

Aus dem Institut für Physiologie und Pathophysiologie
Geschäftsführender Direktor: Prof. Dr. Dominik Oliver
des Fachbereichs Medizin der Philipps-Universität Marburg

New principles in collective cell migration during
***Drosophila* organ development**

Inaugural-Dissertation zur Erlangung
des Doktorgrades der Naturwissenschaften

dem Fachbereich Medizin der Philipps-Universität Marburg

vorgelegt von
Maik Christian Bischoff
aus Mainz

Marburg, 2020

Angenommen vom Fachbereich Medizin der Philipps-Universität Marburg am: 26.11.2020

Gedruckt mit Genehmigung des Fachbereichs Medizin

Dekan, i.V. der Prodekan:	Prof. Dr. R. Müller
Referent:	Prof. Dr. Sven Bogdan
1. Korreferent:	Prof. Dr. Alexander Brehm

Table of Contents

Table of Contents	I
Index of Figures.....	III
Abbreviations.....	IV
1. Introduction.....	2
1.1 Creating motion from potential energy: modes of motility.....	2
1.1.1 Actin treadmilling: the basic force generator	3
1.1.2 Actin regulation: the key process for persistent motion	4
1.1.3 The molecular clutch: regulation of substrate adhesion	8
1.1.4 Lamellipodia independent types of motility	10
1.1.5 Dimensionality in cell migration	11
1.1.6 Principles of directionality.....	13
1.2 „The social behaviour of cells” –migrating in a collective	13
1.2.1 Initiation of collective migration	14
1.2.2 Collectiveness among individual cells: mesenchymal collective cell migration	16
1.2.3 Locomotion with constant adhesion: epithelial collective cell migration	18
1.3 The <i>Drosophila</i> testis myotube migration system.....	20
1.4 Aim of the work	23
2. Material and Methods.....	24
2.1 Fly genetics	24
2.1.1 List of mutant fly stocks	24
2.1.2 List of transgenic fluorescence reporter fly stocks	24
2.1.3 List of transgenic Gal4 and UAS fly stocks	24
2.1.4 Characterization of Gal4 driver stocks	24
2.1.5 Gal4/UAS based screen for adult testis phenotypes	25
2.2 Microscopic image processing.....	25
2.3 Quantification Methods.....	25
2.3.1 Indirect measurement of cell cohesion using <i>beatVC</i> Gal4 mosaic expression.....	25
2.4 Molecular Biology	26
2.4.1 List of Plasmids	26
2.4.3 PCR.....	26
2.4.4 DNA gel electrophoresis.....	27
2.4.5 DNA restriction with restriction endonucleases	27
2.4.6 Directional cloning using the pENTR TOPO System	28
2.4.7 Subcloning using the Gateway technology.....	28
2.4.8 Generation of chemically competent <i>E. coli</i>	28
2.4.9 Transformation of <i>E. coli</i>	29
2.4.10 Purification of plasmids from transformed bacteria (Mini, Midi)	29
2.4.11 RNA isolation	29
2.4.12 cDNA synthesis	30

2.4.13 DNA sequencing.....	30
2.4.14 Transgenesis of <i>Drosophila melanogaster</i> based on the PhiC31 system	30
2.4.15 List of synthetic oligonucleotides (primer).....	31
2.4.16 List of newly created vectors.....	32
2.4.17 List of newly created GTPase sensor fly stocks	32
3. Publications.....	33
3.1 Publication 1	33
3.2 Publication 2	55
Maik C. Bischoff¹, Sebastian Lieb², Renate Renkawitz-Pohl³ and Sven Bogdan^{1*}	56
4. Additional Results and Discussion.....	109
4.1 Pupal testis myotube development occurs in three steps and can be studied in explants	109
4.2 Migrating testis myotubes use a filopodia-based mode of motility	110
4.3 FGF signalling affects migration but likely not as a chemoattractant.....	113
4.4 Collective behaviour resembles contact stimulation of migration (CSM).....	114
4.5 CSM requires differential matrix adhesion	116
4.6 Cohesion is enforced by purse-string-like dynamics via supracellular actin cables	117
4.7 Regulation of substrate adhesion seems to be orchestrated by Rho-GTPases	118
4.8 Testis nascent myotube migration could be an example for invasive cancer-like motility.....	121
4.9 Conclusion	124
5. Summary.....	125
5.1 Zusammenfassung.....	126
6. References	127
7. Appendix	161
7.1 Supplementary figures	161
7.2 Vector Maps.....	170
7.3 Gal4 driver lines screened for genital disc/testis nascent myoblast expression	170
7.4 UAS effector screen for adult testis shaping defect	172
7.5 List of mutant fly lines analysed for adult testis shaping defects.....	179
7.6 Author Contributions	180
7.6.1 Publication 1	180
7.6.2 Publication 2.....	180
7.7 Verzeichnis der akademischen Lehrer/-innen.....	181
7.8 Danksagung.....	182
7.9 Ehrenwörtliche Erklärung	183

Index of Figures

Figure 1. Modes of migration in 2D and 3D environments.....	12
Figure 2. Modes of collective cell migration.....	15
Figure 3. Testis nascent myotube migration.....	22
Figure 4. Rho-GTPases in testis myotube CSM compared to CIL.....	120
Supplementary figure S1. The development of the <i>Drosophila</i> testis myotube layer	161
Supplementary figure S2. Reduction of <i>htl/dof</i> causes severe muscle coverage defects when using specific myoblast driver lines.....	163
Supplementary figure S3. Reduction of <i>ths</i> in the testis terminal epithelium and the seminal vesicle epithelium causes testis muscle coverage defects.	164
Supplementary figure S4. Ectopic expression of <i>pyr</i> in the testis terminal epithelium and the seminal vesicle epithelium causes testis muscle coverage defects.	165
Supplementary figure S5. Mosaic-like expression of <i>htl</i> -RNAi suggests plithotactic direction of immobilized cells.	166
Supplementary figure S6. Cdc42 and Rac activity sensors are derived from GTPase binding domains of different targets.	167
Supplementary figure S7. Collagen localization studies suggests two basement membrane-like ECM-layers covering myotube/pigment cell layer from both sides.....	168
Supplementary figure S8. Pan-mesodermal reduction of <i>Mmp2</i> causes migration defects.....	169

Abbreviations

(excluding genes, domains, cell lines, IUPAC code for nucleotide bases and amino acids)

% (v/v)	percent by volume
% (w/v)	percent by weight
µm	micrometer
ADP	adenosine diphosphate
APF	after pupae formation
approx.	approximately
ATP	adenosine triphosphate
BL-[number]	stock from <i>Bloomington Drosophila Stock Center</i>
BP	base pairs
<i>cf.</i>	<i>confer</i> (compare)
C-terminus	carboxyl-terminus
dATP	deoxyriboseadenine triphosphate
dCTP	deoxyribosecytidine triphosphate
DGRC	<i>Drosophila</i> Genomics Resource Center
dGTP	deoxyriboseguanine triphosphate
DNA	deoxyribonucleic acid
dNTP	deoxyribose Nucleoside triphosphate
Drf	Diaphanous related proteins
dTTP	deoxyribose thymidine triphosphate
<i>E. coli</i>	<i>Escherichia coli</i>
<i>e.g.</i>	<i>exempli gratia</i> (for example)
ECM	extracellular matrix
EGFP	enhanced green fluorescent protein
EMT	epithelial–mesenchymal transition/transformation
F-actin	filamentous actin
fig.	figure
G-actin	globular actin
Gal4	galactose-responsive transcription factor
GAP	GTPase-activating protein
GD[number]	RNAi construct from <i>P-element RNAi library</i> (<i>Vienna Drosophila Resource Center</i>)
GDP	guanine diphosphate
GEF	guanine nucleotide exchange factor
GFP	green fluorescent protein

Abbreviations

GTP	guanine triphosphate
GTPase	guanine nucleotide-binding proteins
h	hour
IUPAC	<i>International Union of Pure and Applied Chemistry</i>
KB	kilo base pairs
kDa	kilo Dalton
KK[number]	RNAi construct from <i>phiC31 RNAi library (Vienna Drosophila Resource Center)</i>
l	liter
LB	lysogeny broth
m	meter
min	minute
ml	milliliter
NIG[number]	stock from <i>National Institute of Genetics (Japan)</i>
NPF	nucleation promoting factor
N-terminus	amino-terminus
-P	-phosphate
PCR	polymerase chain reaction
P _i	inorganic phosphate
PIP2	phosphatidylinositol 4,5-bisphosphate
pub.	publication
RNA	ribonucleic acid
RNAi	ribonucleic acid interference
rpm	revolutions per minute
sec	second
TRiP[number]	RNAi construct from <i>Transgenic RNAi Project (Harvard)</i>
U	unit
UAS	Upstream activating sequence
V	Volt
v[number]	stock from <i>Vienna Drosophila Resource Center</i>

1. Introduction

Cell migration is one of the fundamental processes in the cell biology of metazoans. It is vital in immune response, development, and constitutes one of the hallmarks of cancer cells^{371,187,553}. The basic underlying cellular processes are evolutionary highly conserved and seem to even predate metazoans and multicellular life in general. Motion of prokaryotes relied mostly on flagellate-powered swimming. Early eukaryotes developed a new basic type of motility: amoeboid crawling^{412,279,151}.

It is long-known that single-cell eukaryotes such as *Amoeba* species move, using actin-dependent pseudopodia^{15,16}. Other branches in the tree of eucaryote life also possess the capacity to use amoeboid movement. Heath and Steinberg (1999) showed that fungi have this ability²⁰⁰. In using amoeboid migration based on actin-containing pseudopodia-like structures, cells of the amphibia infecting parasitic fungus *Batrachochytrium dendrobatidis* can reach speeds similar to *Dictyostelium* amoebae. This process depends on the dynamics of the fundamental actin-related protein 2/3 (Arp2/3) activators of the Wiskott–Aldrich Syndrome family (WASp/WAVE family)^{151,515,524}. Holistic sequence analysis and comparison of genes of the WAVE/WASp family revealed that the earliest eukaryotes must have already possessed a homologue. Accordingly, eukaryotes without WASp such as plants seem to have lost them during their evolution. It can be concluded that the capacity to migrate may be one of the ancestral and defining features of eukaryotic cells in general.²⁴⁸

Of course, the development of multicellularity constitutes a drastic change in the surrounding environment of cells. Still, rather than fundamentally changing the basic modes of motility, cells in multicellular organisms seem to have merely adjusted their migratory behaviours to cope with the new challenges. In summary, two fundamental properties changed. Firstly, the surface to migrate on altered, resulting in a variety of migration modes as summarized in section 1.1. Secondly, contact with neighbouring cells became a crucial factor, resulting in a complex network of interaction, comprising *e.g.* direct physical interaction and long-distance crosstalk. Ultimately, these conditions resulted in something Michael Abercrombie, a pioneer in the fields of cell migration, named the “social behaviour” of cells¹. The highest level of “social” organization is achieved in collective cell migration, summarized in section 1.2.

1.1 Creating motion from potential energy: modes of motility

It was also Michael Abercrombie and colleagues, who provided a first detailed description of cellular motility^{2–4,8,5}. As an experimental system, they chose fibroblasts derived from embryonic chick heart and neonatal mouse muscle. Using phase-contrast microscopy, they observed a leading flat fan-like cellular protrusion they termed “lamellipodium”. This structure seemed to be the engine behind the cell movement, pushing against the leading edge by adding material to its front. At the same time, the rear seemed to retract. Dorsally in the lamellipodium, Abercrombie *et al.* observed a constant retrograde flow

of particles. Electron microscopy gave the resolution to characterize the material as “microfilaments” or actin^{2-4,8,5}. Electron dense particles were recognized as substrate adhesions. Based on their observations, Abercrombie *et al.* proposed the mechanism later termed “Abercrombie-cycle” as a mode of motility for migratory cells^{2-4,8,5}. It can be broken down into four steps: 1. **Protrusion**: microfilaments get elongated at the leading edge, pushing it forward. 2. **Substrate adhesion**: via adhesive molecules, microfilaments are tethered to the substratum to build an anchor to push against. 3. **Retraction**: the cell actively retracts in the rear. 4. **Loss of substrate adhesion**: in the rear part of the cell, matured adhesions get disassembled and loose contact to the substratum.^{2-4,8,5} These rules laid the foundation for decades of cell migration research. Although they may simplify the process, they still correctly describe the mechanics inside a lamellipodium. Years of research has broadened our understanding of cell migration. The molecular mechanisms behind force generation and lamellipodial migration are addressed in section 1.1.1–1.1.3. However, the lamellipodium does not constitute the only cellular structure capable of promoting migration. Other mechanisms of migration are addressed in section 1.1.4 & 1.1.5.

1.1.1 Actin treadmilling: the basic force generator

There are two known actin-dependent processes which can convert chemical into kinetic energy: Myosin-driven contractility and actin polymerization. Protrusive forces in most known migration processes rely on actin elongation ^{reviewed in 403}. Monomeric G-actin is a globular protein of about 42 kDa. It contains a medial Adenosine triphosphate (ATP)/Adenosine diphosphate (ADP) binding cleft. A high concentration of Ca²⁺ or Mg²⁺ increases ATP/ADP association. Lowering the concentration shifts the balance, favouring dissociation. Monomers lacking nucleotides are denatured as a consequence^{267,235,451,120}. G-actin-ATP is more likely to bind G-actin-ATP than G-actin-ADP to generate filamentous (F) actin and thereby building a double-helical microfilament³⁸⁹. For actin molecules, being a part of a filament increases the rate of hydrolyzation to actin-ADP, which may be a stochastic process^{47,230}. Nucleotide exchange to the ATP-bound form is never occurring in F-actin, meaning that actin-ATP can only be restored in its monomeric form³⁸³. Because the phosphate residue dissociates very slowly, there is an actin-ADP-Pi intermediate step. It is identical in polymerization rate as actin-ATP. For a filament to grow, new G-actin-ATP must be bound before hydrolyzation is completed. If the binding of new G-actin-ATP happens at a slower rate than hydrolyzation, the filament shortens because terminal actin-ADP tends to dissociate. If the process is faster than hydrolyzation, the filament effectively elongates. The free energy accessible during this process can be utilized to exert force.^{383,154,122,253,210,480}

Under physiological conditions, the initial hurdle lies in bringing a minimum number of actin molecules together to reach a stable phase. Actin-dimers and trimers are unstable but if a nucleus of more than four actin-molecules assembles, polymerization continues. As expected in a stochastic process, the duration of this initial lag in polymerization depends on the total actin concentration in the medium^{454,101,145,363}. Monomeric G-actin is an inherently asymmetric protein. One end of the molecule

is much more prone to polymerization than the other. This end is referred to as “barbed” in contrast to the slowly polymerizing “pointed” end. Accordingly, the filament has a barbed and a pointed end, too. If the actual actin concentration is higher than the critical concentration elongation occurs in both directions but at a faster rate on the barbed end. The critical actin-concentration is reached when the depolymerization-rate at the pointed end equals the polymerization-rate at the barbed end. This process – in which the net length of the filament stays in a dynamic equilibrium – is called “treadmilling”^{541,83,384,493,153,542,59,466}, reviewed in 62,387,385

The treadmilling process constitutes the very basis of all actin polymerization-based modes of cellular motility. Nevertheless, physiological concentrations of G-actin would yield a speed of roughly $0.04 \mu\text{m}/\text{min}$ ³⁸⁷. Since a lot of cells reach higher velocities, it becomes clear that mechanisms exist to optimize the treadmilling process and thereby to obtain a faster yet steady turnover. Enhancement of polymerization and depolymerization-rate and nucleation can be performed by numerous actin regulators as summarized in the following section.^{reviewed in 75,387,403,259,405}

1.1.2 Actin regulation: the key process for persistent motion

There is a large number of proteins regulating actin dynamics. To address them all exceeds the scope of this work. It can be summarized, that for a faster treadmilling process a faster polymerization and depolymerization rate are necessary. A rate-limiting step in polymerization is the concentration of G-actin-ATP. The protein Profilin catalyses nucleotide exchange in G-actin, and thereby restores the G-actin-ATP pool, resulting in a drastically faster polymerization rate^{reviewed in 381}. Meanwhile, a faster depolymerization rate of actin-ADP is enhanced by Actin depolymerizing factors (ADF)/cofilin^{reviewed in 31}. A factor slowing down the polymerization rate is actin-capping. Especially barbed-end-capping by Capping Protein (CP) is utilized to inhibit further elongation of the filament.^{reviewed in 127}

Another strategy to accelerate treadmilling is to promote the *de-novo* nucleation of filaments. In principle, there are three kinds of nucleators known. Firstly, tandem-monomer-binding nucleators like Spire and Cordon-bleu comprise a cluster of G-actin binding sequences which simply bring monomeric actin molecules together and thereby foster nucleation⁴⁰¹. The same principle seems to be used by Enabled (Ena)/Vasodilator-stimulated phosphoprotein (VASP) to nucleate and elongate filaments^{reviewed in 37}. Secondly, there is Arp 2/3 and thirdly, there are Formins as nucleators which will be addressed in more detail in the following.

Arp 2/3. In the first half of the 1990s, numerous unconventional actin-related proteins with unknown functions were discovered^{98,290,100,289,382,96,155,143,341,99,196,452}. These were later termed actin-related proteins 1–11 (Arp1–Arp11)⁴⁴⁸. Many members of the Arp family were later found to participate in chromatin remodelling (Arp4–9)³⁶¹ or dynein transport as part of the dynactin complex (Arp1&11)³³. A complex of two such factors named Arp2 and Arp3 that was firstly purified from *Acanthamoeba castellanii*, however, would turn out to be the core unit of the complex which takes a leading role in actin nucleation^{306,239,344,343}. It was found that Arp2/3 complex induces nucleation of a new filament by

attaching monomeric G-actin to an already existing mother-filament with its barbed end pointing outwards and thereby creating a 70° branching point. Arp2/3 takes the role of a hinge or y-piece, interconnecting mother and daughter filament. This is possible because Arp2 and Arp3, as actin-related proteins, can bind to actin molecules^{239,18,343,46}. Thereby, Arp2/3 creates a dendritic network of branched F-actin³⁸⁶. Shortly after its discovery, it was shown *in vivo* in zebrafish (*Danio*) and frog (*Xenopus*) keratinocytes and in yeast that Arp2/3 induced membrane pushing is the main force responsible for protruding the lamellipodium^{491,490,551,338}. Arp2/3 was also found concentrated in lamellipodia of fibroblasts, the model system in which the Abercrombie-cycle was originally discovered^{304,438}, and in the leading edge of carcinoma cells²⁷. It can be concluded that the Arp2/3 complex is the crucial factor in lamellipodia based motility.

Crystallography of bovine Arp2/3 revealed that the entire complex consists of 7 subunits. Five of them (ARPC1–5) keep the crucial Arp2 and Arp3 subunits apart from each other, incapacitating nucleation^{547,410}. Approaches using cryogenic electron microscopy substantiated the notion that Arp2/3 lies directly in the actin branch and elucidated the exact position of each component of the complex. In contrast, all activators except Cortactin dissociate after nucleation of the new branch occurred^{128, reviewed in 387,176}. Even before it was elucidated by its crystal structure how the Arp2/3 complex is autoinhibited, it was clear that a promoting factor is necessary for inducing dendritic nucleation. In 1997–1999, the Wiskott–Aldrich syndrome family (WASp/WAVE family) was discovered.^{305,552,307,413}

Wiskott–Aldrich syndrome protein (WASp) was originally characterized to be responsible for the Wiskott–Aldrich syndrome. It was presumed to have a function in lymphocytes and thrombocytes in which it was demonstrated to be expressed^{112,359,113,111}. WASp binds to Arp2/3 to promote dendritic nucleation by bringing Arp2 and Arp3 subunits in contact. It was the first example of a nucleation promoting factor (NPF) which could link surface receptor activation to dendritic network formation reviewed in 205. WASp and its homolog N-WASp, which was first thought to be neuronally expressed but later showed to be ubiquitously present, contain a C-terminal VCA domain. It comprises the monomeric G-actin binding Verprolin homology (VPH; V-site; WASp homology domain 2, WH2) domain and the Arp2/3 binding acidic residue (CA)-site^{332,328,307,413}. Deletion analysis of WASp and physical binding assays demonstrated that the C-terminus with the VCA domain binds to the p21-Arc motif of Arp2/3. In N-WASp, it was illustrated that the V-site, which showed to be indispensable for the actin regulation function, directly binds to monomeric G-Actin. Overexpression of the VCA-domain resulted in ectopic Arp2/3 localization and perturbation of lamellipodia-formation^{332,307}. Before its NPF-function was fully understood, WASp was shown to be an activator of actin polymerization downstream of Cell division control protein 42 (Cdc42) using genetic tools. Later, physical interaction was confirmed. WASp contains a Cdc42/Rac interactive binding (CRIB) motif which was shown to procure binding to Cdc42 and Ras-related C3 botulinum toxin substrate (Rac) GTPases^{22,494,63}. Overexpression of N-WASp (but not WASp) and active Cdc42 induces ectopic filopodia in cultured cells³³⁰. It was known before that overexpression of active Cdc42 induces actin spikes^{356,256}. Interestingly, the additional expression of N-

WASp massively increased the length of these, whereas expression of N-WASp alone did not affect the cell morphology. This led to the assumption that N-WASp needs Cdc42-GTP binding to be activated. It was also shown to physically interact with Cdc42³³². N-WASp was also found to function downstream of phosphatidylinositol-4,5-bisphosphate (PIP2) as it contains a pleckstrin homology (PH) domain, like WASp³²⁸. When not activated, N-WASP seems to be in a folded conformation in which the CRIB Domain contacts the C Site. Thereby, the VCA-domain, which is needed for Arp2/3 activation, is masked. To activate N-WASp, PIP2 must bind to PH-domain and Cdc42 to the CRIB-domain. This causes conformational changes which will expose the VCA-domain and thereby promote N-WASp function.^{206,414,581,392,330,242,413 reviewed in 500}. Phosphorylation by the Src-family of tyrosine kinases seems to enhance WASp/N-WASp function^{484,516,432,102}.

Suppressor of cAR (SCAR) is another member of the Wiskott–Aldrich syndrome family which was firstly found in *Dictyostelium*. A loss of the heterotrimeric G-protein-coupled receptor cAR perturbs tip formation in the multicellular development phase of *Dictyostelium*. Expressing SCAR can rescue that phenotype. A knockdown leads to aberrations in F-actin localization³⁸. Its vertebrate homolog, **WASP family Verprolin-homologous protein (WAVE, SCAR1)** induces membrane ruffles when overexpressed in Swiss 3T3 fibroblast. WAVE also contains a VCA domain, similar in function to the one found in WASp^{305,331,307}. Rac1 was found to be an activator of WAVE. Rac was shown before, to be the main regulator of lamellipodia, inducing membrane ruffles when overexpressed^{404,256}. Expression of dominant-negative Rac1 in Swiss 3T3 fibroblasts leads WAVE to change its location from the cytosol to ectopic membrane ruffles. Expression of an inactive WAVE^{ΔPH}, rescues the membrane ruffle phenotype. Active Cdc42 induced filopodia could not be rescued. Based on these results, it seemed as WAVE gets activated by Rac1, although it contains no GTPase binding domain (GBD)/CRIB-motif³³¹. This could be explained when it was found that WAVE is part of a pentameric complex, the WAVE regulatory complex (WRC), that in addition comprises the following subunits: **1.** specifically Rac1-associated protein-1 (Sra1), **2.** p53-inducible protein 121 (PIR121), **3.** Nck-associated protein 1 (Nap1) or its mouse paralog hematopoietic protein-2 (Hem2), and **4.** Abelson interacting protein 1 (Abi1)^{224,166,457}. The 3D structure of this complex causes Sra1 to mask the VCA-Domain and thereby inhibiting NPF function^{226,110,90}. The allosteric release of the autoinhibited stage of the WRC is the target of a multitude of regulative mechanisms. Most notably, Rac1 was shown to be the main regulator^{reviewed in 109,259,90}. Besides, ADP-ribosylation factor 1 (Arf) can cooperate, to activate WAVE²⁵⁰. Phosphorylation of the WRC by numerous kinases seems to play a role, too^{329,243}. It was shown *in-vitro* that full WRC activation requires phosphorylation, prenylated Rac1, and PI(3,4,5)P3, presumably ensuring that WAVE activation is restricted to the membrane^{286,360}. Crystallographic data indicated that a Rac1-binding is built by a part of the Sra1-surface and possibly part of the meander-region of WAVE⁹⁰. Cryo-electron microscopy later revealed that there is another Rac1-binding site on the opposite side of Sra1. Analytical ultracentrifugation confirmed both, the newly found site (D-site) and the known site (A-site), to bind Rac1. The D-site has a 40fold higher affinity to Rac1. Pyrene-assays demonstrated that

both sides are required for WRC activation⁸⁷. Very recent findings based on cell culture data indicated that the A-site suffices for WRC function. In contrast, the D-site appears only to enhance the function without being mandatory⁴³⁹.

There are **several further WASp family NPFs** which activate Arp2/3 in different cellular processes or act redundantly. Their common feature is the WCA domain ^{reviewed in 421}. In *Drosophila*, WHAMY was discovered to be a fly-specific paralog of WASp which underwent a duplication of the CRIB domain. Unlike WASp, WHAMY seems to bind specifically active Rac1 and not Cdc42. Accordingly, it appears to be important for – and localized in filopodia and lamellipodia⁶⁰.

Formins. The third group of F-actin nucleators consists of the Formins. Formin 1 was found in mice and originally termed Limb deformity (Ln) as its alleles *ld^{HD}* and *ld^{ln2}* cause strong defects in the patterning of developing mouse limbs^{227,577,560,303,561}. Shortly after *diaphanous (dia)* had been characterized in *Drosophila*⁸¹, the Formin Bni1p was found in yeast²⁴⁷. In mammals, there are 15, and in *Drosophila* six different genes encoding Formins ^{reviewed in 58}. Early studies revealed that yeast Formins elongate and nucleate F-actin and induce actin cable formation^{426,132,427,131,394}. In metazoan cells, predominantly Diaphanous-related Formins (Drfs) were discovered to take a major role in filopodia assembly^{373,49,567}. Other roles of Formins were found in lamellipodia formation^{431,50,567}, cellular junctions ^{reviewed in 52}, vesicle transport^{294,378,285,449,25}, stress fibers^{225,216,501,275,374,450,447,433,165,434}, and many more cellular processes. Formins are large proteins consisting of more than 1000 amino acids and comprise a formin homology domain 1 (FH1) and 2 (FH2), that have actin-binding capability. In some, further actin-binding motifs, like WH2 domains, can be found at the C-terminus. Drfs, the most abundant type in animals, typically contain an N-terminal GBD, a diaphanous inhibitory domain (DID), a dimerization domain (DD), and a C-terminal a diaphanous autoregulatory domain (DAD). When not activated, Drfs are in an autoinhibited state, in which the DID binds the DAD. Rho-GTPase binding to the GBD allosterically releases this binding, activating Formins.^{91,208,202,207,395,81,293,92,532}

To deploy NPF function, Formins dimerize to antiparallel dimers that can bind to actin barbed ends^{582,252,565,394}. This process prevents capping proteins from inhibiting elongation^{53,459,339,254,197,583}. The FH2 domain alone suffices to induce actin nucleation. Yet, it is very inefficient when only Profilin-actin, which is the most abundant actin under physiological circumstances, serves as substrate^{91,339,463,565}. For instance, binding of Profilin-actin to a potentially existing WH2 or the FH1 domain can accelerate the nucleation process^{85,368,178,202,252,254,427,221}. Subsequently, Formin can also act as potent elongator. It is not entirely understood, how Formins enhance elongation. In the current model it is believed that FH2 domains of both monomers are responsible for the attachment to the barbed end of the growing filament in a step-wise process: there seems to be a continuous alternating binding of each FH2 domain that has consecutive “open states” where actin can be bound and “closed states” where no monomers can be added. The FH1 is very flexible and thereby can enhance elongation by directly delivering Profilin-actin complexes to the FH2 domain. How this process works exactly, remains elusive^{368,251,583,365,339,416,523,252,565,255,369,370}. Cell culture studies, targeting the Drf Formin-like 2 (FMNL2)

revealed that its elongation function seems to outplay its nucleation function in lamellipodial driven motility. Arp2/3 complex works as a nucleator creating barbed ends that are elongated by FMNL2^{50,236}.

The interplay of actin regulators in the lamellipodium is steered by Rho-GTPases. Rho-GTPases work as molecular switches that either bind to guanosine triphosphate (GTP) or guanosine diphosphate (GDP). In their GTP-bound form, they activate downstream effectors like actin regulators. The Rho-GTPases **Rac1**, **Cdc42**, and Ras homolog family member A (**RhoA**) take roles in establishing and maintaining asymmetry as “master-regulators”^{10,356,404,406,191,117}. Rac-GTP activates the Arp2/3 complex at the leading edge via WRC. Arp2/3 branching nucleation constantly creates new barbed ends as a substrate, used by Formins and Ena/VASP for further elongation. Thereby the typical fan-like structure of the lamellipodium is created^{1387,420,271,50,236}. It is important to note that relative to the substrate the branched actin network itself remains stationary due to the molecular clutch mechanism explained in the following. For example, by using photoactivation experiments this can be shown directly⁵⁰⁵. It should also be mentioned that polymerization does not only occur at the tip but also inside the sheet of the lamellipodium⁵³⁸. Cdc42-GTP activates WASp in the lamellipodium and probably in filopodia^{305,413} which explore the environment. In the very rear of the cell, RhoA induces retractive fibre formation and activates Rho-associated protein kinase (Rock), which in turn activates Myosin II ^{reviewed in 527}. This allows for a controlled retraction of the trailing edge. The leading edge in lamellipodial migrating cells does not only contain the lamellipodium but behind it a region of contractile actin fibres called the lamella³⁸⁸ (fig 1 a). This promotes persistent motion based on actomyosin contractility. Yolland *et al.* suggest in a recent publication that global cellular flow of actin, rather than the very narrow lamellipodial protrusive area, guarantees persistent motion in cells⁵⁷⁰. Findings like this demonstrate that the significance of lamellipodial dynamics must be re-evaluated in the future to understand the basics of persistent cellular motion.

1.1.3 The molecular clutch: regulation of substrate adhesion

In 1988, Mitchison and Kirschner proposed a new explanatory model for adhesion in cellular locomotion. They summarized that the actin-flow in cells is constant, yet cellular motion is variable. Like in a car where the motor is consistently running a clutch is necessary as a regulator to switch force submission on and off. Accordingly, this principle was termed “molecular clutch”³³³. Its task is to physically link the extracellular matrix (ECM) to the treadmilling F-actin and to detach from the substrate as an answer to signalling/mechanical cues. If the link is established, retrograde flow is “slowed down”, and F-actin polymerization advances the leading edge instead of treadmilling rearwards.
reviewed in 526

An F-actin binding complex centred around the ECM-binding protein Integrin promotes this function. Integrin is a heterodimeric transmembrane receptor comprising an α and a β subunit²²⁰. It binds to ECM (like fibronectin) using the extracellular domains and numerous linkers using intracellular domains^{220,217,576}. Integrin can bind the protein Talin²¹³ which in turn can bind F-actin²⁰³. Furthermore,

Integrin can be attached to F-actin via α -actinin³⁶⁴. There is also an indirect linkage between F-actin/Talin and F-actin/ α -actinin via Vinculin^{168,64,233,174}. The adhesive complexes built by these proteins can also comprise further molecular players as Paxillin, p120Cas, and many more^{562, reviewed in 526}. Integrin based adhesions can also have a signalling function, most prominently performed by the adhesion complex binding tyrosine kinases Focal adhesion kinases (FAK) and Src (cSrc=Abbreviation for cellular sarcoma)^{reviewed in 562}. FAK localizes to focal adhesions using its focal adhesion targeting (FAT) domain^{209,440}. FAK auto-phosphorylates to bind Src which thereby further phosphorylates FAK^{69,266,441}. FAK is known to positively regulate RhoA via one of its GEFs⁵⁷⁸. Src activates by binding to FAK and is crucial to regulate focal adhesion turnover and thereby cell behaviour and motility^{141,193,296}.

In cellular protrusions during migration, adhesion complexes can assemble in clusters, generally termed “Integrin-mediated adhesions”^{40,28}. This process could be induced by mechano-sensing of F-actin polymerization generated force⁴⁰⁹ or interaction of Arp2/3 with vinculin and FAK^{107,455}. In the initial stage, these complexes are called “**nascent adhesions**”. Their assembly seems to rely on force but is independent of actomyosin contractility, reflecting their position in the leading edge^{171,159,486,409,93} (fig. 1 a). Rather, it seems to be actin polymerization itself that triggers their formation^{170,14,575}. At the rear end of the lamellipodium, nascent adhesions can either get disassembled⁹³ or triggered by Myosin II, turn to so-called “**focal complexes**”^{167,539,517,30} (fig. 1 a). Focal complexes possess Talin, Vinculin, Paxillin, and FAK but no α -actinin^{170,575}. Their dynamics are known to be regulated by Rac1 and Cdc42³⁵⁶. Focal complexes can either disassemble or if clusters are large enough or mature into “**focal adhesions**”, accompanied by the binding of α -actinin^{186,103,575,536}. These are tethered to actomyosin contractile fibres in the lamella region of the cell²¹⁶ (fig. 1 a). Their assembly and disassembly are known to be regulated by Rho/Rock activity^{404,517,97,215,409}. Mature focal adhesions must resist higher tension forces than nascent adhesions¹⁶². The crucial factor for adhesion stability seems to be Talin⁵⁷⁹. FAK appears to promote Talin recruitment in nascent adhesions²⁸⁴. In focal adhesions there is a positive feedback loop as the amount of Talin and Vinculin binding increases, the more force is applied^{177,180}. If due to actomyosin contractility a lot of force is applied Talin gets stretched, exposing more Vinculin binding sites, increasing stability further^{reviewed in 70}. Recently, in a detailed and large systemic approach, the roles of guanine nucleotide exchange factors (GEFs) and GTPase-activating proteins (GAPs) in Rho-GTPase activation/deactivation was deciphered. Interestingly, about one-quarter of all GEFs and GAPs, predominantly Rac1 regulators, are associated with Integrin based adhesions. There was a clear spatial distinction between Rac1-GEFs, which were present close to the membrane, and Rac1-GAPs rearwards at the lamella-region. Accordingly, Rac1 activating GEFs were found in nascent adhesions and Rac1 deactivating GAPs in focal adhesions. These findings explain how the spatiotemporal regulation of Rac1 is guaranteed by Rac1 regulators to safeguard maturation of substrate adhesions³⁴².

1.1.4 Lamellipodia independent types of motility

The dynamics described so far apply to the so-called lamellipodial (or fibroblast-like/mesenchymal⁵⁶⁶) migration type (fig. 1 a). It is important to note that there are numerous other modes of motility. Bleb-based motility is a migration mode independent of treadmilling but relying on F-actin/Myosin-interaction. When moving by blebbing, the cell uses the potential energy in its hydrostatic pressure via controlled rupture of the cortical actin cytoskeleton or by loosening the connection between cortex and membrane, using actomyosin contractility^{86,reviewed in 367,514} (fig. 1 b). This causes the membrane to “bulge”, and thereby to protrude. Interestingly, in some cell types, as in *Danio* mesoderm progenitors, membrane blebs and lamellipodia can coexist¹¹⁹. Other cell types can switch between bleb-based motility and lamellipodia-based motility^{545,41}. Walker carcinosarcoma cells, for instance, can switch from lamellipodia-based motility to blebbing when positioned in non-adhesive environments⁴⁷¹. Lobopodia are cylindrical shaped protrusions that combine characteristics of lamellipodia and blebs (fig. 1 d). They contain Integrin-based adhesions but are fuelled by hydrostatic pressure, released by actomyosin contractility. Originally discovered in protozoans, this mode of motility was found to be used by fibroblasts in three-dimensional ECM environments which were linearly elastic^{465,261,376}. Amoeboid movement is used by many authors as an umbrella term, describing all actin and actomyosin based modes of motility, including lamellipodia/lamella-based motility and blebbing²⁷⁹ (Note: some authors use amoeboid motility as a synonym for bleb-based motility⁵⁶⁶). Lämmermann and Sixt presented an intelligible classification of all amoeboid modes of motility subdivided by three major forces: (substrate) adhesion (A), (actomyosin) contraction (C) and (filament) polymerization (P)²⁷⁹. Using the “ACP” model, depending on which force the respective type of motility relies upon, every mode can be characterized. Classical fibroblast motion relies equally on polymerization, adhesion, and contraction (ACP). Bleb-based movement relies mostly on contraction (aCp), whereas lobopodia-based motility makes use of contraction and adhesion (ACp). Through this model, it becomes clear that different modes of motility are merely combinations of a single toolbox of mechanics. They need to be applied, varied, or changed as an answer to certain physical environments or cues. There are intermediate modes, simultaneous use of different forms and versatile cells that change their means of migration to cope with different surroundings.

Filopodia are thin rod-like dynamic cell protrusions containing bundled actin. They get elongated by formins like Dia or by Ena/VASP and are regulated by different Rho-GTPases. Actin bundlers such as Fascin or α -actinin build the scaffold, to keep F-actin filaments densely packed. Very often, filopodia are found to be anchored in the lamellipodium^{134,133,188,reviewed in 228}. Filopodia were firstly characterized in sea urchin embryos⁵²¹. Findings in the same model organism firstly shed light on their role in long-range cell-cell communication^{237,309}. In the “classical” view, their role is considered largely explorative. They can sense chemoattractants and thereby promote chemoattraction¹⁷. Invadopodia are viewed by some authors as a subtype of filopodia²²⁸. Thereby, the ability to digest ECM can be considered a potential filopodial feature. Furthermore, filopodia in some cells bear integrin-based adhesion, sharing

similarities with those described in lamellipodia. They can be localized at the tip, the base or inside the shaft^{288,437,118,415,163}. The exact role and composition remain elusive, but it seems they resemble focal adhesions. They can mature into such when passing over to the lamellipodium⁵⁵⁶. Adhesions at the tip probably take a role in sensing ECM rigidity, enabling durotaxis^{232,556}.

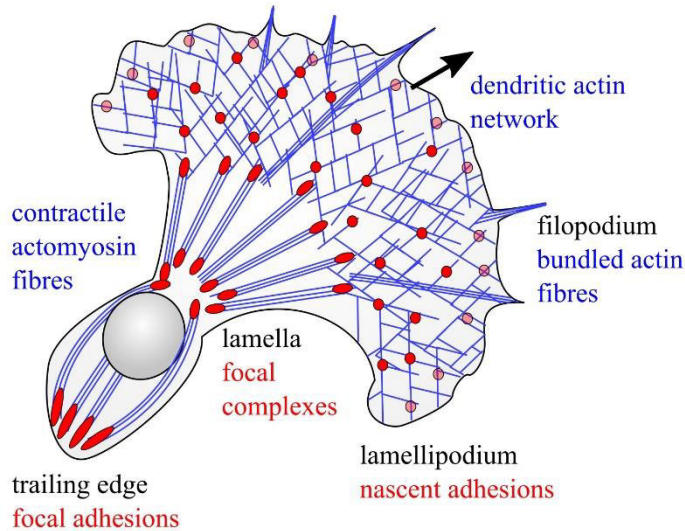
Filopodia can exert pushing force by F-actin polymerization. The mechanics of filopodia have been well-examined, using biophysical approaches and mathematical models^{56,84}. An interesting consequence of these findings is that filopodia could bear the potential to drive migration instead of lamellipodia or lobopodia. Gustafson and Wolpert proposed this kind of migration when they were working on primary mesenchyme cell migration in sea urchin embryogenesis without calling the structures filopodia as they were not defined yet. Later, this idea has been dismissed in favour of a more explorative role of filopodia³²³. Whether endothelial filopodia have a protruding function during angiogenesis, is a matter of discussion¹⁴². But it was shown that a loss of filopodia in *Danio* endothelia still allows for migration, demonstrating the importance of lamellipodial dynamics in angiogenesis³⁷⁹. In mouse embryonic fibroblasts, it was shown that the receptor tyrosine kinase Ror2 induces filopodia downstream of Wnt5a. Incapacitating filaminA binding to Ror2 leads to a loss of filopodia and Wnt5a induced migration. Thereby it can be deduced, that filopodia can act as a motor for migration³⁵⁵. Cancerous and other versatile cell types can deploy numerous migration modes as an answer to environmental cues. It has been observed multiple times that cancer cells possess many highly dynamic filopodia²²⁸. Their loss or upregulation strongly influences metastasis^{20,77,462}. Therefore, it is likely that filopodial migration is part of their repertoire and thereby should be addressed in the future.

1.1.5 Dimensionality in cell migration

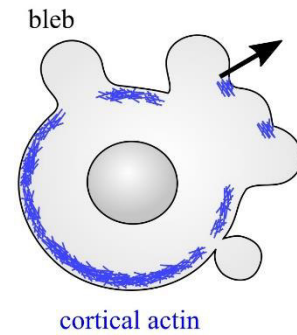
An especially important distinction is whether cells migrate in one dimension (1D, along a single fibril) two dimensions (2D, fig. 1 a, b) or three dimensions (3D, fig. 1 c–e). Inherently versatile cells like fibroblasts and leukocytes but also cancer cells have to migrate through complex 3D environments and thereby deploy a multitude of migration modes^{161,566}. In the case of lamellipodial and bleb-based motility, there is a 3D analogue to the “2D-version”^{566,376} (fig. 1 c, e). Lobopodial motion is inherently three-dimensional (fig. 1 d). Cancer cells in 3D can dynamically switch between all these modes^{357,367,214}. A major challenge coming with 3D migration is confinement by the ECM or other physical barriers. Experiments using microfluidic chambers have shown that the nucleus poses the rate-limiting step when squeezing through such barriers but perinuclear Arp2/3-based nucleation allows for nuclear deformation⁵¹¹. Leucocytes, for instance, choose their migration trajectories based on where the nucleus can fit through when confronted with mazes containing pores of different sizes⁴²³. Instead of simply coping, some cells also modify their environment to facilitate 3D movement. One way to achieve this lies in degrading ECM with proteolytic enzymes like matrix metalloproteases (MMPs)⁶¹. Protrusions containing such proteases and digesting their environments exist in 2D and 3D migration modes and are known as invadopodia or podosomes^{61,357,482,108,228}. Proteolytic ECM remodelling is a

behaviour not only exhibited by cancer cells but also by cells in development, like sprouting endothelia in *Danio* angiogenesis^{534,51}.

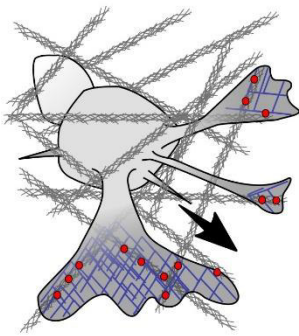
a 2D lamellipodia



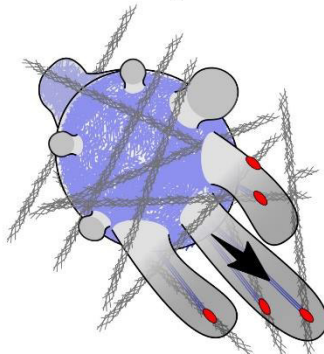
b 2D bleb-based motility



c 3D lamellipodia



d lobopodia



e 3D bleb-based motility

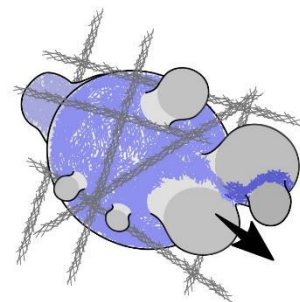


Figure 1. Modes of migration in 2D and 3D environments. Lamellipodia based migration relies on treadmilling of the dendritic actin network and contraction of contractile actomyosin fibres (a). Differently matured Integrin-based adhesions (red) transmit the force to the matrix. Cells can also migrate via blebs by locally disrupting the cortical actin cytoskeleton (b). lamellipodia and bleb-based motility can also be utilized in 3D environments (c, e). Lobopodia use hydrostatic pressure and thereby resemble blebs but comprise Integrin-based adhesions (d). They possess traits of blebs and lamellipodia. F-actin: blue.

1.1.6 Principles of directionality

It is crucial in highly coordinated processes such as wound closure and development that cells reach their assigned destination. There are multiple ways of how signals can steer and coordinate migration. In **chemotaxis**, a spatial gradient of a chemical attractant is established and sensed by cells ^{reviewed in 308}. In a highly complex procedure adjacent tissues or other migrating cells must create a source and a sink for the chemoattractant ^{reviewed in 68}. There are different means of how chemoattraction can be integrated by migrating cell groups ^{reviewed in 508}. The most common one is the use of an externally created gradient as a directional cue. For instance, in *Drosophila* tracheal sprouting, tracheal tip cells express the Fibroblast Growth Factor receptor (FGFR) Breathless (Btl) and migrate along a gradient of the FGF-Ligand Branchless (Bnl)^{489,244}. The cell with the highest Btl activation induces lateral inhibition via Delta/Notch in adjacent cells inhibiting protrusion in them and becomes a highly protrusive leader-cell^{287,82,169}. Consequently, sprouting trachea will always follow a Bnl gradient. On the other hand, FGF-Ligands can also work as a non-directional cue. It has been shown in wound scratch essays using Human Umbilical Vein Endothelial Cells (HUVECs) that they migrate due to FGF-cues. But different from Trachea-cells in *Drosophila*, they already possess asymmetry without a signal because cells at the wound edge have just one open side to protrude. In this model, FGF has been shown to induce migration without the source of the signal being important⁵³¹. A directional gradient must not be established by adjacent tissues but can be generated by the migrating group itself. In *Danio* lateral line, it became evident that polarized expression of a receptor in medial parts of the cluster can locally reduce ligand concentration which in turn affects trailing cells. Ectopic expression of the receptor perturbs migration^{481,121}. There are also models known in which it is not a leader that drags followers but instead, cells pushing from behind that can react to chemoattractant. This mode is known as “rear-wheel drive” chemotaxis⁴⁶¹. In **haptotaxis**, instead of a soluble chemical, ECM-bound cues guide cell migration ^{reviewed in 407}. ECM can also be deposited by leader cells for followers to migrate on, to control their migration routes³⁵². **Durotaxis** refers to migration along an ECM stiffness gradient ^{reviewed in 300}. Additionally, there is a great number of ECM features that can regulate and fine-tune collective and single-cell migration⁵⁶⁶. Another factor contributing to migration directionality is stress caused by physically attached cells. This behaviour exhibited by cohesively migrating cells is called **plithotaxis**^{502,519}.

1.2 „The social behaviour of cells” –migrating in a collective

Swarm behaviour is a basic property observed in many types of so-called “active matter”. This term from theoretical physics describes a collective of agents or particles that transform energy from their surroundings into motion. Examples of active matter include liquid crystals, animal swarms, or human crowds. In 1995, the Hungarian scientist Tamás Vicsek introduced a general model, explaining how

simple rules in these systems can result in the complexity observed in swarm behaviour. He discovered that it suffices if every agent adapts its motion angle to the adjacent particles with a degree of uncertainty. The basic rules he introduced can be observed in nature across scales, especially in biological systems ^{reviewed in 115}. It has been shown that they also apply to clusters of cells during migration ^{495reviewed in 190}. The question which arises is, by which mechanisms cells can reach this high degree of organization comparable to flocks of starlings and shoals of herrings.

Interaction between cells is multifaceted and ranges from physical interaction to a multitude of ways to communicate via different signals. Cells can affect each other's micro-environment or directly crosstalk. Therefore, it is self-evident that migrating cells will influence each other. Michael Abercrombie has already recognised the crucial role of "social" behaviour in migrating fibroblasts upon contact, in 1954. It is still an ongoing matter of discussion, at which point, migration of multiple cells can be considered "collective cell migration". Peter Friedl and Darren Gilmour define three hallmarks: Firstly, a physical and functional connection throughout migration. Secondly, multi- or supracellular polarity. Finally and as an optional point, a modification of the tissues along the migration path¹⁴⁷. This very restrictive definition would not include cells with a transient connection that can also influence each other's migratory behaviour. Therefore, Roberto Mayor and colleagues introduced a new definition referred in various reviews. According to their view, the defining feature of collective migration is that cells migrate more efficiently in a group than solely and influence each other by interactions with their neighbours^{322,509,510}. Pernille Rørth came to a similar conclusion, as her definition states that cells are collectively migrating if they move together, make contact at least some of the time, and affect each other's behaviour in some way⁴¹⁷. She also addressed the question of why cells should migrate in groups and formulated four reasons. Firstly, they do so if tissues must change position while remaining intact. Secondly, inherently immobile cells can be dragged, employing cell-cell adhesion. Thirdly, cells can coordinate and thereby properly shape tissues. Lastly, some decisions can only be made in a collective as described in the Vicsek-Model⁵²⁸. Force measurements have shown that a migrating sheet exerts more force on the substratum as single cells⁴²². This finding demonstrates a basic feature of all collective processes in which the whole is more than the sum of its parts. Collective cell migration is one of the most essential processes in metazoan development ^{reviewed in 436,544}, cancer motility/metastasis ^{reviewed in 147}, and wound healing ^{reviewed in 458}. In the following section it will be described how cells achieve a sense of direction and are guided as a collective. Further on, it will be clarified how cells migrate collectively in section 1.2.2–1.2.3, by comparing different model systems ranging from development to wound closure and cancer cell motility.

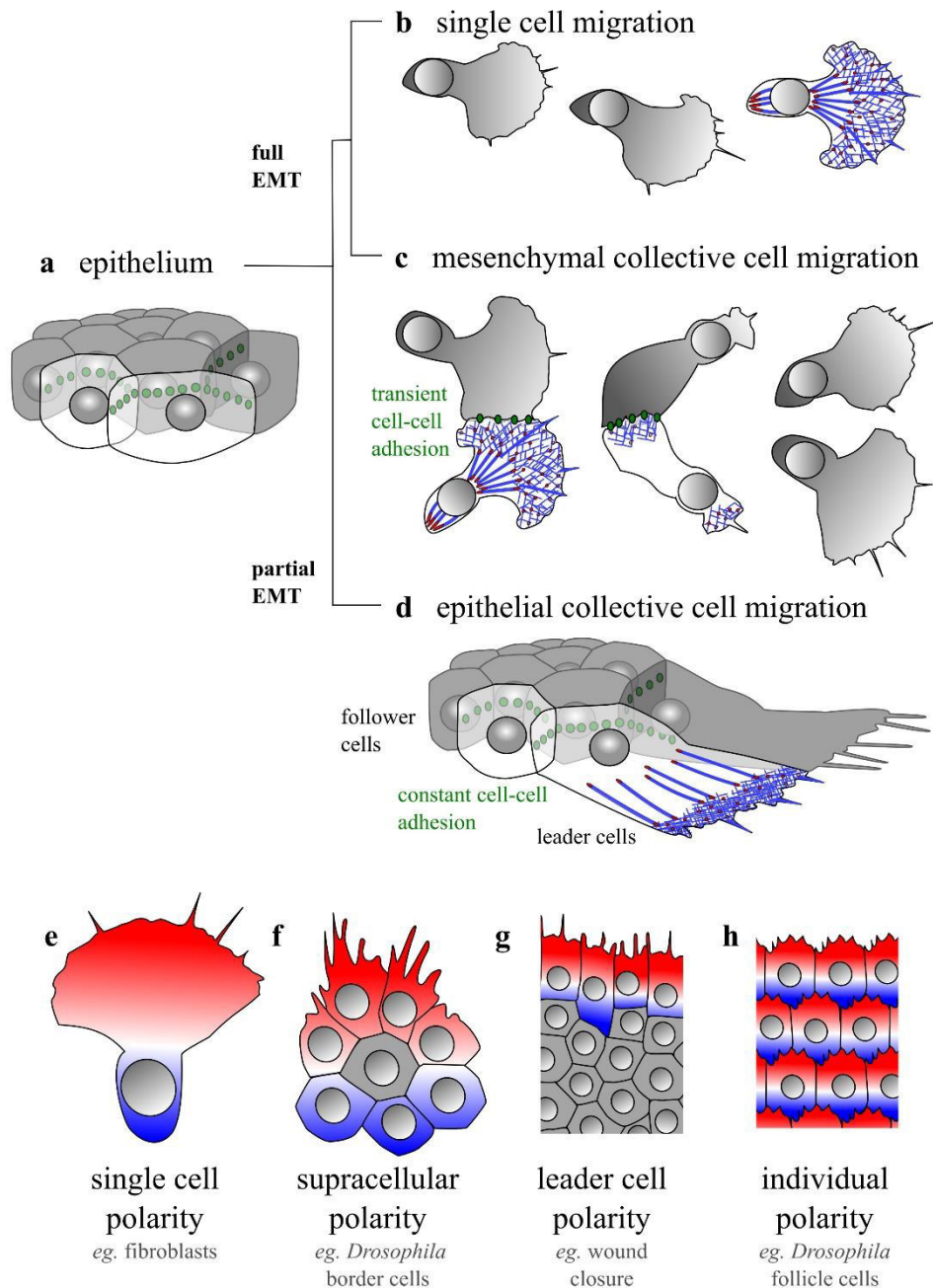
1.2.1 Initiation of collective migration

A wide range of cues is necessary to allow cells to migrate in groups. Signals of different sources such as adjacent tissues, neighbouring cells, or the substrate must be integrated. Usually, the first step is marked by the initiation of a migratory stage¹⁸⁹. To migrate, cells that are organized in epithelia or

endothelia must undergo an epithelial-mesenchymal transition (EMT) in which they lose their planar polarity in favour of a front-rear polarity. This process can be the consequence of changes in ECM stiffness^{543,402,34}. A decision that needs to be made simultaneously is whether cells migrate solely or in a collective. Several mechanisms have been introduced over time. It appears, that in some systems, ECM degradability takes a major role. Less degradable ECM seems to be a potential inductor of collective strand-like migration in cell culture^{reviewed in 518}. It has also been shown that hypoxia can induce collectively migrating clusters in epithelial cancer cells²⁹¹. Very recently, Protein phosphatase 1 (Pp1) was shown to be an activator of collective motility in *Drosophila* border cell migration, by promoting E-Cadherin-based cell-cell adhesion and restricting contractile actomyosin cables to the periphery. Depletion caused cells to dissociate and migrate using different modes of locomotion⁸⁹.

Yamada and Sixt classified migration modes by the “strength” of EMT. A non-migration epithelium (fig. 2 a) can undergo complete EMT, resulting in individually migrating cells (fig. 2 b). It can undergo partial EMT, resulting in migrating mesenchymal cells that are still transiently coupled via cell-cell adhesions (fig. 2 c, see section 1.2.2). Alternatively, it can pass EMT except for some leader-cells, resulting in the dynamics referred to as epithelial migration (fig. 2 d, see: section 1.2.3). EMT induced front-rear polarity is marked by the polarized activation of Rho-GTPases as Rac1, Cdc42, and RhoA and follows in principle the same rules as in single-cell migration³²². There seem to be three major modes of how this is achieved in detail. In less cohesive cells every cell undergoes EMT and has a front-rear polarity which is always reestablished upon contact⁴⁷⁹ (fig. 2 e). There are also some models in which the entire cluster behaves like a single cell as front cells have protrusive dynamics and follower cells are retractive. This phenomenon was termed “supracellular polarity”^{399,460,461} (fig. 2 f). In the classical model, only a part of the cells undergoes EMT and thereby reach a migratory stage (fig. 2 g). These leader cells sense cues and drag epithelial followers using actin cables. In some epithelial sheets, like the *Drosophila* follicular epithelium, every single cell is front-rear-polarized^{319,473} (fig. 2 h).

Figure 2. Modes of collective cell migration (next page). Non-migrating epithelia (A) can adopt different modes of collective motility after EMT. They can become undergo full EMT and become mesenchymal to migrate individually (B). Mesenchymal single cells can still exhibit collective behaviour like CIL (C). They can also undergo partial EMT and migrate as epithelia with (pseudo-)mesenchymal leader cells (D). Migrating cells are polarized through spatially restricted activation of small GTPases. Single migrating cells usually possess a front (red) and a rear (blue). In a supracellular unit, multiple cells are polarized like a single cell (F). “Classical” migrating epithelial sheets possess front-rear polarized leaders. Followers maintain an apico-basal organization (G). In some epithelia, every single cell has a front-rear-polarization. A–D based on⁵⁶⁶, E–H based on⁴⁶⁰.



1.2.2 Collectiveness among individual cells: mesenchymal collective cell migration

Eric Theveneau and Roberto Mayor established a classification of migration modes with a gradient ranging from solely migrating cells to migrating epithelia with constant cell-cell adhesion. Mesenchymal collective cells constitute an intermediate type⁵⁰⁹. This type is characterized by short-lived cell-cell contacts of mostly individually migrating cells accompanied by an exchange of information (fig. 2 c). A common trait of many cell types that migrate as individuals or establish transient cell-cell adhesion is “**contact stimulation of locomotion**” (CIL). This term refers to a process in which two cells upon contact either cease migration or migrate in opposite directions⁴⁷⁹. Originally, it was found and termed by Michael Abercrombie in 1954 using cultured fibroblasts^{1,6}. The first *in vivo* evidence of CIL came from the neural crest cell model in *Xenopus*⁷⁸. Neural crest cells are highly migratory cells that

delaminate from the neural tube during gastrulation while undergoing EMT. They migrate in several distinct streams dorsoventrally to build many tissues during development including smooth muscles, bone, cartilage, neurons, glia, endocrine cells and connective tissue^{265,506,435,317,71,318,336}. Inside a stream individual cell behaviour becomes obvious as cells quickly exchange neighbours²⁶⁵. During their migration, neural crest cells are polarized, building prominent lamellipodia. Before CIL was revealed to play a role, Wnt signalling was found to be important for neural crest migration^{317,71,318}. CIL occurs when cells directly contact while transient N-Cadherin-based adhesions are built⁴³⁵, followed by repolarization of both cells away from the point of contact⁷⁸. The traction force which is built up due to these new lamellipodia provokes divergent migration⁴³⁵. At the contact site, Wnt/PCP signalling activates RhoA, resulting in “rear”-dynamics⁷⁸. N-Cadherin/Par3^{506,336} signalling, on the other hand, inhibits Rac1, ensuring repolarization^{506,435}. In conclusion, repolarization is guaranteed by RhoA activation and Cdc42/Rac1 inhibition at the contact site^{506,36,23,336,114}. Additionally, focal adhesions are disassembled at the point of contact, inhibiting force transmission⁵⁰⁷. Consequently, cells at the edge of the migrating cohort exhibit much more prominent protrusions than cells inside the sheet. On top, CIL serves as a kind of collision control, ensuring through repulsion that a monolayer is built and maintained³²¹. Interestingly, cells exhibiting CIL are more persistent than solely migrating cells, allowing them to migrate in distinct streams. On a larger scale, CIL has a unifying effect on the directionality of cells⁷⁸. To allow that, several mechanics must work in parallel. It has been shown that cells not only exhibit repulsive behaviour upon direct contact. On a larger scale, there is a common attraction, enforcing cohesion⁷⁹. Chemoattraction via CXCL12/SDF-1 ensures that the cluster migrates to its destination^{506,507}. Flanking the migration paths, lateral repulsive cues guarantee movement in a coherent stream without cells expanding left or right^{160,411,574,467,129,246}. Numerous mathematical and computational models exist, describing how CIL and the aforementioned parallel mechanisms affect collective behaviour^{558,74,114,295}. In other model organisms, the basic mechanisms of CIL have also been demonstrated *in vivo*, e.g. in *Drosophila* macrophages⁴⁷⁸ and mouse Cajal-Retzius cells⁵²⁹.

A very specialized type of contact inhibition constitutes the dynamic referred to as “chase and run”. *Xenopus* epithelial placodes, which later give rise to sensory organs, exhibit slow motility. They chemically attract neural crest cells but show CIL-like repulsion, when contacted by them. In this self-perpetuating cycle, neural crest cells “chase” placode cells which in turn gain motility and “run”⁵⁰⁷. Placode cells are not the only type of cohesive cells that undergo CIL. *Danio* prechordal plate cells migrate in an epithelium, interconnected via E-Cadherin. Cells need collectiveness to migrate since transplanted single cells are immotile¹²⁵. The follicle epithelium surrounding the *Drosophila* egg chamber is not a rigid structure but constantly rotates around the inner cells (oocyte, nurse cells). This migration of a planar polarized epithelium seems to be driven by a CIL-like process in which cells inhibit protrusions in their neighbours via semaphoring(Sema-5c)-signalling⁴⁷³. Chick cephalic neural crest behaves very much like *Xenopus* neural crest but cells are interconnected by long filopodia which are thought to exist for long-range communication. It is shown that cell content is shared through these

finger-like protrusions. This causes a CIL response in connected cells much farther apart than in *Xenopus* neural crest cells. As in *Xenopus*, the resulting interconnected network causes cells to polarize toward the free edges.^{262–264,326,503}

1.2.3 Locomotion with constant adhesion: epithelial collective cell migration

The collective migration of epithelial cell sheets is well studied^{150,417,322,509,147,544,149}. Numerous model systems exist in cell culture but also *in vivo* during development. Some of these systems will be elucidated in the following. In epithelial collective migration, only partial EMT in some “steering-” or leader-cells occurs (fig. 2 d). In the “classical” view these leaders pull follower cells due to constant cell-cell adhesion, *e.g.* via Cadherins^{reviewed in 149, 326}. These are cell-surface trans-membrane proteins that enable Ca²⁺-dependant cell-cell adhesion in many different tissues^{reviewed in 456,496,504,183}. Cadherins can cluster to so-called adherens junctions^{reviewed in 198}. In these, the intracellular domains of Cadherin can bind β -catenins, which in turn recruit α -catenins^{reviewed in 571,366}. α -catenins procure actin-binding via recruitment of adaptors like Vinculin⁵⁴⁶. Usually, cadherins only allow homophilic binding. Therefore, mixed cells expressing different Cadherins segregate by their respective Cadherin-types⁴⁹⁷. In vertebrate neurulation, two classical Cadherin types have been described: E-Cadherin and N-Cadherin^{396,497–499}. N-Cadherin is typically expressed in mesenchymal cells, as explained above. The switch from E- to N-cadherin constitutes one of the hallmarks of EMT in many different tissues and in cancer cells^{reviewed in 548}. In the early vertebrate ectoderm, E-cadherin is used to build a continuous epithelial sheet. Presumptive cells of the neural tube undergo a switch to N-Cadherin and thereby segregate³⁹⁶. E-Cadherin as the typical epithelial type, has been shown to play an important role in many kinds of epithelial cell migration, like for example in blood vessel sprouting^{375,9} and in some types of cancer^{297,76}. Cohesion in epithelial sheets can be supported by trans-cellular actin cables linked via cell-cell adhesions⁵³⁰. In extreme examples, follower-cells possess no migratory capacity at all which causes them to completely cease migration if separated from leaders by mechanical perturbation. In these cases, leader-cells migrate alone^{550,298,73}.

A basic principle in cell biology, stated by Abercrombie in 1960 in a publication concerned with the properties of cancer cells, is that epithelia do not accept open edges and react with protrusions⁷. An open edge always gives a sense of directionality without polarizing guidance cues. This principle has been shown several times to be used by epithelial monolayers in **wound scratch assays**^{354,48,390}. During wound closure, cells at the front are motile due to the inherent asymmetry. However, cells inside the layer also contribute to protrusion^{135,137,362,531,390}. Through mechanical coupling, the motion of adjacent cells in epithelia is partially synchronized^{528,531,390}. Interestingly, forces seem not only to be generated in a substratum-dependent fashion but also by cell-cell interaction since it was shown that a retrograde flow of adherens junctions exerts force from cell to cell³⁷². Not only epithelial monolayers but also fibroblasts react to open spaces with polarization in direction of the free edge. Although, after migration starts they turned out to migrate in a completely non-collective fashion³¹⁶. The *Drosophila dorsal*

closure strongly resembles wound closure as observed in scratch assays³¹⁴. Originally, it was thought to be organized by a trans-cellular contractile actin cable in a purse-string-like manner⁵⁷³. By mechanically perturbing this structure, it was shown that closure still works and thus seems to rely on multiple processes^{241,229,218}. Dorsal closure seems to be a combination of actin polymerization-based protrusive and actomyosin contractility-based constrictive processes. These findings demonstrate another basic rule of epithelial monolayers; convex membrane curvature on open epithelia edges causes protrusive dynamics, and concave membrane curvature causes actin-cables (“purse-string”) to close the opening or wound^{398, reviewed in 269}. Most closure processes probably rely on both principles.

***Drosophila* border cell migration** provides an example of invasive collective motility in 3D ^{reviewed in 334}. The border cell cluster consists of two immotile polar cells, that are enwrapped in six to eight motile cells that were recruited from the follicle epithelium. The follicle epithelium surrounds the entire egg-chamber, a structure composed of the oocyte and large nurse cells. The polar cells induce follicle cells to delaminate and undergo EMT, by secreting Unpaired (Upd), a Janus-kinase/Signal transducer and activator of transcription proteins (JAK/STAT)-Ligand that activates the JAK/STAT-pathway in follicle cells^{39,464}. This causes activation of the transcription factor Slow border cells (Slbo) which in turns promotes expression of FAK, the actin bundler *singed* (*sn*), *E-cadherin* and *Drosophila* β -catenin *armadillo* (*arm*)^{335,54,537}. These, and many more downstream factors of Slbo promote follicle cells to surround polar cells, to invade the nurse cells, and subsequently to migrate to the oocyte where it forms the later sperm entry point (micropyle). During migration, there is a constant change in cell position among the motile cells in the cluster^{334,335,391,418,43}. The guidance cue seems to be based on chemoattractants produced by the oocyte and the nurse cells. PDGF- and VEGF-related factor 1 (PVF1) and epidermal growth factor (EGF) seem to have redundant function in the first part of the migration, posteriorly towards the egg^{124,123}. Ectopic expression of the ligands is shown to mislead the cluster^{324,325}. The second part of the migration, dorsally along the oocyte depends on EGFR und Gurken¹²³. During the first part of the migration, the cluster is led by one cell which has more pronounced protrusions than the rest of the cluster. As there is a constant change of position the leader-state fluctuates and cannot be inherent to one specific cell. Its amount of protrusion was shown to be regulated by Rac1 activity downstream of PVR activation. The cell with the highest degree of PVR activation stands out as the cell with most Rac1-GTP activity and thereby builds the longest protrusions, safeguarding directionality. A dominant-negative form of Rac1 or a loss of PVR impairs migration as all cells build protrusions^{347,223,391,535,140,43}. Rac1 was directly shown to be polarized inside the cluster, demonstrating that the border cell can be classified as “supracellular polarized”^{397,67,460,140}. It was shown that photoactivation of Rac1 suffices to redirect migration of the cluster. Photoactivation of a dominant-negative version of Rac1 leads to protrusions in all cells and a loss of leader-follower distinction⁵³⁵. Interestingly, the invasive migration of the border cell cluster does not rely on ECM/Integrin dynamics as there is no matrix between nurse cells. Traction force appears to be generated in a cell-cell dependent manner via E-Cadherin as its depletion perturbs the migration of the entire cluster. Using direct tension

measurements, the role of E-Cadherin in motion could be elucidated in detail^{353,67}. At the same time, E-Cadherin is also needed for the cohesion of the cluster^{299,380}. Cohesions seems to be ensured also via trans-cellular contractile actin-cables at the periphery of the cluster^{204,19}.

A lot of tumour cells, especially of epithelial origin, invade collectively, using multiple modes^{428,148,reviewed in 95}. Examples for such tumours are colorectal carcinomas, melanomas, breast cancer, rhabdomyosarcomas, oral squamous cell carcinomas, fibrosarcomas, and endometrial carcinomas^{349,147,201,146}. Collectively invading cancer cells have been documented in clinical specimens of patients with advanced stages of cancer⁹⁵. They can be also directly observed *in vivo* after implantation, using murine skin-fold chambers¹³. In Madin–Darby canine kidney (MDCK) cells substrate adhesions seems to be restricted to the migration front, revealing a clear leader-role of the first rows of cells⁴²². In different cancer cell types in culture it could be shown that cells in the cluster are interconnected via Cadherins like E-Cadherin to pull follower cells^{540,268,13,24,95}. However, migration in an epithelial-like conformation is not the only mode used by cancer cells. Some types invade in a strand-like fashion with every cell undergoing incomplete EMT^{315,32}. A crucial factor for tumour invasion is the secretion of matrix proteases, typically MMPs^{554,468,348}. In MDCK cells it has been shown that overexpression of MMPs suffices to promote invasive migration into tissue⁴⁶⁸. An exciting finding was that the role of invading leader cells can be taken over by fibroblasts which can mechanically bind and guide tumour cells by building migratory tracks. Fascinatingly, both cell types relied on different Rho-GTPases. Fibroblasts need RhoA for migration whereas cancer cells relied on Cdc42. In both cases, Myosin II seemed to be the downstream effector. Nevertheless, it seems as the cell types rely on different migration mechanics¹⁵⁸.

1.3 The *Drosophila* testis myotube migration system

The common fruit fly, as one of the most versatile model organisms with a toolbox for genetic perturbations and modification, is ideally suited for research on collective motility. Its testes are covered in a multinucleated smooth-like musculature at the imago stage⁴⁸⁸. Testis and muscles originate from spatially distinct anlagen that coalesce during pupal development in an intricate process. The larval testis comprises germ cells and gonadal mesoderm cells. The former arises from pole cells set aside early in development that enter the embryo through the hindgut primordium and are contacted by mesodermal cells which give rise to the gonadal mesoderm⁴³⁰. In larvae and pupae up to 30 h after pupae formation (APF), testes lie spatially separated from other tissues, except for the fat body in the body cavity (fig. 2 a). The genital imaginal disc in larvae builds most somatic parts of the male genitalia including the seminal vesicles, the paragonia, the ejaculatory duct, and the sperm pump (fig. 3 a)^{88,130,94,199}. It is located terminally in larvae and early pupal stages. Prospective testis myoblasts are adhered to it, covering its distal tips (the prospective seminal vesicles, sv, fig. 3 a) in multiple layers (fig. 3 a, in red)^{260,12,130,257}. In pupae 30 h APF, the testes and the prospective seminal vesicles coalesce through an epithelial fusion of

the seminal vesicle epithelium and the testis terminal epithelium (tte, fig. 3 a)^{351,476,477,257}. Shortly before and during this process, the mononucleated myoblasts fuse to multinucleated testes nascent myotubes (myotubes, fig. 3 a,b)^{488,260}. Subsequently, myotubes start to migrate on the testes shortly before and after connection to the genital disc is established (fig. 3 b)^{351,476,477,260,257}. They do not move on its surface but between an outer layer of pigment cells that in turn expands over the seminal vesicles and the cysts which contain the germ cells (fig. 3 b, magnification)²⁵⁷. This finding might speak for a potentially invasive migration mechanism.

There are multiple **related cell migration model systems**. In comparison with what is already known about *Drosophila* myogenesis, the fact that migration occurs in a multinuclear myotube state is atypical. During embryonal myogenesis and flight muscle development it is always mononuclear myoblasts, more precisely fusion competent myoblasts (FCM) in embryogenesis and dorsal longitudinal muscle (DLM) myoblasts during flight muscle formation, that possess the ability for locomotion ^{reviewed in 195,184}. FCMs migrate in a Rac1, Rac2, and WAVE dependent manner¹⁷². Not much is known about the regulation except that Dumbfounded (Duf), expressed in founder cells, seems to be an attractive cue⁴²⁴. DLM myoblasts migrate on nerve cells^{138,139}, using filopodial protrusions^{116,453,173}. There is nothing known about FCMs and DLM using collective migration. When compared to male genital myogenesis both processes would be analogous to the migration of myotubes onto the genital disc prior to the migration steps described here. Migration-like processes involving multinuclear myotubes in *Drosophila* are only known for myofiber guidance to the attachment sites subsequent to fusion ^{445,reviewed in 184}. In a complex process, comprising multiple phases, embryonal myotubes elongate on two opposite ends, in a more or less oblique fashion roughly extending in dorsal and ventral direction, depending on their exact position in the segment. During this process, filopodial protrusions at the two opposite leading edges seem to generate the necessary force. This highly coordinated process is guided by numerous factors acting as guidance cues including Derailed (Drl), Slit, and Kon-Tiki (Kon)^{445,446}. Recently, FGF-signalling via the ligands Thisbe (Ths)/Pyramus (Pyr), binding to the FGFR heartless (Htl), was introduced to support myotube guidance by regulating Rac1 activity and thereby promoting lamellipodial dynamics⁵⁶⁸.

During vertebrate muscle repair and myogenesis, satellite cell migration, which normally starts at the niche and ends at the site of muscle trauma, is a well-studied phenomenon due to numerous cell-culture approaches^{reviewed in 175}. It is a chemically stimulated lamellipodia-based single-cell migration, sharing more traits with fibroblast motility than with testis myoblast migration. Testis myotubes seem to resemble vertebrate smooth muscles which might justify a comparison. Yet, it must be noted that *Drosophila* contains no smooth muscle actin as all fly actin orthologs cluster with vertebrate cytoplasmic actins²³⁰. Smooth muscle cells line the vascular, digestive, urinary, and reproductive system as a contractile layer and have to migrate during development and repair¹¹. Vascular smooth muscle migration also seems to use “canonical” fibroblast dynamics and chemoattraction via multiple pathways^{reviewed in 11,301}. In culture it was shown that vascular smooth muscle cells undergo invasive migration, using the same principles already shown for other 3D-migrating cells^{reviewed in 301}. Interestingly, smooth muscle cell migration in cell culture wound scratch assays can be perturbed by a loss of N-Cad which may indicate a collective dynamic³⁰².

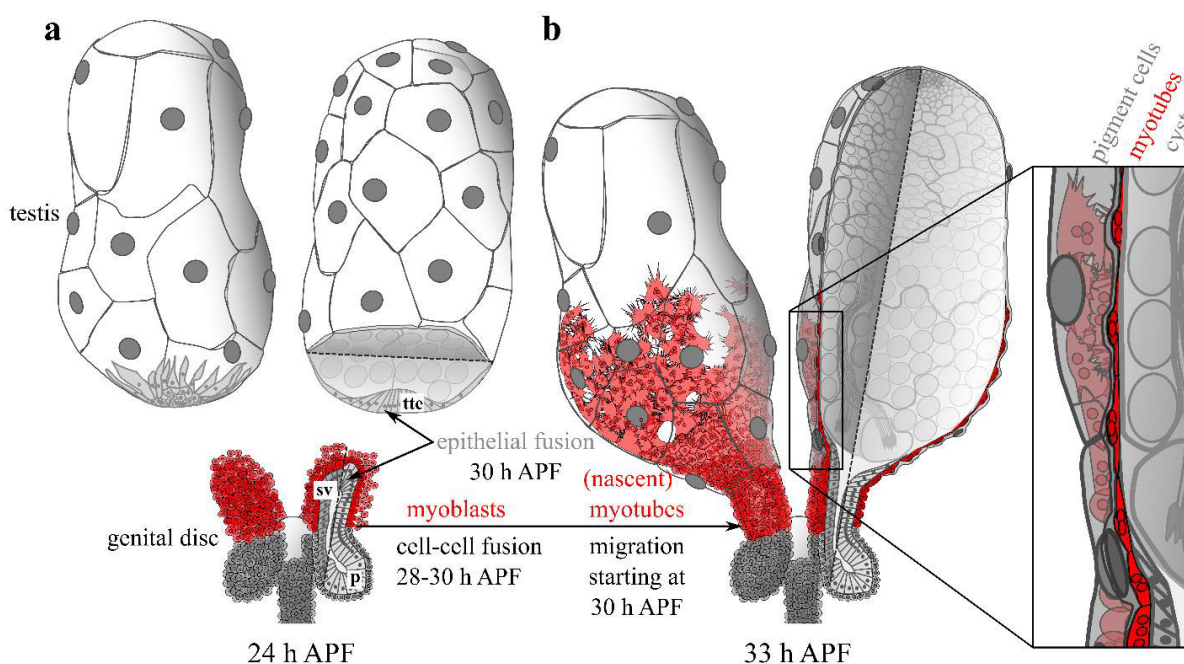


Figure 3. Testis nascent myotube migration. 24 h APF testes and genital disc lie spatially distinct (a). At 28–30 h APF, myoblasts (red) fuse to nascent multinuclear myotubes. At 30 h APF the testis terminal epithelium (tte) and the seminal vesicle (sv) epithelium fuse to a continuous tube. Subsequently, migration starts. At 30 h APF migration is in the process (b). Migrating myotubes move in the narrow space between pigment cells and the cyst (magnification). p = prospective paragonia. Modified from pub. 2

1.4 Aim of the work

The objective of the present work is to gain insights into collective dynamics in development and to find key mechanisms that could potentially also be used by cancer cells or in tissue repair. To accomplish this, *Drosophila* testis explants should be established as a new live-cell imaging model for collective cell migration. This model may combine the advantages of mechanical, genetic, and pharmacological perturbation with high visual resolution. Testis myotube migration has the potential to be a valuable tool as the entire germ cell-containing portion is enclosed by pigment cells and thereby a self-contained system like the egg chamber in the border cell migration model. To achieve similar usability, exact conditions for live-cell imaging must be determined and genetic driver tools that allow for tissue- and time-specific expression of target genes must be identified.

Using these tools, potential actin regulators promoting myotube migration ought to be found. Preliminary studies suggest that migration of testis myotubes is mostly Arp 2/3 independent¹⁵². This could indicate that myotubes use atypical locomotion mechanisms. Cancerous and other versatile cells, important in immune response and tissue repair, can deploy numerous migration modes as an answer to their environment. Therefore, the discovery of new types of motility is vital and bears the potential to find new implements in the toolbox of migratory cells. An important factor could be that myotubes migrate in a thin gap beneath the pigment cells. Therefore, migration seems neither 2D, nor truly 3D but rather an intermediate form. The aim is to find which adaptations in migratory mechanisms permit locomotion under such circumstances. These cannot be simulated in cell culture. Therefore, the testis myotube migration system may create opportunities for novel approaches.

Early experiments have shown that migration of testicular nascent myotubes appears to be in close contact with neighbours. Therefore, complex collective dynamics seem likely. The question arises, which mechanisms steer the potentially collective motility of testis myotubes. It could be extrinsic factors, as chemoattractants or intrinsic factors, allowing self-regulation. In this regard, the role of cell-cell contacts in collective dynamics must be addressed. The aim is to find how they contribute to cohesion, directionality, and collective cell behaviour.

2. Material and Methods

In this section, only additional materials and methods, regarding experiments that were not part of the publications and manuscripts in this work, are listed. For all further materials and methods: See section 3.

2.1 Fly genetics

Fly genetics were employed according to the methods described elsewhere²¹. RNAi based experiments were carried out at 25 °C.

2.1.1 List of mutant fly stocks

Lists of the used mutant lines are attached (section 7.5).

2.1.2 List of transgenic fluorescence reporter fly stocks

designation	chromosome	fly stock ID/source
<i>UAS-mCD8-EGFP</i>	II	BL-32186
<i>UAS-mCD8-EGFP</i>	III	BL-32185
<i>vkg-EGFP (vkg^{G205})</i>	II	337

2.1.3 List of transgenic Gal4 and UAS fly stocks

Lists of the used Gal4 driver stocks and UAS stocks (except for fluorescence reporter lines, see section 2.1.2) are attached (sections 7.3 and 7.4).

2.1.4 Characterization of Gal4 driver stocks

To find new putative driver tools deployable in testis myoblast research *Janelia FlyProject*^{231,377} was searched. *Janelia FlyProject* provides expression data in the larval genital disc²³⁴. Candidates with a promising pattern were ordered and tested by crossing them with *UAS-mCD8-EGFP* (BL-32186). A list of characterized driver lines is attached in section 7.3.

2.1.5 Gal4/UAS based screen for adult testis phenotypes

It could be shown that missing myotube coverage of the adult testis is accompanied by testis shaping defects that are visible in low magnification light microscopy⁴¹⁹. Based on that a fast screening method was established. Gal4 driver virgins are crossed with UAS constructs (*e.g.* RNAi)⁵⁷ and kept on 25 °C. 1–3 days old male offspring are dissected using surgical forceps under a dissecting microscope (*Leica Stemi 508*). Testes are analysed regarding their shape. A club-like shape with a dilated hub region is defined as “*medium migration defect*”. A slightly dilated hub region is defined as a “*weak migration defect*”. If more than 50% of the testis volume is dilated phenotypes are considered “*strong migration defects*” (*cf.* pub.2 Fig S1a). A list of all lines tested is attached. (section 7.4)

2.2 Microscopic image processing

Microscopy is carried out as described in the enclosed publications (pub. 1, pub. 2). In addition, image stitching is employed on *Zeiss* Apotome-fluorescence micrographs to allow for high-resolution images covering the entire testis. Multiple images of a structure are stitched using the Fiji-Plugin *Grid/Collection stitching*³⁹³.

2.3 Quantification Methods

2.3.1 Indirect measurement of cell cohesion using *beatVC* Gal4 mosaic expression

beatVC Gal4 is used to drive expression of *UAS-mCD8-EGFP* and a respective UAS construct. Male prepupae are collected from the offspring and timed 48 h APF. Testes are prepared as described previously⁴¹⁹. Phalloidin Atto-565 (*Sigma Aldrich*) is used to mark F-actin. Images are taken and stitched as explained in section 2.2. The Fiji tool *segmented line* is used to measure the migration distance of GFP positive cells. With the same tool, the total migration distance is measured 10 times by measuring and averaging the distance between the testis basis and the farthest point where myotubes could be detected. Excel is used to quantify the output. Boxplots and statistical testing are performed as described in pub 2.

2.4 Molecular Biology

2.4.1 List of Plasmids

designation	source	comment
pENTR/D-Topo	Invitrogen	gateway compatible entry vector.
pUASTattb-rfa-GFP	Raiko Stephan, 2008 Dissertation	gateway compatible destination vector with a GFP tag and an <i>attB</i> site for <i>Drosophila</i> germline transformation via the phiC31 integrase vector system.
pUASTattb-GFP-rfa	Raiko Stephan, 2008 Dissertation	gateway compatible destination vector with a GFP tag and an <i>attB</i> site for <i>Drosophila</i> germline transformation via the phiC31 integrase vector system.
pOT2 LD47929	DGRC	Sra1 cDNA clone. Template for generation of pUAS _t -Sra1.Asite-eGFP, pUAS _t -Sra1-eGFP.Asite pUAS _t -Sra1.Dsite-eGFP pUAS _t -Sra1-eGFP.Dsite
pFLC-I RE12101	DGRC	WASp cDNA clone. Template for generation of pUAS _t -WASp.Crib-eGFP pUAS _t -Crib.WASp-Asite
pUASTattb-whamy long-GFP	Brinkmann et al., 2016 ⁶⁰	long form of <i>whamy</i> cloned in pUASTattb-rfa-GFP ⁶⁰ . Template for generation of pUAS _t -Whamy.Crib-eGFP pUAS _t -Crib.Whamy -Asite

2.4.3 PCR

(Saiki et al., 1985, Mullis & Faloona 1987)^{429,345}

(Q5 High-Fidelity DNA Polymerase (*M0591*), NEB)

Components used in a PCR reaction (25 µl):

component	volume/amount	final concentration
Plasmid DNA	1 µl/1 ng	0.04 ng/µl
forward primer	1.25 µl	0.5 µM
reverse primer	1.25 µl	0.5 µM
dNTP's	0.5 µl	200 µM
5xQ5 Buffer	5 µl	1x
Q5 polymerase	0.25 µl	0.5 U
ddH₂O	15.75 µl	

Thermocycling conditions used:

duration	temperature	step	
30 sec	98 °C	initial denaturation	
10 sec	98 °C	denaturation	35 cycles
30 sec	70 °C	primer annealing	
7-42 sec (30 sec/kb)	72 °C	elongation	
2 min	72 °C	final elongation	
	4 °C	cooling	

2.4.4 DNA gel electrophoresis

(5x DNA Loading Buffer, Blue (*Bioline*), GelRed (*Biotium*), HyperLadder 1KB: (*Bioline*))

TAE buffer (50x): 2 M Tris, 5.7% (v/v) acetic acid, 50 mM EDTA in ddH₂O (pH 8.5).

Gels for preparative and analytic applications are produced by solving 1% (w/v) agarose in TAE buffer (1x). 0.005 % (v/v) *GelRed* is added after the mix cooled down below 60 °C. The gel polymerizes in a gel tray (Compact XS/S, *Biometra*). Gels are run in TAE in a standard gel chamber (Compact XS/S, *Biometra*). PCR-product or plasmids are mixed with loading dye and ddH₂O. *HyperLadder 1KB* is used as a molecular weight size marker (“DNA-Ladder”). Horizontal agarose electrophoresis is performed at 100 V. Bands are analysed or extracted using a standard gel documentation system (*MWG Biotech*).

2.4.5 DNA restriction with restriction endonucleases

(EcoRV HF (*NEB*, 20,000 U/ml), NotI HF (*NEB*, 20,000 U/ml), CutSmart (*NEB*))

DNA concentration is measured using a microvolume spectrophotometer (NanoDrop, *ThermoFisher*). For each reaction, 0.5 µg DNA, 2.5 µl CutSmart buffer and 0.25 µl (5 U, 10fold “overdigestion” as recommended by *NEB*) enzyme are mixed. Water is added to a total volume of 25 µl. The reaction mix is incubated for 30 min at 37 °C. For analytic DNA gel electrophoresis, the restriction mix is mixed with loading buffer without further dilution in water.

2.4.6 Directional cloning using the pENTR TOPO System

(pENTR/D-TOPO Cloning Kit (*ThermoFischer*))

Primers are designed to include a CACC-sequence on the 5' end of the forward primer. They are designed in a way that the domain of interest is fused with the GFP-Tag in frame. The domain of interest is amplified using the standard-PCR procedure (section 3.4.3). DNA concentration is measured using a microvolume spectrophotometer (NanoDrop, *ThermoFischer*). The cloning reaction was set according to the manufacturer's instructions without any alterations and transformed into chemically competent *E. coli* (section 3.4.8, 3.4.9)

2.4.7 Subcloning using the Gateway technology

(Clonase Gateway LR Clonase II enzyme-mix (*ThermoFischer*))

Constructs are cloned into the Gateway System compatible vectors pUAST-attb-rfa-EGFP or pUAST-attb-EGFP-rfa. The cloning reaction is set according to the manufacturer's instructions and transformed into chemically competent *E. coli*.

2.4.8 Generation of chemically competent *E. coli*

(Mandel & Higa 1970)³¹¹

(*E. coli* (DH10B))

LB medium⁴²: 1% (g/v) bacto tryptone, 0.5% (g/v) yeast extract, 85.5 mM NaCl in ddH₂O (pH 7.0).

50 mM CaCl₂ in H₂O: 7.85 g CaCl₂ · 2H₂O in 1 l ddH₂O.

50 mM CaCl₂ in glycerol: 7.85 g CaCl₂ · 2H₂O in 70 ml ddH₂O and 30 ml 50% (v/v) glycerol.

E. coli are incubated in LB medium overnight at 37 °C and 200 rpm. The medium is diluted 1/80 in LB medium and incubated at 37 °C/200 rpm until OD₆₀₀=0.3. The medium is centrifuged at 4 °C/4000 rpm for 10 min. The supernatant is discarded. The pellet gets dissolved in 50 ml 50 mM CaCl₂ (in H₂O, ice-cold). The mix is centrifuged at 4 °C/4000 rpm for 10 min. The supernatant is discarded. The pellet gets dissolved in 50 ml 50 mM CaCl₂ (in H₂O, ice-cold) and is incubated on ice for 2.5 h. The mix is centrifuged at 4 °C/3000 rpm for 8 min. The supernatant is discarded. The pellet gets dissolved in 15 ml 50 mM CaCl₂ (in glycerol, ice-cold). Bacteria are stored in aliquots of 100 µl at -80 °C.

2.4.9 Transformation of *E. coli*

(Maniatis *et al.*, 1985)³¹²

SOB medium¹⁹²: 2% (w/v) bacto tryptone, 0.5% (w/v) yeast extract, 10 mM NaCl, 2.5 mM KCl, 10 mM MgCl₂ und 10 mM MgSO₄ in ddH₂O (pH 7.0).

SOC medium¹⁹²: SOB medium (autoclaved) and 20 mM glucose in ddH₂O.

LB_{amp} selective plate: LB medium with 100 µg/ml ampicillin, 1.5% (w/v) agar (high purity).

LB_{kana} selective plate: LB medium with 100 µg/ml kanamycin A, 1.5% (w/v) agar (high purity).

2 µl of the cloning reaction mix is added to chemically competent *E. coli* (section 2.4.8). They are incubated on ice for 30 min. Cells are heat shocked for 40 sec at 42 °C. Subsequently, they are transferred on ice. 250 µl of SOC is added. Tubes are incubated for an hour at 37 °C/500 rpm. 100 µl are spread on selective plates containing either kanamycin A or ampicillin.

2.4.10 Purification of plasmids from transformed bacteria (Mini, Midi)

(E.Z.N.A. Plasmid DNA Mini Kit I (*omega*), Plasmid Plus Midi Kit (*Qiagen*))

Transformed *E. coli* are amplified in liquid culture overnight. Clones are picked from selective plates, using a pipette tip and transferred in LB medium containing 100 µg/ml of the respective antibiotic. They are incubated at 37 °C with shaking. 3 µl of liquid culture is incubated for Mini-preparation and 250 µl in the case of Midi-preparation. The steps of purification over columns, using a vacuum pump, were carried out according to the manufacturer's instructions.

2.4.11 RNA isolation

(RNeasy Mini Kit (*Qiagen*))

All steps are performed, using RNase-free material. 5×10^6 S2R+ cells⁴⁴⁴ are centrifuged for 5 min at 300 G. The pellet is dissolved in 350 µl RLT-Buffer (containing 10 µl/ml β-mercaptoethanol) by inverting the reaction tube. The lysate is centrifuged 3 min at 13,000 rpm. The supernatant is transferred in a new reaction tube and mixed with 350 µl 70 % (v/v) ethanol and transferred onto an RNeasy spin column. The column is centrifuged for 15 sec at 8000 rpm, the flow-through is discarded. 500 µl Buffer RW1 is added. The column is centrifuged for 15 sec at 8000 rpm, the flow-through is discarded. 500 µl Buffer RPE is added. The column is centrifuged for 15 sec at 8000 rpm, the flow-through is discarded. To dry

it, the column is transferred to a new collection tube and centrifuged for 1 min at 13,000 rpm. The collection tube is replaced by a reaction tube and 30 μ l. RNase-free water is added. The column is centrifuged for one min at 8000 rpm. RNA concentration is measured using a microvolume spectrophotometer (NanoDrop, *ThermoFisher*). The product is stored at -20 °C.

2.4.12 cDNA synthesis

(SensiFAST cDNA Synthesis Kit (*Bioline*))

All steps are performed, using RNase-free material. 1 μ g RNA, 4 μ l (5x) TransAmp Buffer (includes oligo dT primers and random hexamer primers), 1 μ l (=1 U) Reverse Transcriptase are mixed in RNase free water to a final volume of 20 μ l. They are mixed gently by pipetting. The following program is used in a thermal cycler.

duration	temperature	step
10 min	25 °C	primer annealing
15 min	42 °C	reverse transcription
5 min	85 °C	inactivation
	4 °C	cooling

cDNA concentration is measured using a microvolume spectrophotometer (NanoDrop, *ThermoFisher*). The reaction product is stored at -20 °C.

2.4.13 DNA sequencing

All sequencing was performed by *Microsynth Seqlab GmbH*. Samples were prepared according to their instructions.

2.4.14 Transgenesis of *Drosophila melanogaster* based on the PhiC31 system

(Bateman et. al., 2006, Bischof et. al., 2007, Groth et. al., 2004, Horn et. al., 2005, Oberstein et. al., 2005, Thorpe et. al., 2000, Venken et. al., 2006)^{35,513,181,358,44,212,525}

Injection and PhiC31 Integrase-mediated transgenesis were performed by BestGene Inc. They make use of the FlyC31 system. The service type “H” was chosen. Samples were prepared according to their instructions.

2.4.15 List of synthetic oligonucleotides (primer)

designation	sequence	annealing temperature
EGFP_WhamyCrib_F	CACCTACACATACGCCTACATCTCCG	70 °C
EGFP_WhamyCrib_R	TTATGGCTGCGCCTGAAGATCACTTTTTGG	70 °C
WhamyCrib_EGFP_F	CACCATGGAGGATTACACATACGCCT	70 °C
WhamyCrib_EGFP_R	CTGAAGATCACTTTTTGGTGCCAT	70 °C
WASpCrib_EGFP_F	CACCATGAAGAAGCGCAAGGTGACCAAGG	70 °C
WASpCrib_EGFP_R	CGAAGCCAGGACATTGTTGCTCT	70 °C
EGFP_WASpCrib_F	CACCGACAAGAAGCGCAAGGTGACCAAGG	70 °C
EGFP_WASpCrib_R	CTAAGCCAGGACATTGTTGCTCTGTATGAAGTCGTAG	70 °C
Sra1Dsite_EGFP_F	CACCATGCTGATCCAGGGCTCGCTGCT	70 °C
Sra1Dsite_EGFP_R	TAGCTCTGTCTTCGCGTCCGGA	70 °C
EGFP_Sra1Dsite_F	CACCCCACTGATCCAGGGCTCGCTG	70 °C
EGFP_Sra1Dsite_R	TCACTCTGTCTTCGCGTCCGGATATTGCACGAT	70 °C
Sra1Asite_EGFP_F	CACCATGGGCAAGTTTATCAACATGTTTGCCGTGCT	70 °C
Sra1Asite_EGFP_R	CTTGCACTCCTCGTTGTGCTGATG	70 °C
EGFP_Sra1Asite_F	CACCCTAGGCAAGTTTATCAACATGTTTGCCGTGC	70 °C
EGFP_Sra1Asite_R	CAGCTACTTGCACTCCTCGTTGTGCTGATGC	70 °C
MbtCrib_EGFP_F	CACCATGTTCTCGAAGAAGAAAAGAAACCGCTGATC	70 °C
MbtCrib_EGFP_R	CTTCAGATCGAGAATCTCGGTGGG	70 °C
EGFP_MbtCrib_F	CACCATGTTCTCGAAGAAGAAAAGAAACCGCTGATCTC	70 °C
EGFP_MbtCrib_R	CTACAGATCGAGAATCTCGGTGGGCGTAATCTC	70 °C

2.4.16 List of newly created vectors

designation	size
pENTR/D-TOPO-Whamy.Crib-EGFP	3273 BP
pENTR/D-TOPO-EGFP-Whamy.Crib	3276 BP
pENTR/D-TOPO-WASp.Crib-EGFP	2811 BP
pENTR/D-TOPO-EGFP-WASp.Crib	2811 BP
pENTR/D-TOPO-Sra1.Asite-EGFP	4035 BP
pENTR/D-TOPO-EGFP-Sra1.Asite	4041 BP
pENTR/D-TOPO-Sra1.Dsite-EGFP	2745 BP
pENTR/D-TOPO-EGFP-Sra1.Dsite	2745 BP
pENTR/D-TOPO-Mbt.Crib-EGFP	2799 BP
pENTR/D-TOPO-EGFP- Mbt.Crib	2799 BP
pUAST attB-Whamy.Crib-EGFP	10.017 BP
pUAST attB-EGFP-Whamy.Crib	10020 BP
pUAST attB-WASp.Crib-EGFP	9555 BP
pUAST attB-EGFP-WASp.Crib	9555 BP
pUAST attB-Sra1.Asite-EGFP	10779 BP
pUAST attB-EGFP-Sra1.Asite	10785 BP
pUAST attB-Sra1.Dsite-EGFP	9489 BP
pUAST attB-EGFP-Sra1.Dsite	9489 BP
pUAST attB-Mbt.Crib-EGFP	9543 BP
pUAST attB-EGFP- Mbt.Crib	9543 BP

2.4.17 List of newly created GTPase sensor fly stocks

genotype	chromosome	injection stock
<i>w, y;; w^{mini}, UAS^t-Whamy.Crib-EGFP</i>	III	ZH-86Fb (BL- 24749)
<i>w, y;; w^{mini}, UAS^t-WASp.Crib-EGFP</i>	III	ZH-86Fb (BL- 24749)
<i>w, y;; w^{mini}, UAS^t-Sra1.Asite-EGFP</i>	III	ZH-86Fb (BL- 24749)
<i>w, y;; w^{mini}, UAS^t-Sra1.Dsite-EGFP</i>	III	ZH-86Fb (BL- 24749)
<i>w, y;; w^{mini}, UAS^t-mbt.Crib-EGFP</i>	III	ZH-86Fb (BL- 24749)

3. Publications

3.1 Publication 1

Biology Open 2017, **6** (12): 1876–1888.

Myotube migration to cover and shape the testis of *Drosophila* depends on Heartless, Cadherin/Catenin, and myosin II

Silke Rothenbusch-Fender, Katharina Fritzen, **Maik C. Bischoff**, Detlev Buttgereit, Susanne F. Oenel, and Renate Renkawitz-Pohl

RESEARCH ARTICLE

Myotube migration to cover and shape the testis of *Drosophila* depends on Heartless, Cadherin/Catenin, and myosin II

Silke Rothenbusch-Fender^{1,2}, Katharina Fritzen¹, Maik C. Bischoff^{1,2}, Detlev Buttgereit¹, Susanne F. Oenel^{1,2,*} and Renate Renkawitz-Pohl^{1,2,‡}

ABSTRACT

During *Drosophila* metamorphosis, nascent testis myotubes migrate from the prospective seminal vesicle of the genital disc onto pupal testes and then further to cover the testes with multinucleated smooth-like muscles. Here we show that DWnt2 is likely required for determination of testis-relevant myoblasts on the genital disc. Knock down of fibroblast growth factor receptor (FGFR) *heartless* by RNAi and a dominant-negative version revealed multiple functions of Heartless, namely regulation of the amount of myoblasts on the genital disc, connection of seminal vesicles and testes, and migration of muscles along the testes. Live imaging indicated that the downstream effector Stumps is required for migration of testis myotubes on the testis towards the apical tip. After myoblast fusion, myosin II is needed for migration of nascent testis myotubes, in which Thisbe-dependent fibroblast growth factor (FGF) signaling is activated. Cadherin-N is essential for connecting these single myofibers and for creating a firm testis muscle sheath that shapes and stabilizes the testis tubule. Based on these results, we propose a model for the migration of testis myotubes in which nascent testis myotubes migrate as a collective onto and along the testis, dependent on FGF-regulated expression of myosin II.

KEY WORDS: DWnt2, Thisbe, Stumps, FGF, Testes tubules, Muscles

INTRODUCTION

Cell migration is essential for many developmental and physiological processes throughout the animal kingdom, and is also implicated in diseases, e.g. cancer metastasis (Roca-Cusachs et al., 2013). In *Drosophila*, various single as well as collective cell migration processes have been described, such as border cell migration in the ovary and embryonal mesoderm migration (Pocha and Montell, 2014).

In the current study, we focus on the migration of muscle cells during the development of the male reproductive tract of *Drosophila*. The five different organs of the inner male reproductive system of *Drosophila* develop from two different tissues. The testes are of

gonadal origin located in segment A5, whereas the somatic parts arise from a single genital imaginal disc (hereafter called genital disc) in segments A8/A9/A10 (Estrada et al., 2003; Greig and Akam, 1995; Stern, 1941). During metamorphosis, the genital disc and pupal testes grow towards each other, and the developing seminal vesicles fuse with the terminal epithelium of the testes (Kozopas et al., 1998; Nanda et al., 2009; Stern, 1941). Nascent myotubes migrate over the developing seminal vesicles onto the pupal testes and build the muscle sheath surrounding the adult testis (Kozopas et al., 1998; Kuckwa et al., 2016). This musculature is composed of multinucleated, smooth-like myofibers (Susic-Jung et al., 2012).

Myoblasts of the genital disc build muscle sheaths for all parts of the male reproductive system (Susic-Jung et al., 2012). The myoblasts that form the testis muscle sheath originate from a common pool and accumulate during the first day of metamorphosis on the prospective seminal vesicles of the genital disc (Fig. 1A). Founder-cell-like (FC-like) myoblasts and fusion-competent-myoblast-like (FCM-like) cells start to fuse around 28 h after puparium formation (APF) to build multinucleated myotubes (Kuckwa et al., 2016). Around 30 h APF, the multinucleated nascent myotubes begin to migrate from the genital disc towards the testis, contact the gonad at the distal end, and migrate further to cover the entire testis (Fig. 1A') (Kozopas et al., 1998; Kuckwa et al., 2016). Migration of testis myotubes is independent of successful fusion of testis-relevant myoblasts (Kuckwa et al., 2016). Early evidence indicated that this migration process might be dependent on the presence of the Wnt ligand DWnt2 in addition to, or as a consequence of, the failure of pigment cell migration, since in DWnt2 mutant males smooth-like muscles do not accumulate on the testis (Kozopas et al., 1998).

Another relevant pathway for the development of the male reproductive organs of *Drosophila* is fibroblast growth factor (FGF) signaling. The FGF receptor (FGFR) Breathless (Btl) and its ligand Branchless recruit larval mesodermal cells, which become epithelial and give rise to paragonia and seminal vesicles (Ahmad and Baker, 2002). Btl is also essential for cell migration during embryonal tracheal development (Glazer and Shilo, 1991) and for directed cell migration of midline glial cells (Klämbt et al., 1992). The second FGFR in *Drosophila*, Heartless (Htl), becomes activated by its ligands Thisbe (Ths) and Pyramus (Pyr) (Gryzik and Müller, 2004; Stathopoulos et al., 2004) and is implicated in various migration processes. Htl is expressed in the mesoderm during gastrulation (Shishido et al., 1993), where it is necessary for the epithelial-mesenchymal transition, i.e. the dorsolateral migration of individual mesodermal cells along the ectoderm (Gisselbrecht et al., 1996). Htl is also needed during ovarian muscle tissue development (Irizarry and Stathopoulos, 2015). Htl-dependent FGF signaling also guides the migration of founder cells of the longitudinal midgut muscles during *Drosophila* embryogenesis (Kadam et al., 2012; Reim et al., 2012). During migration, these longitudinal founder cells fuse with

¹Philipps-Universität Marburg, Fachbereich Biologie, Entwicklungsbiologie, Karl-von-Frisch Straße 8, 35043 Marburg, Germany. ²DFG Research Training Group, Membrane Plasticity in Tissue Development and Remodeling, GRK 2213, Philipps-Universität Marburg, 35043 Marburg, Germany.

*Present address: Philipps-Universität Marburg, Fachbereich Medizin, Institut für Physiologie und Pathophysiologie, Molekulare Zellphysiologie, Emil-Mannkopf-Str. 2, 35032 Marburg, Germany.

‡Author for correspondence (renkawit@biologie.uni-marburg.de)

 R.R.-P., 0000-0002-4695-0824

This is an Open Access article distributed under the terms of the Creative Commons Attribution License (<http://creativecommons.org/licenses/by/3.0>), which permits unrestricted use, distribution and reproduction in any medium provided that the original work is properly attributed.

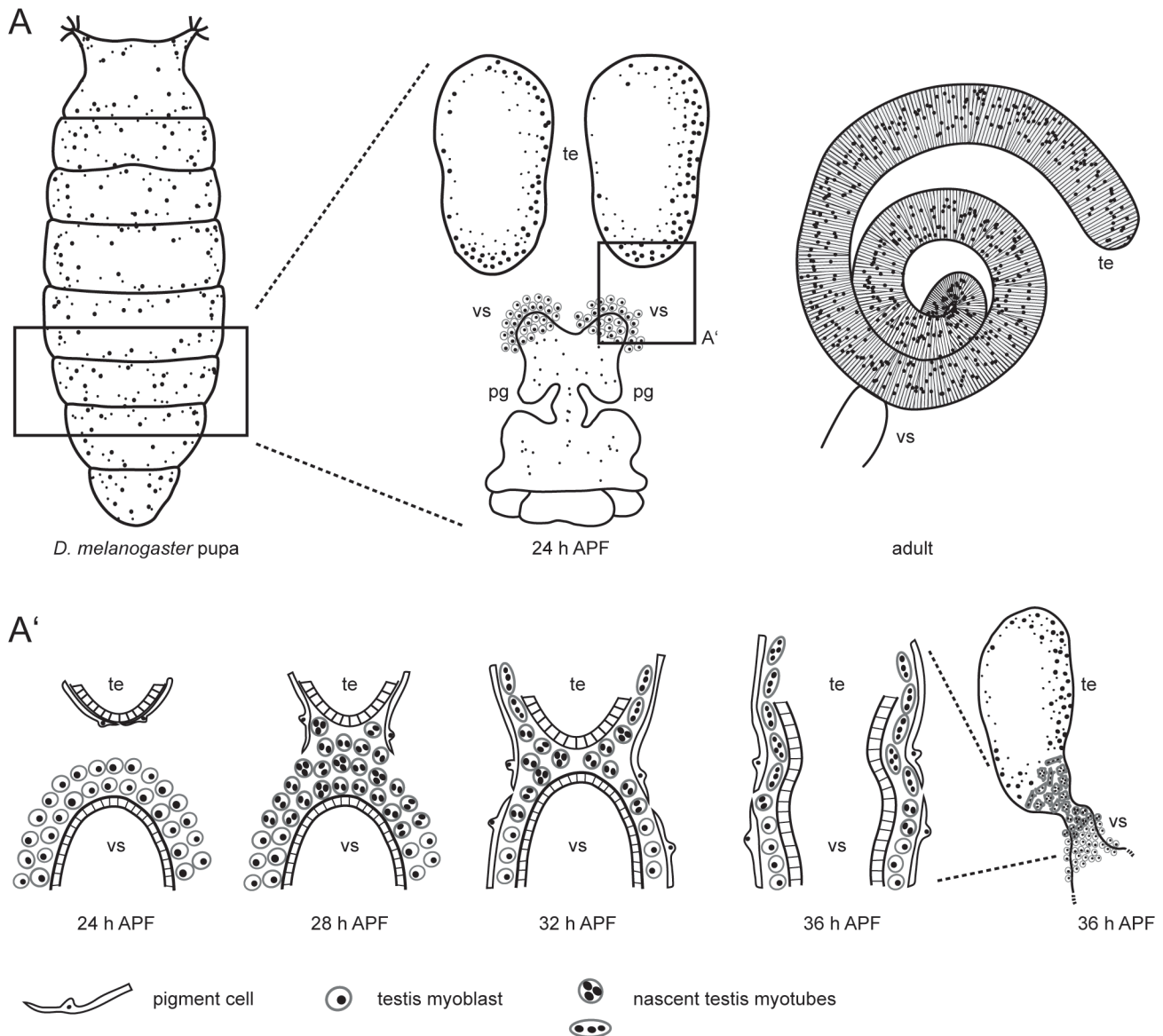


Fig. 1. Scheme of *Drosophila* testis myotube migration. (A) The male reproductive tract develops during metamorphosis. At 24 h APF, the single genital disc and paired testes (te) are separate organs. The seminal vesicles (vs) and the paragonia (pg) already start to grow. In the adult, the tubular testis is connected to the seminal vesicle. (A') During metamorphosis, the prospective seminal vesicles and testes grow towards each other and fuse. On genital discs 24 h APF, testis-relevant myoblasts accumulate on the prospective seminal vesicle. Pigment cells cover the pupal testis. At 28 h APF, myoblasts fuse to build multinucleated testis myotubes. These nascent testis myotubes migrate beneath the pigment cells onto the pupal testis, while pigment cells migrate from the testis onto the developing seminal vesicle. By 36 h APF, the epithelia of seminal vesicles and the terminal epithelium of the testes have fused. Modified after Bodenstein (1950), Kozopas et al. (1998), Kuckwa et al. (2016).

fusion-competent myoblasts to build syncytia. Rudolf et al. (2014) have shown that this migration and fusion process is dependent on cytoskeletal rearrangements, particularly Arp2/3-induced actin polymerization. The function of cytoskeleton components and their regulators is also implicated in other cell migration processes. In vertebrate cells, Arp2/3 is needed for actin nucleation in lamellipodia-dependent cell migration (Campellone and Welch, 2010), while non-muscle myosin II plays a fundamental role in promoting directional cell migration (Vicente-Manzanares et al., 2009).

In *Drosophila*, cadherins such as Shotgun (Shg, the *Drosophila* homologue of E-Cadherin) and Cadherin-N (Cad-N) can mediate adhesion between neighboring cells. Catenins, such as beta-catenin, mediate the link between cadherins and the cytoskeleton (Bulgakova

et al., 2012). Exemplarily, during the epithelial-mesenchymal transition in the *Drosophila* embryo, a series of changes in cell polarity, cell adhesion, and motility occur. Cells undergo a switch from an adhesive state towards a migrating state (Lim and Thiery, 2012). Thereby, the transcription factor Snail down-regulates epithelial genes, e.g. Shg, while Twist induces the transcription of Cad-N in the mesoderm (Leptin and Grunewald, 1990).

Here, we report first insights into the migration process of nascent myotubes from the prospective seminal vesicle onto the pupal testis and further towards the apical tip of the testis. Based on our results, we propose a model that links Ths- and Htl-dependent FGF signaling to myosin II-dependent processes during the migration of nascent myotubes from the genital disc onto the testes.

RESULTS

The adhesion molecule Cadherin-N is essential for building a continuous testis sheath

Since the *Drosophila* adult testis is encircled by a tight muscle sheath, we asked whether cadherins mediate the adhesion between myotubes in the testis muscle sheath before, during, and after migration. In expression analyses, we used Mef2-Gal4-driven UAS-mCD8-GFP flies to visualize myoblasts on genital discs and pupal testes at distinct time points. We observed that on genital discs 30 h APF, Shg (Cad-E) was expressed in the epithelium of the prospective seminal vesicle but was hardly detectable in myoblasts (Fig. 2A–A’).

By contrast, Cad-N was detected in the membranes of nascent myotubes on genital discs 30 h APF (Fig. 2B–B’) as well as on testes at 30 h APF (Fig. 2C–C’). Nascent myotubes of testes 44 h APF expressed Cad-N in correlation to their stage of migration. Specifically, myotubes at the basal testis end already started to elongate and to build a sheath, and expressed Cad-N (Fig. 2D,D’), whereas Cad-N was barely detected in nascent myotubes near the apical tip in mCD8-GFP-labeled myotubes in an optical section (Fig. 2D,D’). In the testis sheath of adult males, Cad-N was distinctly localized in the adjacent membranes of multinucleated myotubes (Fig. 2E).

Hence, we then knocked down *cad-N* by RNA interference (RNAi) with the driver line UAS-Dcr-2;;Mef2-Gal4 specifically in myoblasts. This resulted in a disturbed morphology of the testis. In the wild type, the adult testis is a long, thin tubule of 2.5 coils (Fig. 2F). In the RNAi-mediated knock-down of *cad-N*, the adult testis was partly irregular in shape and had roughly only one coil (Fig. 2G). The testis muscle sheath exhibited holes, which indicated that the myotubes were not properly attached to one another (Fig. 2G’). Genital discs 24 h APF exhibit Duf-expressing FC-like and sticks and stones (SNS)-expressing FCM-like myoblasts on prospective seminal vesicles (Kuckwa et al., 2016). In differential interference contrast (DIC) images, FC-like and FCM-like cells are visible (Fig. S2A), Cad-N expression is largely restricted to FC-like myoblasts (Fig. S2A’). *mefGAL4*-driven knock-down of Cad-N was efficient in FC-like myoblasts, whereas expression was hardly affected in myoblasts lying over the paragonia (compare Fig. S2B’ to wild type Fig. S2A’). At 44 h APF, *cad-N* knock-down testes displayed nascent myotubes, which were distributed all over the testes (Fig. S2C’). In contrast to wild-type testes (Fig. S2C), the nascent myotubes in these *cad-N* knock-down testes are less elongated and their number seemed to be reduced (Fig. S2C). Nevertheless, adult males with this phenotype were able to produce offspring (89%, Fig. S1).

Furthermore, we down-regulated Armadillo (Arm), the beta-catenin homologue in *Drosophila* (Peifer et al., 1992), specifically in myoblasts. Adult testes with down-regulated *arm* had about two coils (Fig. 2H). The testis muscle sheath exhibited numerous small holes, which indicated that the adhesion between single myotubes was disturbed (Fig. 2H’). These males also had a reduced fertility (60%, Fig. S1). Cad-N expression between adjacent myotubes was preserved upon *arm* knock-down, whereas no Cad-N expression was detected when testis myotubes did not adhere to each other (Fig. 2I).

We conclude that Cad-N in cooperation with Arm is involved in testis myotube migration and is necessary both to stabilize the testis muscle sheath and to shape the testis.

Non-muscle myosin II regulates the migration of nascent myotubes onto the testes

Many migratory processes depend on the actin-myosin network (Campellone and Welch, 2010; Vicente-Manzanares et al., 2009).

Using myoblast-specific RNAi experiments, we therefore investigated the relevant myosins of nascent myotubes as they populated the testis. Down-regulation of the light or heavy chain of non-muscle myosin II led to drastic defects.

When we myoblast-specifically knocked down *spaghetti squash* (*sqh*), the regulatory light chain of non-muscle myosin II (Karess et al., 1991). The testes were smaller than in the wild type (Fig. 3A), and had bulky tips and 1.5 coils in adult males (Fig. 3C). The muscle sheath did not cover the entire testes and had numerous holes; single myofibers appeared shorter (Fig. 3C’) than in the wild type (Fig. 3B). These males had reduced fertility (43%, Fig. S1).

Testes morphology and musculature were also disturbed when *zipper* (*zip*), the non-muscle myosin II heavy chain (Mansfield et al., 1996), was down-regulated. Adult testes had 1.5 coils and a bulky head (Fig. 3D), comparable to the phenotype observed in the *sqh* knock-down, and the muscles resembled a broad-meshed net rather than a sheath (Fig. 3D’). In contrast to *sqh* knock-down males, the fertility of *zip* knock-down males was preserved (100%, Fig. S1). This was surprising because the *sqh* and *zip* knock-down phenotypes resembled each other and are components of myosin II. The observed differences in male fertility might be due to an unpredicted off-target in the *sqh* RNAi line.

As an example, we first analyzed adult *sqh* knock-down testes in more detail. Cad-N was expressed between the few remaining adjacent myotubes (Fig. S2D), which suggested that the muscle sheath defect was not due to faults in Cad-N-mediated attachment of single myotubes. Instead, it was likely caused by insufficient population of the testis with muscles. We further analyzed the status of the extracellular matrix by monitoring Terribly reduced optic lobes (Trol) (Voigt et al., 2002), which is expressed in the testis muscle sheath (Susic-Jung et al., 2012). Expression of Trol revealed no changes in adult *sqh* knock-down testes (Fig. S2E,F), which indicated extracellular matrix integrity. At 44 h APF, pupal testes with myoblast-specific *sqh* knock-down were populated with fewer nascent myotubes than wild-type testes (Fig. S2H, compare to G). However, the testis shape was not affected at this time of development.

Taken together, these data led us to conclude that non-muscle myosin II is required for testis myotube migration and that correct shaping of the testis depends on the presence of an intact tight muscle sheath.

DWnt2 signaling controls determination of testis-relevant myoblasts

It has been previously suggested that DWnt2 plays a role in the migration of myoblasts from the prospective seminal vesicle onto the testes (Kozopas et al., 1998). Therefore, we analyzed the testis shape and muscle sheath of two amorphic *DWnt2* alleles in *trans* (*DWnt2^L*, *DWnt2^O*; Kozopas et al., 1998). The resulting flies were not able to hatch, and pharate lethal. The development and morphology of testes was variable in these flies, as has also been recently observed by Linnemannstöns et al. (2014). The most abundant phenotypes were deformed and not elongated adult testes that did not resemble the wild-type adult testis shape (Fig. 4A). Instead, the shapes were comparable to those of pupal testes (Fig. 4C). Testis stability was decreased, and germ cells leaked (Fig. 4C, arrow). Unlike the wild-type musculature (Fig. 4B), smooth-like muscles were not detected on these testes, but some multinucleated actin-rich structures that contained repetitive actin filaments resembling striated muscles were visible (Fig. 4C’,C’’, arrows). The leaking cysts with elongated spermatids that appeared shortly before individualization (Fig. 4D, arrow) indicated that germ

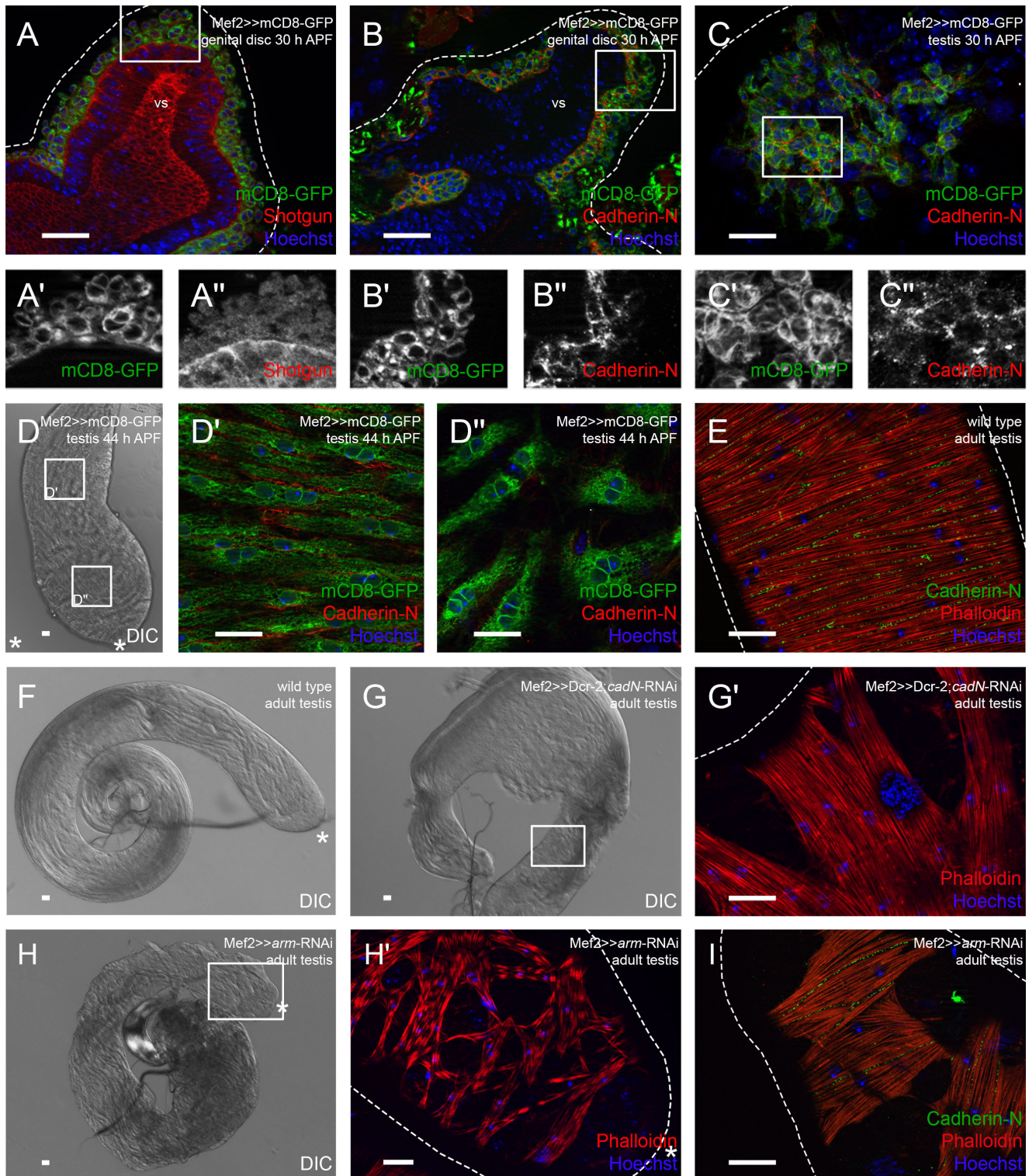


Fig. 2. Knock-down of *Cadherin-N* or *Armadillo* strongly reduces the adhesion between testis myotubes. Immunofluorescence analyses of genital discs and testes. (A) Seminal vesicles 30 h APF stained or marked with anti-Shotgun (red), GFP (green; myoblasts and myotubes on genital discs and pupal testes marked with *Mef2*>>*mCD8-GFP*), and Hoechst (blue; nuclei). (A', A'') Enlargement of boxed area in A, stained or marked as indicated. (B) Genital discs 30 h APF and (C) testis 30 h APF stained or marked with anti-Cad-N (red), GFP (green), and Hoechst (blue), magnification of prospective seminal vesicle is shown. (B', B'', C', C'') Enlargement of boxed area in B and C stained or marked as indicated. (D–D'') Testis 44 h APF. (D) Differential interference contrast (DIC) micrograph of testis 44 h APF, (D', D'') enlargement of boxed area in D stained or marked with anti-Cad-N (red), GFP (green), and Hoechst (blue). (E) Adult testis stained with Hoechst (blue), Phalloidin to visualize F-actin (red), and anti-Cad-N (green). (F) DIC micrograph of wild-type testis. (G) DIC micrograph of *cad-N* knock-down testis; (G') enlargement of boxed area in G showing Phalloidin (red) and Hoechst (blue) staining of testis muscle sheath. (H) DIC micrograph of *arm* knock-down testis; (H') enlargement of boxed area in H showing Phalloidin (red) and Hoechst (blue) staining of testis muscle sheath. (I) Adult *arm* knock-down testis stained with Hoechst (blue), Phalloidin to visualize F-actin (red), and anti-Cad-N (green). Dotted lines reflect approximate shape of the organ. Asterisk, hub region; vs, seminal vesicle. Scale bars: 20 μ m.

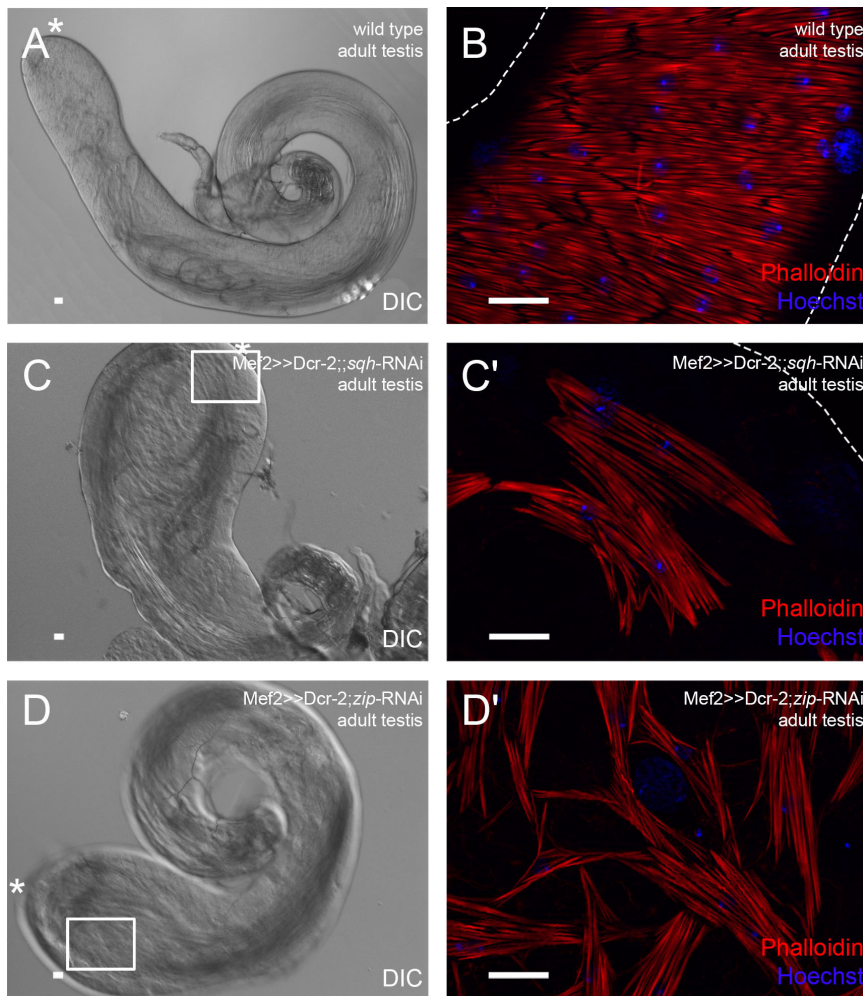


Fig. 3. Myoblast-specific down-regulation of non-muscle myosin II leads to inefficient population of the testis with muscles. Analysis of adult (A,B) wild-type testes, (C,C') *sqh* knock-down testes, and (D,D') *zip* knock-down testes. (A,C,D) DIC micrograph; asterisk, hub region. (B,C',D') Phalloidin staining to visualize F-actin (red), and Hoechst staining of nuclei (blue). C' and D' are enlargements of areas boxed in C and D, respectively. Dotted lines reflect approximate shape of the organ. Scale bars: 20 μ m.

cell maturation proceeded normally. This is in agreement with our earlier observations that spermatogenesis *in vitro* in cultured isolated cysts proceeds until shortly before individualization, independently of the presence of the testis muscle sheath (Awe and Renkawitz-Pohl, 2010; Gärtner et al., 2014). Other organs of the reproductive system showed no obvious defects (data not shown), which suggested a selective effect on testis-relevant myoblasts.

From these data, we concluded that *DWnt2^L/DWnt2^O* mutant flies fail to determine testis-specific myoblasts from the common pool of myoblasts. However, this does not exclude an additional later role of *DWnt2* during migration of muscles onto the testes.

Heartless-dependent FGF signaling is essential for the migration of nascent myotubes onto the testis

FGF signaling is involved in various migration processes throughout the animal kingdom (Itoh and Ornitz, 2011; Ornitz and Itoh, 2015; Shilo, 2016). Therefore, we examined the role of FGF signaling in the migration of nascent testis myotubes. We analyzed the expression of Stumps, the intracellular adaptor protein specific for FGFRs, which is also known as Heartbroken (Hbr) and Downstream of FGF (Dof) (Imam et al., 1999; Michelson et al., 1998a; Vincent et al., 1998), using a specific antibody (Vincent et al., 1998) on genital discs. At 24 h APF, Stumps was detected in the cytoplasm of myoblasts in the inner layer, the so-called FC-like myoblasts (Fig. 5A–A"). Nascent myotubes on genital discs 30 h APF (Fig. 5B–B") and testes 30 h APF (Fig. 5C–C") also expressed Stumps in the cytoplasm. We investigated the potential expression

pattern of Htl on male genital discs in an Htl-Gal4 driver line that has been shown to drive expression in the epithelial sheath of the ovary (Irizarry and Stathopoulos, 2015). We observed Htl-driven mCD8-GFP expression in myoblasts on the prospective seminal vesicles at 24 h APF (Fig. 5D) and 30 h APF (Fig. 5E). Notably, Stumps was expressed in FC-like Htl-positive myoblasts on developing seminal vesicles at 24 h APF (Fig. 5D–D") and in all nascent myotubes at 30 h APF (Fig. 5E–E"), which suggested that FGF signaling might be activated during migration.

In *Drosophila*, Stumps is a unique adaptor protein in FGF signaling that can be activated by two FGFRs (Vincent et al., 1998). Myoblast-specific knock-down of the FGFR Btl did not result in any defects in testis musculature or shape, but resembled the wild-type situation (Fig. S3A). By contrast, we observed very drastic defects when the FGFR Htl was knocked down. Specifically, all flies were pharate lethal, and most testes were not attached to the seminal vesicles and did not elongate (Fig. 6C). The testes did not contain muscles, and the sheath consisted solely of pigment cells (Fig. 6C', arrowhead). Nevertheless, spermatogenesis appeared to be normal in these testes since we observed bundles of spermatids shortly before or during individualization (Fig. 6C', arrow). This indicates that the presence of testis muscles is not essential for germ cell maturation, as we also observed in hypomorph *DWnt2* alleles (Fig. 4). In the *htl* knock-down, the other organs of the male reproductive system were malformed and partly degraded, and muscles were mainly absent (data not shown). This might be due to myoblast determination defects, since *htl* knock-down genital discs 24 h APF contained fewer myoblasts than wild-

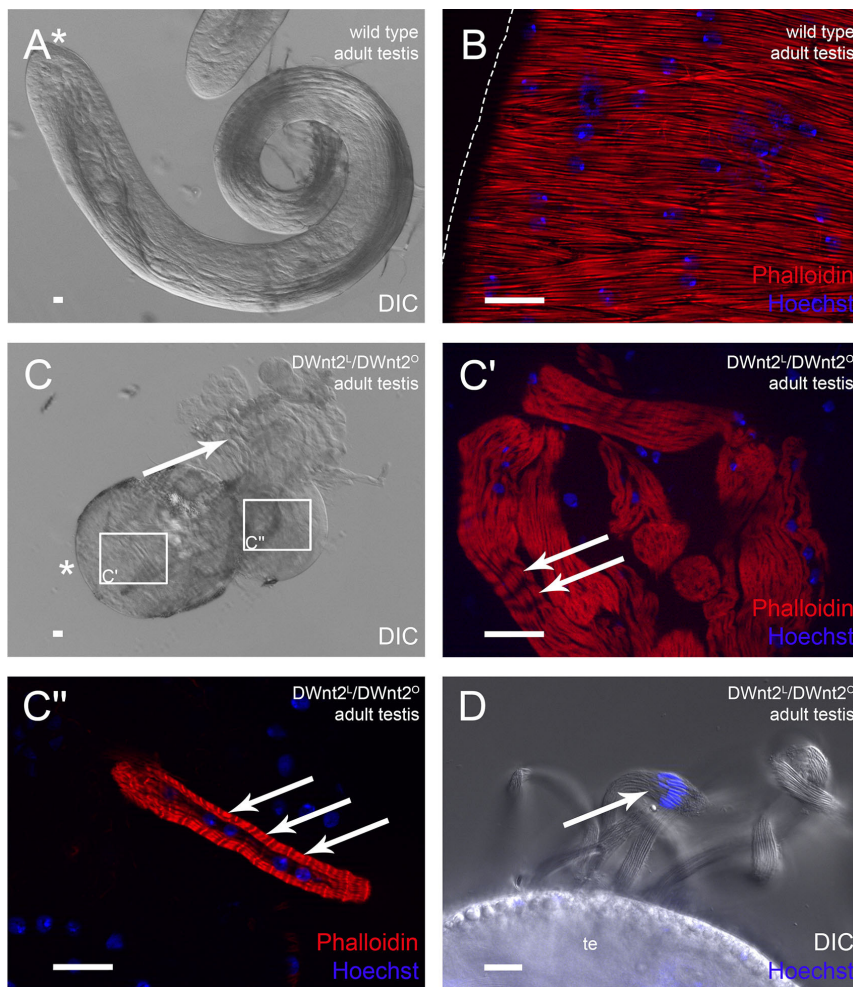


Fig. 4. DWnt2 affects testis muscle determination. Analysis of adult (A,B) wild-type testes and (C-D) DWnt2^L/DWnt2^O testes. (A,C) DIC micrographs; arrow, leaking sperm; asterisk, hub region. (C',C'') Enlargement of the respective boxed areas in C stained with Phalloidin to visualize F-actin (red) and Hoechst to visualize nuclei (blue). Arrows, thin actin filaments. (D) DIC micrograph and Hoechst staining (blue) of adult DWnt2^L/DWnt2^O testis. Arrow, nuclei of leaking spermatid bundles. Scale bars: 20 μm.

type genital discs 24 h APF. This was especially the case in the posterior part of the genital discs, where myoblasts for the muscle sheaths of the ejaculatory duct and sperm pump are localized (Fig. S3B,C, arrows). At 30 h APF, prospective seminal vesicles of *htl* knock-down genital discs contained fewer nascent myotubes than the wild type (compare Fig. S3F-F'' to Fig. 5B). This is in agreement with the observed Htl-driven expression of mCD8-GFP in most myoblasts on genital discs 24 h APF (Fig. S3D). Myoblast-specific expression of a dominant-negative (DN) version of Htl lacking the kinase domain (Michelson et al., 1998b) resulted in a milder phenotype than the *htl* knock-down, comparable to the other *htl*-RNAi line (Table S1). The adult testes were elongated and coiled, but had bulky tips as observed with the DN-version of Htl (Fig. S3E). The testis muscles covered the organs except for the tips (Fig. S3E'). To gain further insight into which FGF ligand activates Htl in nascent myotubes, we analyzed the testis shape and musculature of hypomorph *ths*^{e02026}/*Df(2R)ths238* mutants. Adult testes had approximately two coils and a very bulky tip (Fig. 6D). The smooth-like testis muscle sheath had numerous holes, and the testis tip was free of muscles (Fig. 6D') as previously observed for DN-version of Htl and knock down by the RNAi line BL35024. Unfortunately, we could not analyze the other FGF ligand Pyr because no hypomorph alleles were available.

When we down-regulated *stumps* specifically in myoblasts, a strong phenotype was generated, comparable to that of the *htl* knock-down. But unlike the strongest *htl* knock-down testes, adult testes with reduced Stumps levels were attached to seminal vesicles, and about

30% of the testis sheath contained muscles. All flies were pharate lethal, and most testes attached to the seminal vesicles did not elongate (Fig. 6E). The muscles did not build a complete sheath but remained at the basal end of the testis, and the muscle pattern was disturbed (Fig. 6E'). On the adult *stumps* knock-down testis, Cad-N was normally expressed in the membranes between adjacent myofibers, where muscles formed an intact sheath (Fig. 6F). However, where myofibers did not attach to one another, no Cad-N was detected (Fig. 6F). No Stumps expression was visible in *stumps* knock-down genital discs 24 h APF, which indicated a strong down-regulation of *stumps* (Fig. S3G-G''). After *stumps* knock-down – in contrast to the *htl* knock-down (Fig. S3F-F'') – we observed many myoblasts lying over the seminal vesicles (Fig. S3G-G''). Stumps expression on *htl* knock-down genital discs 24 h APF remained unchanged in testis-relevant myoblasts (Fig. 6G-G''). At 40 h APF, mCD8-GFP-positive nascent myotubes were visible on both wild-type (Fig. 6H) and *stumps* knock-down testes (Fig. 6I), which indicated that the initial migration process was intact upon *stumps* knock-down.

These results suggest that Htl-controlled FGF signaling activated by Ths is essential for the correct migration of nascent myotubes on testes.

Stumps is necessary for proper myotube migration on the testis *ex vivo*

To gain further insights into the migration process on the testis, we established *ex vivo* live imaging of co-cultures of pupal testes and

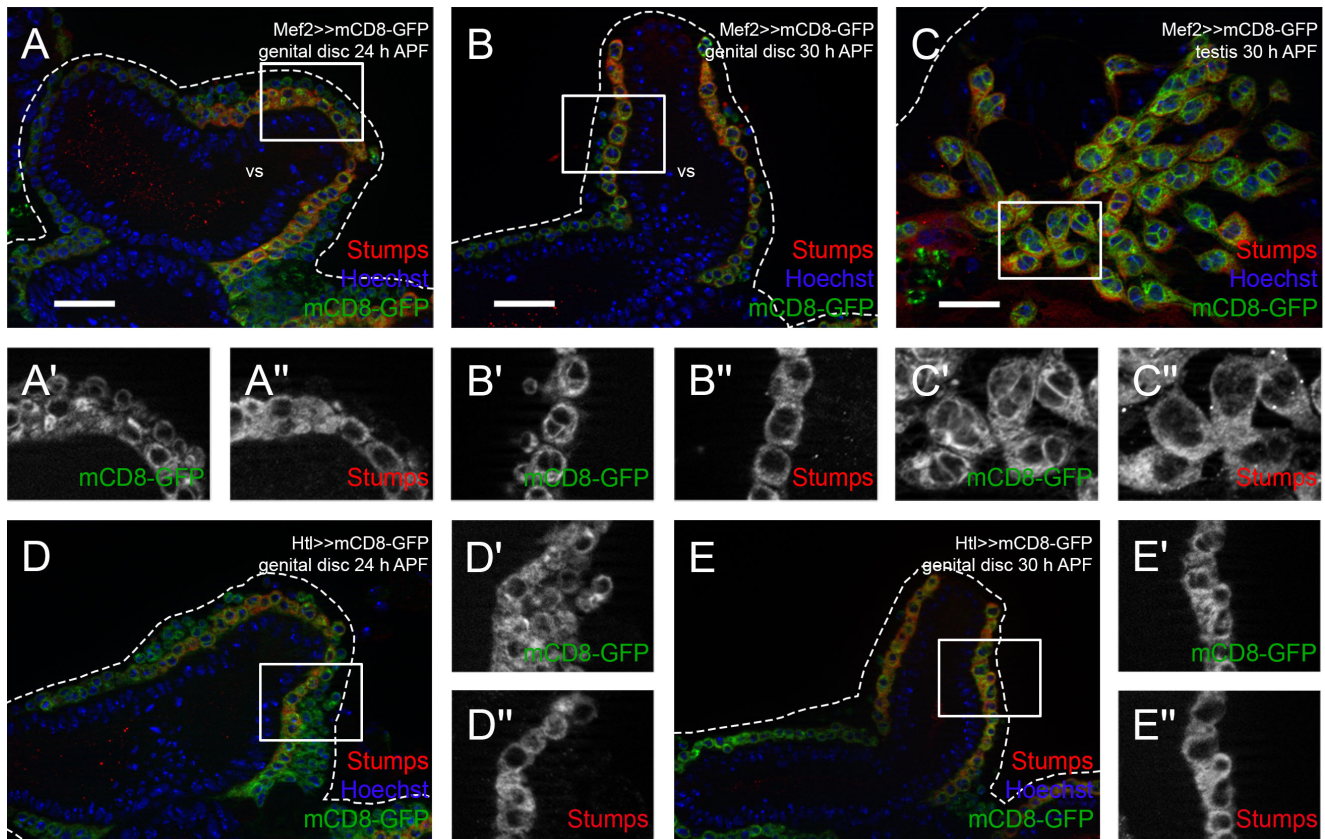


Fig. 5. FGF signaling components are expressed during migration of testis myotubes. Immunofluorescence analysis of *Stumps*. Myoblasts and nascent myotubes on (A-A'') wild-type genital discs 24 h APF, (B-B'') wild-type genital discs 30 h APF (magnifications of prospective seminal vesicles are shown), and (C-C'') pupal testis 30 h APF stained or marked with anti-*Stumps* (red), *Mef2*-driven *mCD8-GFP* (green), and *Hoechst* (blue; nuclei). (A', A'', B', B'', C', C'') Enlargement of boxed areas in A, B, and C, respectively, marked with GFP or stained with anti-*Stumps*. (D-E'') Myoblasts and myotubes on *Htl-Gal4* >> *mCD8-GFP* genital discs at (D-D'') 24 h APF (magnification of prospective seminal vesicle is shown) and (E-E'') 30 h APF, stained or marked with anti-*Stumps* (red), *Htl*-driven *mCD8-GFP* (green), and *Hoechst* (blue). (D', D'', E', E'') Enlargement of boxed area in D and E, respectively, marked with *Htl*-driven *mCD8-GFP* or stained with anti-*Stumps*. Dotted lines reflect approximate shape of the organ. vs, seminal vesicle. Scale bars: 20 μ m.

genital discs. For investigating the migrating nascent myotubes on the testis itself, we used 40 h APF testes expressing myoblast-specific *mCD8-GFP*. The testes were still attached to part of the developing seminal vesicles, but not to the genital disc. When live imaging started, approximately 60% of the pupal testis surface was already covered with multinucleated nascent myotubes (Fig. 6J, arrowhead). Four hours later, the myotubes had spread out and migrated towards the apical region (Fig. 6J', arrowhead). After nine hours, myotubes covered about 80% of the pupal testis surface (Fig. 6J'', arrowhead). During live imaging, the testis grew in length.

We then tested the effect of down-regulated *stumps* on the migration process on pupal testes. We cultured *stumps* knock-down testes 40 h APF expressing myoblast-specific *mCD8-GFP*. These testes were also still attached to a part of the developing seminal vesicle. When live imaging started, approximately 30% of the pupal testis was covered with nascent myotubes (Fig. 6K, arrowhead). After four hours, myotubes covered about 40% of the testis (Fig. 6K', arrowhead). After nine hours, myotubes still covered no more than 40% of the testis (Fig. 6K'', arrowhead). Strikingly, the morphology of the nascent myotubes was affected; the cells seemed smaller than in the control (Fig. 6K, compare to J) and did not spread out on the testis during live imaging. In addition, the testis grew only little in length.

From these results, we conclude that *Stumps* is essential for the migration of nascent myotubes on pupal testes, and that when *Stumps* is efficiently reduced, testes can grow and even attach to the

developing seminal vesicles, but nascent myotubes fail to fully cover the testes.

Non-muscle myosin II expression depends on Heartless signaling

So far, we gained evidence for Heartless-dependent migration of nascent myotubes along the testes and showed that knock-down of *Cad-N* (Fig. 2G-G') and *Sqh* (Fig. 3) lead to distortion of the coverage of testes with muscles. We now asked whether the expression of *Cad-N* or *Sqh* or both depends on Heartless signaling. As the *htl-RNAi* line with the strongest phenotype after myoblast-specific activation had no muscles on the testis, we applied a second *htl-RNAi* line (BL35024) in our analysis, which resembles the *Htl-DN* (Fig. S3E) phenotype and the *thisbe* hypomorph mutant and thus had muscles on the testes. As RNAi-mediated knock-down of *Stumps* (Fig. S3G-G') was very efficient (Fig. S3G-G''), we focused on *stumps* in our analysis in parallel to the *htl-RNAi* line BL35024.

We observed *Cad-N* expression in nascent myotubes migrating along the testis and in the mature musculature (Fig. 2D-E). We asked whether reducing Heartless signaling impairs expression of *Cad-N* in pupal testes (arrows in Fig. 7A-C). *Cad-N* was expressed at the site of contact (Fig. 7A) in wild type and after knock-down of either *Htl* (Fig. 7C) or *Stumps* (Fig. 7B), which indicates that *Cad-N* expression is independent of *Htl* signaling. At 44 h APF in the *Stumps* knock-down mutant, nascent myotubes were less tightly

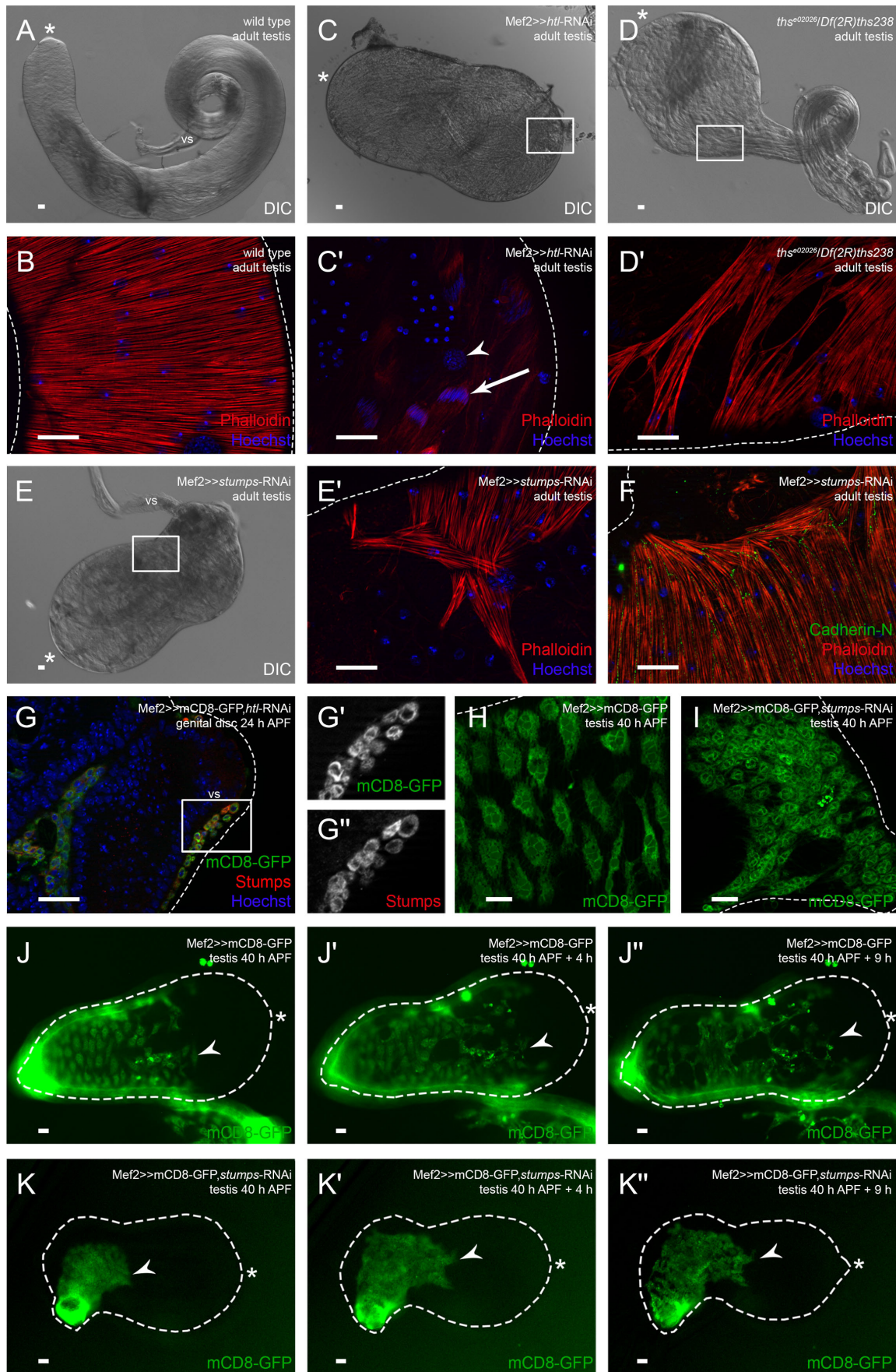


Fig. 6. See next page for legend.

Fig. 6. *Ths*-activated *Heartless* is essential for populating the testis with myotubes. Analysis of *htl* and *stumps* knock-down and *ths* mutant. (A) DIC micrograph of adult wild-type testis. (B) Phalloidin staining to visualize F-actin (red), and Hoechst staining of nuclei (blue). (C) DIC micrograph of adult *htl* knock-down (v6692) testis. (C') Enlargement of boxed area in C showing adult *htl* knock-down testis stained with Phalloidin (red; F-actin) and Hoechst (blue; nuclei); arrowhead, pigment cell nuclei; arrow, spermatids during individualization. (D) DIC micrograph of adult *ths* mutant testis. (D') Enlargement of boxed area in D showing adult *ths* mutant testis stained with Phalloidin (red) and Hoechst (blue). (E) DIC micrograph of adult *stumps* knock-down testis. (E') Enlargement of boxed area in E showing adult *stumps* knock-down testis stained with Phalloidin (red) and Hoechst (blue). (F) Adult *stumps* knock-down testis stained with anti-Cad-N (green), Phalloidin (red), and Hoechst (blue). (G-G'') *htl* knock-down genital disc 24 h APF stained or marked with anti-Stumps (red), GFP (green), and Hoechst (blue); magnification of prospective seminal vesicle is shown. (G', G'') Enlargement of boxed area in G marked with GFP or stained with anti-Stumps. (H) Myoblasts on wild-type testis 40 h APF marked with Mef2-driven mCD8-GFP (green). (I) Myotubes of *stumps* knock-down testis 40 h APF marked with GFP (green). (J-K'') Live imaging over time of testes 40 h APF expressing Mef2-driven mCD8-GFP to reveal the migration of nascent myotubes in an *ex vivo* culture of (J-J'') wild-type testis and (K-K'') *stumps* knock-down testis. Dotted lines reflect the approximate shape of the organ. Arrowheads, the front of migrating nascent myotubes; asterisk, hub region; vs, seminal vesicle. Scale bars: 20 μ m.

packed and many Cad-N-positive filopodia were visible at the contact sites between neighboring myotubes (Fig. 7B).

Next we asked whether Sqh, the light chain of myosin II, is expressed dependent on Htl signaling. At 44 h APF, Sqh localized to the filopodia of nascent myotubes on wild-type testes, and Sqh was enriched at the ends of stretching myotubes (Fig. 7D). In the *htl*-RNAi knock-down situation, however, nascent myotubes were less densely packed and had started to stretch while encircling the testis tube. In this situation, Sqh expression was not obviously disturbed (Fig. 7F). This is not surprising since in the less efficient *htl*-RNAi

line showed a weak phenotype comparable to the dominant-negative version. By contrast, we did not detect Sqh in the poorly stretched nascent myotubes after efficient reduction of Stumps in the parallel experiment (Fig. 7E) (for knock down phenotype with respect to testis shape see Fig. 6E). We propose that Heartless signaling via Stumps directly or indirectly activates the synthesis of Sqh, the regulatory light chain of myosin II.

DISCUSSION

Wnt signaling does not directly affect testis myotube migration but affects determination of testis-relevant myoblasts

DWnt2 functions in pigment cell determination and possibly also in the migration of nascent myotubes onto pupal testes in addition to, or as a consequence of, the failure of pigment cell migration (Kozopas et al., 1998). We checked whether amorphic DWnt2 alleles have migration defects. In agreement with the results of Kozopas et al. (1998) and Linnemannstöns et al. (2014), an amorphic allelic combination of *DWnt2* produced small testes of various sizes. Kozopas et al. (1998) observed only a small amount of muscles on adult DWnt2 mutant testes. We showed that smooth-like muscles were absent from the testis sheath. Surprisingly, a few striated muscles were visible on these testes.

The results presented here led us to tentatively conclude that DWnt2 affects cell fate determination of testis-relevant myoblasts. Indeed, it has been shown that Wnt signaling specifies cell identity of a subset of somatic muscle founder cells in *Drosophila* embryogenesis (Baylies et al., 1995) and during many other determinations of the fate of the cell (Bertrand, 2016; Munoz-Descalzo et al., 2015). However, an additional later role in the migration of testis myotubes cannot be excluded.

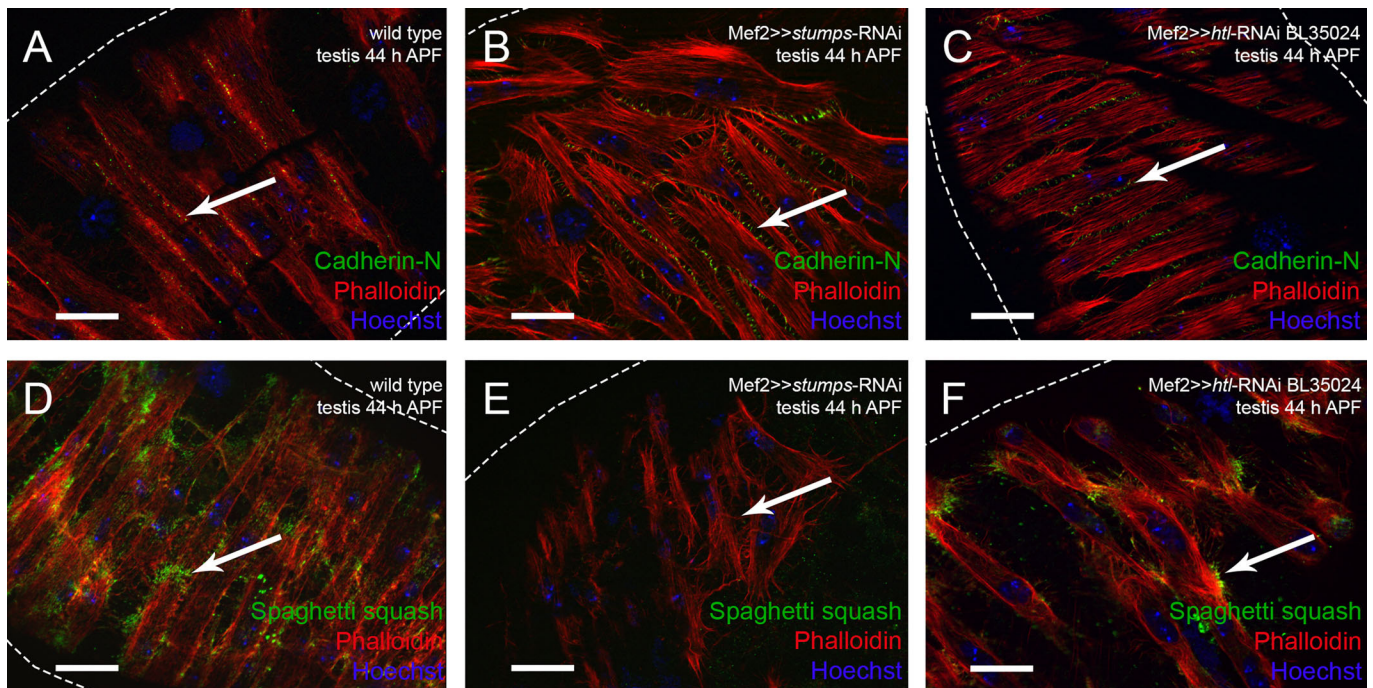


Fig. 7. Expression of the myosin II subunit Spaghetti squash is not detectable after knock-down of Stumps. (A-F) Visualization of muscles on testes by Phalloidin (red). (A-C) Expression of Cad-N in (A) wild type, (B) *stumps* knock-down, and (C) *htl* knock-down. (D-F) Sqh expression in (D) wild type (Z-stacks, 27 images with 0.48 μ m per layer), (E) *stumps* knock-down (Z-stacks, 12 images with 0.52 μ m per layer), and (F) *htl* knock-down (Z-stacks, 9 images with 0.24 μ m per layer). Arrows in A-C indicate Cad-N and in D-F indicate Sqh; dotted lines indicate border of testis.

Multiple roles of Heartless-dependent FGF signaling during the development of the male reproductive system

The FGF receptor Btl is required for migration of glia and tracheal cells (Klämbt et al., 1992). In our study, down-regulation of the FGFR Btl, specifically in myoblasts, did not result in migration defects of testis myotubes. Conversely, knock-down of *htl* led to adult testes of a severely reduced size that remained free of muscles or to less drastic phenotypes, depending on the RNAi fly line chosen.

The *htl* knock-down yielded two further phenotypes. One phenotype was the drastically reduced number of non-testes-relevant myoblasts building the genital discs 24 h APF, while testis-relevant myoblasts were present on the developing seminal vesicles. This might be due to decreased proliferation of myoblasts on genital discs, since myoblasts undergo mitosis around 16 h APF (Kuckwa et al., 2016). Alternatively, this might be due to survival or determination defects. The second phenotype was the lack of a connection between the seminal vesicles and the testes. Knock-down of *htl* by one RNAi line caused testes development to stop early, whereas the dominant-negative version of Htl (Fig. 8A) and a weaker RNAi line (BL 35024) resulted in testes shapes that pointed towards a much later stop in development. Testes of hypomorph mutants of the Htl ligand Ths (Fig. 8A) showed a remarkably similar phenotype. This suggests that Ths is an important ligand of Htl in this system.

Stumps was expressed in FC-like myoblasts and nascent myotubes adjacent to the epithelium on genital discs and testes. In addition, down-regulation of the adaptor protein *stumps* yielded drastic defects in covering the testes with myotubes. This could be caused by a reduced number of myotubes or by a migration defect. We observed a fairly normal amount of myoblasts lying over the seminal vesicles. This and the disruption of migration of these myotubes in *ex vivo* cultures of testes argue for a migration defect in addition to morphology defects. *stumps* knock-down pupal testes 40 h APF exhibited many nascent myotubes, which indicated that initial migration occurred. However, we cannot exclude that we were unable to detect a low level of Stumps in immunofluorescence assays and that such a low amount could be sufficient for initial migration onto the testes.

Our results led us to conclude that migration of nascent myotubes on the testis depends on FGF signaling via Ths, Htl, and Stumps. Future research will focus on unravelling the distinct functions of FGF signaling via Heartless during muscle development in the male reproductive system.

Non-muscle myosin II drives the migration of nascent testis myotubes dependent on Heartless signaling

Down-regulation of non-muscle myosin II (i.e. *zip* or *sqh*) resulted in adult testes that were not fully covered with muscles, which indicated that non-muscle myosin II is necessary for the migration of nascent testis myotubes. Myosin II is also required for proper detachment and migration of border cells during egg chamber development (Combedazou et al., 2016; Majumder et al., 2012), and *Drosophila* tubulogenesis (Saxena et al., 2014; Nie et al., 2014). Signaling through epidermal growth factor receptor activates non-muscle myosin II (Saxena et al., 2014; Combedazou et al., 2016). Here, we propose that Heartless-mediated FGF signaling directly or indirectly induces non-muscle myosin II, which promotes migration of nascent testis myotubes. This might explain migration and morphological defects of myotubes *in vivo* and *ex vivo*.

Cadherin-N and Armadillo are expressed during cell migration and for stabilizing the testis muscle sheath

Cad-N was expressed in myoblasts and nascent myotubes of genital discs and pupal testes as well as in the membranes of adult testis myotubes. In contrast to the epithelial-mesenchymal transition during embryogenesis (Leptin and Grunewald, 1990), no change in expression from Shg to Cad-N was observed when the nascent myotubes started to migrate. During the initial migration onto and along the testis, Cad-N was expressed, which suggests a collective mode of cell migration. We propose that lack of Cad-N or Arm leads to disturbances in collective cell migration. As a consequence, far fewer myotubes spread over the testes, and residual myotubes cannot yield a tight sheath of muscles. This leads to thickened areas in the testes, where the population of muscles is low. Therefore, we in turn propose that Cad-N in cooperation with Arm is furthermore essential for mediating cell adhesion between single testis myotubes, thereby stabilizing the testis muscle sheath and the tubular and coiled shape of the testes. In contrast, to *Sqh* we gained no evidence for Htl dependent expression of Cad-N.

Testis shaping depends on an intact muscle sheath

Shaping of adult testes was disturbed to varying degrees depending on the genetic background (Fig. 8). The shape resembled that of different developmental time points in the wild type (Fig. 8A). Mutants with amorphic DWnt2 alleles, *htl* knock-down, or *stumps* knock-down showed hardly any shaping. These phenotypes correlate with the total absence or presence of only a few testis muscles. Hypomorph Ths mutants as well as the expression of a dominant-negative version of Htl led to a less severe phenotype that matched the shaping defects produced by down-regulating *htl* with another RNAi fly line. These adult testes resembled those of the wild type at 72 h APF. Knock-down of *cadN*, *arm*, *sqh*, or *zip* led to adult testes whose shape, but not the degree of coverage of the testes with muscles, resembled that of wild-type testes at 54–72 h APF. At 42 h APF, nascent myotubes reach the testis tip in the wild type (Kuckwa et al., 2016). This is also the case when *cadN*, *arm*, *sqh*, or *zip* is down-regulated specifically in myoblasts. However, already at this stage, fewer myotubes were present on knock-down testes (Fig. 7), which supports our conclusions that Cad-N and non-muscle myosin II are required for the migration of testis myotubes and that an intact muscle sheath is required for the shaping of the testis.

Conclusions and model

Based on our results, we propose a model in which testis myotube migration is divided into two Htl- and Cad-N-dependent phases. (i) After myoblast fusion, when Stumps and Cad-N are distributed along the plasma membrane of nascent testis myotubes that are in close contact to the adjacent epithelium of the prospective seminal vesicles, FGF signaling initiates collective migration of nascent testis myotubes from the prospective seminal vesicle onto the testis (Fig. 8B). (ii) The coverage of the testes with muscles is achieved by collective cells migrating towards the testis tip, and this migration requires myosin II and the formation of a network of nascent myotubes with Cad-N-positive connections (Fig. 8C).

We propose that the ligand Ths and possibly also Pyr binds Htl in nascent myotubes and thereby activates FGF signaling via Stumps during both phases of migration; the source of these ligands needs to be determined. Downstream, components of MAPK signaling, such as Erk, could be activated, which might cause changes in transcription

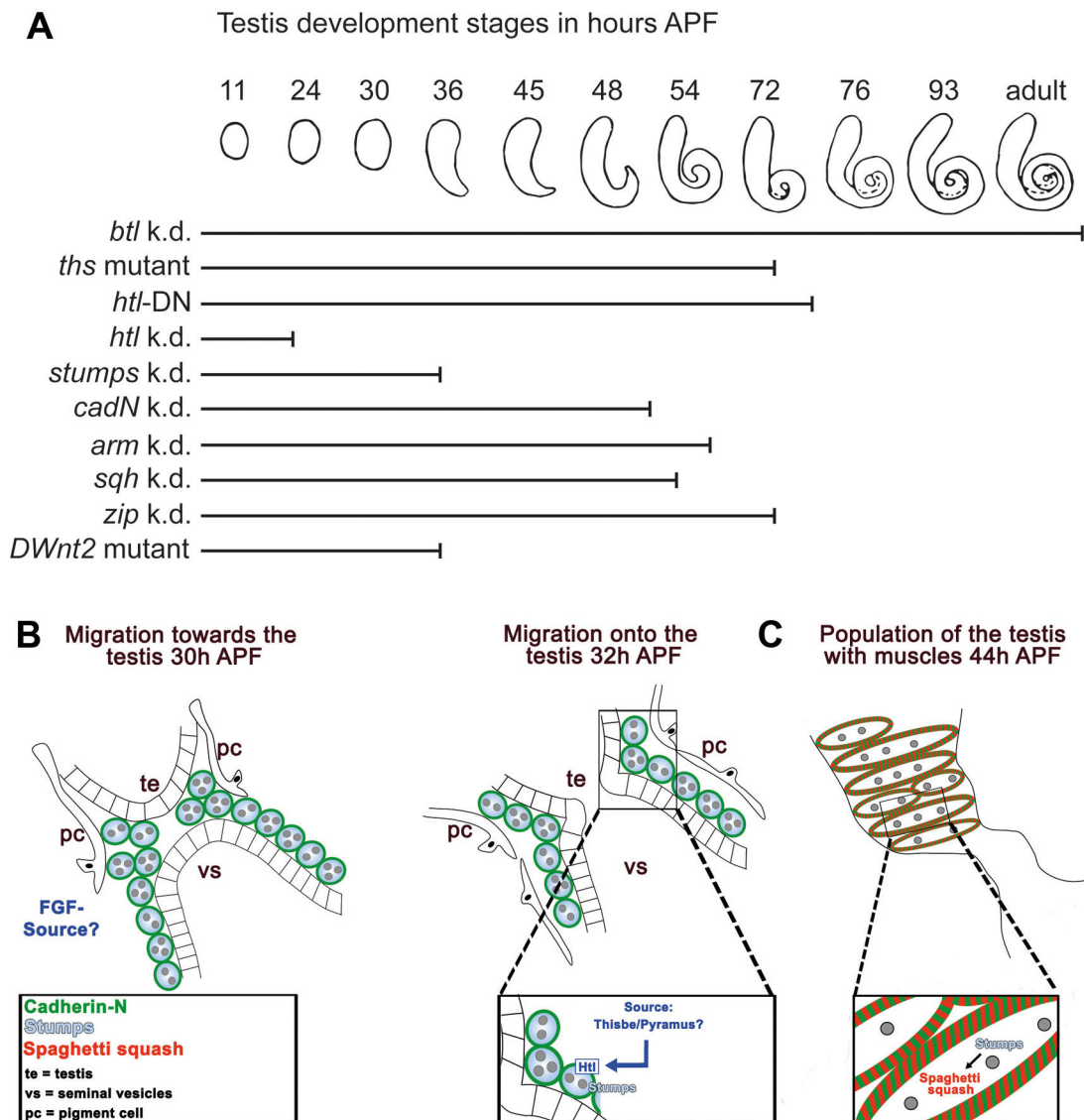


Fig. 8. Model of testis myotube migration. (A) Summary of shaping defects of knock-down/mutant testes. Stages of testis development in wild-type males during metamorphosis, from 11 h APF to adult. Bars indicate the stage to which to mutant testes develop [myoblast-specific knock-down (k.d.) mutants, mutant testes expressing the dominant-negative (DN) Htl protein, or a DWnt2 mutant]. According to the affected gene or genetic manipulation, testis development correlates to different stages of wild-type development. For example, down-regulation of *btl* does not interrupt testis development, whereas *htl* knock-down leads to a very early stop in development. (B,C) Two-phase model of testis myotube migration. (B) Phase one represents the Htl dependent migration of nascent myotubes onto the testis before and after fusion of the epithelium of the seminal vesicle (vs) and the terminal epithelium (te) of the testes. Pigment cells (pc) migrated towards the vs. The FGF ligand Ths and possibly Pyr are secreted by an unknown source. (C) In phase two, nascent myotubes are already on the testis and migrate further towards the tip. Cad-N mediates adhesion between adjacent myotubes. Stumps might control the migration process, likely via non-muscle myosin II. *Sqh* expression depends on Stumps, which suggests *Sqh* regulation by Htl signaling. Note that after an initial phase one, both phases run in parallel until all myotubes reach the testis.

of different target genes. Indeed, we observed Htl-dependent expression of *Sqh*. We hypothesize that Thisbe/Heartless-induced MAPK signaling might link to the actin cytoskeleton via non-muscle myosin II, thereby facilitating cytoskeletal changes needed for cell migration (Fig. 8B).

Our data provide first insights into the Thisbe/Heartless-dependent regulation of myotube migration via myosin II expression from the seminal vesicle to and along the testes, which is dependent on successful connection of these tissues. Future studies aiming at identifying missing components and functions to fully elucidate testis myoblast specification and myotube migration will require the establishment of more specific tools, such as driver lines specifically active in testes myoblasts and myotubes.

MATERIALS AND METHODS

Fly stocks

Flies were kept and RNAi crossings were carried out on standard medium at 25°C. *w¹¹¹⁸* (BL6326) was used as the wild-type reference. The following transgenic flies were used: Mef2-Gal4 (Ranganayakulu et al., 1995), Htl-Gal4 (BL40669), UAS-Dcr-2;;Mef2-Gal4 (BL25756), UAS-htl-DN (BL5366), and UAS-mCD8-GFP (BL32186). For RNAi experiments, the following fly lines were used: UAS-*cadN*-RNAi (v1092, v1093, v101642), UAS-*arm*-RNAi (BL31304, BL35004), UAS-*sqh*-RNAi (BL32439, BL33892), UAS-*zip*-RNAi (BL36727, BL37480), UAS-*btl*-RNAi (BL40871, v27106), UAS-*htl*-RNAi (BL35024, v6692), and UAS-*stumps*-RNAi (v21317, v105603). We conducted all RNAi experiments with at least two different fly lines per gene; the differences were in knock-down efficiencies or effects of second site insertions, as described in Vissers et al. (2016). An overview of all produced

phenotypes is given in Table S1. The *ths* mutant was generated by crossing *ths*⁶⁰²⁰²⁶/CyO. actin-GFP (Stathopoulos et al., 2004) and *Df(2R)ths238*/CyO. actin-GFP (Kadam et al., 2009). For DWnt2 experiments, DWnt2^L (BL6909, Kozopas et al., 1998) and DWnt2^O (BL6958, Kozopas et al., 1998) flies were used. BL flies were ordered from Bloomington *Drosophila* Stock Center (Bloomington, IN, USA), and v flies were obtained from Vienna *Drosophila* RNAi Center (Vienna, Austria).

Fertility tests

One adult male of the F₁ generation from RNAi crossings was mated with three virgin females (w¹¹¹⁸) over seven days. After two weeks, the efficiency of the matings was examined. All fertility tests were carried out at 25°C.

Immunofluorescence

Pupae selection, genital disc dissection, and immunofluorescence were carried out as described elsewhere (Kuckwa et al., 2016) and were repeated at least three times. The following antibodies were used: anti Duf/Kirre (1:500, Kreisköther et al., 2006), anti-Cadherin-N (1:100, DSHB DN-Ex #8), anti-Shotgun (1:100, DSHB DCAD2), anti-Stumps (Dof, 1:1000; gift from Maria Leptin, University of Cologne, Germany; Vincent et al., 1998), antiSqh [1:10, 64 h incubation time; anti Phospho-Myosin Light Chain 2 (ser19), #3671 Cell Signaling; dilution according to Saxena et al., 2014; Nie et al., 2014] and anti-Trol (Perlecan domain V, 1:2000; gift from Stefan Baumgartner, Lund University, Sweden; Friedrich et al., 2000). The following secondary antibodies were used: anti-rat Cy3 (1:500; Jackson ImmunoResearch Laboratories), anti-rat Alexa Fluor[®] 488 (1:500; Jackson ImmunoResearch Laboratories), anti-rabbit DyLight 488 (1:500; Vector Laboratories), anti-rabbit DyLight 549 (1:500; Vector Laboratories). For visualization of F-actin, we used Phalloidin-Atto 565 (4 nmol l⁻¹; 94072, Sigma-Aldrich, St. Louis, MO, USA); to visualize nuclei, Hoechst 33342 was used (3.2 µg ml⁻¹; 62249, Thermo Fisher Scientific, Waltham, MA, USA).

Live imaging of ex vivo cultures

Male white prepupae were collected at 0 h APF and aged on a moistened filter. Genital discs and pupal testes were dissected in culture medium and transferred into a tissue culture treated µ-Dish^{35mm,high} (81156, ibidi, Martinsried, Germany) containing 2 ml culture medium Shields and Sang M3 Insect Medium (S8398, Sigma-Aldrich) was made according to Aldaz et al. (2010) by filtering and supplementing with 2% fetal bovine serum (S0113, Biochrom AG, Berlin, Germany), 0.5% penicillin-streptomycin (P11-010, PAA, Cambridge, UK), and 0.1 µg ml⁻¹ Ecdysone (H5142, Sigma-Aldrich). Culture medium worked successfully for up to 4 days when stored at 4°C. A Zeiss AxioObserver Z.1 inverse microscope was used for live imaging. A Z-stack was acquired every 15 min for up to 10 h.

Image acquisition and processing

Conventional fluorescent images and optical sections were captured with a Zeiss AxioObserver Z.1 inverse microscope with ApoTome function. Images were taken and processed with AxioVision LE64 (Carl Zeiss Microscopy GmbH, Jena, Germany), figures were assembled with Adobe Photoshop CS6 (Adobe Systems Incorporated, San José, CA, USA), and models were generated in Adobe Illustrator CS6 (Adobe Systems Incorporated). Charts were generated in Microsoft Excel 2016 (Microsoft Corporation, Redmond, WA, USA).

Acknowledgements

We thank Katja Gessner for secretarial assistance, Peer Fender for graphic design expertise, Ljubinka Cigoja for help in dissecting and fly work, Hedda Wassum for initial experiments, Karen Linnemannstons for advice on ex vivo testes cultures, Angelike Stathopoulos for fly lines, Maria Leptin and Stefan Baumgartner for antibodies, and Karen A. Brune for linguistic revision of the manuscript.

Competing interests

The authors declare no competing or financial interests.

Author contributions

Conceptualization: S.R.-F., K.F., R.R.-P.; Methodology: S.R.-F., K.F., M.C.B.; Validation: S.R.-F., K.F., M.C.B., D.B.; Investigation: S.R.-F., K.F., M.C.B., D.B.;

Writing - original draft: S.R.-F., K.F., R.R.-P.; Writing - review & editing: R.R.-P.; Visualization: M.C.B., D.B., S.F.O.; Supervision: S.F.O., R.R.-P.; Project administration: R.R.-P.; Funding acquisition: R.R.-P.

Funding

This work was supported by the Deutsche Forschungsgemeinschaft [Re 628/16-1, GRK 1216 and GRK 2213].

Supplementary information

Supplementary information available online at <http://bio.biologists.org/lookup/doi/10.1242/bio.025940.supplemental>

References

- Ahmad, S. M. and Baker, B. S. (2002). Sex-specific deployment of FGF signaling in *Drosophila* recruits mesodermal cells into the male genital imaginal disc. *Cell* **109**, 651-661.
- Aldaz, S., Escudero, L. M. and Freeman, M. (2010). Live imaging of *Drosophila* imaginal disc development. *Proc. Natl. Acad. Sci. USA* **107**, 14217-14222.
- Awe, S. and Renkawitz-Pohl, R. (2010). Histone H4 acetylation is essential to proceed from a histone- to a protamine-based chromatin structure in spermatid nuclei of *Drosophila melanogaster*. *Syst. Biol. Reprod. Med.* **56**, 44-61.
- Baylies, M. K., Martinez Arias, A. and Bate, M. (1995). wingless is required for the formation of a subset of muscle founder cells during *Drosophila* embryogenesis. *Development* **121**, 3829-3837.
- Bertrand, V. (2016). Beta-catenin-driven binary cell fate decisions in animal development. *Wiley Interdiscip. Rev. Dev. Biol.* **5**, 377-388.
- Bodenstein, D. (1950). The postembryonic development of *Drosophila*. In *Biology of Drosophila* (ed. M. Demerec), pp. 275-367. New York: John Wiley & Sons, Inc.
- Bulgakova, N. A., Klapholz, B. and Brown, N. H. (2012). Cell adhesion in *Drosophila*: versatility of cadherin and integrin complexes during development. *Curr. Opin. Cell Biol.* **24**, 702-712.
- Campellone, K. G. and Welch, M. D. (2010). A nucleator arms race: cellular control of actin assembly. *Nat. Rev. Mol. Cell Biol.* **11**, 237-251.
- Combedazou, A., Choesmel-Cadamuro, V., Gay, G., Liu, J., Dupre, L., Ramel, D. and Wang, X. (2016). Myosin II governs collective cell migration behaviour downstream of guidance receptor signalling. *J. Cell Sci.* **130**, 97-103.
- Estrada, B., Casares, F. and Sánchez-Herrero, E. (2003). Development of the genitalia in *Drosophila melanogaster*. *Differentiation* **71**, 299-310.
- Friedrich, M. V. K., Schneider, M., Timpl, R. and Baumgartner, S. (2000). Perlecan domain V of *Drosophila melanogaster*. Sequence, recombinant analysis and tissue expression. *Eur. J. Biochem.* **267**, 3149-3159.
- Gärtner, S. M. K., Rathke, C., Renkawitz-Pohl, R. and Awe, S. (2014). Ex vivo Culture of *Drosophila* pupal testis and single male germ-line cysts: dissection, imaging, and pharmacological treatment. *J. Vis. Exp.* **91**, e51868.
- Gisselbrecht, S., Skeath, J. B., Doe, C. Q. and Michelson, A. M. (1996). heartless encodes a fibroblast growth factor receptor (DFR1/DFGF-R2) involved in the directional migration of early mesodermal cells in the *Drosophila* embryo. *Genes Dev.* **10**, 3003-3017.
- Glazer, L. and Shilo, B. Z. (1991). The *Drosophila* FGF-R homolog is expressed in the embryonic tracheal system and appears to be required for directed tracheal cell extension. *Genes Dev.* **5**, 697-705.
- Greig, S. and Akam, M. (1995). The role of homeotic genes in the specification of the *Drosophila* gonad. *Curr. Biol.* **5**, 1057-1062.
- Gryzik, T. and Müller, H.-A. J. (2004). FGF8-like1 and FGF8-like2 encode putative ligands of the FGF receptor Htl and are required for mesoderm migration in the *Drosophila* gastrula. *Curr. Biol.* **14**, 659-667.
- Imam, F., Sutherland, D., Huang, W. and Krasnow, M. A. (1999). stumps, a *Drosophila* gene required for fibroblast growth factor (FGF)-directed migrations of tracheal and mesodermal cells. *Genetics* **152**, 307-318.
- Irizarry, J. and Stathopoulos, A. (2015). FGF signaling supports *Drosophila* fertility by regulating development of ovarian muscle tissues. *Dev. Biol.* **404**, 1-13.
- Itoh, N. and Ornitz, D. M. (2011). Fibroblast growth factors: From molecular evolution to roles in development, metabolism and disease. *J. Biochem.* **149**, 121-130.
- Kadam, S., McMahon, A., Tzou, P. and Stathopoulos, A. (2009). FGF ligands in *Drosophila* have distinct activities required to support cell migration and differentiation. *Development* **136**, 739-747.
- Kadam, S., Ghosh, S. and Stathopoulos, A. (2012). Synchronous and symmetric migration of *Drosophila* caudal visceral mesoderm cells requires dual input by two FGF ligands. *Development* **139**, 699-708.
- Karess, R. E., Chang, X., Edwards, K. A., Kulkarni, S., Aguilera, I. and Kiehart, D. P. (1991). The regulatory light chain of nonmuscle myosin is encoded by spaghetti-squash, a gene required for cytokinesis in *Drosophila*. *Cell* **65**, 1177-1189.
- Klämbt, C., Glazer, L. and Shilo, B.-Z. (1992). breathless, a *Drosophila* FGF receptor homolog, is essential for migration of tracheal and specific midline glial cells. *Genes Dev.* **6**, 1668-1678.

- Kozopas, K. M., Samos, C. H. and Nusse, R.** (1998). DWnt-2, a *Drosophila* Wnt gene required for the development of the male reproductive tract, specifies a sexually dimorphic cell fate. *Genes Dev.* **12**, 1155-1165.
- Kreisköther, N., Reichert, N., Buttgerit, D., Hertenstein, A., Fischbach, K.-F. and Renkawitz-Pohl, R.** (2006). *Drosophila* Rolling pebbles colocalises and putatively interacts with alpha-Actinin and the Sls isoform Zormin in the Z-discs of the sarcomere and with Dumbfounded/Kirre, alpha-Actinin and Zormin in the terminal Z-discs. *J. Muscle Res. Cell Motil.* **27**, 93-106.
- Kuckwa, J., Fritzen, K., Buttgerit, D., Rothenbusch-Fender, S. and Renkawitz-Pohl, R.** (2016). A new level of plasticity: *Drosophila* smooth-like testes muscles compensate failure of myoblast fusion. *Development* **143**, 329-338.
- Leptin, M. and Grunewald, B.** (1990). Cell shape changes during gastrulation in *Drosophila*. *Development* **110**, 73-84.
- Lim, J. and Thiery, J. P.** (2012). Epithelial-mesenchymal transitions: insights from development. *Development* **139**, 3471-3486.
- Linnemannstöns, K., Ripp, C., Honemann-Capito, M., Brechtel-Curth, K., Hedderich, M. and Wodarz, A.** (2014). The PTK7-related transmembrane proteins off-track and off-track 2 are co-receptors for *Drosophila* Wnt2 required for male fertility. *PLoS Genet.* **10**, e1004443.
- Majumder, P., Aranjuez, G., Amick, J. and McDonald, J. A.** (2012). Par-1 controls myosin-II activity through myosin phosphatase to regulate border cell migration. *Curr. Biol.* **22**, 363-372.
- Mansfield, G. S., Al-Shirawi, D. Y., Ketchum, A. S., Newbern, C. E. and Kiehart, D. P.** (1996). Molecular organization and alternative splicing in zipper, the gene that encodes the *Drosophila* non-muscle myosin II heavy chain. *J. Mol. Biol.* **255**, 98-109.
- Michelson, A. M., Gisselbrecht, S., Buff, E. and Skeath, J. B.** (1998a). Heartbroken is a specific downstream mediator of FGF receptor signalling in *Drosophila*. *Development* **125**, 4379-4389.
- Michelson, A. M., Gisselbrecht, S., Zhou, Y., Baek, K.-H. and Buff, E. M.** (1998b). Dual Functions of the heartless fibroblast growth factor receptor in development of the *Drosophila* embryonic mesoderm. *Dev. Genet.* **22**, 212-229.
- Munoz-Descalzo, S., Hadjantonakis, A. K. and Arias, A. M.** (2015). Wnt/Beta-catenin signalling and the dynamics of fate decisions in early mouse embryos and embryonic stem (ES) cells. *Semin. Cell Dev. Biol.* **47-48**, 101-109.
- Nanda, S., DeFalco, T. J., Loh, S. H. Y., Phochanukul, N., Camara, N., Van Doren, M. and Russell, S.** (2009). Sox100B, a *Drosophila* group E Sox-domain gene, is required for somatic testis differentiation. *Sex. Dev.* **3**, 26-37.
- Nie, J., Mahato, S. and Zelhof, A. C.** (2014). The actomyosin machinery is required for *Drosophila* retinal lumen formation. *PLoS Genet.* **10**, e1004608.
- Ornitz, D. M. and Itoh, N.** (2015). The fibroblast growth factor signaling pathway. *Wiley Interdiscip. Rev. Dev. Biol.* **4**, 215-266.
- Peifer, M., McCrea, P. D., Green, K. J., Wieschaus, E. and Gumbiner, B. M.** (1992). The Vertebrate adhesive junction proteins beta-catenin and plakoglobin and the *Drosophila* segment polarity gene *armadillo* form a multigene family with similar properties. *Cell* **118**, 681-691.
- Pocha, S. M. and Montell, D. J.** (2014). Cellular and molecular mechanisms of single and collective cell migrations in *Drosophila*: themes and variations. *Annu. Rev. Genet.* **48**, 295-318.
- Ranganayakulu, G., Zhao, B., Dokidis, A., Molkentin, J. D., Olson, E. N. and Schulz, R. A.** (1995). A series of mutations in the D-MEF2 transcription factor reveal multiple functions in larval and adult myogenesis in *Drosophila*. *Dev. Biol.* **171**, 169-181.
- Reim, I., Hollfelder, D., Ismat, A. and Frasch, M.** (2012). The FGF8-related signals Pyramus and Thisbe promote pathfinding, substrate adhesion, and survival of migrating longitudinal gut muscle founder cells. *Dev. Biol.* **368**, 28-43.
- Roca-Cusachs, P., Sunyer, R. and Trepats, X.** (2013). Mechanical guidance of cell migration: lessons from chemotaxis. *Curr. Opin. Cell Biol.* **25**, 543-549.
- Rudolf, A., Buttgerit, D., Jacobs, M., Wolfstetter, G., Kesper, D., Pütz, M., Berger, S., Renkawitz-Pohl, R., Holz, A. and Önel, S. F.** (2014). Distinct genetic programs guide *Drosophila* circular and longitudinal visceral myoblast fusion. *BMC Cell Biol.* **15**, 27.
- Saxena, A., Denholm, B., Bunt, S., Bischoff, M., Vijayaraghavan, K. and Skaer, H.** (2014). Epidermal growth factor signalling controls myosin II planar polarity to orchestrate convergent extension movements during *Drosophila* tubulogenesis. *PLoS Biol.* **12**, e1002013.
- Shilo, B.-Z.** (2016). New twists in *Drosophila* cell signaling. *J. Biol. Chem.* **291**, 7805-7808.
- Shishido, E., Higashijima, S., Emori, Y. and Saigo, K.** (1993). Two FGF-receptor homologues of *Drosophila*: one is expressed in mesodermal primordium in early embryos. *Development* **117**, 751-761.
- Stathopoulos, A., Tam, B., Ronshaugen, M., Frasch, M. and Levine, M.** (2004). Pyramus and thisbe: FGF genes that pattern the mesoderm of *Drosophila* embryos. *Genes Dev.* **18**, 687-699.
- Stern, C.** (1941). The Growth of Testes in *Drosophila* I. The relation between vas deferens and testis within various species. *J. Exp. Zool.* **87**, 113-158.
- Susic-Jung, L., Hornbruch-freitag, C., Kuckwa, J., Rexer, K.-H., Lammel, U. and Renkawitz-pohl, R.** (2012). Multinucleated smooth muscles and mononucleated as well as multinucleated striated muscles develop during establishment of the male reproductive organs of *Drosophila melanogaster*. *Dev. Biol.* **370**, 86-97.
- Vicente-Manzanares, M., Ma, X., Adelstein, R. S. and Horwitz, A. R.** (2009). Non-muscle myosin II takes centre stage in cell adhesion and migration. *Nat. Rev. Mol. Cell Biol.* **10**, 778-790.
- Vincent, S., Wilson, R., Coelho, C., Affolter, M. and Leptin, M.** (1998). The *Drosophila* protein Dof is specifically required for FGF signaling. *Mol. Cell* **2**, 515-525.
- Vissers, J. H. A., Manning, S. A., Kulkarni, A. and Harvey, K. F.** (2016). A *Drosophila* RNAi library modulates Hippo pathway-dependent tissue growth. *Nat. Commun.* **7**, 10368.
- Voigt, A., Pflanz, R., Schäfer, U. and Jäckle, H.** (2002). Perlecan participates in proliferation activation of quiescent *Drosophila* neuroblasts. *Dev. Dyn.* **224**, 403-412.

Suppl Figures and Tables

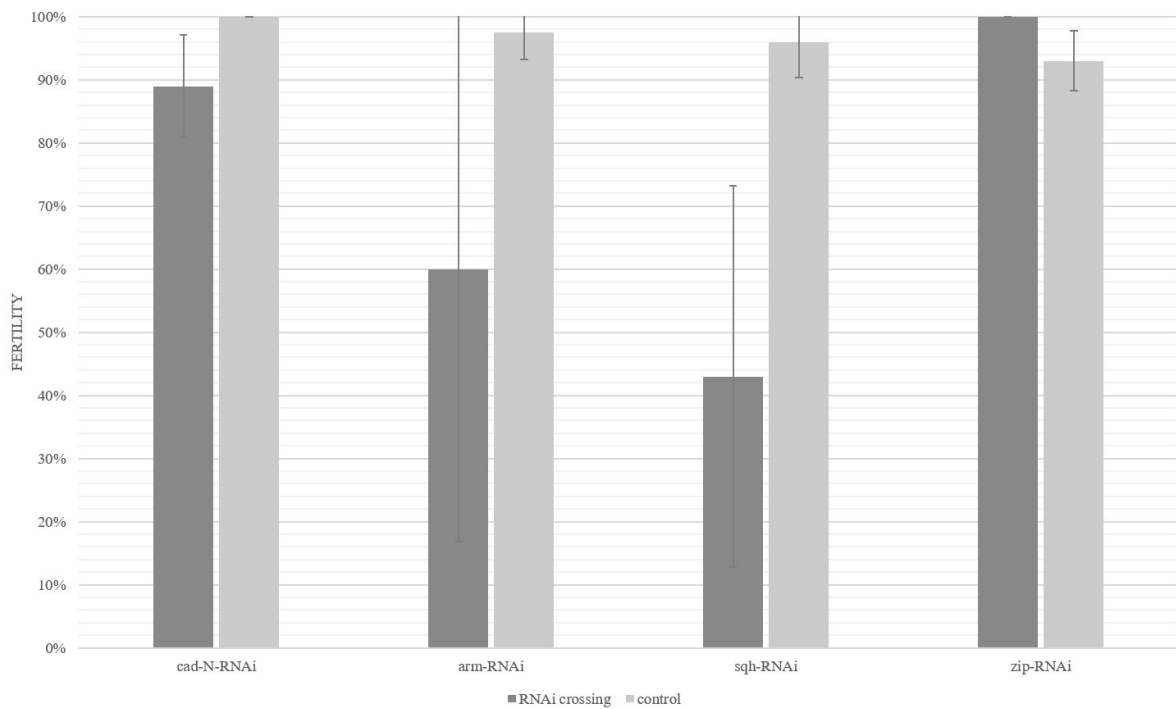


Figure S1: Fertility of males after RNAi knock-down experiments. Mef2- or Mef2>>Dcr2-driven RNAi males were crossed with three wild type virgin females. For controls, RNAi males were tested under the same circumstances. Neither *cad-N* knock-down nor *zip* knock-down resulted in reduced male fertility. Fertility of the males was reduced only upon down-regulation of *sqh* and *arm*. $n = 30$.

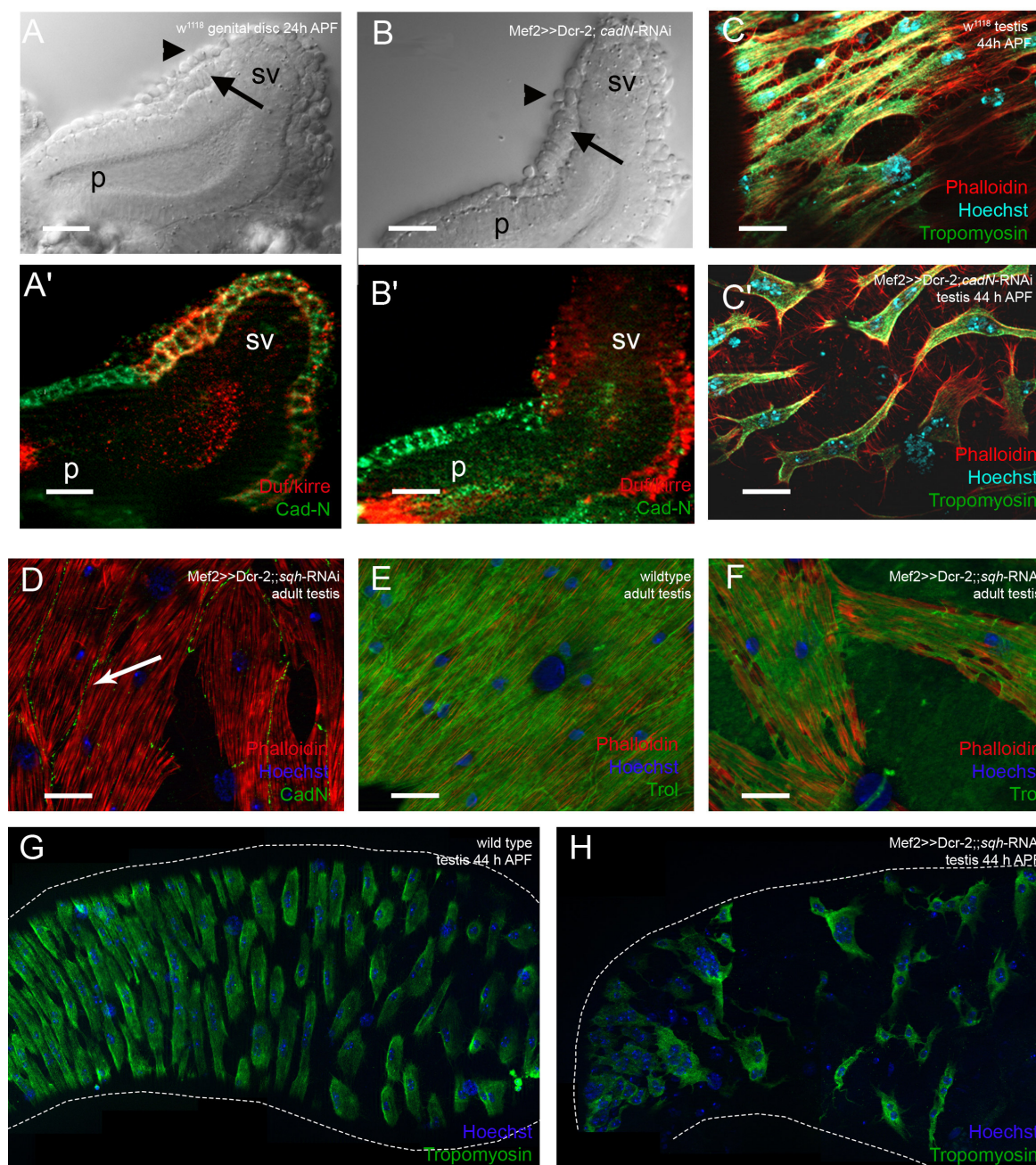


Figure S2: Reduction of Cad-N or Spaghetti squash does not influence expression of Trol in adult testes but disturbs efficient population of the testes with muscles. (A, B) Differential interference contrast (DIC) micrograph of testis 44 h APF; 8A'-H: immunofluorescence; Phalloidin (red) labels F-actin, and Hoechst (blue) visualises nuclei. (A) On genital discs of wild type males FC-like (arrow) and FCM-like (arrowhead) myoblasts are visible in interference contrast. (A') The adhesion protein Duf/Kirre was expressed in FC-like

myoblasts on seminal vesicles 24 h APF. B) After knock down of *cad-N*, FC-like (arrow) and FCM-like myoblasts (arrow head) were detectable and B') Duf/Kirre expression was maintained. (C, C') At 44 h APF, pupal *cad-N* knock-down testes (C') contain nascent myotubes with less elongated shapes; the number of myotubes might be reduced (compare to C, wild type). (D) Cad-N was expressed between adjacent myotubes (arrow) in *sqh* knock-down testes. (E) The ECM protein Trol was expressed in the muscle sheath of wild type testes and (F) in the irregular-shaped muscles upon *sqh* knock-down. (G) Pupal wild type testes at 44 h APF. (G) Pupal *sqh* knock-down testes at 44 h APF showed little defects in shape (compare to F), but are covered with fewer nascent myotubes. Scale bars, 20 μ m.

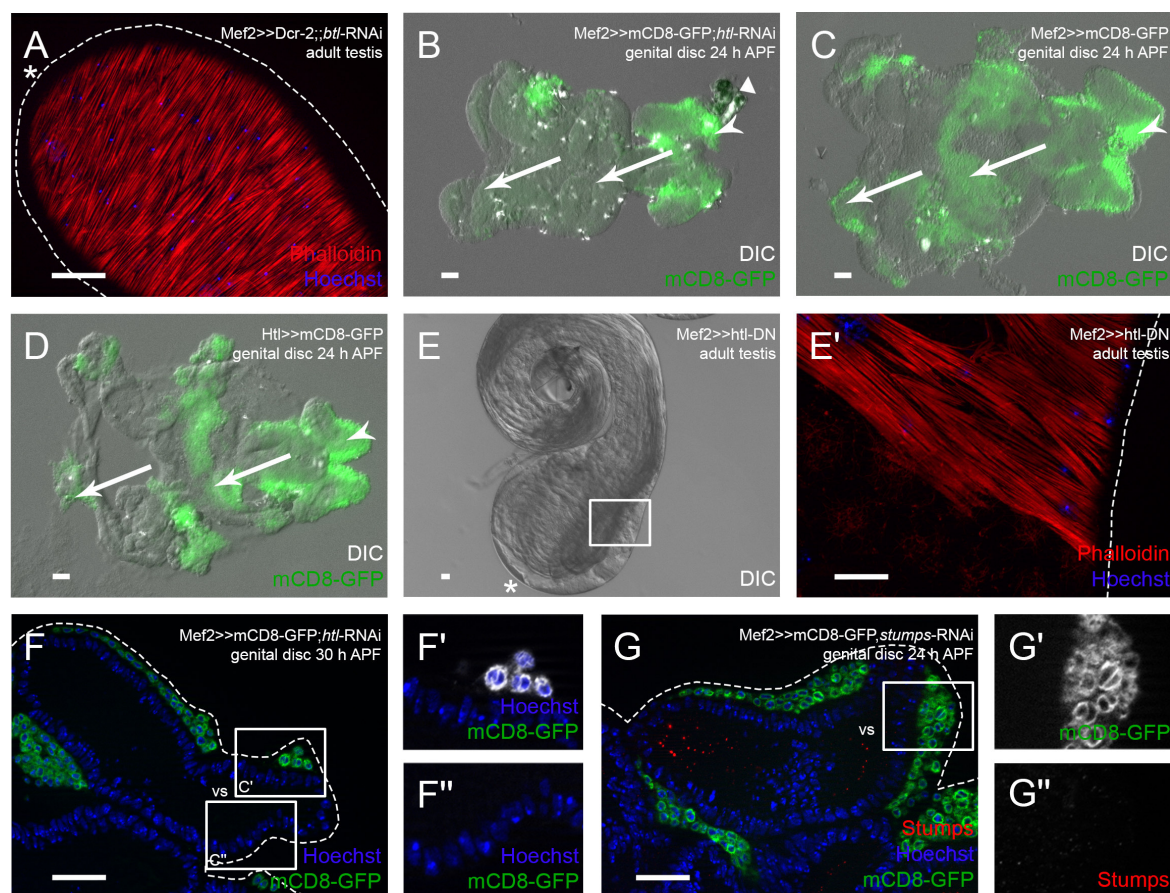


Figure S3: Analysis of FGF-signaling components (A) Down-regulation of *htl* did not affect the adult testis muscle sheath. (B) Upon *htl* knock-down, the number of myoblasts on genital discs 24 h APF was severely reduced in the posterior part (compare to C; arrows), whereas testis-relevant myoblasts accumulated over the prospective seminal vesicle. Triangle indicates fat tissue. (C) Myoblasts on genital discs 24 h APF. (D) *Htl*-Gal4 drives expression in posterior myoblasts (arrows) and in testis-relevant myoblasts (arrowhead) on genital discs 24 h APF. (E) Myoblast-specific expression of *Htl*-dominant negative (DN) produced an adult testis with a bulky tip. (E') In the *htl*-DN background, testis muscles did not cover the bulky tips. (F–F'') At 30 h APF, *htl* knock-down (BL35024) seminal vesicles exhibited a severely reduced number of myotubes. F' and F'' show enlargements of the respective boxed areas in F. (G–G'') On *stumps* knock-down genital discs 24 h APF, *Stumps* was not expressed. Phalloidin (red) visualizes F-actin, Hoechst (blue) labels nuclei. On genital discs, myoblasts and nascent myotubes are marked with *Mef2*-driven *mCD8-GFP*. Asterisk marks testis hubs. Dotted lines reflect approximate organ shape. Scale bars, 20 μm.

Table S1: Phenotypes of RNAi fly lines

RNAi fly line	Testis phenotype	Predicted off-targets
Mef2>>Dcr-2; <i>cadN</i> -RNAi v1092	shape: not coiled properly muscle sheath: not continuous	none
Mef2>>Dcr-2; <i>cadN</i> -RNAi v1093*	shape: not coiled properly muscle sheath: not continuous	none
Mef2>> <i>cadN</i> -RNAi v101642	shape: wt muscle sheath: some holes	CadN2
Mef2>>Dcr-2;; <i>sqh</i> -RNAi BL32439*	shape: small and thickly muscle sheath: not encircling	none
Mef2>>Dcr-2;; <i>sqh</i> -RNAi BL33892	shape: wt muscle sheath: holes	none
Mef2>>Dcr-2;; <i>zip</i> -RNAi BL36727	shape: small and thickly muscle sheath: big holes	none
Mef2>>Dcr-2; <i>zip</i> -RNAi BL37480*	shape: coiled with big testis tip muscle sheath: holes	none
Mef2>> <i>arm</i> -RNAi BL31304*	shape: many thickenings muscle sheath: short muscles, holes	Sequoia (zink finger protein)
Mef2>> <i>arm</i> -RNAi BL35004	shape: wt muscle sheath: wt	none
Mef2>>Dcr-2;; <i>btl</i> -RNAi BL40871	shape: wt muscle sheath: wt	none
Mef2>>Dcr-2; <i>btl</i> -RNAi v27106*	shape: wt muscle sheath: wt	none
Mef2>>Dcr-2;; <i>htl</i> -RNAi BL35024	shape: coiled with big testis tip muscle sheath: no muscles at tip	none
Mef2>> <i>htl</i> -RNAi v6692*	shape: small and round, no connection to vs muscle sheath: no muscles	none
Mef2>> <i>stumps</i> -RNAi v21317*	shape: variable, small and round, but connected to vs muscle sheath: variable, no muscles at apical region	none

Mef2>> <i>stumps</i> -RNAi v105603	shape: variable, small and round, but connected to vs muscle sheath: variable, big regions without muscles	none
---------------------------------------	---	------

wt = wild type; vs = seminal vesicle; * = presented in Results

3.2 Publication 2

Filopodia-based contact stimulated collective migration drives tissue morphogenesis

Maik C. Bischoff, Sebastian Lieb, Renate Renkawitz-Pohl, Sven Bogdan

Filopodia-based contact stimulated collective migration drives tissue morphogenesis

Maik C. Bischoff¹, Sebastian Lieb², Renate Renkawitz-Pohl³ and Sven Bogdan^{1*}

¹ Institute of Physiology and Pathophysiology, Dept. of Molecular Cell Physiology, Philipps-University Marburg, Germany.

² Computer Graphics and Multimedia Programming, Philipps-University Marburg, Germany.

³ Developmental Biology, Philipps-University Marburg, Germany.

*) to whom correspondence should be addressed

sven.bogdan@staff.uni-marburg.de

Key words

Drosophila, testis myotubes, collective cell migration, contact inhibition of locomotion, CIL, contact stimulation of migration, cell-matrix adhesion, cell shape, lamellipodia, filopodia, cell motility, actin, Arp2/3, WAVE, formins, Cdc42, Rac, Rho, N-cadherin, actomyosin, computer simulation

Abstract

Cells migrate collectively to form tissues and organs during morphogenesis. Contact inhibition of locomotion (CIL) drives collective migration by inhibiting lamellipodial protrusions at cell-cell contacts and promoting polarization at the leading edge. Here, we report on a CIL-related collective cell behavior of myotubes that lack lamellipodial protrusions, but instead use filopodia to move as a cohesive cluster in a formin-dependent manner. Genetic, pharmacological and mechanical perturbation analyses reveal essential roles of Rac2, Cdc42 and Rho1 in myotube migration. They differentially control not only protrusion dynamics but also cell-matrix adhesion formation. Here, active Rho1 GTPase localizes at retracting free edge filopodia. Rok-dependent actomyosin contractility does not mediate a contraction of protrusions at cell-cell contacts but likely plays an important role in the constriction of supracellular actin cables.

We propose that contact-dependent asymmetry of cell-matrix adhesion drives directional movement, whereas contractile actin cables contribute to the integrity of the migrating cell cluster.

Introduction

The ability of cells to migrate as a collective is crucial during tissue morphogenesis and remodeling^{1,2}. The molecular principles of collective cell migration share features with the directed migration of individual cells. The major driving forces in migrating single cells are Rac-mediated protrusions of lamellipodia at the leading edge, formed by Arp2/3 complex dependent actin filament branching and Rho-dependent actomyosin driven contraction at the cell rear^{3,4}. Cells can migrate directionally in response to a variety of chemical cues, recognized by cell surface receptors that initiate downstream signaling cascades controlling the activity or recruitment of Rho GTPases. Directional cell locomotion is also controlled by mechanical stimuli such as upon cell-cell contact⁵⁻⁷. A well-known phenomenon is contact inhibition of locomotion (CIL), whereby two colliding cells change direction after coming into contact^{8,9}. Mayor and colleagues provided first mechanistic evidence how CIL might act *in vivo* as the driving force to polarize neural crest cells that derived from the margin of the neural tube and disperse by migration during embryogenesis^{10,11}.

In neural crest cells, CIL involves distinct stages of cell behavior including cell-cell contact, protrusion inhibition, repolarization, contraction and migration away from the collision¹². The initial cell-cell contact requires the formation of transient cadherin-mediated cell junctions. Once the cells come in close contact, a disassembly of cell-matrix adhesions near the cell-cell contact and the generation of new cell-matrix adhesions at the free edge occur. Such mechanical crosstalk between N-cadherin-mediated cell-cell adhesions and integrin-dependent cell-matrix adhesions has been recently described *in vivo* during neural crest cell migration in both *Xenopus* and zebrafish embryos¹³. However, the loss of cell-matrix adhesions at cell contacts alone is not sufficient to drive CIL. A subsequent repolarization of the cells away from the cell-cell contact and thereby the generation of new cell-matrix adhesions and protrusions at the free edge are required to induce cell migration away from the collision. In neural crest cells, this depends on the polarized activity of the two Rho GTPases, Rac1 and RhoA¹⁴. A model of CIL has been proposed in which a contact-dependent intracellular Rac1/RhoA gradient is formed that generates an asymmetric force driving directed cell migration¹⁵. N-cadherin binding triggers a local increase of RhoA and inhibits Rac1 activity at the site of contact^{14,16}. Thus, Rac1-dependent

protrusions become biased to the opposite end of the cell-cell contact and cells migrating away from the collision.

Overall, CIL has been successfully used to explain contact-dependent collective migration of loose clusters of mesenchymal cells such as neural crest cells and hemocytes¹², but it is still unclear whether mechanisms governing CIL might also contribute to the migratory behavior of cohesive cell clusters or epithelia^{5,7}.

Here, using an integrated live-cell imaging and genetic approach, we identified a CIL related, contact-dependent migratory behavior of highly cohesive nascent myotubes of the *Drosophila* testis. Myotubes lack lamellipodial cell protrusions, but instead form numerous large filopodia generated at both N-cadherin-enriched cellular junctions at cell-cell contacts and integrin-dependent cell-matrix sites at their free edge. Filopodia-based myotube migration requires formins and the Rho family small GTPases Rac2, Cdc42 and RhoA, whereas the Arp2/3 complex and its activator, the WAVE regulatory complex (WRC) seem only to contribute to filopodia branching. Rac2 and Cdc42 differentially control not only protrusion dynamics but also cell-matrix adhesion formation. Unlike CIL, RhoA is not activated at cell-cell contacts, but rather gets locally activated along retracting protrusions. Genetic and pharmacological perturbation analysis further revealed an important requirement of Rho/Rok-driven actomyosin contractility in myotube migration.

In summary, we propose a model in which N-cadherin-mediated contact dependent asymmetry of cell-matrix adhesion acts as a major switch to drive cell movement towards the free space, whereas contractile actin cables contribute to the integrity of the migrating cell cluster.

Results

Long-term live imaging of *Drosophila* smooth-like testes muscles as a new collective cell migration model

At 24h after puparium formation (APF), both testes lay free in the body cavity (Figure 1a). The genital disc provides the myoblasts and other somatic parts of the reproductive system such as the seminal vesicles^{17,18}. Testes myoblasts adhere to the epithelium of the seminal vesicles (Figure 1a, sv) and fuse to small syncytia shortly before the connection between seminal vesicles and terminal epithelia (Figure 1a, te) has been formed (Figure 1a, b^{19,20}). Between 28-30h APF this connection has been

established (Figure 1, see arrow between a and b). At 30 h APF nascent myotubes (Figure 1b, mt in red) start to migrate beneath the pigment cell layer (Figure 1b, pc) to and along the testes towards the apical end (Figure 1b²¹). At 40 h APF, myotubes cover the whole pupal testis as a thin muscular sheet²².

To better understand how myotubes cover the testis, we established a protocol for *ex vivo* organ cultivation and long-term imaging (7 h) of isolated 33h APF pupal testes (Figure 1c). We used the muscle-specific *mef2*-Gal4 or the *heartless*-Gal4 (*htl*-Gal4) driver to express a UAS-LifeAct-EGFP transgene either in myotubes or in both, myotubes and pigment cells respectively (see supplementary figure S2a). This method provides an excellent experimental system for studying the highly dynamic migratory cell behavior of myotubes and to visualize their actin-rich protrusions over several hours at high resolution. Spinning disc live imaging microscopy of 33 h APF old testes onwards revealed that myotubes migrate collectively on an ellipsoid surface constrained by the outermost layer of pigment cells and the basal membrane enclosing the inner cysts (Figure 1d, e; supplementary movie M1). To better track the migratory behavior of individual cells within the cell cluster we additionally labeled the cells by co-expression of the membrane marker mCD8-RFP enabling precise 4D (xyz and t) trajectory mapping using the Imaris software (Figure 1f; supplementary movie M2). Since all mathematical directionality descriptors for 2D migration (biased angle, persistence angle, straightness, etc.) are based on Euclidean geometry, we had to transform our 3D(+time) datasets into corresponding 2D(+time) datasets for precise cell quantification. A simple xy-projection would neglect curvature and lead to wrong results. Preexisting tools using unwrapping algorithms and Riemannian manifold learning were not compatible with our system²³. Instead of an unwrapping algorithm fit for every kind of surface, but with some restrictions in angle and distance accuracy, we developed a Mercator-projection based process, which allows for high angle-accuracy but neglects distances (illustrated in supplementary figure S3 b-f).

Dissecting the cell trajectories of wild type myotubes revealed a directional cell behavior with maximal cell movement into the base-apex direction with a speed about 0.37 $\mu\text{m}/\text{min}$ over a distance of about 130 μm (Figure 1f', Figure 4q, supplementary figure S2g; supplementary movie M2). Once myotubes reached the testis apex they started to elongate and form large actin bundles that aligned perpendicular to the pupal testis surface (Figure 1g, supplementary movie M1, middle). After completing pupal

development, myotubes form a densely packed muscle sheath surrounding the elongated, tubular adult testis (Figure 1h, h').

Myotube migration depends on formin-dependent filopodial membrane protrusions

Strikingly, migrating myotubes largely lacked lamellipodial protrusions, but instead formed numerous filopodia-like protrusions (from here on referred to as filopodia; Figure 1i; supplementary movie M3). Expression of LifeAct-EGFP together with a nuclear targeted EGFP transgene in myotubes in a mosaic-like fashion further showed that myotubes also formed prominent filopodial protrusion between neighboring cells (Figure 1j.; supplementary movie M4). To better characterize the distribution of filopodia in these cells, we quantified the directionality of filopodia of cells by measuring the orientation angle as illustrated in figure 1m and m'. This analysis revealed no strong bias in filopodia generation or directionality in cells within the cluster (Figure 1n) and surprisingly also at the front edge of the cluster (Figure 1o). To statistically analyze this, we differentiate the filopodia (in cells at the front edge) in those which are assembled at the cell front (pointing to the testis apex) and those at the "rear" (pointing to the testis base; Figure 1kl). To account for irregular cell shapes, we calculated the density (number/ μm) by measuring edge length. There was no significant difference in filopodia density between front and rear. Thus, the directionality of collective myotube migration cannot be simply predicted by filopodia number or direction.

We next determined how central actin nucleators such as formins and the Arp2/3 complex contribute to filopodia formation and myotube migration. Treatment with the specific Arp2/3 inhibitor CK-666²⁴ did not strongly affect the overall cell cluster morphology compared to control cells incubated with DMSO (Figure 2a, b and c; supplementary movie M5). Likewise, cells depleted of the *arp3* subunit or *wave* by RNA interference (RNAi) showed moderate changes in cell morphology despite prominent fusion defects (see mononucleated myotubes marked by co-expression of the mCD8-RFP marker excluded from the nuclei in figure 2e; supplementary movie M6). Similar to CK666 treatment, *arp3* and *wave* depleted cells were still able to migrate persistently in a directed fashion (Figure 2b-e'; supplementary figure S2h. However, cells depleted of the *arp3* subunit or treated with CK666 showed a significantly reduced migration

speed and distance along the x-axis (compare migratory tracks in figure 2a, b and d; quantification in figure 2h supplementary figure S2g). Thus, the Arp2/3-WRC pathway promotes motility, but seems to be dispensable for directed migration of myotubes.

By contrast, treatment with the pan-formin small-molecule inhibitor SMIFH2²⁵ strongly affected cell morphology and completely disrupted collective myotube migration (Figure 2f, g and g'; supplementary movie M7; quantification in figure 2h, S2 g). Compared to CK666 treatment, cells treated with SMIFH2 showed a prominent reduced number of dynamic, but instead highly branched filopodia-like protrusions (Figure 2k; supplementary movie M7). Interestingly, cells co-treated with CK666 and SMIFH2 completely lacked these branched filopodial protrusions suggesting that their formation or branching depends on a still prominent Arp2/3 complex activity in SMIFH2 treated cells (Figure 2l). Supporting this notion, cells only depleted for Arp3 showed a reduction in filopodia branches resulting in a significant reduction of protrusions (Figure 3a, b; quantification in c). Consistently, an Arp3-EGFP transgene localized close to newly forming branches as we recently found in dendrite branchlet formation of *Drosophila* larval sensory neurons (arrowheads in Figure 3d, e²⁶). Interestingly, we also found a strong accumulation of the Arp3-EGFP at cell-cell contacts, an observation made in different cell systems (asterisks in Figure 3e').

Taken together, these findings suggest that Arp2/3 activity is required in filopodia-branching, whereas the activity of formins are essential to generate filopodial protrusions. RNAi-mediated suppression of single *Drosophila* formins did not result in prominent protrusion or migration defects (see supplementary table 1), suggesting a potential redundant and synergistic functions of different formins in protrusion formation.

Migrating myotubes preferentially form more stable cell-matrix adhesions at their free edge

It is generally believed that filopodia may promote mesenchymal migration by promoting cell-matrix adhesiveness at the leading edge to stabilize the advancing lamellipodium²⁷. Migrating myotubes lack lamellipodia, but instead filopodia appear to be critical for myotube migration as inhibition of their formation by interfering with formin function results in a complete loss of migration. Expression of a cell-matrix adhesion

targeting reporter (FAT-EGFP²⁸) revealed that migrating myotubes indeed formed numerous cell-matrix anchorage sites at the base, along the shaft, and at the tip of filopodia (Figure 3f; supplementary movie M8). Multiple cell-matrix adhesions were built in a single filopodium, giving them a beaded appearance (Figure 3g; supplementary movie M8). Cell-matrix adhesions formed along filopodia shafts subsequently seemed to move rearwards, along a retrograde flow of bundled actin filaments, eventually getting disassembled in the outer rim of the cell body (Figure 3g; supplementary movie M8). Co-expression with a LifeAct-RFP reporter marked especially thicker actin bundles attached to large, more elongated cell-matrix adhesion structures that shows a more classical appearance of matrix adhesions found in lamellipodia (Figure 3h-h’’).

Remarkably, the number of cell-matrix adhesions within single cells at the front edge of the cluster correlates with the presumed direction of migration towards the testis tip (Figure 3k). Cells formed an increased number of cell-matrix adhesions at the migrating front (pointing to the testis apex; figure 3i) when compared to the rear. An even more pronounced difference becomes apparent, when instead of comparing front and rear, cell-matrix adhesions are divided into those build at the free edge (excluding free edge regions comprising actin cables marked in blue) versus the cell-cell edge as illustrated in figure 3j, k. Quantitative analysis of matrix adhesion dynamics further showed that cell-matrix contacts formed at free edges showed significantly increased lifetime compared to those close to cell-cell contacts (Figure 3l-l’’; supplementary movie M9; quantification in figure 3n). This asymmetric distribution of cell-matrix adhesion implies that polarization along the cell edge of myotubes does not require specialized leader cells, as observed in endothelial cells or border cell migration²⁹. It rather appears to be a response on exhibiting free edge and potentially can occur in every cell within the cluster. Consistently, an increase of free edges within the cell cluster was accompanied with the formation of new matrix adhesions as ablation experiments showed. Myotubes immediately migrated when exposed to an empty space and filled the gaps within laser-induced wounds (Figure 3o; supplementary movie M10).

Reduced N-cadherin expression promotes single cell migration at the expense of collective directionality

Reduced cell-matrix adhesion density of myotubes in contact might be due to an enhanced disassembly of cell-matrix complexes at cell-cell contacts as previously reported for neural cells undergoing CIL¹³. Migratory myotubes predominantly express N-cadherin as a key adhesion molecule of cell-cell contacts³⁰, which is essential in early *Drosophila* embryogenesis³¹. N-cadherin was not only found along adjacent membranes of myotube sheets at the testis base (Figure 4a, b, b'), but were also highly enriched along the bridges of interdigitating filopodia (Figure 4c, c', e, e'). In contrast, single myotubes without any cell neighbor that were rarely observed (Figure 4f, f') completely lacked N-cadherin clusters at their free edge filopodia. Live imaging of migrating myotubes expressing a N-Cad-EGFP transgene confirmed a highly dynamic accumulation at cell-cell contacts and along filopodia forming initial contacts between neighboring cells (Figure 4g; see also supplementary movie M11).

To further test the importance of N-cadherin-dependent cell-cell contacts in controlling the collective behavior of myotubes we used an RNAi approach to downregulate N-cadherin expression in myotubes by using the *mef2*-Gal4 driver (Figure 4h, i; supplementary movie M12). Expression of two different RNAi transgenes efficiently downregulates N-cadherin protein level as shown by immunostainings of adult testes (Supplementary figure S2 h, i, quantification in S2 j). Myotubes depleted for N-cadherin are still able to migrate, and even change more frequently their relative positions with each other within the moving cluster (Figure 4h, i; supplementary movie M12). Expression of different *N-cad* RNAi transgenes resulted in an obvious increase of free cell edges with prominent cell-matrix adhesions (Figure 4j, k; supplementary movie M13) and increased gaps between migrating myotubes (Figure 4l, m) in a dosage-dependent manner, but did not affect the cell number or cell size (Supplementary figure S2b, c, d and e). Consistently, suppression of N-cadherin led to a significantly decreased neighbor permanency suggesting that indeed a reduced N-cadherin function weakened cell-cell adhesions (Figure 4n). Quantitative analysis of the migration pattern of individual cells further revealed prominent changes of the migratory behavior. Overall, the total migration distance along the x-axis was not affected indicating that N-cadherin-depleted cells migrate as far as wild type cells (Figure 4o; supplementary movie M12). However, N-cadherin-depleted cells migrate

significantly less directional but faster compared to wild type cells (Figure 4p, q). Thus, myotubes did not display a leader-follower cell dynamics, in which leader cells drag inherently passive followers cells by means of strong cell-cell cadherin contacts. By contrast, N-cadherin-mediated cell-cell contacts seem to be required for the directionally coordinated migratory behavior of myotubes.

Migrating myotubes need cell-cell contact to achieve directionality

To further test whether myotubes require cell-cell contacts for their directional cell migration, we performed laser ablation experiments. Isolation of single myotubes by laser ablation of the adjacent neighboring cells on the testis created a situation, in which a cell is surrounded by free edge. After the ablation, the isolated cells immediately ceased directional migratory behavior and cells formed numerous filopodial protrusions pointing in all directions (Figure 5a-c; supplementary movie M14). Once those cells got in close contact to adjacent cells, they started to migrate forward along those migratory sheets as a collective (Figure 5d, e; supplementary movie M14). Single cell tracking before and after cell-cell contact confirmed a contact-dependent migratory cell behavior of myotubes, a phenomenon that is reminiscent of CIL (Figure 5e-g). Remarkably, such a contact-stimulated migratory behavior could not be observed between two individual cells, which were still connected by cell-cell junctions but isolated from remaining cell cluster by laser ablation (Figure 5h; supplementary movie M15). Cell pairs neither migrated away from each other nor became polarized pointing protrusions into opposite directions, but instead always stuck together with constant contact distance over time (Figure 5 i, j supplementary movie M15).

Rac2 and Cdc42 functions play important roles in myotube migration shaping testis morphology

Cell adhesions are not only required to mechanically couple cells within the cluster, but also to link adhesion complexes to the actin cytoskeleton controlling the protrusion dynamics and directionality³². Rho GTPases are critical molecular players that regulate adhesions and motility during single and collective cell migration^{33,34}.

To identify such key players contributing to myotube migration we used an RNAi approach to screen numerous candidate genes (see supplementary table 1). Defects in testis myotube migration during pupal metamorphosis can be identified by a

prominent disturbed morphology of adult testis (supplementary figure S1a-l; ³⁰. The adult testis is a pair of thin tubules of 2.5 coils and ~2 mm in length surrounded by a sheath of multinuclear smooth-like muscles ^{19,30}. Defective N-cadherin-mediated cell-cell adhesion resulted characteristic holes in the muscle sheet ¹⁹, where myotubes were not properly attached to one another (supplementary figure S1a, c, e). In contrast, defects in myotube migration resulted in an abnormal testis morphology with reduced coils and bulky tips (Supplementary figure S1a, f-k). Depending on the phenotypic strength the muscle sheath only partially or completely failed to cover the entire testis resulting into strong elongation/coiling defects (supplementary figure S1a). Strong abnormalities were observed following RNAi-mediated suppression of Cdc42 and Rac2 functions, one of the two very similar *rac* genes in *Drosophila* ³⁵. In both cases, the adult testes were smaller than in the wild type with reduced coils and bulky tips (Supplementary figure S1f, g). The muscle sheath either did not cover the entire testes with numerous large holes. In comparison, suppression of Arp2/3 complex subunits and single subunits of the WAVE regulatory complex (WRC ³⁶) such as WAVE and the Rac-effector Sra-1, resulted into more moderate morphological defects compared to *rac2* or *cdc42* depletion. Adult testes deficient for Arp3, WAVE and Sra-1 still had about 1.5 to 2 coils, however many myotubes also did not reach the testis apex resulting into bulky tips (Supplementary figure S1h-j).

Rac2 and Cdc42 are required for myotube migration by differentially regulating cell-matrix adhesions

Compared to suppression of the Arp2/3-WRC pathway, knockdown of Rac2 functions led to stronger defects in membrane protrusions and cell migration suggesting that Rac2 might have additional roles in myotube migration (Figure 6a, d; compare quantification in supplementary figure S2g). *rac2*-depleted cells showed a severely changed cell morphology with thinner and highly dynamic filopodial protrusions. These filopodia were unable to adhere stably (Figure 6g, g'; supplementary movie M16, M17). Supporting this notion, live-cell imaging of *rac2* knockdown cells using the FAT-EGFP reporter revealed a prominent loss of cell-matrix adhesion contacts (Figure 6l, supplementary movie M18). Since *mef2*-Gal4 driven FAT-EGFP is still normally enriched in integrin-dependent adhesion structures such as muscle attachment sites

of the larval body wall musculature, a general impact of Rac2 function on matrix adhesion can be excluded (Supplementary figure S1m, n).

Suppression of Cdc42 function also severely impaired migration speed resulting in a strongly reduced migration distance on the x-axis (Figure 6b, e; supplementary movie M15; compare quantification in supplementary figure S2g). However, compared to *rac2*-depleted cells, *cdc42*-deficient myotubes showed an increase of thin and prolonged filopodia (Figure 6g, g'; supplementary movie M17, M19). Overall, the *cdc42*-depleted myotubes showed an elongated cell shape with numerous gaps between adjacent cells. Live-cell imaging of *cdc42* knockdown cells using the FAT-EGFP reporter revealed a significantly increased lifetime of cell-matrix adhesions (Figure 6m; quantification in figure 6n; supplementary movie M18). Compared to wild type cells, the cell-matrix adhesions remained much longer, even when they reached the trailing end of a migrating cell (Supplementary movie M18). In summary, Rac2 and Cdc42 are both required for myotube migration, but appear to differentially regulate cell-matrix adhesions.

Activated Rho1 is not enriched at cell-cell contacts

The activity of Rho1^{37,38}, the *Drosophila* homologue of RhoA, appears to be as essential for myotube migration as Cdc42 and Rac2. RNAi-mediated suppression of Rho1 but not RhoL activity in myotubes indeed resulted in strong morphological defects of the testes, and even under low RNAi transgene expression (using *lbe*-Gal4 driver) *rho1* depleted myotubes showed strong migration defects (see supplementary figure S1k, table 1). Suppression of the same RNAi transgenes using the *mef4*-Gal4 driver resulted into an early pupal lethality (data not shown, supplementary table 1).

Different from neural crest cells undergoing CIL, activated Rho1 was not enriched at cell-cell contacts between myotubes (Figure 7a). Live imaging of migrating myotubes coexpressing a Rho1-GTP biosensor or Anillin Rho-binding domain fused to GFP (Anil.RBD-GFP³⁹ and a LifeAct-RFP transgene uncovered highly dynamic, local pulses of Rho1 activity along retracting filopodial protrusions at free edges (Figure 7a, b; supplementary Movie M20). Rho1 activation appeared to be synchronous with backward movement of retracting filopodial protrusions (Figure 7b; supplementary Movie M20). Once a protrusion has been completely retracted, activated Rho1 disappeared. Remarkably, retracting protrusions were often followed by new forward-

directed protrusions at the same region without any Rho1 signal (Figure 7b, Supplementary Movie M20). Thus, migrating myotubes are not simply polarized along a front-rear axis.

Myotube migration requires Rok-dependent actomyosin contractility

Rho1 is known to control myosin II-dependent contraction through the protein kinase Rok shaping cells into tissue in a large variety of morphogenetic events during development^{40,41}. To test whether Rok-dependent actomyosin-mediated contractility is required for myotube collective migration, we first inhibited contractility by treating *ex vivo* cultured pupal testes with the specific Rok inhibitor Y-27632⁴² and with blebbistatin⁴³ or rather its photostable derivate para-nitro-blebbistatin⁴⁴, which targets the action of the myosin II (Figure 7c, Supplementary Movie M21). Compared to control cells treated with DMSO, we found similar striking changes in cell morphology in a time-dependent manner that eventually disturb myotube cell migration (Figure 7c, e, f; supplementary Movie M21). Following treatment with Y-27632 or blebbistatin, the myotube cell cluster was still able migrate, but became dramatically elongated with long interconnecting cell processes as expected for a tissue under stretch. As consequence, the cell cluster showed large gaps between individual cells, which dramatically increased in the total size over time (see quantification in figure 7h). Consistently, RNAi-mediated depletion of both the regulatory light chain of the myosin II (*spaghetti squash, sqh*) and the myosin II heavy chain (*zipper, zip*) phenocopies the pharmacological inhibition of Rok (Figure 7d, g, supplementary Movie M21; quantification in figure 7h). Migratory defects and the inability to tighten up the cell cluster finally led to small adult testes with reduced coils and bulky tips with numerous large holes in the muscle sheet similar to those depleted of Rho1 (compare figure 7k, l with supplementary figure S1b, k). In conclusion, these data show an important role of Rok-driven actomyosin contractility in collective myotube migration. Together, our data do not support that actomyosin-dependent contractility is required for myotube forward movement, but rather contribute to the integrity of the migrating cell cluster.

Discussion

Myotube migration – a new model system for collective cell migration

In this study, we established a new model system for studying collective cell migration in organ culture that allows high-resolution long-term live-imaging microscopy combined with genetic, pharmacological, and mechanical perturbation analysis. Our data implies that a contact-dependent migration mechanism acts as a driving force to polarize *Drosophila* myotubes and to promote their directional movement along the testes. A contact-stimulated migration has been already observed in cultured cells many years ago, but the molecular mechanisms underlying this phenomenon has been never analyzed in more detail ⁴⁵. Thomas and Yamada observed that both primary neural crest cells and two neural-crest-derived cell lines barely moved when isolated in suspension, but could be stimulated up to 200-fold to migrate following contact with migrating cells ⁴⁵. This process might help to ensure the cohesion and coordination of collectively migrating myotubes to form dense muscular sheets in the walls of developing hollow organs. Those muscle fibers that race ahead will immediately cease migration when they lose contact with their neighbors. That is exactly what we observed in our experiments. After ablation, an isolated myotube awaits restimulation by the other cells of the migrating cluster. Consistently, reduced N-cadherin function promotes single cell migration toward the free space at the expense of collective directionality. The contact-dependent behavior of myotubes also resembles contact inhibition of locomotion (CIL), a well-characterized phenomenon ¹⁶. CIL regulates the *in vivo* collective cell migration of mesenchymal cells such as neural crest cells by inhibiting protrusions forming within the cluster at cell-cell edges and by driving actin polymerization at their free edge ⁴⁶.

Different from neural crest cells, myotubes did not migrate as loose cohorts, but maintain cohesiveness (see model in figure 8). In the context of more-adhesive cells, a CIL-related mechanism, termed “frustrated” CIL has been proposed by which cell-cell junctions can determine the molecular polarity of a collectively migrating epithelial sheet ^{47,48}. The authors provided evidence that cell-cell junctions determine the molecular polarity through a network of downstream effectors that independently control Rac activity at the cell free end and Rho-dependent myosin II light chain (MLC) activation at cell-cell junctions ^{47,48}. At the first glance myotubes do not show an obvious polarized cell morphology with prominent polarized protrusions. Instead,

myotubes form numerous competing protrusions in all directions. However, protrusions pointing to the free space preferentially form more stable cell-matrix adhesions as anchorage sites for forward protrusions, whereas the lifetime of cell-matrix adhesions at cell-cell contacts is decreased. Thus, a contact-dependent asymmetry in matrix adhesion dynamics seems to be important for the directionality of migrating myotubes, a molecular polarity that has been also found in neural crest cells undergoing CIL^{13,49}. Only when one of the adhesions of competing protrusions disassembles, pulling of the cell body towards the competing protrusions might contribute to symmetry breaking and directionality of collective migration (see model in figure 8).

Rho GTPases differentially regulate myotube migration

We further provide evidence for a differential requirement of the Rho GTPases, Rac2 and Cdc42 in regulating cell-matrix adhesion. *cdc42* knockdown cells formed less cohesive clusters and showed a significant increase of cell-matrix adhesion lifetime probably due to a decrease cell-matrix adhesion turnover. In contrast, Rac2 depletion resulted in a prominent loss of cell-matrix adhesions, a phenotype that has already been described in *Rac1*^{-/-} mouse embryonic fibroblasts⁵⁰. Thus, we propose a model in which cell-matrix adhesions are downregulated at N-cadherin-dependent cell-cell contacts, a process that requires Cdc42 functions. To finally test whether a contact dependent reduction of cell-matrix adhesion in filopodia is sufficient to explain the observed collective cell behavior, we developed a simplified simulation model with a few rules governing cell behavior such as protrusive filopodia, matrix adhesion, cell-cell adhesion, and membrane resistance (Supplementary movie M22). Unlike comparable computer models^{51,52}, single cells do not possess directional information. A cell's position is defined by the geometric center of all its filopodia, whose emergence/disappearance/elongation causes translation of the centroid, perceived as motion. Upon cell-cell contact, filopodia lose their cell-matrix adhesion and thereby their grip on the ECM, but keep connections through cell-cell adhesions. These adhesions are recognized by both contributing cells to calculate their respective centroids (see supplementary material). Using these simple rules, we could indeed model myotube collective migration, provided that cells are positioned in a confined area mimicking the unfolded testis surface (Supplementary movie M22 2A, 2B). If filopodia disappear directly after contact, cells exhibit a different cell behavior that is

very reminiscent of CIL (Supplementary movie M22 2C). This simplified model further confirms our observation that local regulation of cell-matrix adhesion suffices to drive collective motility.

Actomyosin function ensures the integrity of cohesive myotube cluster during migration

Myotube migration also requires Rho1 the *Drosophila* homologue of RhoA. Different from cells undergoing CIL, in migrating myotubes activated Rho1 was not enriched at cell-cell contacts between myotubes, but rather localized as local pulses along retracting filopodial protrusions at free edges. The effects of tensile forces have to be addressed separately in the future, by establishing one of the many existing force measurement techniques such as transition force microscopy (TFM) or using *in vivo* FRET-based tensions sensors in this system. We show that loss of Rok activity, *sqh* and *zip* phenocopies *rho1* knockdown suggesting that a canonical pathway controls myotube migration in which Rho1 acts through Rok kinase to activate myosin II contractility. This finding supports the notion that in testis myotubes, unlike many other cell types, locally restricted Rho-GTPase regulation outweighs global Rac/Rho regulation along the cell-rear axis to achieve directionality. Previous studies demonstrated that myosin II-dependent contraction is essential for coordinating the CIL response in colliding cells. In myotube migration, Rok-dependent actomyosin contraction seems to be not required to drive the myotube cluster forward, but rather contractile actin cables contribute to the integrity of the migrating cell cluster. Thus, myotube cluster behave more like a collectively migrating monolayered epithelial sheet during gap closure⁵³. While myotubes migrate into any given free space, they leave larger gaps within the cell sheet surrounded by prominent circumferential actin cables. Constriction of these supracellular actin cables necessarily might lead to gap closure observed in wildtype, but not in cells defective for RhoRok-driven actomyosin contractility.

Filopodia based-myotube migration depends on the differential function of formins and the Arp2/3 complex

Efficient mesenchymal cell migration on two-dimensional surfaces is thought to⁵⁴ require the Arp2/3 complex generating lamellipodial branched actin filament networks that serve a major engine to push the leading edge forward .

Interestingly, epithelial and mesenchymal cells form more filopodia when the Arp2/3 complex is absent⁵⁵⁻⁵⁷. Under these conditions, mesenchymal cells lack lamellipodia and adopt a different mode of migration only using matrix-anchored filopodial protrusions. Our data further provide evidence for a filopodia-based cell migration in a physiological context during morphogenesis. This migration mode largely depends on formin as central known actin nucleators generating filopodia^{33,58}. Our data also suggest that the Arp2/3 and its activator, the WRC contribute to a more efficient myotube migration by promoting filopodia branching, and thereby increasing the number of cell-matrix adhesions, thus increased anchorage sites. Overall, filopodia-based migration enables the cell to regulate discrete subunits of membrane protrusions as an answer to the environment. The sum of filopodial protrusions adds up to a net cell locomotion that occurs similarly during lamellipodial migration (please compare figure 8). Filopodial matrix adhesion complexes not only provide anchorage sites, but also allow cells to directly restructure their microenvironment by membrane-bound matrix proteases. There is indeed increasing clinical evidence suggesting filopodia play a central role in tumor invasion^{27,59}. Similar to invading cancer cells myotubes rather migrate through a 3D microenvironment composed of extracellular matrix restricted by pigment cells from the outside of the testis. Thus, it will be interesting to determine to what extent extracellular matrix restructuring by metalloproteinases is required for myotube migration.

Taken together, our data suggest that contact-stimulated filopodia-based collective migration of myotubes depends on a CIL-related phenomenon combining features and molecular mechanisms described in mesenchymal and epithelial sheet migration as well. We propose a model in which contact-dependent asymmetry of cell-matrix adhesion acts as a major switch to drive directional motion towards the free space, whereas contractile actin cables contribute to the integrity of the migrating cell cluster.

Experimental procedures

Drosophila Genetics

Fly husbandry and crossing were carried out according to the standard methods ⁶⁰. Crossings and all UAS-Gal4-based Experiments including RNAi were performed at 25 °C. The following fly lines were used: *mef2*-Gal4 ⁶¹, *beatVC*-Gal4 (BL-40654), *htl*-Gal4 (BL-40669), *lbe*-Gal4 (BL-47974), UAS-LifeAct-EGFP (BL-35544), UAS-LifeAct-RFP (BL-58715), UAS-GFP nls (BL-4775), UAS-mcd8-RFP (BL-32219), UAS-myr-mRFP (BL-7119), cell-matrix adhesion sensor UAS-fat-GFP ²⁸; RhoA-activity sensor Ubi-Anillin.RBD-GFP ³⁹. All UAS-RNAi lines we used are summarized in table 1 (Supplementary data). CyO/Sco; TM2/TM6B was used as a tool for multi-step crossings, control crossings were conducted using *w*¹¹¹⁸.

Immunohistochemistry and fluorescence staining

Adult and pupal testis fixation and antibody staining was performed as described elsewhere ¹⁹. The following antibody was used: anti-Cadherin-N (1:500, DSHB DN-Ex #8). The following secondary antibodies were used: Alexa Fluor 488 (*Molecular Probes*). Alexa Fluor Phalloidin 568 (*Molecular Probes*) staining on pupal testes was carried out during the secondary antibody incubation for 2 h (1:1000 in PBS). Adult testes were stained overnight (1:1000 in PBS). DAPI (*Molecular Probes*) was performed for 10 min.

Microscopy/4D live cell imaging of testicular nascent myotubes

Fixed pupal testes were embedded in Fluoromount-G (SouthernBiotech) and imaged on object slides. Adult testes were imaged in live-culture dishes in PBS, to maintain their natural shape. Light micrographs were taken with a Leica M165 FC stereo microscope equipped with a Leica DFC7000 T CCD camera. All fluorescent microscopic stills were taken with a Leica TCS SP8 with a HC PL APO CS2 20x/0.75 dry objective. 4D live cell imaging was performed on developing testes of 33 h APF pupae. Prepupae were collected and timed as described elsewhere ³⁰. Life imaging of pupal testes was performed like on egg chambers, as described before ⁶². Images were taken on a Zeiss Observer.Z1 with a Yokogawa CSU-X1 spinning disc scanning unit and an AxioCam MRm CCD camera (6.45 µm x 6.45 µm). Long-term imaging was performed using a LD LCI Plan-Apochromat 25x/0.8 Imm Korr DIC oil-immersion

objective over 7 h, with a z-stack every 5 min. Close-ups were taken with a C Plan-Apochromat 63x/1.4 oil-immersion objective over 2 h, with a z-stack every 2 min. Laser ablation of single cells on the testis was performed with a Rapp TB 355 laser.

Chemical inhibitors

Live imaging experiments with chemical inhibitors were performed exactly as described above. All inhibitors were pre-solved in DMSO and stored at -20°C. The following inhibitors were used: CK666 (100 μ M, *Sigma-Aldrich*), Formin inhibitor SMIFH2 (10 μ M, *Abcam*), para-nitro-blebbistatin (10 μ M, Cayman Chemical), Rok inhibitor Y-27632 (10 μ M, Cayman Chemical).

Data processing and quantification with Fiji

Filopodia angles were obtained by manually tracking filopodia tips using the *Multiple Points* tool. The center of mass was calculated in Fiji. Testes for single cell analysis (marked with beatVC-Gal4 >> lifeact-EGFP) were always oriented with the testis tip, the presumptive destination, pointing left (See Figure 1m'). The angle of the vector between filopodia tip and center of mass was calculated in R using the package *matlib*. Rose plots were generated using the package *ggplot2*. Membrane length for filopodia density (number per μ m membrane) was quantified with the *Free Hand Line* tool and R. For single cell analysis of oriented images, points left of a virtual horizontal line crossing the center of mass (front) were compared to points on the right-hand side (rear, see Figure 1k). For processing and quantification of adhesion defects on still images a ROI with a defined size (120 x 220 px), in the middle of the migrating sheet was chosen. To obtain a black-and-white image for further analysis, a threshold was set (min: 299, max: 300). The cell number inside the ROI was counted. All further values were assessed using the *Analyze>Analyze Particles*-Tool. Area per cell was derived from the total area/cell number. Free cell edge was derived from the sum of all perimeters, as they constitute the length of black-to-white border, which is tantamount to the free cell edge. The gap number was derived from the number of coherent particles, when black-and-white picture are inverted (see also supplementary figure S2 B, C). The size of gaps during live imaging was measured with *Analyze>Analyze Particles*-Tool, too. Only gaps larger than 20 μ m² were analyzed. Corrected total cell

fluorescence (CTCF) was measured on sum-projections based on the method established elsewhere⁶³.

Data processing and quantification of 4D life image stacks

Manual tracking of migrating myotubes was performed using the *spots*-module in the Imaris 9.3 software. For drift correction, the *reference frame* module was used. The x-axis was positioned as axis from the genital disc to the testis hub. Excel was used for all processing and quantification. **Distance on X** is defined as the difference between the x-Values of the same track at t=0 and t=7 h on unprojected and unsmoothed 3D-data. It was used as a measuring tool instead of speed, as fluctuations in manual tracking strongly affects velocity especially in slow cells.

Neighbor permanency is defined as $\frac{\text{Number of remaining neighbors at } t=7 \text{ h}}{\text{Number of neighbors at } t=0}$. Neighbors are defined as the 6 closest cells to a given cell at t=0. A value of 1 means, that all neighbors were kept.

Smooth data. As the manual tracking process is fluctuation-prone, we developed a process, taking this uncertainty into account. The *smoothing* process takes every spot as the center of a 10 μm circle and finds the track with the smallest angles, through these areas. The process is reiterated 30 times. Weak phenotypes could potentially lead to false negative results, but false positive phenotypes get much less likely. (Summary and Formula in Fig. S3A, Data after processing: Fig. S3B)

Mercator projection.

[1] An approximation of the central axis is performed by splitting the dataset in 10 subsets along the x-axis. In every subset, yz-coordinates of the center point are approximated by triangulation using the leftmost, rightmost and uppermost points. A central axis is derived from the point of gravity of the first 5 subsets and the last 5 subsets. Based on that, the x-axis is moved with a rotation matrix. This process gets reiterated three times. (Summarized in Fig. S3 B-C)

[2] An yz-vector \vec{r}_n from every point's respective yz-coordinate to the yz-coordinate of the central axis is generated. Its magnitude is the radius $|\vec{r}_n|$ of this point. The maximal radius of all points is $|\vec{r}_{max}|$. The formula of the central angle θ depends on the position of the yz coordinates of every respective point.

$$\text{IF } y_n < y_{axis} \text{ AND } z_n > z_{axis} \quad \theta = 2 * \pi - \cos^{-1} \left(\frac{\vec{r}_n * \begin{pmatrix} 1 \\ 0 \end{pmatrix}}{|\vec{r}_n| * \begin{pmatrix} 1 \\ 0 \end{pmatrix}|} \right)$$

$$\text{IF } y_n > y_{axis} \text{ AND } z_n > z_{axis} \quad \theta = -\cos^{-1} \left(\frac{\vec{r}_n * \begin{pmatrix} 1 \\ 0 \end{pmatrix}}{|\vec{r}_n| * \begin{pmatrix} 1 \\ 0 \end{pmatrix}|} \right)$$

$$\text{IF } z_n < z_{axis} \quad \theta = \cos^{-1} \left(\frac{\vec{r}_n * \begin{pmatrix} 1 \\ 0 \end{pmatrix}}{|\vec{r}_n| * \begin{pmatrix} 1 \\ 0 \end{pmatrix}|} \right)$$

A new y-coordinate is generated using the formula: $\frac{\pi/2 - \theta}{\pi/2} * |\vec{r}_{max}| * \pi/2$

(summarized in Fig. S2 C-E).

[3] To correct the x-axis with respect to $|\vec{r}_n|$, all datapoints are sorted by x-coordinate. x_n^1 is the x-coordinate of a given spot before correction. x_{n-1}^1 is the point preceeding this point. Its corresponding point after correction is x_n^2 (Summarized in Fig. S3 E-F).

For the very first point the formula is: $x_1^1 = x_1^2$

For all further points : x_n^1 : the formula is $x_n^2 = x_{n-1}^2 + (x_n^1 - x_{n-1}^1) * \frac{|\vec{r}_{max}|}{|\vec{r}_n|}$

Track speed mean was measured in motility lab using smoothed tracking data, in order not to quantify manual tracking inaccuracies.

Biased angle to x-axis. The usual “biased angle” method measures the bias towards a predefined point. As myotubes do not migrate towards a point, but along a defined axis, we measured the angle-distribution to the x-axis to analyze myotube directionality. As angles get strongly affected by speed, this method can only compare cells with the same “distance on x” value (summarized in Fig. S3 F). Rose plots were generated in R using the *ggplot2* package.

Meandering distance. To compare the directionality of samples with different speeds, their meandering distance $|\vec{d}_2|$ was measured according to the following formula. The median for all tracks on the testis was calculated. $\vec{d}_1 =$

$$\left(\begin{array}{c} x_n - x_n \\ y_n - y_{mean \text{ per track}} \end{array} \right) \quad |\vec{d}_2| = |\vec{d}_1| * \frac{|\vec{r}_n|}{|\vec{r}_{max}|}$$

Cell-matrix adhesion lifetime was measured with the *spots* module of the Imaris 3.0 software on 2D maximum projections.

Cell distance over time between cells isolated by ablation was quantified in R based on Imaris tracking data using the packages *matlib*, *reshape2*, *tibble* and *beeswarm*.

Statistical Analysis

All statistical tests were performed using Prism 7 (GraphPad). Multiple comparisons were done using parametric or nonparametric Anova, and for single comparisons welsh's t-test or Mann-Whitney-test was used. Depending on normal distribution, assessed with the Shapiro-Wilk test, either parametric or non-parametric tests were used.

Image Processing and graphic editing

For image processing and graphic editing, the following software tools were used: Zen Blue (Zeiss), LasX (Leica), Fiji (ImageJ 1.51), Imaris 9.3 (Bitplane), Inkscape 0.91. R Studio 1.2.5042 (RStudio, Inc.) and packages therein mentioned above. For displaying cell tracks, Motility lab was used (Miller, unpublished)

Computer simulation of testis myoblast behavior. The software was programmed using Unity 2019.2.2f1 (Unity Technologies). A single cell in this model (see also supplementary movie M22) is not simulated as a single agent but consists of multiple simulated protrusion points (black dots). Their geometrical center (centroid) is calculated constantly and constitutes the cells "position". Protrusion points radially move away from the centroid, mimicking filopodia elongation, but must counter membrane resistance that gets the higher the farther away the point moves from the centroid. On its way every protrusion point creates its own "cell-matrix adhesions" (red dots). They mediate a filopodium (= protrusion points & all its adhesions) static friction which is needed to counter membrane resistance. If membrane resistance is higher than adhesion the entire filopodium gets translated towards the centroid. Protrusion points and cell-matrix adhesions have a lifetime. New protrusion points are generated in a fixed distance from the centroid (grey circle) where the local density is lowest to recapitulate our finding that there is no asymmetry in myotube filopodia assembly. When a protrusion point touches the "adhesion radius" (grey circle) of another cell it loses its cell-matrix adhesions mimicking the measured shortened lifetime of real cell-matrix adhesions. The protrusion point is then turned into an "adhesion point" (green dot) which is recognized by both cells as one of their protrusion points to calculate their respective centroids. For more details see also supplementary material.

Acknowledgements

We thank the Bloomington Stock Center and VDRC for fly stocks. We thank Thomas Lecuit for providing the Rho1-biosensor. We thank Susanne Önel for providing the Arp3-GFP transgene. We thank Chi-Hon Lee for providing the flies bearing UAS-N-cad-EGFP transgene. We thank Christian Klämbt and Jörg Grosshans for helpful discussion. We thank Caroline Zedler and Franziska Lehne for critical reading of the manuscript. This work was supported by GRK 2213 graduate school program of the Deutsche Forschungsgemeinschaft (DFG) to R. R.- P. and S.B.

Figures

Figure 1 *Myotubes form numerous filopodial membrane protrusions instead of lamellipodia and migrate collectively onto the testis*

a, b. Graphics of the *Drosophila* testis at 24h and 33 h after pupae formation (APF). **a.** Myoblasts (mb, red) arising from the genital disc, adhere to the epithelium of the seminal vesicles (sv) and fuse to small syncytia shortly before the connection between seminal vesicles and terminal epithelia (te). **b.** After epithelial fusion nascent myotubes (mt) migrate between the basal lamina separating the testicular cyst cells and a layer of pigment cells (pc) from the testis base towards the apex. **c.** Schematic of the *ex vivo* technique enabling life imaging of *Drosophila* testis development with a spinning disc microscope. **d.** Only one testis of the pair (compare to c) which was prepared is depicted, as in 25x magnification (compare to d) only one testis can be seen. **e.** Wild type testis 33 h APF 350 min in *ex vivo* culture. UAS-LifeAct-EGFP was driven using the *htl-Gal4* driver line, which promotes expression in migrating myotubes (m) and pigment cells (pc). The dashed line in “0 min” represents the area depicted in 100–420 min. Scale bar, 50 μ m. **f, f’.** Migration of myotubes was tracked using the Imaris software. *mef2-Gal4* was used to drive UAS-LifeAct-EGFP, expressed only in myotubes. **f.** An overlay of microscopic data and track data are shown. Source data are provided as a Source Data file. **f’.** Only track data is shown. Scale bar, 100 μ m. **e.** Top view of a testis 46 h APF in 420 min *ex vivo* culture. *mef2-Gal4* drives UAS-LifeAct-EGFP expression. **g.** Subsequent to migration, testis myotubes start to encircle the testis, generating ring muscles. The testis starts to change its shape. The dashed line

in h represents the area depicted in 0/285 min. Scale bar, 100 μm . **h.** Confocal image of an adult testis stained with phalloidin and DAPI. Due to constriction by building muscles in pupal development, the testis gained its typical coiled shape³⁰ Scale bar, 100 μm ; close-up in **h'**. **i.** Close-up of myotubes at the front edge of the migrating sheet 60 min in *ex vivo* culture. *mef2-Gal4* drives UAS-LifeAct-EGFP expression. Cells at the front of the migrating cluster appear like the cells within the cluster depicted in h, as they project filopodia-like structures in all directions. The actin cytoskeleton appears in stress fiber-like thick bundles. Scale bar 10 μm . **j.** Close-up of two myotubes during migration 60 min in *ex vivo* culture. *beatVC-Gal4* promotes expression of UAS-LifeAct-EGFP and UAS-GFP-nls in a mosaic fashion, allowing for the analysis of single cells within the migrating sheet. Nuclei of neighboring cells are marked by yellow asterisks. Even cells within the cluster, enwrapped by neighboring cells, appear to have filopodia-like protrusions and a general mesenchymal phenotype. Scale bar, 20 μm . **l.** Quantification of filopodia number per cell edge length in cells at the migration front. Source data are provided as a Source Data file. Directionality of filopodia of cells was quantified by measuring the orientation angle as illustrated in **m** and **m'**. Quantification revealed no strong bias in filopodia direction neither of cells **n.** within the myotube cluster nor **o.** of cells at the migration front. Source data are provided as a Source Data file.

Figure 2 *Formins are essential in myotube collective migration and filopodia dynamics, but not the Arp 2/3 complex.*

a. Migration tracks of testis myotubes 33 h APF in 420 min *ex vivo* culture, treated with DMSO as a control. Source data are provided as a Source Data file. **b, c.** CK666 (100 μM) treatment of a testis 33 h APF in 420 min *ex vivo* culture. Upon Arp2/3 complex activity inhibition, migration is reduced. Especially cells at the testis base appear to be affected. *mef2-Gal4* drives UAS-LifeAct-EGFP and UAS-mCD8-RFP expression. **b.** Migration tracks of testis myotubes upon CK666 treatment. Source data are provided as a Source Data file. **c.** Life imaging micrographs. mCD8-RFP in green and LifeAct-EGFP in white. The dashed line in c represents the area depicted in 0-420 min. Scale bar, 50 μm . **d, e.** Migration is also mildly reduced by *arp3* RNAi. *mef2-Gal4* drives UAS-LifeAct-EGFP, UAS-mCD8-RFP and the RNAi construct *UAS-arp3^{KK102278}* (Vienna v108951). **d.** Migration tracks of testis myotubes upon *arp3* RNAi. **e, e'**. Life imaging

micrograph. Source data are provided as a Source Data file. mCD8-RFP (green) is depicted in **e**. (Note: mononucleated myotubes marked by co-expression of the mCD8-RFP marker excluded from the nuclei). Overlay with LifeAct-EGFP (white) in **e'**. The dashed line in **e'** represents the area depicted in 0-350 min. Scale bar, 50 μm . **f, g**. Upon Formin suppression through SMIFH2 (10 μM) treatment, migration is completely disrupted. *mef2-Gal4* drives UAS-LifeAct-EGFP and UAS-mcd8-RFP expression. **f**. Migration tracks of testis myotubes upon SMIFH2 treatment. Source data are provided as a Source Data file. **g, g'**. Life imaging micrographs. mCD8-RFP (green) is depicted in **g**. Overlay with LifeAct-EGFP (white) in **g'**. The dashed line in **g'** represents the area depicted in 0-350 min. Scale bar, 50 μm . **h**. Quantification total migration distance along x-axis. Source data are provided as a Source Data file. **i-k**. Close ups of front-row myotubes upon different treatments. **i**. Upon DMSO treatment, cell morphology and filopodia composition were not affected. **j**. Arp2/3 suppression by CK666 treatment leads to mild defects. No branched filopodia are built, the overall morphology is unaffected. **k**. Formin suppression by SMIFH treatment leads to strong morphological defects. Cells are contracted, filopodia generate more branches. **l**. CK666 in addition to SMIFH2 co-treatment leads to a loss of branched filopodia. Cells are contracted even stronger.

Figure 3 *Migrating myotubes form stable cell-matrix adhesions at their free edge and adherens junctions at their cell-cell edge*

a, b. Close ups of front-row myotubes **a**. wild type and **b**. *arp3* knock-down marked by Lifeact-EGFP expression. Scale bar, 10 μm . **c**. Quantification of filopodia tip number per cell edge length. Source data are provided as a Source Data file. **d**. Spinning disc microscopy still images of a front-row myotube expressing an Arp3-EGFP transgene. The arrowheads mark positions where Arp3 is enriched at filopodial branch points. Scale bar, 10 μm . **e**. Spinning disc microscopy still images of a front-row myotube co-expressing Arp3-EGFP and Myr-RFP. The arrowhead marks a position of Arp3 at a distinct filopodial branch. Scale bar, 10 μm . **f, g**. Close-up of myotubes at the front edge of the migrating sheet, 6 min in *ex vivo* culture. Cell-matrix adhesions (green) are assembled in the shafts of free edge-filopodia. Filopodia elongate, generating new adhesions in a beaded string-like manner. Scale bar: 10 μm . **g**. Some filopodia build branches. UAS-FAT-EGFP (cell-matrix adhesion marker and UAS-Myr-RFP was

driven by *mef2-Gal4*. Scale bar: 10 μm . **h, h', h''**. FAT-EGFP and LifeAct-RFP were driven by *mef2-Gal4*. **h**. Dashed lines represent the area magnified in **h'** and **h''**. **h'**. Matrix adhesions are found at filopodia tips (white arrowheads) and appear enriched at the free edge of cells in contrast to their cell-cell edges. Thick actin cables are marked by yellow arrowheads. **h''**. Cell-matrix adhesions colocalize with bundled actin fibers (white arrowheads). **h', h''**. Scale bar, 10 μm . **i, j, k**. Quantification revealed **i**. a significant bias in directionality of cell-matrix adhesions, **j**. an increased number of cell-matrix adhesions at the cell front (pointing to the testis apex) and **k**. an increased number of cell-matrix adhesions at the free-edge compared to cell-cell edges (excluding free edge regions with prominent actin filament bundles marked as “actin cables” in blue) as illustrated. Source data are provided as a Source Data file. **l, m**. Cell-matrix adhesions in nascent myotubes during migration. FAT-EGFP was driven by *mef2-Gal4*. Quantified matrix adhesions at the free edge are depicted in red and at the cell-cell edge in green. Scale bar: 10 μm . **l**. Front edge of the migrating sheet. **l'**. Magnification at 0 min. **l''**. Magnification at 40 min. **m**. Following cells in the same sheet as in **h**. **m'**. Magnification at 0 min. **m''**. Magnification at 40 min. **n**. The quantification revealed that cell-matrix adhesions longevity is significantly higher at the “free edge” compared to the “cell-cell-edge”. $n=3$ testes. Source data are provided as a Source Data file. **o**. Cell-matrix adhesions in myotubes in the middle of the migrating sheet 33 h APF in *ex vivo* culture before and after laser ablation. *mef2-Gal4* drives UAS-FAT-EGFP expression. Before ablation only few and scattered cell-matrix adhesions can be observed in “follower” myotubes. After laser ablation, cells adjacent to the ablation site start to generate cell-matrix adhesion containing protrusions along the newly arose free edge (arrowhead). Scale bar: 10 μm .

Figure 4 *Reduced N-cadherin expression increases free edge, promoting cell-independent behavior at the expense of collective directionality*

a-f. Confocal images of a wild type 33 h APF testis stained with an anti-N-cadherin antibody. F-Actin was stained using Phalloidin and nuclei were marked with DAPI. **a**. Overview of the testis base. The areas marked with dashed lines are magnified in **B, C** and **E, F**, respectively. Scale bar: 50 μm . **b**. On the genital disc adjacent to the testis base, nascent myotubes appear epithelial with N-cadherin localized evenly along the cell edge. **c, c'**. In contrast, at the front edge of the migrating sheet, N-cadherin

localized in foci at the tip of filopodia-like structures interconnecting cells (white arrowhead). **d, e, e'**. The same is true for cells within the sheet. **f, f'**. In rare cases, completely isolated cells could be observed. No N-cadherin staining can be detected in such cells. **b, c, e, f**. scale bar: 10 μm . **g**. Spinning disc microscopy still images of myotubes expressing a Ncad-EGFP transgene. The arrowheads mark positions where Ncad-EGFP is enriched at cell-cell junctions. Scale bar, 10 μm . **h, i**. *mef2-Gal4* was used to drive expression of UAS-LifeAct-EGFP and UAS-Ncad-RNAi construct. **h**. Wild type (WT) testis 33 h APF in *ex vivo* culture. *mef2-Gal4* drives expression of UAS-LifeAct-EGFP. Overview at $t = 0$ min at the left side. Scale bar: 50 μm . Time steps from 0 min to 45 min in *ex vivo* culture at the right side. Scale bar: 20 μm . **h'**. Migration tracks of WT myoblasts. Source data are provided as a Source Data file. **i**. *n-cadherin* knock down in myotubes. Compare to A. Single cells are not as strongly attached to each other. Myotubes are sometimes completely isolated as in WT (yellow asterisk) ($t = 0$ min, 45-60 min). **i'**. Migrations tracks upon knock down of *N-cadherin*. Source data are provided as a Source Data file. **j, k**. 18 min life culture demonstrates that an increased free edge in every single cell (yellow asterisk) through N-cad RNAi results in more cell-matrix adhesion-producing filopodia. The arrowhead marks a retracting protrusion. UAS-FAT-EGFP and *UAS-NcadRNAi* was driven by *mef2-Gal4*. Scale bar: 20 μm . **l, m**. Quantification with Fiji. Graphical representation of the values is depicted. A ROI of the same size of 8 stills of each respective genotype was compared with Fiji Particle Analysis after conversion to black-and-white pictures (see also supplementary figure S2B, C). **l**. The number of gaps between cells is significantly increased. **m**. As proxy for free edge, we used the perimeter of the white-to-black edge. Cell free edge is significantly increased in *N-cad* RNAi animals. Source data are provided as a Source Data file. **n**. Neighbour-permanency is significantly reduced when N-cadherin is knocked down (using two independent RNAi transgenes). Source data are provided as a Source Data file. **o**. To assess, how far cells were able to migrate on the testis, the difference of x values (x-axis = defined as the axis from base to apex) of testis myotubes at $t = 0$ min and $t = 420$ min was calculated. The mean of each testis was compared. Upon N-Cadherin reduction, myotubes come as far as in WT. Source data are provided as a Source Data file. **p**. As a tool for directionality, biased angle in regard to the testis axis was measured. Datasets were smoothed and Mercator-projected before (see also supplementary figure S3). The mean angle (0-180°) of every track is blotted. N-Cadherin reduction causes myotubes to migrate less directional. The same

is true using a second RNAi line. Source data are provided as a Source Data file. **q.** Quantification of track speed mean in $\mu\text{m}/\text{sec}$. RNAi line #1 is subject to wider fluctuation but not significantly faster. RNAi line #2 is significantly faster than wild type (WT). Source data are provided as a Source Data file.

Figure 5 *Migrating myotubes need cell-cell contact to achieve directionality.*

a-g. Isolation of a single nascent myotube by laser ablation. **a.** Overview of a testis after laser ablation (33 h APF). *htl-Gal4* drives UAS-LifeAct-EGFP expression. Scale bar, 100 μm . **b.** Close-up on the ablation site. **c.** Same site as in b, before ablation. Scale bar in c and c': 20 μm . The dashed line represents the area affected by laser ablation. **c'.** Behavior of the isolated cell from B after ablation. The isolated cell (yellow asterisk) shows no forward motion if it has no contact to adjacent cells (upper row). After contact is established, it moves along in the migrating sheet (bottom row). **d, e.** To quantify the directionality of the isolated cell, cell motion was tracked using the Imaris software. The isolated cell before contacting to the migrating sheet is depicted in red, after contacting it is depicted in green. As a control, adjacent cells were tracked. They are showed in blue. Source data are provided as a Source Data file. **f, g.** As a measurement tool, we used the biased angle to x-axis. The mean angle (0-180°) of every track is blotted. When isolated, cells lose their directionality, but regain it after establishing contact to adjacent cells. The color code is the same as in **e, f**. n= 5 testes. Source data are provided as a Source Data file. **h-j.** Isolation of two adjacent myotubes by laser ablation. **h.** Overview of a testis after laser ablation (33 h APF). *htl-Gal4* drives LifeAct-EGFP (grey) and Myr-RFP (magenta) expression. The dashed line represents the area affected by laser ablation. Scale bar, 100 μm . **h'.** Behavior of the two isolated myotubes from h. after ablation. Scale bar in c and c': 20 μm . **i.** Rose plot shows the distribution of the biased angle to x-axis. Source data are provided as a Source Data file. **j.** Measurement of the distance between two myotubes over time. Source data are provided as a Source Data file.

Figure 6 *Rac2 and Cdc42 regulate filopodia matrix adhesion to enable myotube collective migration*

a, c, i, j. *rac2* knockdown was induced by expression of the *UAS-rac2*^{NIG.8556R} RNAi transgene together with UAS-LifeAct-EGFP, using *mef2-Gal4*. **a.** *rac2* knockdown in

myotubes on testis 33 h APF in *ex vivo* culture. Myotube migration almost completely ceases. Tracks are depicted in D. The dashed line in “0 min” represents the area depicted in 50–420 min. Scale bar: 50 μ m. Source data are provided as a Source Data file. **b, d, i, j.** *cdc42* knockdown was induced by expression of the *UAS-cdc42^{TRiP.JF02855}* (#1) or the *UAS-cdc42^{KK108698}* (#2) RNAi transgenes, together with *UAS-LifeAct-EGFP*, using *mef2-Gal4*. Source data are provided as a Source Data file. **b.** *cdc42* knock down in myotubes on testis 33 h APF in *ex vivo* culture. Myotube migration is disrupted. Cells change their shape, generating massive filopodia-like structures, in comparison to WT. Tracks are depicted in **e**. The dashed line in “0 min” represents the area depicted in 50–420 min. Scale bar: 50 μ m. Source data are provided as a Source Data file. **f-h.** Close-up of myotubes 33 h APF in *ex vivo* culture with corresponding color-coded projection in **f'-h'**. Scale bar: 10 μ m. **f, f'**. Wild type (WT) myotubes. **g, g'**. *rac2* RNAi causes a fast assembly and disassembly of filopodia. **h, h'**. *cdc42* RNAi leads to very stable filopodia in comparison to wt. Filopodia are prolonged, even between nascent myotubes, rendering close cell-cell contact harder to achieve, thus the entire sheet appears less dense as in WT. **i.** Quantification of migration distance on x-axis (compare to Fig 3J). Source data are provided as a Source Data file. **j.** Quantification of median meandering distance. Source data are provided as a Source Data file. **k.** Cell-matrix adhesions in myotubes during migration. *UAS-FAT-EGFP* was driven by *mef2-Gal4*. Scale bar: 10 μ m. **l.** Cell-matrix adhesions are completely lost upon *rac2* suppression by RNAi. **m.** Cell-matrix adhesions remain much longer upon *cdc42* reduction, even reaching the trailing end of a migrating cell. **n.** Quantification of cell-matrix adhesion lifetime. As shown in H, a cell-cell edge cannot be clearly defined upon knock down of *cdc42*, thus just the free edge was compared. *cdc42* reduction increased lifetime of cell-matrix adhesions significantly, compared to WT, n = 3 testes for WT and *cdc42* RNAi. Source data are provided as a Source Data file.

Figure 7 *Rho/Rok-driven actomyosin contractility is essential for myotube migration.*

a, b. Close-ups of myotubes at the front edge of the migrating sheet 30 min in *ex vivo* culture. *mef2-Gal4* drives *UAS-LifeAct-RFP* and the Rho1 sensor Anillin-RBD-EGFP. *UAS-LifeAct-RFP* is enriched along the membrane in actin cables. To depict all actin structures, gamma was set on 0.09. In the boxes in the upper right corner, details with gamma=1 are depicted. **a.** Rho1-Sensor activity is found in free edge filopodia (white

arrowheads, as LifeAct-RFP rapidly bleached out in filopodia tips, EGFP signal appears partially outside the cell). When analyzed with $\gamma=1$, it becomes clear that Rho1-sensor is only present at parts of the edge containing actin cables. After the Rho signal appears, the corresponding part of the cell retracts, and the Rho1 signal immediately disappears. During retraction, the LifeAct-RFP signal at the retractive site goes back to normal intensity. **b.** Rho1 sensor activity does not seem to mark rear polarity. Filopodia can protrude (left column, yellow line, then activate RhoA and retract (middle column, yellow line). Subsequently, neighboring filopodia can elongate again (middle and left column, yellow line). **c.** myotubes expressing LifeAct-EGFP on testis 33 h APF in *ex vivo* culture treated with the Rok inhibitor Y-27632. **d.** *sqh* knockdown was induced by expression of the *UAS-sqh* RNAi transgene together with UAS-LifeAct-EGFP using *mef2-Gal4*. Myotube cell cluster were still able migrate with reduced speed and become dramatically elongated with long interconnecting cell processes. The dashed line in “0 min” represents the area depicted in 50–420 min. Scale bar: 50 μm . Tracks are depicted in **e.** wild type (WT), **f.** Y-27632 treatment and **g.** *sqh* knockdown. Source data are provided as a Source Data file. **h.** Measurement of the gap size within cell cluster over time. Source data are provided as a Source Data file. **i.** Quantification of migration distance on x-axis. Source data are provided as a Source Data file. **j.** Quantification of the median meandering distance. Source data are provided as a Source Data file. **k, l.** Confocal images of adult testes expressing **k.** a *sqh* RNAi transgene **l.** a *zip* RNAi transgene under the *mef2-Gal4* driver, the muscle sheet is stained with phalloidin (red) and nuclei are stained with DAPI (cyan). Scale bar: 100 μm .

Figure 8 Proposed model

a. Comparison between filopodia-based and lamellipodia-based cell migration. Lamellipodia-based migration requires the Arp2/3 complex generating branched actin filament networks that serve as the major engine to push the leading edge forward, whereas filopodia support mesenchymal migration by promoting cell-matrix adhesiveness at the leading edge stabilizing the advancing lamellipodium or by sensing the environment. In filopodia-based migration, it seems that filopodia replace the lamellipodium as the motor of motility. We assume that polymerization of bundled actin filaments through formins pushes parts of the membrane. Arp2/3 complex contributes to filopodia branching and thereby provides new barbed ends generating

new filopodia. **b.** Key features and cell behavior in testis myotube migration compared to **c.** migrating mesenchymal neural crest cells undergoing CIL. Different from neural crest cells, myotubes did not migrate as loose cohorts, but maintain cohesiveness. Unlike neural crest cells, migrating myotubes are not simply polarized along a front-rear axis and do not form a contact-dependent intracellular Rho gradient that initiates cell polarization driving directed cell migration. In myotube migration, a contact-dependent asymmetry of cell-matrix adhesion rather acts as a major switch to drive locomotion towards the free space. Individually or loosely connected migrating cells, like neural crest cells are able to migrate persistently due to classical front-rear polarity. By contrast, testis myotubes rely on constant cohesion to break symmetry. Supracellular contractile actin cables contribute to the integrity of the migrating cell cluster and thereby to cohesion.

Supplementary material

Supplementary figures

Figure S1

a. Graphical representation of types of adult testis defects as a consequence of partial loss of adhesion or migration. **b-l.** Adult testes with different genetic backgrounds. Upper left corner: light micrograph of several testis showing the phenotypic range, upper right corner: light micrograph of a single testis. Bottom: confocal image of a testis. muscle sheet stained with phalloidin (red) and nuclei stained with DAPI (cyan). **b.** Wild type adult testis with a curled shape and an organized and entirely closed muscle sheet. **c, d.** Expression of a *N-cad* RNAi transgene #1 driven by *mef2-Gal4* leads to small holes in the muscle sheet in a dose dependent-manner³⁰. **c.** one copy of the RNAi transgene #1; **d.** two copies of the same RNAi transgene #1. **e.** Expression of a stronger *N-cad* RNAi transgene #2 causes much stronger defects with large holes within the muscle sheet (yellow arrowheads). **f.** *rac2* RNAi driven by *mef2-Gal4* leads to strong migration defects with a strongly dilated tip, partially uncovered, partially covered in disorganized muscles. **g.** *cdc42* RNAi driven by *mef2-Gal4*, resembles *rac2* RNAi with slightly milder defects. **h, i, j.** *arp3*, *wave* and *sra-1* RNAi driven by *mef2-Gal4*, leads to mild migration defects with a slightly dilated tip and small uncovered areas. **k.** *rho1* RNAi driven by *lbe-Gal4*. Even using a weak driver line, prominent migration defects can be observed. **l.** *Ncad2* RNAi driven by *mef2-Gal4* resembles wild

type testis without any defects. **m, n.** Confocal images of FAT-GFP driven by *mef2-Gal4* in larval body wall muscles 6/7. Muscle attachment sites, marked by FAT-GFP are not affected by *rac2* RNAi, indicating that *rac2* depletion has no general impact on matrix adhesion or integrin expression, but specifically affects cell-matrix adhesions in migratory cells. Using sibling flies, no cell-matrix adhesions can be detected in migrating myoblasts.

Figure S2

a. Graphical representation of the expression patterns of the Gal4 driver lines used (in green). Compare to Fig. 1B. **b, c.** Overview and ROI's (120 x 220 px) in WT (B) and *N-cad* RNAi (C) on which quantification in D/E and Fig. 3E, F is based. Marked with yellow dashed lines in the overview. **d.** Cell number inside ROI's. Cell number is not affected upon *N-cad* RNAi. Source data are provided as a Source Data file. **e.** Area per cell inside ROI's. Cell Area is not affected upon *N-cad* RNAi. Source data are provided as a Source Data file. **f, g, h, i.** Comparison of neighbor permanency (f.), distance on x-axis (g.), directionality based on biased angle (H) and based on meandering distance (I), for all genotypes. For every genotype, all trackable cells on 5 testes were analyzed. The number of tracks for every genotype equals the number of data points in h. Source data are provided as a Source Data file. **i, j.** Confocal images of adult testis muscle sheet stained with a specific anti-NCad antibody (green), phalloidin (red) and DAPI (blue). **i.** In wildtype (WT) Ncadherin localizes along the cell-cell junction. **j.** Expression of a *ncad* RNAi transgene strongly reduce anti-NCad immunostaining as quantified in **k.** for two independent RNAi transgenes. Source data are provided as a Source Data file.

Figure S3

Myotubes migrate on the surface of an ellipsoid, thus on a two-dimensional surface, that is curved in space. This curvature did not allow to apply mathematical rules based in flat geometry. 3D migration tools do not consider the limitations of the surface, to which myotubes are bound but assume they can move freely. Instead, we developed a Mercator projection-based process, which allows for high angle-accuracy but neglects distances. **a.-f.** Steps of Mercator projection are shown (see material and methods for details). Source data are provided as a Source Data file.

Supplementary table 1

A list of the RNAi transgenes used in this study, and phenotypic strength using different Gal4 driver lines.

Supplementary methods (simulation model)

Description of the simulation model and details on mathematical modeling.

Supplementary movies*Supplementary movie M1*

Spinning disc microscopy time-lapse movie of *ex vivo* cultured wild type testes (33h APF) expressing (left) LifeAct-EGFP in myotubes and pigment cells using the *htl-Gal4* driver, (middle) LifeAct-EGFP only in myotubes using the *mef2-Gal4* driver, and (right) LifeAct-RFP and a nuclear EGFP in myotubes and pigment cells using the *htl-Gal4* driver. Scale bar: 50 μ m.

Supplementary movie M2

Spinning disc microscopy time-lapse movie of an *ex vivo* cultured wild type testis (33h APF) expressing a LifeAct-EGFP transgene using the *mef2-Gal4* driver. The migration of myotubes was tracked using the Imaris software. An overlay of microscopic data and track data are shown. Scale bar: 30 μ m.

Supplementary movie M3

Spinning disc microscopy time-lapse movie of migrating myotubes (marked by LifeAct-EGFP expression) at the front edge of the migrating sheet 60 min in *ex vivo* culture. Scale bar 10 μ m.

Supplementary movie M4

Spinning disc microscopy time-lapse movie of migrating myotubes expressing LifeAct-EGFP and a nuclear EGFP in a mosaic fashion 60 min in *ex vivo* culture, allowing for the analysis of single cells within the migrating sheet. Scale bar 30 μ m.

Supplementary movie M5

Spinning disc microscopy time-lapse movie of an *ex vivo* cultured testis (33h APF) expressing a LifeAct-EGFP transgene, treated with 100 μ M CK666. Upon Arp2/3 complex activity inhibition, migration is reduced. Especially cells at the testis base appear to be affected. Scale bar: 50 μ m.

Supplementary movie M6

Spinning disc microscopy time-lapse movie of an *ex vivo* cultured testis (33h APF) co-expressing an *arp3* RNAi together with a LifeAct-EGFP transgene in all myotubes using the *mef2-Gal4* driver. Migration is also mildly reduced by *arp3* RNAi. Scale bar: 50 μ m.

Supplementary movie M7

Spinning disc microscopy time-lapse movie of an *ex vivo* cultured testis (33h APF) expressing a LifeAct-EGFP transgene, treated with 10 μ M SMIFH2. Myotube migration is completely suppressed. Scale bar: 50 μ m.

Supplementary movie M8

Spinning disc microscopy time-lapse movie of migrating myotubes expressing the cell-matrix adhesion reporter FAT-EGFP and a membrane marker Myr-RFP. Scale bar: 10 μ m.

Supplementary movie M9

Spinning disc microscopy time-lapse movie of migrating myotubes expressing the cell-matrix adhesion reporter FAT-EGFP tracked using the Imaris software. Quantified cell-matrix adhesions at the free edge are depicted in red and at the cell-cell edge in green. Scale bar: 20 μ m.

Supplementary movie M10

Spinning disc microscopy time-lapse movie of migrating myotubes expressing the cell-matrix adhesion reporter FAT-EGFP in the middle of the migrating sheet 33 h APF in *ex vivo* culture before and after laser ablation (position is marked by an asterisk). Scale bar: 10 μ m.

Supplementary movie M11

Spinning disc microscopy time-lapse movie of migrating myotubes co-expressing NCad-EGFP and LifeAct-RFP in the middle of the migrating sheet 33 h APF in *ex vivo* culture. Scale bar: 10 μm .

Supplementary movie M12

Spinning disc microscopy time-lapse movie of *ex vivo* cultured (left) wild type testes compared to (right) testis expressing an *N-cad* RNAi transgene. Myotubes are marked by LifeAct-EGFP transgene expression in all myotubes using the *mef2-Gal4* driver. Scale bar: 50 μm .

Supplementary movie M13

Spinning disc microscopy time-lapse movies of migrating wildtype myotubes (left) compared to myotubes depleted of N-cadherin (right) visualized by the cell-matrix adhesion reporter FAT-EGFP. Scale bar: 10 μm .

Supplementary movie M13

Spinning disc microscopy time-lapse movie of an *ex vivo* cultured testis (33h APF) co-expressing a *rac2* RNAi together with a LifeAct-EGFP transgene in all myotubes using the *mef2-Gal4* driver. Myotube migration is almost completely disrupted. Scale bar: 50 μm .

Supplementary movie M14

Spinning disc microscopy time-lapse movie of *ex vivo* cultured wild type testis (33h APF) expressing LifeAct-EGFP using the *htl-Gal4* driver. The isolated single myotube by laser ablation is marked by an asterisk. Scale bar 100 μm .

Supplementary movie M15

Spinning disc microscopy time-lapse movie of *ex vivo* cultured wild type testis (33h APF) expressing LifeAct-EGFP using the *htl-Gal4* driver. The isolated myotube pair by laser ablation is marked by an asterisk. Scale bar 100 μm .

Supplementary movie M16

Spinning disc microscopy time-lapse movie of an *ex vivo* cultured testis (33h APF) co-expressing a *rac2* RNAi together with a LifeAct-EGFP transgene in all myotubes using

the *mef2-Gal4* driver. Myotube migration is almost completely disrupted. Scale bar: 50µm.

Supplementary movie M17

Spinning disc microscopy time-lapse movie of an *ex vivo* cultured (left) wild type testis compared to (right) testis expressing a *cdc42* RNAi transgene. Migration is strongly affected by *cdc42* RNAi. Cells change their shape, generating massive filopodia-like structures, in comparison to WT Scale bar: 50µm.

Supplementary movie M18

Spinning disc microscopy time-lapse movies of (right) wild type myotubes, (middle) *rac2* depleted myotubes and (right) *cdc42* depleted myotubes together with a LifeAct-EGFP transgene, 40 min in *ex vivo* culture. Scale bar 20 µm.

Supplementary movie M19

Spinning disc microscopy time-lapse movies of (right) wild type myotubes, (middle) *rac2* depleted myotubes and (right) *cdc42* depleted myotubes marked by the cell-matrix adhesion reporter FAT-EGFP, 40 min in *ex vivo* culture. Scale bar 20 µm.

Supplementary movie M20

Spinning disc microscopy time-lapse movie of migrating myotubes co-expressing the Rho1 activity reporter and LifeAct-RFP to visualize protrusion dynamics. Rho-Sensor activity is found in retracting free edge filopodia (yellow arrowheads). Note that the ubiquitously expressed Rho1 sensor also marks ring canals in the *Drosophila* germline cyst (white arrowheads). Scale bar: 10 µm.

Supplementary movie M21

Spinning disc microscopy time-lapse movies of *ex vivo* cultured (from left to right) testis treated with (A) the Rok inhibitor (Y27632), (B) treated with the blebbistatin, expressing a (C) *sqh* and (D) *zip* RNAi transgene. Migration is strongly affected. Scale bar: 50µm.

Supplementary movie M22

Computer simulation model. Cells were positioned at one end of a confinement roughly mimicking the unfolded testis surface. **(A)** If cells behave according to the default setting, meaning that just adhesion but not filopodia lifetime is affected by contact, then all free space gets covered while cells keep their cohesion. **(B)** Isolated cells keep their cohesion as well, but randomly migrate, until they are contacted by the expanding sheet. After contact, they move along, as part of the sheet. **(C)** When filopodia disassemble shortly after contact, the behaviour resembles CIL, as there is a short phase of protrusion asymmetry, shifting the centroids apart from each other. Shortly after contact the repulsive motion ceases, as new filopodia emerge, until another cell moves close. All space gets covered, but there is no cohesion between cells. (A-C) In all scenarios a clumping of cells can be observed at the testis base. It seems to be a consequence of the interaction with the barrier which has no counterpart in a three dimensional limitless but finite surface. It is thereby an artefact with no meaning for the simulation (for more details about the simulation see supplementary material).

References

- 1 Scarpa, E. & Mayor, R. Collective cell migration in development. *J Cell Biol* **212**, 143-155, doi:10.1083/jcb.201508047 (2016).
- 2 Friedl, P. & Mayor, R. Tuning Collective Cell Migration by Cell-Cell Junction Regulation. *Cold Spring Harb Perspect Biol* **9**, doi:10.1101/cshperspect.a029199 (2017).
- 3 Ridley, A. J. Rho GTPase signalling in cell migration. *Curr Opin Cell Biol* **36**, 103-112, doi:10.1016/j.ceb.2015.08.005 (2015).
- 4 Schaks, M., Giannone, G. & Rottner, K. Actin dynamics in cell migration. *Essays Biochem* **63**, 483-495, doi:10.1042/EBC20190015 (2019).
- 5 Mayor, R. Collective Cell Migration: Wisdom of the Crowds Transforms a Negative Cue into a Positive One. *Current Biology* **29**, R205-R207 (2019).
- 6 Mayor, R. & Etienne-Manneville, S. The front and rear of collective cell migration. *Nat Rev Mol Cell Biol* **17**, 97-109, doi:10.1038/nrm.2015.14 (2016).
- 7 Yamada, K. M. & Sixt, M. Mechanisms of 3D cell migration. *Nat Rev Mol Cell Biol*, doi:10.1038/s41580-019-0172-9 (2019).
- 8 Abercrombie, M. & Heaysman, J. E. M. Observations on the Social Behaviour of Cells in Tissue Culture .1. Speed of Movement of Chick Heart Fibroblasts in Relation to Their Mutual Contacts. *Exp Cell Res* **5**, 111-131 (1953).

- 9 Abercrombie, M. & Heaysman, J. E. M. Observations on the Social Behaviour of Cells in Tissue Culture .2. Monolayering of Fibroblasts. *Exp Cell Res* **6**, 293-306 (1954).
- 10 Lin, B., Yin, T., Wu, Y. I., Inoue, T. & Levchenko, A. Interplay between chemotaxis and contact inhibition of locomotion determines exploratory cell migration. *Nat Commun* **6**, 6619, doi:10.1038/ncomms7619 (2015).
- 11 Roycroft, A. & Mayor, R. Michael Abercrombie: contact inhibition of locomotion and more. *Int J Dev Biol* **62**, 5-13, doi:10.1387/ijdb.170277rm (2018).
- 12 Stramer, B. & Mayor, R. Mechanisms and in vivo functions of contact inhibition of locomotion. *Nat Rev Mol Cell Bio* **18**, 43-55 (2017).
- 13 Roycroft, A. *et al.* Redistribution of Adhesive Forces through Src/FAK Drives Contact Inhibition of Locomotion in Neural Crest. *Dev Cell* **45**, 565-579 e563, doi:10.1016/j.devcel.2018.05.003 (2018).
- 14 Theveneau, E. *et al.* Chase-and-run between adjacent cell populations promotes directional collective migration. *Nat Cell Biol* **15**, 763-+ (2013).
- 15 Scarpa, E. *et al.* Cadherin Switch during EMT in Neural Crest Cells Leads to Contact Inhibition of Locomotion via Repolarization of Forces. *Dev Cell* **34**, 421-434, doi:10.1016/j.devcel.2015.06.012 (2015).
- 16 Carmona-Fontaine, C. *et al.* Contact inhibition of locomotion in vivo controls neural crest directional migration. *Nature* **456**, 957-961, doi:10.1038/nature07441 (2008).
- 17 Bate, M. & Martinez Arias, A. *The Development of Drosophila melanogaster*. (Cold Spring Harbor Laboratory Press, 1993).
- 18 Estrada, B., Casares, F. & Sanchez-Herrero, E. Development of the genitalia in *Drosophila melanogaster*. *Differentiation* **71**, 299-310, doi:10.1046/j.1432-0436.2003.03017.x (2003).
- 19 Kuckwa, J., Fritzen, K., Buttgereit, D., Rothenbusch-Fender, S. & Renkawitz-Pohl, R. A new level of plasticity: *Drosophila* smooth-like testes muscles compensate failure of myoblast fusion. *Development* **143**, 329-338, doi:10.1242/dev.126730 (2016).
- 20 Nanda, S. *et al.* Sox100B, a *Drosophila* Group E Sox-domain Gene, Is Required for Somatic Testis Differentiation. *Sex Dev* **3**, 26-37, doi:10.1159/000200079 (2009).
- 21 Kozopas, K. M., Samos, C. H. & Nusse, R. DWnt-2, a *Drosophila* Wnt gene required for the development of the male reproductive tract, specifies a sexually dimorphic cell fate. *Genes Dev* **12**, 1155-1165, doi:10.1101/gad.12.8.1155 (1998).
- 22 Susic-Jung, L. *et al.* Multinucleated smooth muscles and mononucleated as well as multinucleated striated muscles develop during establishment of the male reproductive organs of *Drosophila melanogaster*. *Dev Biol* **370**, 86-97 (2012).

- 23 Liepe, J. *et al.* Accurate Reconstruction of Cell and Particle Tracks from 3D Live Imaging Data. *Cell Syst* **3**, 102-107, doi:10.1016/j.cels.2016.06.002 (2016).
- 24 Nolen, B. J. *et al.* Characterization of two classes of small molecule inhibitors of Arp2/3 complex. *Nature* **460**, 1031-U1121, doi:10.1038/nature08231 (2009).
- 25 Rizvi, S. A. *et al.* Identification and characterization of a small molecule inhibitor of formin-mediated actin assembly. *Chem Biol* **16**, 1158-1168, doi:10.1016/j.chembiol.2009.10.006 (2009).
- 26 Sturner, T. *et al.* Transient localization of the Arp2/3 complex initiates neuronal dendrite branching in vivo. *Development* **146**, doi:10.1242/dev.171397 (2019).
- 27 Jacquemet, G., Hamidi, H. & Ivaska, J. Filopodia in cell adhesion, 3D migration and cancer cell invasion. *Curr Opin Cell Biol* **36**, 23-31, doi:10.1016/j.ceb.2015.06.007 (2015).
- 28 Nagel, B. M., Bechtold, M., Rodriguez, L. G. & Bogdan, S. Drosophila WASH is required for integrin-mediated cell adhesion, cell motility and lysosomal neutralization. *J Cell Sci* **130**, 344-359, doi:10.1242/jcs.193086 (2017).
- 29 Theveneau, E. & Linker, C. Leaders in collective migration: are front cells really endowed with a particular set of skills? *F1000Res* **6**, 1899, doi:10.12688/f1000research.11889.1 (2017).
- 30 Rothenbusch-Fender, S. *et al.* Myotube migration to cover and shape the testis of Drosophila depends on Heartless, Cadherin/Catenin, and myosin II. *Biol Open* **6**, 1876-1888, doi:10.1242/bio.025940 (2017).
- 31 Iwai, Y. *et al.* Axon patterning requires DN-cadherin, a novel neuronal adhesion receptor, in the Drosophila embryonic CNS. *Neuron* **19**, 77-89 (1997).
- 32 Hunter, M. V. & Fernandez-Gonzalez, R. Coordinating cell movements in vivo: junctional and cytoskeletal dynamics lead the way. *Curr Opin Cell Biol* **48**, 54-62, doi:10.1016/j.ceb.2017.05.005 (2017).
- 33 Rottner, K., Faix, J., Bogdan, S., Linder, S. & Kerkhoff, E. Actin assembly mechanisms at a glance. *J Cell Sci* **130**, 3427-3435, doi:10.1242/jcs.206433 (2017).
- 34 Rottner, K. & Schaks, M. Assembling actin filaments for protrusion. *Curr Opin Cell Biol* **56**, 53-63, doi:10.1016/j.ceb.2018.09.004 (2019).
- 35 Hakeda-Suzuki, S. *et al.* Rac function and regulation during Drosophila development. *Nature* **416**, 438-442, doi:10.1038/416438a (2002).
- 36 Chen, Z. C. *et al.* Structure and control of the actin regulatory WAVE complex. *Nature* **468**, 533-U207, doi:10.1038/nature09623 (2010).
- 37 Hariharan, I. K. *et al.* Characterization of Rho Gtpase Family Homologs in Drosophila-Melanogaster - Overexpressing Rho1 in Retinal Cells Causes a Late Developmental Defect. *Embo J* **14**, 292-302, doi:DOI 10.1002/j.1460-2075.1995.tb07003.x (1995).

- 38 Sasamura, T. *et al.* Molecular cloning and characterization of Drosophila genes encoding small GTPases of the rab and rho families. *Mol Gen Genet* **254**, 486-494, doi:10.1007/s004380050443 (1997).
- 39 Munjal, A., Philippe, J. M., Munro, E. & Lecuit, T. A self-organized biomechanical network drives shape changes during tissue morphogenesis. *Nature* **524**, 351-355, doi:10.1038/nature14603 (2015).
- 40 Settleman, J. Rac 'n Rho: the music that shapes a developing embryo. *Dev Cell* **1**, 321-331, doi:10.1016/s1534-5807(01)00053-3 (2001).
- 41 Hodge, R. G. & Ridley, A. J. Regulating Rho GTPases and their regulators. *Nat Rev Mol Cell Biol* **17**, 496-510, doi:10.1038/nrm.2016.67 (2016).
- 42 Ishizaki, T. *et al.* Pharmacological properties of Y-27632, a specific inhibitor of rho-associated kinases. *Mol Pharmacol* **57**, 976-983 (2000).
- 43 Straight, A. F. *et al.* Dissecting temporal and spatial control of cytokinesis with a myosin II inhibitor. *Science* **299**, 1743-1747, doi:10.1126/science.1081412 (2003).
- 44 Kepiro, M. *et al.* para-Nitroblebbistatin, the non-cytotoxic and photostable myosin II inhibitor. *Angew Chem Int Ed Engl* **53**, 8211-8215, doi:10.1002/anie.201403540 (2014).
- 45 Thomas, L. A. & Yamada, K. M. Contact stimulation of cell migration. *J Cell Sci* **103 (Pt 4)**, 1211-1214 (1992).
- 46 Theveneau, E. & Mayor, R. Collective cell migration of epithelial and mesenchymal cells. *Cell Mol Life Sci* **70**, 3481-3492 (2013).
- 47 Ladoux, B. & Mege, R. M. Mechanobiology of collective cell behaviours. *Nat Rev Mol Cell Biol* **18**, 743-757, doi:10.1038/nrm.2017.98 (2017).
- 48 Desai, R. A., Gao, L., Raghavan, S., Liu, W. F. & Chen, C. S. Cell polarity triggered by cell-cell adhesion via E-cadherin. *J Cell Sci* **122**, 905-911, doi:10.1242/jcs.028183 (2009).
- 49 Bajanca, F. *et al.* In vivo topology converts competition for cell-matrix adhesion into directional migration. *Nat Commun* **10**, 1518, doi:10.1038/s41467-019-09548-5 (2019).
- 50 Guo, F., Debidda, M., Yang, L., Williams, D. A. & Zheng, Y. Genetic deletion of Rac1 GTPase reveals its critical role in actin stress fiber formation and focal adhesion complex assembly. *J Biol Chem* **281**, 18652-18659, doi:10.1074/jbc.M603508200 (2006).
- 51 Woods, M. L. *et al.* Directional Collective Cell Migration Emerges as a Property of Cell Interactions. *Plos One* **9**, doi:ARTN e104969 10.1371/journal.pone.0104969 (2014).
- 52 Szabo, A. *et al.* In vivo confinement promotes collective migration of neural crest cells. *J Cell Biol* **213**, 543-555, doi:10.1083/jcb.201602083 (2016).

- 53 Begnaud, S., Chen, T., Delacour, D., Mege, R. M. & Ladoux, B. Mechanics of epithelial tissues during gap closure. *Curr Opin Cell Biol* **42**, 52-62, doi:10.1016/j.ceb.2016.04.006 (2016).
- 54 Krause, M. & Gautreau, A. Steering cell migration: lamellipodium dynamics and the regulation of directional persistence. *Nat Rev Mol Cell Biol* **15**, 577-590, doi:10.1038/nrm3861 (2014).
- 55 Wu, C. Y. *et al.* Arp2/3 Is Critical for Lamellipodia and Response to Extracellular Matrix Cues but Is Dispensable for Chemotaxis. *Cell* **148**, 973-987, doi:10.1016/j.cell.2011.12.034 (2012).
- 56 Suraneni, P. *et al.* The Arp2/3 complex is required for lamellipodia extension and directional fibroblast cell migration. *J Cell Biol* **197**, 239-251, doi:10.1083/jcb.201112113 (2012).
- 57 Gupton, S. L. *et al.* Cell migration without a lamellipodium: translation of actin dynamics into cell movement mediated by tropomyosin. *J Cell Biol* **168**, 619-631, doi:10.1083/jcb.200406063 (2005).
- 58 Yang, C. & Svitkina, T. Filopodia initiation: focus on the Arp2/3 complex and formins. *Cell Adh Migr* **5**, 402-408, doi:10.4161/cam.5.5.16971 (2011).
- 59 Arjonen, A., Kaukonen, R. & Ivaska, J. Filopodia and adhesion in cancer cell motility. *Cell Adhes Migr* **5**, 421-430, doi:10.4161/cam.5.5.17723 (2011).
- 60 Ashburner, M. *Drosophila*. (Cold Spring Harbor Laboratory, 1989).
- 61 Ranganayakulu, G. *et al.* A series of mutations in the D-MEF2 transcription factor reveal multiple functions in larval and adult myogenesis in *Drosophila*. *Dev Biol* **171**, 169-181, doi:10.1006/dbio.1995.1269 (1995).
- 62 Squarr, A. J. *et al.* Fat2 acts through the WAVE regulatory complex to drive collective cell migration during tissue rotation. *J Cell Biol* **212**, 591-603, doi:10.1083/jcb.201508081 (2016).
- 63 Burgess, A. *et al.* Loss of human Greatwall results in G2 arrest and multiple mitotic defects due to deregulation of the cyclin B-Cdc2/PP2A balance. *Proc Natl Acad Sci U S A* **107**, 12564-12569, doi:10.1073/pnas.0914191107 (2010).

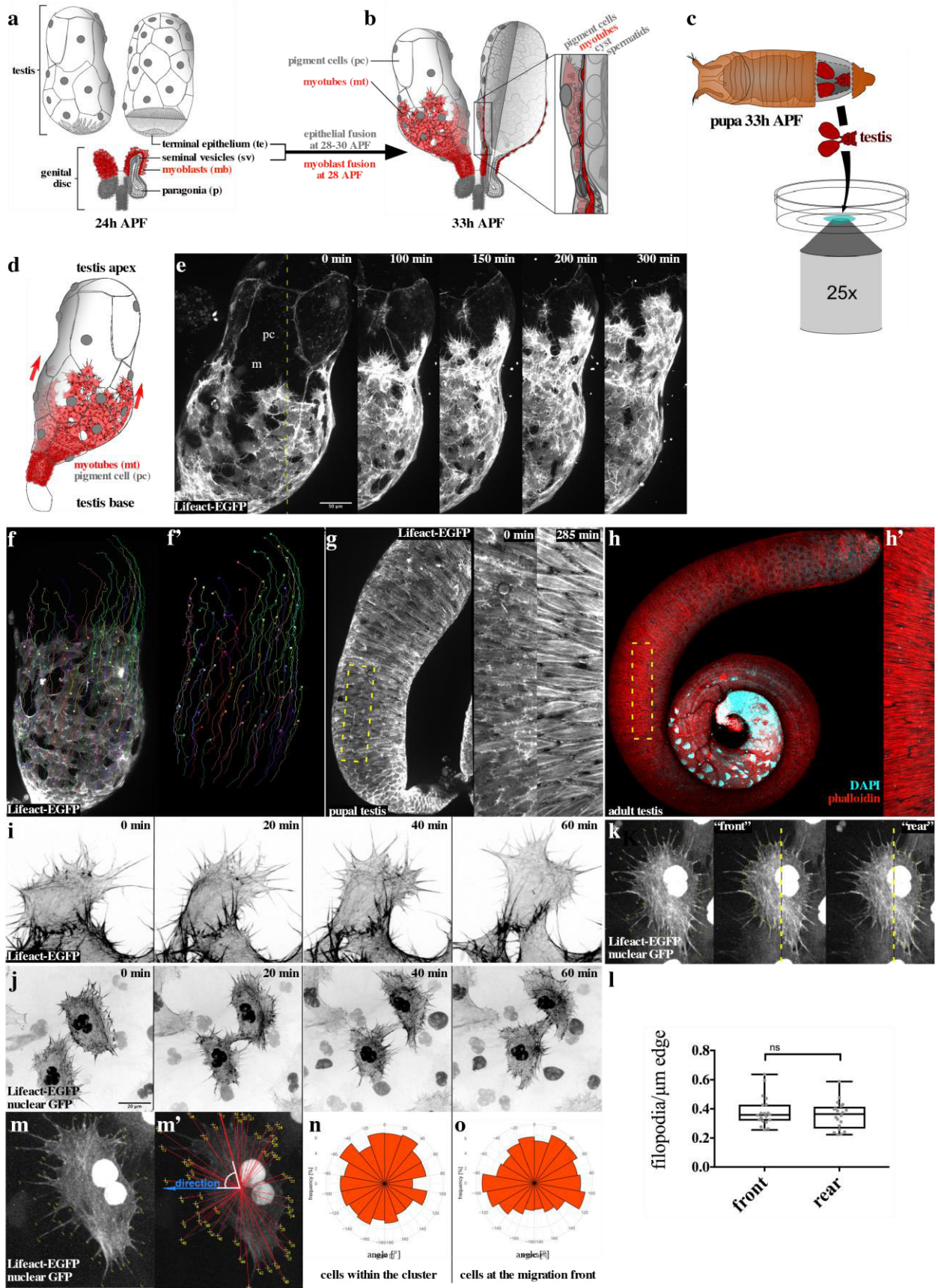


Figure 1

Bischoff et al.,

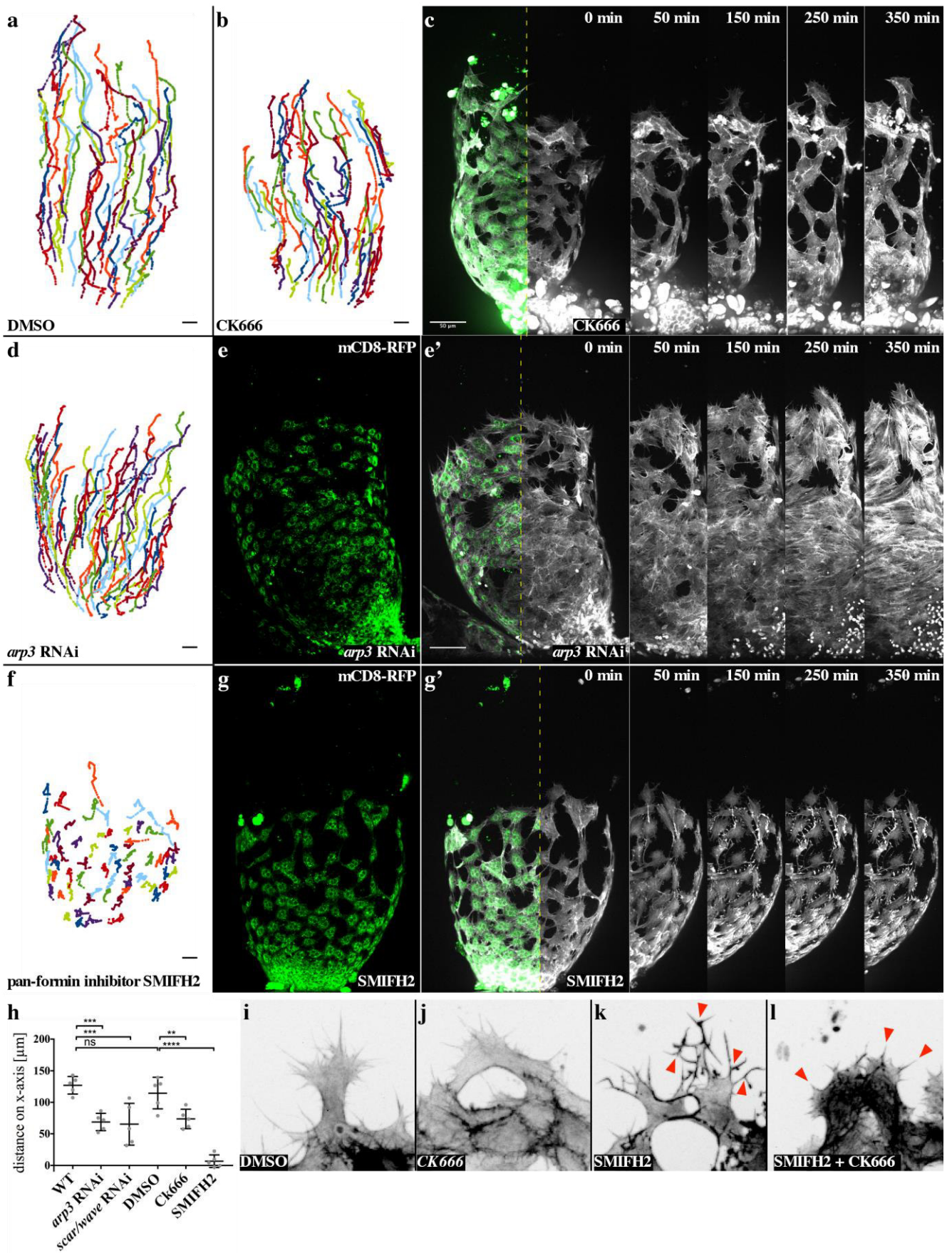


Figure 2

Bischoff et al.,

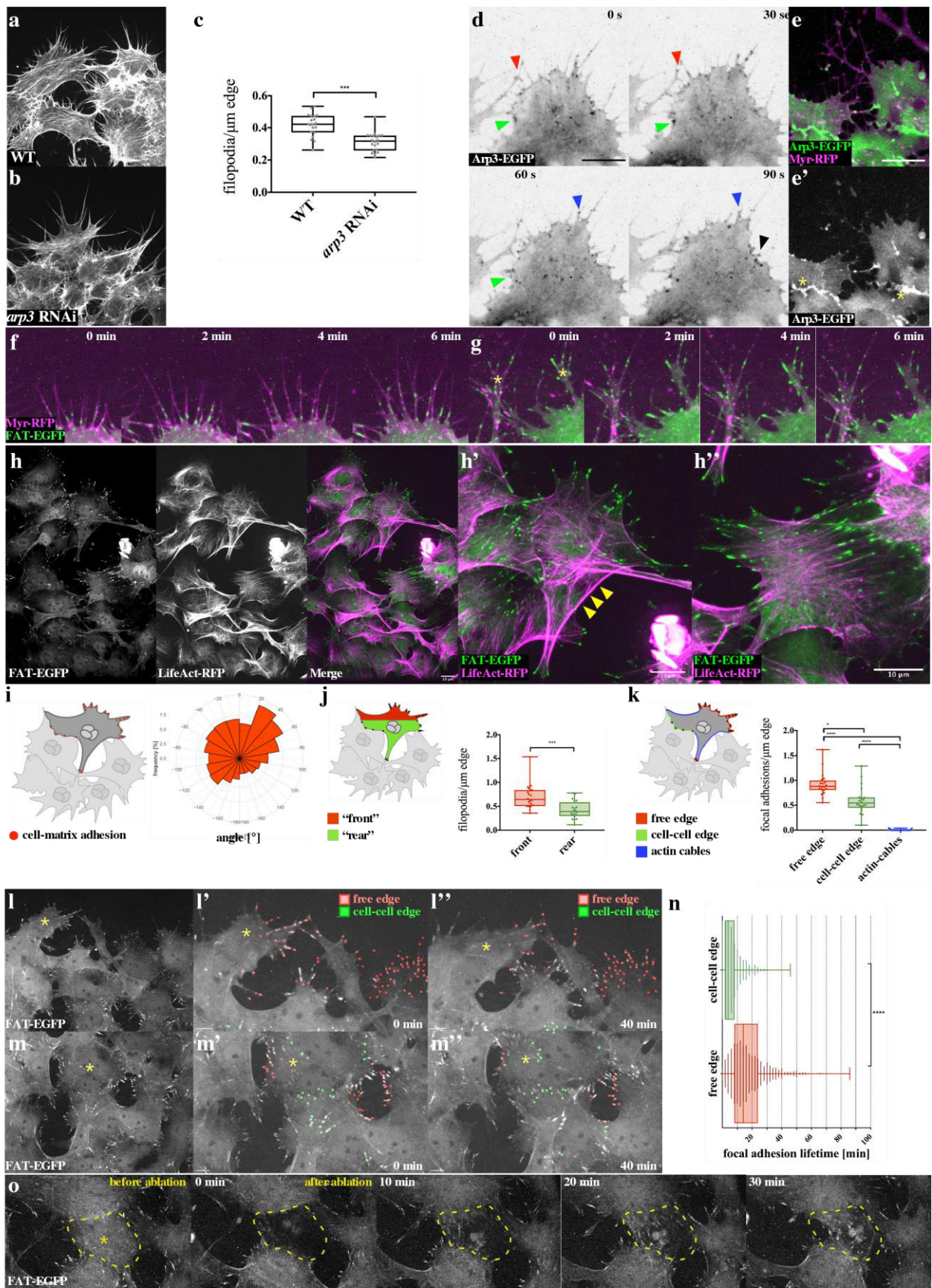


Figure 3

Bischoff et al.,

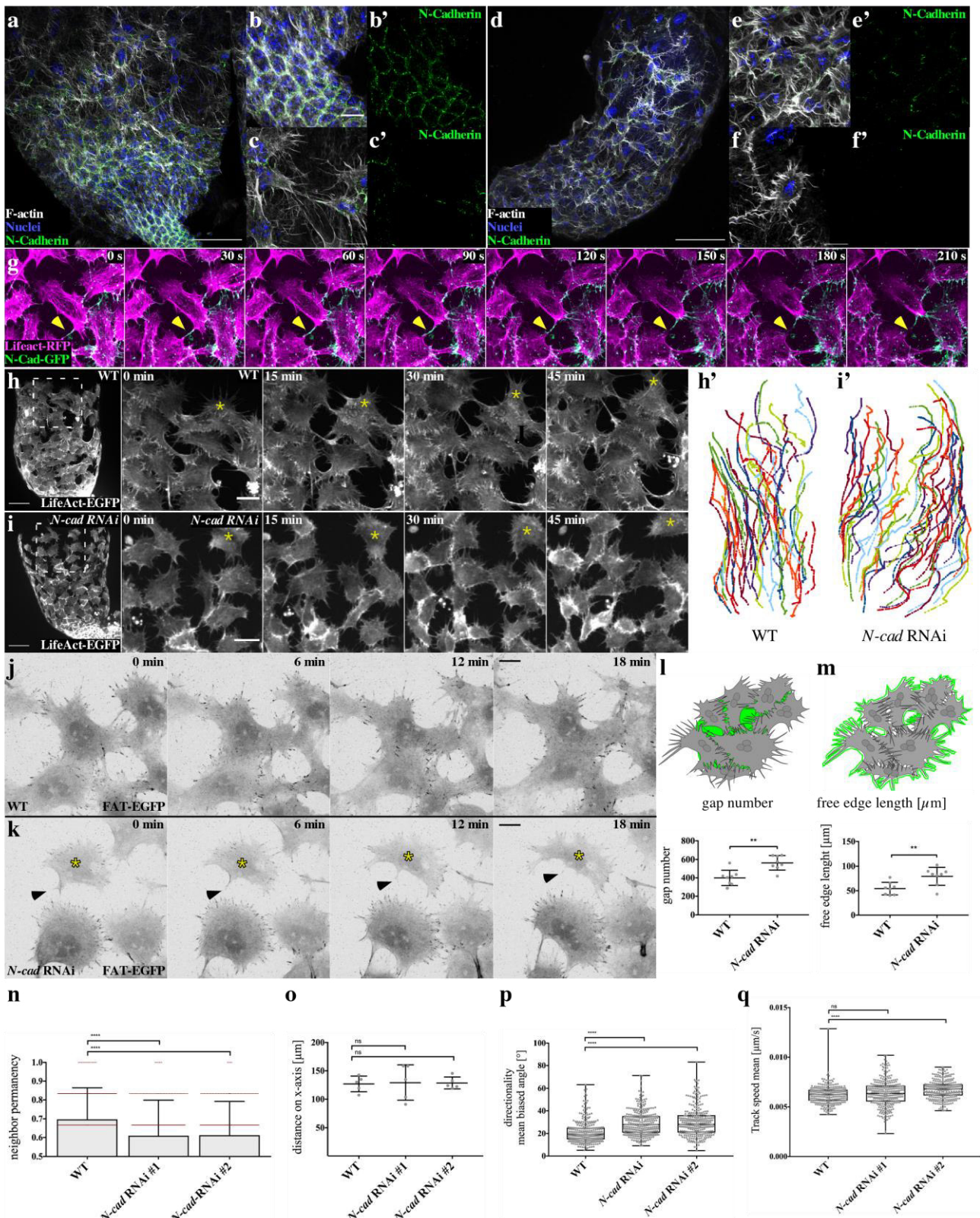


Figure 4

Bischoff et al.,

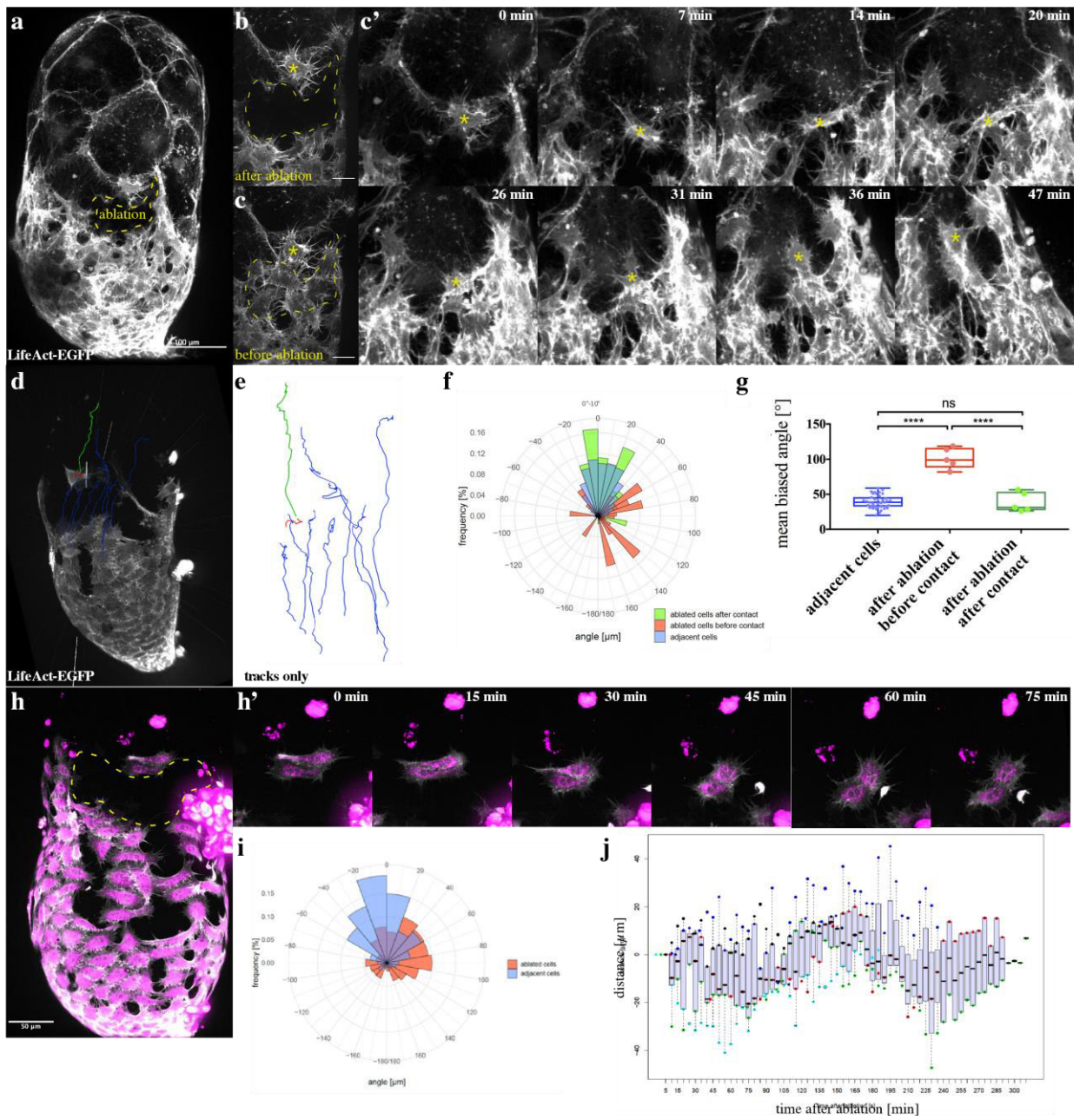


Figure 5

Bischoff et al.,

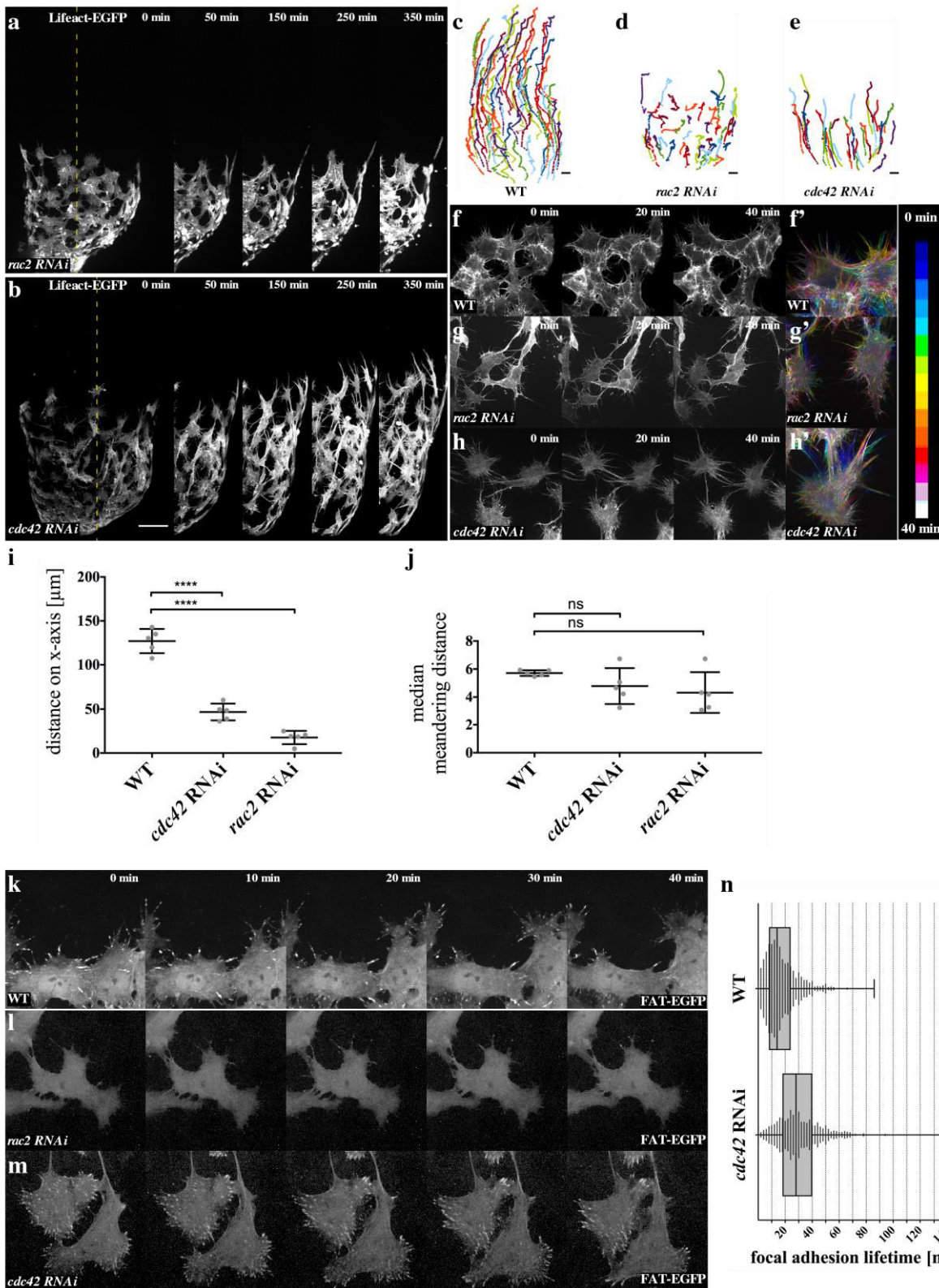


Figure 6

Bischoff et al.,

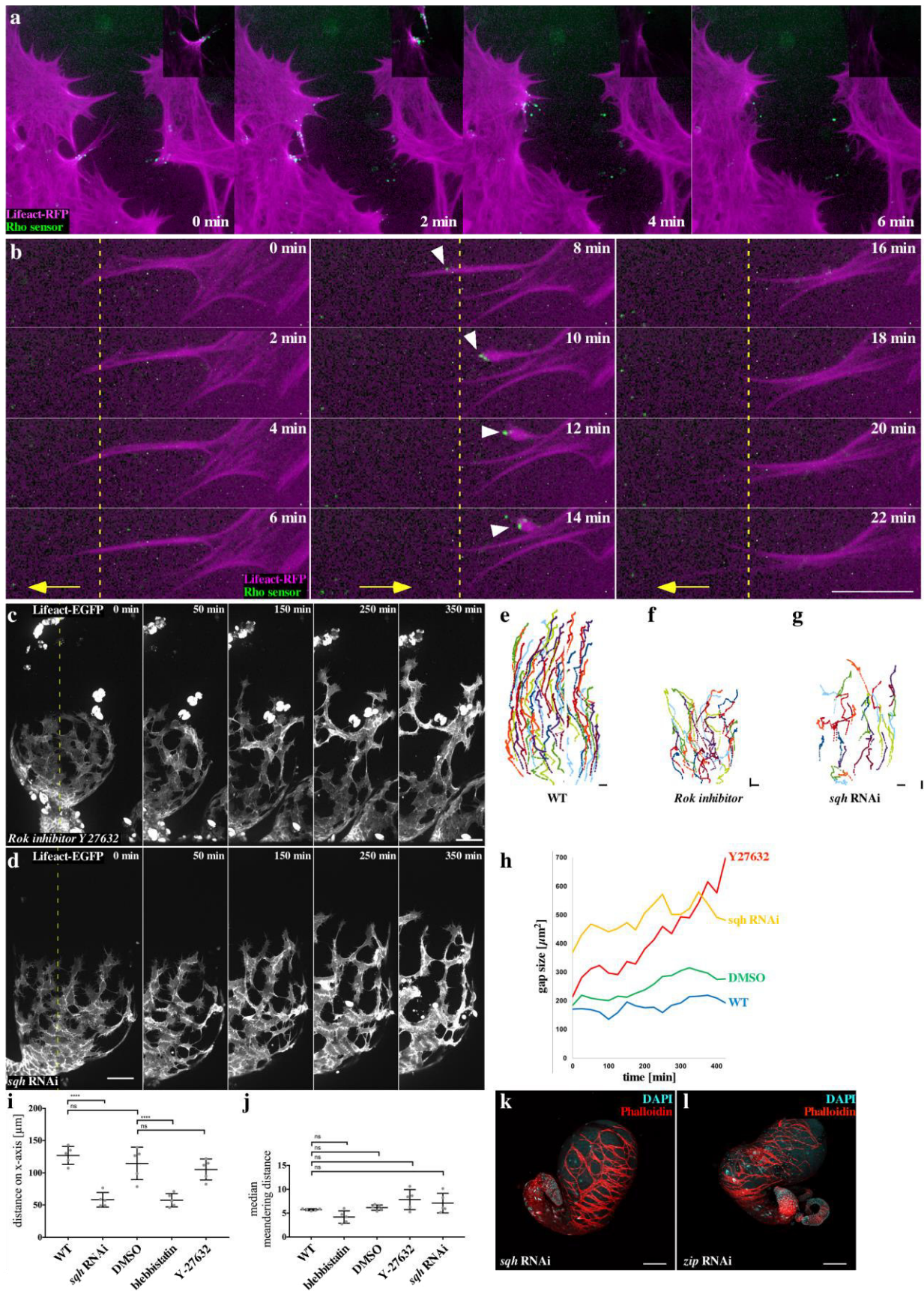


Figure 7

Bischoff et al.,

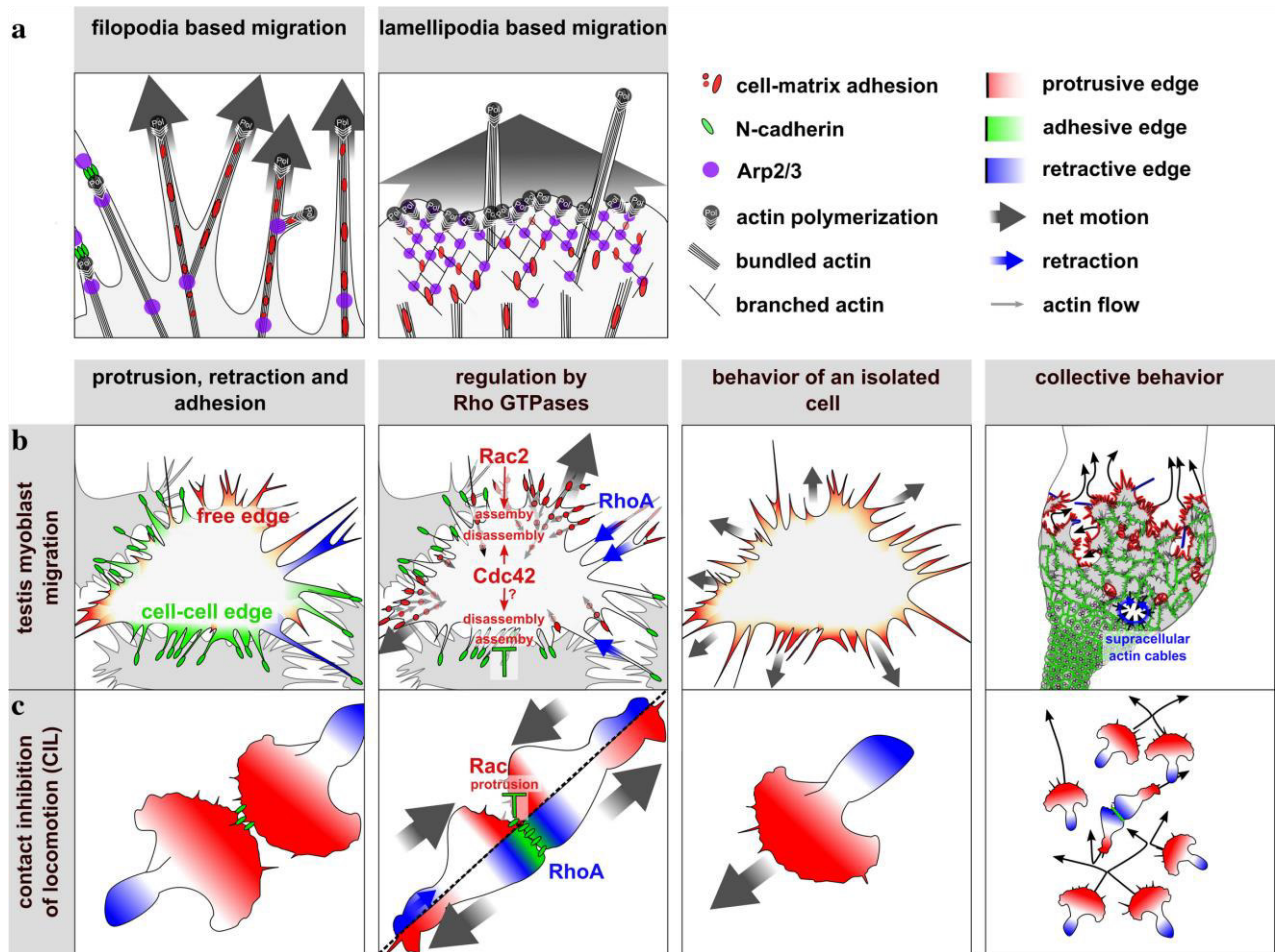
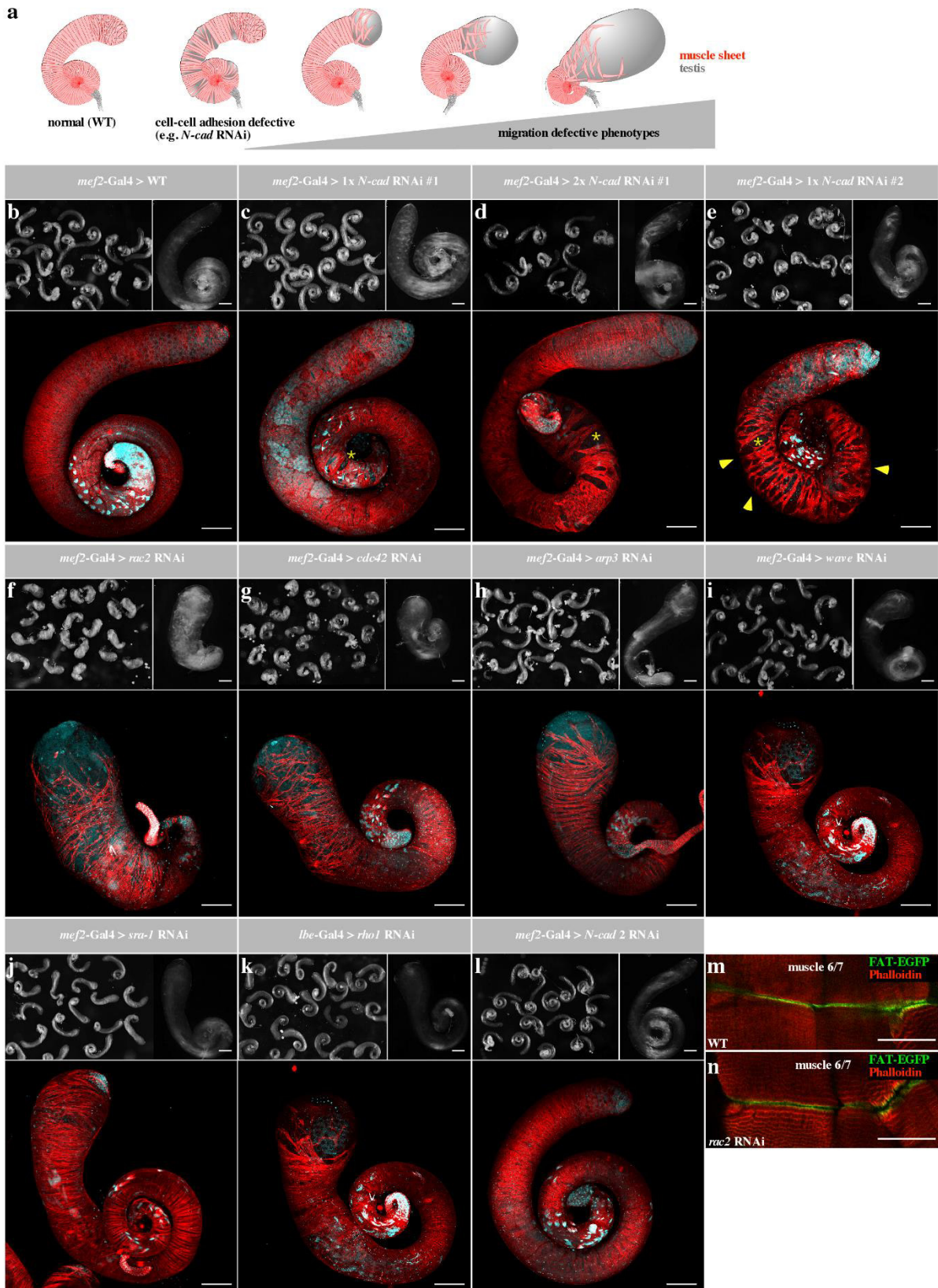


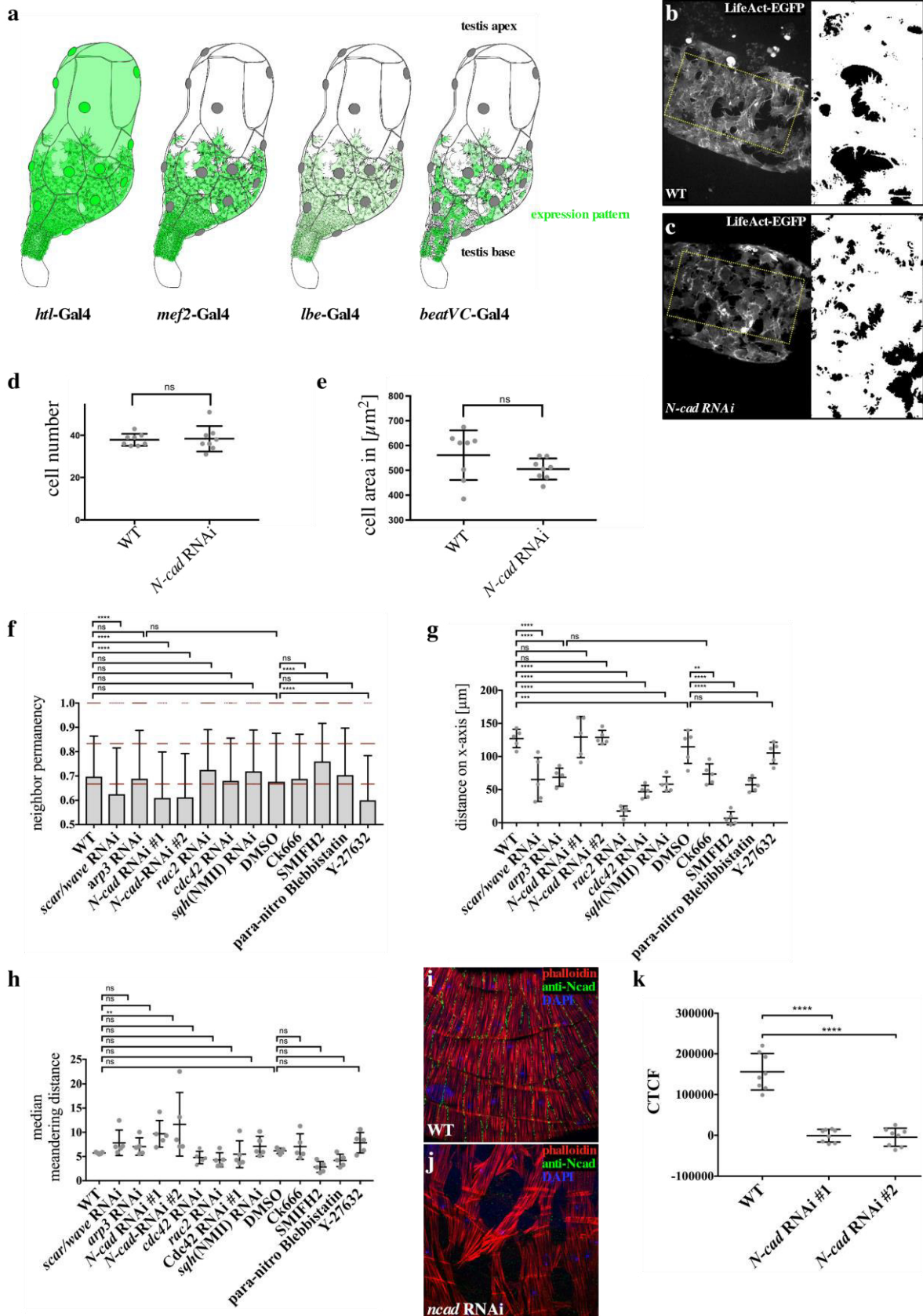
Figure 8
al.,

Bischoff et



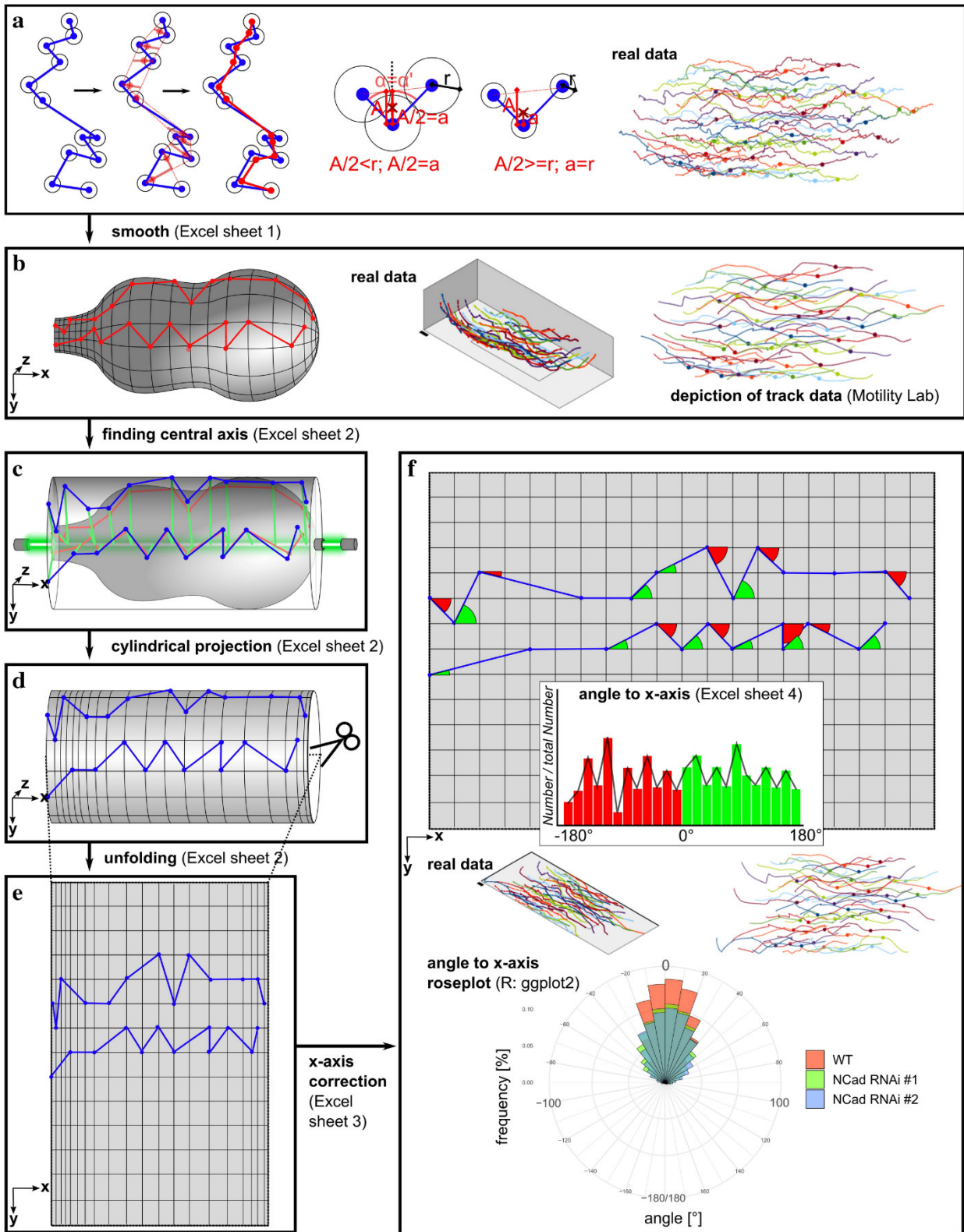
Supplementary figure S1

Bischoff et al.,



Supplementary figure S2

Bischoff et al.,



Supplementary figure S3

Bischoff et al.,

effector	fly line ID	driver	phenotypic strength
UAS-Ncad RNAi	v1092	<i>htl-Gal4</i>	defective adhesion
	v1092	<i>mef-Gal4</i>	defective adhesion
	v1093 (\pm #1)	<i>htl-Gal4</i>	defective adhesion
	v1093	<i>mef-Gal4</i>	defective adhesion
	v101642 (\pm #2)	<i>mef-Gal4</i>	defective adhesion
UAS-Ncad 2 RNAi	v101659	<i>mef-Gal4</i>	no phenotype
	v36166	<i>mef-Gal4</i>	no phenotype
UAS-arp3 RNAi	v108951	<i>htl-Gal4</i>	medium migration defects
	v108951	<i>mef-Gal4</i>	medium migration defects
	v35258	<i>htl-Gal4</i>	medium migration defects
	v35258	<i>mef-Gal4</i>	medium migration defects
	BL-32921	<i>htl-Gal4</i>	no phenotype
	v35260	<i>htl-Gal4</i>	no phenotype
UAS-arp2 RNAi	v29944	<i>Mef-Gal4</i>	medium migration defects
UAS-scar/wave RNAi	NIG 4636R-1	<i>htl-Gal4</i>	medium migration defects
	NIG 4636R-1	<i>mef-Gal4</i>	medium migration defects
	BL-51803	<i>mef-Gal4</i>	medium migration defects
	BL-36121	<i>mef-Gal4</i>	no phenotype
	BL-31126	<i>mef-Gal4</i>	no phenotype
UAS-sra1 RNAi	BL-38294	<i>mef-Gal4</i>	medium migration defects
UAS-rac2 RNAi	NIG-8556R-1	<i>mef-Gal4</i>	strong migration defects
	NIG-8556R-3	<i>mef-Gal4</i>	strong migration defects
	v28926	<i>mef-Gal4</i>	no phenotype
	v50349	<i>mef-Gal4</i>	no phenotype
	v50350	<i>mef-Gal4</i>	no phenotype
UAS-rac1 RNAi	BL-28985	<i>mef-Gal4</i>	no phenotype
	BL-34910	<i>mef-Gal4</i>	no phenotype
	v49246	<i>mef-Gal4</i>	no phenotype
UAS-mtl RNAi	v108427	<i>mef-Gal4</i>	no phenotype
UAS-cdc42 RNAi	BL-28021	<i>htl-Gal4</i>	strong - medium migration defects
	BL-28021	<i>mef-Gal4</i>	strong migration defects
	v100794	<i>mef-Gal4</i>	medium migration defects
UAS-rho1 RNAi	v12734	<i>mef-Gal4</i>	lethal
	BL-27727	<i>mef-Gal4</i>	lethal
	BL-32383	<i>mef-Gal4</i>	lethal
	BL-32383	<i>lbe-Gal4</i>	medium migration defects
	v109420	<i>mef-Gal4</i>	no phenotype
UAS-rhoL RNAi	v102461	<i>mef-Gal4</i>	no phenotype
UAS-dia RNAi	v20518	<i>htl-Gal4</i>	strong migration defects
	v20518	<i>mef-Gal4</i>	no phenotype
	BL-25955	<i>mef-Gal4</i>	no phenotype
UAS-capu RNAi	v34278	<i>htl-Gal4</i>	no phenotype
UAS-form RNAi	v107473	<i>htl-Gal4</i>	no phenotype
	v45594	<i>htl-Gal4</i>	no phenotype
	v42302	<i>htl-Gal4</i>	no phenotype
UAS-daam RNAi	v24885	<i>htl-Gal4</i>	no phenotype
UAS-frl RNAi	v34412	<i>htl-Gal4</i>	no phenotype
	v34413	<i>htl-Gal4</i>	no phenotype
UAS-fhos RNAi	v45837	<i>htl-Gal4</i>	no phenotype
	v45838	<i>htl-Gal4</i>	no phenotype
	v34034	<i>htl-Gal4</i>	no phenotype
	v34035	<i>htl-Gal4</i>	no phenotype
	v108347	<i>htl-Gal4</i>	no phenotype
UAS-sqh RNAi	v7916	<i>mef-Gal4</i>	strong migration defects
	v7917	<i>mef-Gal4</i>	medium migration defects
	v109493	<i>mef-Gal4</i>	medium migration defects
UAS-zip RNAi	v7819	<i>mef-Gal4</i>	strong migration defects
UAS-mys RNAi	v103704	<i>htl-Gal4</i>	lethal
	v103704	<i>mef-Gal4</i>	lethal
	v103704	<i>lbe-Gal4</i>	strong – no migration defects

Supplementary table 1

Bischoff et al.

4. Additional Results and Discussion

4.1 Pupal testis myotube development occurs in three steps and can be studied in explants

Shortly before testis myotube migration starts, testis and seminal vesicle come into close proximity. Then, the testis terminal epithelium and the seminal vesicle epithelium fuse to build a continuous epithelial tube at 30 h APF^{260,257}. After cell-cell fusion, cells are tightly packed in a columnar fashion, containing N-Cadherin^{260,419} (pub. 1, fig. 8). At the imago stage, testes are covered by a smooth-muscle-like sheath of elongated myotubes⁴⁸⁸. As a prerequisite for live-cell imaging approaches, the sequence of events including migration, elongation and testis shaping had to be determined. To achieve this, pupae were timed in steps ranging from 36 to 76 h APF and stained for F-actin and N-Cadherin (fig. S1). It became clear that migration was still going on at 36 h APF and ended at 40 h APF. At that time, the elongation of myotubes starts (fig. S1a–b'). During migration, the shape of the testis does not change dramatically. Cells are still interconnected via N-Cadherin containing tip adhesions in interdigitating filopodia. Subsequently, proximal-distal elongation of the testis from 40–54 h APF is accompanied by an expansion of its surface, causing myotubes to recede from each other (fig. S1 b–e'). Still, cells are linked by finger-like protrusions, seemingly keeping cells together and countering expansion of the substrate. These protrusions are projected in parallel along the elongated myotube. At the same time (40–54 h APF), myotubes become narrower, building increasingly parallel F-actin bundles. After 54 h APF, myotubes broaden, covering the open testis surface and thereby build a continuous sheet (fig. S1 e–g'). This zip-like process ends at 66 h APF and is accompanied by a shortening of interdigitating N-Cadherin bearing filopodia. From 66 h APF onwards, testes seem to elongate slightly, yet myotubes on the surface seem not to change their shape anymore (fig. S1 g–i'). Interestingly, until the adult stage N-Cadherin does not localize along the entire membrane but in distinct foci, revealing small interdigitating rod-like protrusions (see in pub. 2, fig. S2 i). Based on these observations, three steps of pupal testis myotube development can be defined: **1.** myotube migration, approx. 30–40 h APF, **2.** myotube elongation and condensing, approx. 40–54 h APF, **3.** myotube convergence, approx. 54–66 h APF. Linkage via N-Cadherin containing finger-like protrusions is kept throughout development and thereby appears crucial for mechanical linkage countering tensile forces throughout testis development. How cell adhesion affects post-migration stages remains to be elucidated.

Applying this knowledge, *ex vivo* imaging of pupal testes explants was established. There were first attempts of live-cell imaging of testis myotube migration, preceding this work (pub. 1, fig 6 j–k') based on approaches developed to visualize spermatogenesis¹⁶⁴. In these experiments, migration was not clearly visible. For further optimize live-cell imaging, methods from *Drosophila* egg-chamber cultivation were applied and modified⁴⁷⁰. Using these methods, the migration along the testis and the elongation step could be reproduced in culture (pub. 2). The explanted organs could be kept alive for up to 7 h and were imaged from 33 h APF onwards, to visualize and analyse migration. The system allows

for an in-depth analysis of cell dynamics which was so far only feasible in cell culture. Still, this new model brings the merits of an *in vivo* model as all the cellular interfaces resemble the natural configuration. The fly testis explant represents an isolated micro-environment, passing through the same developmental processes during which it interacts with the same substrates as inside the developing animal. The only comparable explant-based system in *Drosophila* is border cell migration ^{reviewed in 334}. Nevertheless, due to their flat structure testis myotubes allow for a detailed analysis of cytoskeletal structures. Live-cell imaging revealed a constant cell-cell adhesion between myotubes, turning it to a genuine model for collective cell migration. Most research regarding collective motility relies on cultured isolated cells. These systems bring many advantages in terms of feasibility and imaging, but also some shortcomings in emulating the biophysical traits comparable with the situation *in vivo*⁴¹⁷. The testis myotube migration model seems to combine the merits of an *ex vivo* system with imaging capacities nearly comparable to 2D cell culture. To facilitate future research in this model-system driver lines from the Janelia Research Campus^{231,377} were screened for expression in myoblasts and adjacent tissues (section 7.3).

4.2 Migrating testis myotubes use a filopodia-based mode of motility

By using the newly established culturing methods, it could be shown that migrating testis myotubes lack lamellipodial structures but possess numerous highly dynamic filopodia-like protrusions. Analysing defects on the matured testis, it has been shown before that WAVE and Arp3 are seemingly not needed for migration but myotube fusion¹⁵². Live-cell imaging of RNAi-based *arp3*, *arp2*, and *wave* depleted myotubes and pharmacological inhibition of Arp2/3 via CK666 confirmed migration to be largely independent of actin-branching. In contrast, perturbation of Formins with SMIFH2 leads to a complete cessation of migration, suggesting that nucleation and elongation of bundled actin outweigh dendritic network formation. Arp2/3 function only seemed to be supportive in migration since detailed mathematical and statistical analysis revealed a slight reduction of the migratory distance during 7 h of live-cell imaging (pub. 2). Recently, border cell motility was also suggested to depend on bundled actin dynamics based on a loss of the bundler Fascin (*singed* in *Drosophila*) disrupting migration²⁷⁴. In this work, it could be shown that treatment with SMIFH2 causes a high number of branched filopodia. The addition of CK666 reversed this effect. Arp3-GFP localized in branch points that rarely occur in wild type myotubes. It may thus be concluded that formin dependent elongation takes the main role in protrusion, whereas Arp2/3 complex dependent dendritic nucleation might contribute to filopodia branching. Consistently, number of filopodia was reduced upon *arp3* RNAi (pub. 2). It is well-established that Formins take a central role in filopodia-formation^{373,49,567}. In contrast, Arp2/3 complex as a factor in filopodia-branching seems unusual. However, the Arp2/3 complex is known to take a role in conventional filopodia assembly. In fibroblast-like motility, filopodia seem to emerge from Arp2/3 induced branch points inside the lamellipodium^{249,469}. During dendrite branchlet formation in

Drosophila sensory neurons, it was demonstrated that Arp2/3 can branch filopodia-like structures containing condensed bundled F-actin⁴⁸³. At the same time, Arp2/3-GFP was shown to localize to these branch points. The findings presented here, suggest that Arp2/3 complex function can support filopodial motility. Presumably, this is caused by a higher number of filopodia tips, increasing Formin dependent elongation of barbed ends.

Using the FAK-localization marker FAT-EGFP³⁵⁰, it could be shown that Integrin-mediated adhesions emerge in filopodia shafts. Filopodia elongate and slide over these adhesions, suggesting a molecular clutch process fuelled by actin polymerization as known from lamellipodial migration^{562, reviewed in 526}. It is recognized that filopodia can contain Integrin-mediated substrate adhesions that are localized either in the tip, the shaft, or the base and bear resemblance with focal adhesions^{288,437,118,415,163}. However, their role was either seen as an initial anchoring point for adhesions that are delivered to the lamellipodium or as a means for probing ECM-rigidity^{232,556}.

Many experiments could show that a loss of lamellipodium in different cell types goes along with the emergence of numerous filopodia. In the earliest approach, the finding that tropomyosin acts negatively on Arp2/3 was applied⁴⁵. Injection of α -tropomyosin in PtK₁ epithelial cells leads to a disruption of lamellipodia and abundant filopodia¹⁸⁸. Cells without lamellipodia are faster. The authors concluded that migration was driven by the actomyosin-based dynamics of the lamella. In another approach, a loss of lamellipodium in Arp3^{-/-} mouse embryonic fibroblasts was shown to be accompanied by more mDia1 and 2 dependent filopodia. Cells had the same speed but were less persistent⁴⁸⁷. Depleting Arp2 and p34Arp in mouse embryonic fibroblasts also perturbed lamellipodia and induced abundant filopodia. Inhibitor experiments demonstrate that the resulting slower random migration is still F-actin polymerisation dependent and not actomyosin-contraction driven. This contradicts the hypothesis that lamella-based motility is used upon Arp2/3 depletion. Interestingly, sensibility to specific migration cues was affected differently. Chemoattraction (via PDGF) remained unaffected, whereas cells could not follow a linear gradient of ECM concentration. This led the authors to the assumption that haptotaxis seems lamellipodia dependent⁵⁶³. Other approaches to disrupt lamellipodia, not targeting Arp2/3 complex, had similar effects on filopodia dynamics. Lamellipodin (Lpd) colocalizes and interacts with Ena/VASP at lamellipodia/filopodia tips in “Rat2” fibroblasts and mouse neuronal cells. Overexpression of Lpd leads to an increase of lamellipodial protrusion while a knock-out causes a loss of lamellipodium and numerous filopodia. This caused reduced cell speed²⁵⁸. These results have been reproduced *in vivo* via Lpd knock-down in mouse melanoblast migration²⁸³. It can be concluded that migration in all the described experimental settings principally still worked with filopodia as the only source of protrusive forces. Thereby it can be deduced that filopodia-driven motility belongs to the toolkit of many cell types and is mostly masked by lamellipodial dynamics.^{188, 487–258}

In cancer cells, it was demonstrated repeatedly that tempering with structural components of filopodia, like Myosin X, affects tumour metastasis^{20,77,462}. Very recently, it was shown that migration of ovarian cancer cells through the mesothelial cell layer, which covers peritoneal organs, depends on

filopodia not lamellipodia or invadopodia. Trans-migration can be increased by overexpressing Fascin 1. Downregulation of Fascin-1 or Myosin X inhibited the process. Additionally, downregulation on Integrin β 1 or N-Cadherin also leads to a drop in the rate of trans-mesothelial migration. Ovarian cancer cells seem to deploy filopodial migration only in certain environments. When in contact with glass only lamellipodia are built but plated on human peritoneal mesothelial cells numerous filopodia emerge⁵⁷². It looks like in this example for cancer trans-migration, the same mechanisms are utilized as in testis myotube locomotion. In the future, it must be elucidated which exact conditions cause cells to switch their migration mode to filopodial rather than lamellipodial motility.

A remarkable finding was that filopodia seemed not to be perturbed but rather elongated by RNAi-based reduction of *Cdc42*. In the “classical” view, *Cdc42* induces filopodial protrusions via WASP³³⁰⁻³⁵⁶. Testis myoblast migration is not the only model in which filopodia were built in a *Cdc42*-independent manner. It was shown in fibroblastoid cells that *Cdc42* is negligible for filopodia and lamellipodia formation¹⁰⁴. The phenotypes observable in *Cdc42* reduced myotubes seem to be a consequence a potential regulative function in substrate adhesion, discussed in section 4.5.

A question not addressed in this work concerns the contribution of actomyosin contractility in filopodial locomotion. Future experiments, based on fluorescence recovery after photobleaching (FRAP)-based visualization of retrograde flow or Förster resonance energy transfer (FRET)-based tension-sensors for example, will have to deduce whether motion arises only by actin polymerization-based pushing or if actomyosin-based pulling contributes as well. During FRET, a donor fluorophore transfers energy to an acceptor fluorophore when the distance between both is under of $\sim 10 \mu\text{m}$. As the more energy is transferred, the closer they come, measuring of FRET-efficiency provides a tool to assess the distance between two tagged molecules²⁷³. When acceptor and donor are separated by a flexible element and brought into load-bearing regions of a protein, the resulting sensors can be used to measure molecular tension²¹¹. Experiments like these have been conducted using Vinculin¹⁸⁰ or Talin⁴⁰⁸. Force measurements via similar FRET-based tension-sensors or alternatively by atomic force microscopy must elucidate the force that can be exerted by filopodia during filopodial migration. Combined with latrunculinA and blebbistatin treatment, the roles of actin-pushing and myosin-pulling could be dissected in detail.

4.3 FGF signalling affects migration but likely not as a chemoattractant

Fibroblast growth factors (FGF) are involved in many developmental processes including proliferation, cell fate decisions, differentiation and cell migration^{105,340}. They are secreted proteins that bind to FGF-receptors (FGFRs) which have tyrosine kinase activity^{reviewed in 105}. *Drosophila* possesses two FGFRs, the aforementioned Btl and Heartless (Htl)^{reviewed in 340}. Htl is activated by its two ligands Thisbe (Ths) and Pyramus (Pyr)^{66,472,182,313}. Downstream of Htl, mitogen activated protein kinase (MAPK)-pathway is activated^{564,156}. This causes the phosphorylation of different transcription factors, thereby altering the transcription profile⁵⁶⁹. In *Drosophila* mesoderm development, Htl seems also to activate the GEF Pebble (Pbl), which in turn activates Rac²²².

An RNAi screen in a previous study indicated that Htl might contribute to testis nascent myotube migration¹³⁶. It was observed that RNAi-based reduction of *downstream of FGF (dof, stumps)* using a pan-mesodermal driver tool causes adult testis coverage defects. These phenotypes were discussed being a consequence of either the regulation of the number of myoblasts on the genital disc, the connection of seminal vesicles, or disturbed cell migration. Downregulation of *htl* but not *btl* leads either to weaker coverage phenotypes or, depending on the RNAi-construct, to a complete loss of testis/genital disc connection (pub. 1)¹³⁶. *htl* RNAi-based loss of function can be phenocopied, using more specific driver tools. *htl*-Gal4 is restricted to myoblasts on imaginal discs, including the genital disc (fig.S 2 c–f, cf. scheme in c with a). *CadN*-Gal4, on the other hand, is restricted to prospective testis myotubes on the genital disc (fig. S2 g–j, cf. scheme in g with a). Weak phenotypes caused by a reduction of *htl* could be phenocopied using a hypomorphic *ths* allele. Thus, it can be concluded that FGF-signalling is significant for myotube coverage of the testis. A *htl*-Gal4 driver was used to deduce *htl* expression. It promotes Gal4 expression under the control of an intronic enhancer, representing large parts of the first intron of *htl*. The driver tool could induce strong *mcd8*-EGFP expression in myoblasts in larval²³⁴ and pupal stages (pub. 1). Immunofluorescence analysis of Ser19 phosphorylated Myosin II in wild type and *stumps* RNA depleted myotubes suggested that Myosin II activation may be downstream of Stumps/Htl activity. Furthermore, RNAi-mediated depletion of the Myosin II heavy chain and light chain genes, *zipper (zip)* and *spaghetti squash (sqh)* phenocopied weak *htl*-RNAi/*ths* hypomorphic allele phenotypes. (pub. 1).

It is known from many model-organisms that continuous gradients of FGF, either due to diffusion or due to gradual expression in tissues, are used to direct collective migration²⁹. The best-established model-system for Htl activation by Ths/Pyr in *Drosophila* is the developing mesoderm. Whether mesodermal cells migrate towards a source or along a gradient of the ligand is still debated but so far not shown²⁶. There are also many models known in which FGF works in a non-directional way, for example by promoting EMT or maintaining a migratory stage^{531,485}. To discriminate between a potential directional or non-directional function in myotube migration, experiments aiming potential sources of ligand were carried out. Reduction of *ths* via RNAi using Gal4 drivers specific for the seminal vesicle epithelium and the testis terminal epithelium (fig. S3 a–b') phenocopied the defects in *ths* hypomorphic allele (fig. S3 e–e'). Weaker coverage defects are yielded when a Gal4 driver is used which only

promotes expression in myoblasts and terminal testis epithelium (Supp fig. 3 c–d', f, f'). Using either Gal4 drivers promoting expression exclusively in seminal vesicle epithelium or myoblasts/myotubes, no phenotypes can be observed (data not shown). This suggests that *Ths* expression in the testis terminal epithelium is largely responsible for normal development, with a possible additional role for the seminal vesicle epithelium. Depleting *pyr* RNAi instead of *ths* RNAi yields no defects (data not shown). Conversely, strong coverage defects occur when using the terminal testis epithelium/seminal vesicle epithelium-driver line to promote ectopic expression of *Pyr* (fig S4 a–b', f–f'). In some cases, it seems as ectopic striated muscles get attracted to the origin of induced *Pyr* expression at the seminal vesicle epithelium (fig S4 g–g'') or the testis terminal epithelium (fig S4 h–h''). Ectopic *Pyr* expression in the seminal vesicle epithelium leads to weak coverage defects with loosely packed myotubes at the testis tip (fig S4 c–d', h–h''). Overexpression of UAS-*Ths* in the seminal vesicle epithelium did not lead to any coverage defects (data not shown). These findings suggest that *Pyr* expression in seminal vesicle/testis terminal epithelia is not needed for migration and even detrimental for normal development. *In situ* hybridization analysis of *ths* in the genital disc about 40 h APF revealed transcript expression in a gradient starting at prospective paragonia, reaching over the seminal vesicle epithelium with its peak at the testis terminal epithelium (Buttgereit, unpublished data). Therefore, it can be hypothesized that FGF ligand *Ths* does not work as chemoattractant during testis myotube migration. It is expressed in tissues adjacent to the starting point of myotube migration where the transformation in a migratory stage occurs. Secretion of *Ths*, which in turn activates *Htl* in myotubes, could induce this EMT-like process and thereby work as a gatekeeper for the testis. It might be crucial for the tight spatiotemporal regulation of the start of migration. This working hypothesis has to be addressed in the future, using the newly established live-cell imaging methods.

4.4 Collective behaviour resembles contact stimulation of migration (CSM)

In a recent *Current Biology* “dispatch”, spotlighting a publication that demonstrates principles of CIL in epithelial cell rotation⁴⁷³, Roberto Mayor gave rise to the question of whether other developmental collective migration processes use modified versions of CIL³²⁰. This might be especially interesting, regarding more cohesive cells. Even before the testis live-cell imaging system was established, it has been shown that myotubes are physically linked during migration. Immunostainings revealed N-Cadherin localization in cell-cell connecting filopodia, thereby creating a network of interconnected myotubes. (fig. S5 a). *beatVC*-Gal4 was found to promote expression in a mosaic pattern among genital disc myoblasts (fig. S5 b–b'). Expression of *htl*-RNAi under the control of *beatVC*-Gal4 caused a range of phenotypes, reaching from an almost complete lack of muscle coverage to mild defects (fig. S5 C, I–V). These results suggest that a loss of *htl* in scattered myotubes during migration causes a disruption of migration in the entire sheet. To test whether physical segregation of *htl*-depleted myotubes from the rest of the cluster occurs, GFP was co-expressed and testes were analysed at 48 h APF (fig. S5 d–e'').

The relative migration distance of affected GFP positive cells was quantified in comparison to unaffected GFP negative cells (fig. S5 f). The maximum migration distance of all cells was strongly affected when compared to wild type (*UAS-GFP* driven by *beat VC*, fig. S5 g). Nevertheless, the relative distance of GFP positive cells remains the same, showing that the position of possibly immotile cells did not alter (fig. S5 h). This indicates a physical link that allows immobilized cells to be dragged utilizing strong cell-cell adhesion. Such a behaviour resembles plithotaxis^{502,519}. Future experiments have to show whether depletion of N-Cadherin in the same background leads to segregation and clustering of GFP+/*htl*-RNAi cells at the basis. It could even partially rescue the coverage phenotype as motile cells gain back their full potential, being “cut off” from their immotile neighbours.

It could be shown, that RNAi based reduction of *N-cadherin* leads to adult myotube adhesion defects (pub. 1,2). During migration, N-Cadherin is localized in cell-cell interconnecting filopodia. A GFP tagged version of N-Cadherin revealed that the link between cells gets constantly renewed by newly emerging finger-like protrusions. RNAi-based depletion using the live-cell imaging system revealed that N-Cadherin is needed for directional behaviour. Reduction leads to a loss of directionality but did not change the total migration distance. What cells lost in persistence they gained in speed (pub. 2). The same observations upon depletion of N-Cadherin could be made during human glial cell migration in a wound scratch assay⁷². By these results, the conclusion can be drawn that reduced cell-cell adhesion in myotubes causes cells to exhibit more “open edge”. This can be hypothesized to be the reason for the loss of persistence. To address this question, single cells were isolated on the testis by laser-based ablation of their neighbours. These cells lost all directionality only to regain it after contact with the migrating sheet is re-established (pub. 2). A similar discovery was made in quail neural crest in which it was shown that cell-cell contact activates migration. Cells separated from the cluster ceased directional migration, a phenomenon termed contact stimulated migration (CSM)⁵¹². Transplantation of single *Danio* prechordal plate cells led to the same result. The major difference is that prechordal plate cells migrate as epithelia interconnected via E-Cadherin¹²⁵. CSM dynamics alone suffices as a sparse explanation for the observed behaviour of myotubes. Chemotaxis requires an attractive or repulsive cue which is established in a highly complex procedure by adjacent tissues. These must create a source and a sink for the chemoattractant/chemorepellent ^{reviewed in 68}. Therefore, a simple self-regulating mechanic of directionality towards the open edge appears less complex. Directionality based on “free edge” resembles behaviour observed in wound scratch essays using epithelial monolayers^{135,137,362,531,390}. Using this analogy, the uncovered parts of the testis can be described as the wound that must be closed.

In contrast to epithelial wound closure, even myotubes inside the sheet contain highly dynamic protrusions and do not show a sign of epithelial polarity. All myotubes in the cluster have a mesenchymal phenotype. Therefore, their migration can be classified as a type of mesenchymal cell migration by the definition of Theveneau and Mayor⁵⁰⁹. Myotube migration resembles a modified version of CIL^{506,78}. In *Xenopus* neural crest, CIL also causes cells to build more prominent protrusions at the free edges of the cluster³²¹. But unlike *Xenopus* neural crest cells, myotubes are constantly adhered to each other due to

the perpetual renewal of filopodial interdigitating. A basic problem in CIL is that it constitutes a repulsive and thereby negative cue, causing cells to disperse. To turn it into a positive driving force additional cell-cell attracting cues are necessary for *Xenopus* neural crest cells to ensure cohesion⁷⁹. In myotubes, physical N-Cadherin-mediated adhesion via filopodia might fulfil this function. The absence of propulsive behaviour was confirmed by isolating a pair of cells through laser ablation. Conversely, *Xenopus* neural crest cell migration is characterized by a constant neighbour exchange due to a lack of constant physical linkage²⁶⁵. To turn CIL into a directive signal in *Xenopus* additional chemoattraction of the cluster is necessary^{506,507}. In myotubes, this seems not to be required as the sheet has to expand onto the free space but cannot move in the opposite direction, unlike neural crest cells. Migration of chick cephalic neural crest cells seems to be more similar to myotubes. Chick neural crest cell CIL-behaviour is characterized by constant cell-cell adhesion via long filopodia through which cell content is shared^{262-264,326,503}. The main difference between these cells and testis myotubes lies in the fact that contact-dependent behaviour seems to be regulated differently. In myotubes, RhoA is not activated at the contact site. Cell-cell contact may lead to a similar outcome but the reason for motion towards the free edge seems mechanically different as discussed in the following section.

4.5 CSM requires differential matrix adhesion

Most CIL-related processes are marked by repulsive behaviours due to retraction at the contact site and protrusion at the free edge⁴⁷⁹. Hence, protrusive direction when measured points away from neighbouring cells or the cell-sheet. In myotubes, it could not be shown that filopodia align with the general direction of migration. Protrusions cannot be used to predict the trajectory but occur circumferentially uniform. Yet, anisotropy could also be reached through asymmetry in substrate adhesion, allowing submission of force only in distinct areas. Such asymmetry could be measured in myotube-migration using FAT-EGFP as a marker for integrin-based adhesions³⁵⁰. At the site of contact, there were shown to be less adhesions with a reduced lifetime. Hence, not all filopodia can assert the same force, presumably causing directional behaviour. Using laser-ablation techniques, it could be demonstrated that cells inside the cluster react with Integrin-mediated adhesions immediately when in contact with a newly created free edge. Therefore, the force of circumferential actin polymerization seems only to be submitted at the free edge of the cluster. Cell-cell connecting filopodia appear largely stall regarding submission of treadmilling, on the other hand, they mechanically link neighbours. This sparse regulation scheme alone suffices to explain the CSM-like behaviour observed. Therefore, it was recreated in a computer simulation where it caused the same dynamics as observed in *ex vivo* culture (pub. 2). Very recently, a much more complex computer model was presented, taking substrate stiffness and cell shape into account. It demonstrated as well that cell-cell adhesion and matrix adhesion are crucial factors for maintaining motion and cohesion of migrating sheets⁵⁸⁰. Contact dependent inhibition

of substrate adhesion is also known from *Xenopus* placode cells upon contact to neural crest cells during their “chase-and-run”-behaviour. Yet, cell-cell contact also influences protrusion via Rac-inhibition⁵⁰⁷.

Whether in myotubes a break of symmetry is enforced by regulating the actin polymerization rate in a contact-dependent manner remains elusive. Stall cell-cell interconnecting filopodia still need actin polymerization to counter membrane tension-force and thereby cannot cease treadmilling^{reviewed in 56}. On a mechanistic level, it suffices to regulate substrate adhesion without acting on polymerization rate. F-actin linked matrix adhesion takes the position of a rate-limiting step in the molecular clutch. If it is lacking locally, no force can be generated even when polymerization thus retrograde flow, remains unaffected. In the presented model, matrix adhesion takes the position of an on/off-switch to convert intracellular force into directed locomotion. Though, F-actin polymerization could be regulated additionally. To address this question, FRAP experiments visualizing retrograde flow or particle analysis have to be conducted to compare cell-cell filopodia with open edge filopodia.

A possible molecular mechanism for the observed behaviour could be Cadherin/Integrin antagonism. This dynamic has been shown numerous times, using different micropatterning assays^{reviewed in 65,126,55}. In glial cell migration, *N-cadherin* depletion causes the same non-directional behaviour as in myotubes⁷². Knockdown causes expansion of Integrin-mediated adhesions around the cell and a wound scratch assay did not yield repolarization as observed in wild type. Similar findings could be made in vascular smooth muscle cells⁴²⁵. In a very recent publication, a potential mechanism was presented which explains contact-dependent protrusive and adhesive behaviour without cell-cell adhesion/juxtacrine signalling at all¹⁵⁷. Physical confinement alone seems to suffice as an explanation. A single cell only in contact with adhesive micro-stripes reacted to these purely physical cues by a reduction of lamellipodial protrusion and matrix adhesion and thereby adopted a follower-like phenotype¹⁵⁷. To uncover the principles of substrate adhesion regulation in testis myotubes, exact measurements of Integrin-mediated adhesions upon a total loss of N-Cadherin have to be conducted. When a loss of matrix-adhesions upon contact still occurs, it means that contact-dependent behaviour is regulated by N-Cadherin-independent signals or it is purely physical. To prove the latter, myotubes have to be isolated from the testis and analyzed in micropatterned environments lacking cell-cell contact but faced with mechanical barriers.

4.6 Cohesion is enforced by purse-string-like dynamics via supracellular actin cables

Mesenchymal CSM-based migration of testis myotubes is a very dynamic process, presumably accompanied by the transmission of stress via cell-cell adhesions. It can be observed that small ruptures in the sheet can grow to holes and thereby disturb cohesion. Open edge was shown to promote substrate adhesion and thereby openings close by protrusion. Yet, circular gaps partially or completely lack protrusions and are enclosed by thick actin cables, passing through multiple cells. Protrusion-less edges still manage to close in a multi-cell cooperative process. A dynamic observed in other tissues can be confirmed in myoblasts; positive membrane curvature causes protrusive dynamics, whereas negative

membrane curvature results in actin cables, closing gaps in a purse-string like manner^{398, reviewed in 269}. Perturbation of Myosin II (*zip* and *sqh*) by RNAi or pharmacological inhibition of Myosin II and Rock causes a phenotype in which holes are not stopped from growing larger. Prominent ruptures are still present in adult testes. This suggests that actomyosin contractility is responsible for the process. Quantification showed a disturbed cohesion and a negatively affected migration distance. Filopodia-based protrusion still seemed to work, suggesting that Myosin II takes no direct role in filopodial motion (pub 2). This observation is reminiscent to border cell migration in which Cadherin-dependent cohesion is also supported by contractile supracellular actin cables^{204,19}. The difference is that border cells are surrounded peripherally by actin-cables, whereas myotubes build them internally.

There are similarities between myotube gap closure and *Drosophila* dorsal closure that originally gave rise to the purse-string analogy⁵⁷³. The same dynamics can be observed in epithelial monolayers during wound closure³⁹⁸. As both systems constitute typical examples of epithelial migration, it becomes clear again that testis nascent myotubes combine traits of mesenchymal cells and epithelia.

4.7 Regulation of substrate adhesion seems to be orchestrated by Rho-GTPases

In CIL, a RhoA/Rac1 gradient with the former at the contact site and the latter at the protrusive free edge steers the cell (summarized in fig. 4 b). As potential regulators for the matrix-adhesion turnover in myotubes, Rac2 and Cdc42 were found (pub. 2). It is long-known that Integrin-mediated adhesions are regulated by Rho-GTPases via Paxilin or FAK^{356,400,522}. A central role in this relationship is taken by Pax-interacting exchange factor beta (β Pix, rtGEF in *Drosophila*). β Pix is a Rac-GEF that binds Paxilin via G protein-coupled receptor kinase interactor 1/2 (Git1/2). Thereby, it activates Rac and inhibits RhoA^{245,520,310}. Conversely, effects on Integrin-mediated adhesions downstream of Rho-GTPase are known. Nobes and Hall observed that Cdc42 and Rac1 induce focal complex assembly³⁵⁶. Later, this role of Rac1 was confirmed^{272,185}. Yet, other findings suggest Rac1 being dispensable for integrin-mediated adhesion assembly⁴⁷⁴. In myotubes, it could be shown that RNAi-based reduction of *Rac2* causes a near-complete loss of FAT-EGFP marked matrix-adhesions. It must be noted that *Drosophila* Rac2 is not a direct homolog of vertebrate Rac2. In insects and vertebrates, Rac diversification occurred independently after the last common ancestor⁵⁴⁹. *Drosophila* Rac2 and Rac1 are nearly identical. In contrast to *Rac2*, reduction of *Cdc42* in myotubes leads to a longer lifetime of matrix adhesions (pub. 2). This is a highly unusual finding. In other systems, only opposite effects have been reported, *e.g.* in mouse skin development⁵⁵⁷. Similar phenotypes have been observed only upon RhoA depletion^{559,539} as actomyosin contractility is thought of as one of the driving forces of Integrin-mediated adhesion disassembly^{reviewed in 219}.

Both, *Rac2* and *Cdc42* reduction in myotubes cause severe migration defects. These could be linked to their influence on matrix adhesion (summarized in fig. 4 a). *Rac2*-RNAi causes short and unstable filopodia explicable by attenuation of substrate adhesion. In contrast, *Cdc42*-RNAi yields elongated

static rod-like protrusions (pub. 2). This phenotype is as previously mentioned unexpected as Cdc42 is known to induce filopodia via WASp. Still, mechanistically it makes sense that filopodia appear prolonged when matrix-adhesion-disassembly is perturbed. Accordingly, force is exerted as expansion not as motion. Similar tail-retraction-defects caused by a lack of adhesion disassembly have been observed upon depletion of RhoA⁵⁵⁹. Therefore, the question arises whether Cdc42 gets activated in a contact dependent-manner as RhoA during CIL^{506,36,23,336,114} (summarized in fig. 4 a).

RhoA can be excluded to have this function in myotubes. Analysis of RhoA activation using the RhoA-activity sensor Anilin.RBD-GFP³⁴⁶ revealed activation in filopodia at the free edge but never at contact sites. Lifeact-RFP is strongly expressed in actin cables that appear in protrusions presumably under tensile stress. RhoA activation always occurs in such filopodia followed by immediate retraction. In some cases, retraction is directly followed by protrusion (pub. 2). These findings demonstrate that RhoA is not a rear-end marker in myotubes but constitutes a short-timed answer to external, probably mechanical, cues (summarized in fig. 4 a). In the future, force measurements will have to elucidate whether these are truly membrane stress. A large body of evidence supports the finding that RhoA can be activated by tensile forces^{reviewed in 292}.

The activation of RhoA in single filopodia and not the rear gave rise to the hypothesis that filopodial migration in testis myotubes works without the “classical” mechanics of Rac/RhoA gradient-based polarization. This may work because filopodial dynamics replacing lamellipodia causes compartmentalization of forces which can be turned on/off in a binary fashion. Circumferential pushing forces can be modulated and orchestrated by controlling substrate adhesion in small regions via GTPase activity. Removing substrate adhesion from one compartment automatically leads to motion in the opposite direction. This small-scale partitioning allows for a spatially tightly structured regulation of forces (summarized in fig. 4 a). Unlike in lamellipodia, GTPase regulation can occur on a minimum scale. Rac2 and Cdc42 seem to have a function in substrate adhesion turn over but their exact roles remain elusive.

To address the function of Rac2 and Cdc42 in CSM, the subcellular localization of activation must be known. Therefore, bio-sensors were created, using the same principle as employed to create Anilin.RBD-GFP. The A and D-site of Sra1 were shown to have a high affinity for Rac⁸⁷ so they were utilized like RBD/CRIB sites in Rho-GTPase sensors⁴⁷⁵ to create highly specific Rac-activity sensors (fig S6 a', b, c). WHAMY, a *Drosophila* WASp paralog, contains two Rac-GTP-specific CRIB-sites⁶⁰ that are kept in tandem to create another Rac sensor (fig S6 a'', b, c). WASp is a classical Cdc42 binding partner^{22,494,63} so its CRIB domain was used to create a Cdc42-activity-sensor (fig S6 a''', b, c). Finally, the *Drosophila pak2* gene *mushroom bodies tiny (mbt)* was shown to specifically bind active Cdc42 but not Rac⁴⁴³. Thus, its CRIB was used to create a second Cdc42 sensor (fig S6 a''', b, c). These sensors will be used in the future to elucidate the exact activity pattern of Rho-GTPases at cell-cell contact sites and free-edges. As mentioned before, it remains to be clarified which role contact-dependent inhibition of actin polymerization plays during myotube CSM. Furthermore, it remains to be explored how Rho-

GTPases affect actin regulation upon contact. FRAP and particle analysis visualizing retrograde flow can be combined with Rho-GTPase depletion-experiments to approach this question. Finally, photoactivatable Rac, which was used to shed light on protrusive dynamics in border cell migration⁵³⁵, can be used to understand the exact role of Rac in myotube migration. This could be achieved by locally activating Rac at cell-cell contacts and, following a measurement of retrograde flow and focal adhesion dynamics.

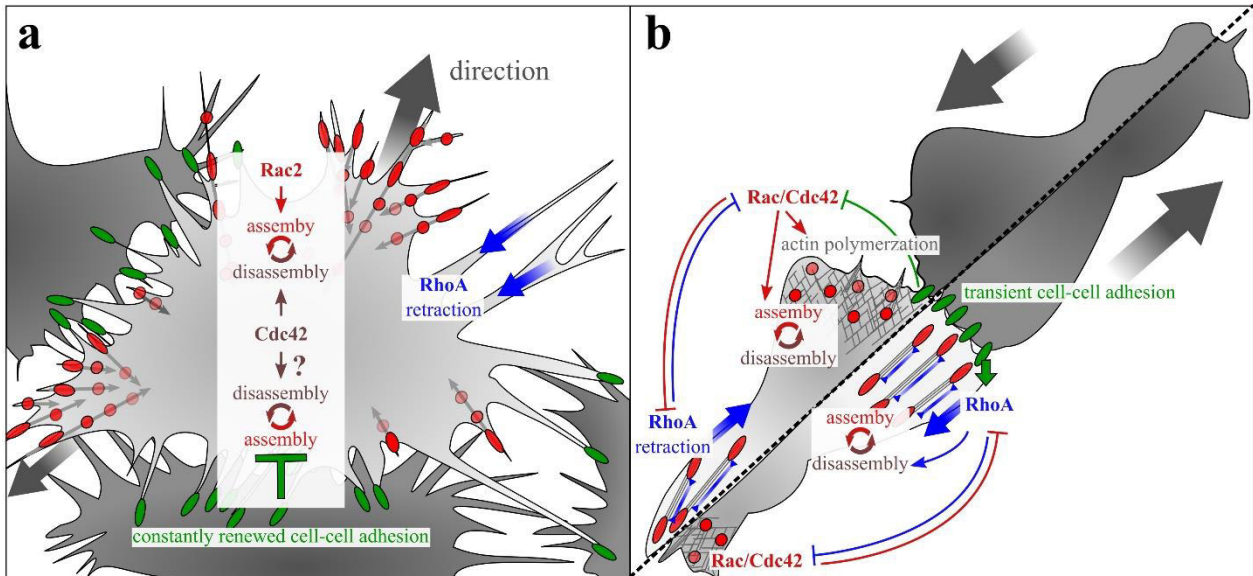


Figure 4. Rho-GTPases in testis myotube CSM compared to CIL. In myotubes (a) small GTPases seem to affect integrin-based adhesion turnover (red). Rac2 appears to affect assembly whereas Cdc42 seems to cause disassembly. In CIL (b) both Rac and Cdc42 are known positive regulators of integrin-based adhesions. Cell-cell adhesion activated RhoA causes nascent adhesion disassembly in accordance with its rear-defining function. In fibroblast-like motility RhoA induces retraction of actomyosin fibres via Myosin II-activation (blue arrow, b). In myotubes RhoA is not activated in the rear or at the contact site, but in free edge filopodia, seemingly exhibiting membrane stress (blue arrow, a). After RhoA activation filopodia retract. Still, in myotubes cell-cell contact seems to inhibit matrix adhesion assembly, potentially via Cdc42 (arrow with ?, a). In CIL and fibroblast-like motility Rac and Cdc42 mainly affect actin-polymerization via WRC/Wasp. This could not be shown in myotubes. Cell-cell contact in myotubes is not transient, like in CIL, but gets constantly renewed, causing cells to adhere and thereby move as a cluster. Thereby cells move in the free space, adhered to their neighbours, and do not repel each other like in CIL (grey arrows in a & b).

4.8 Testis nascent myotube migration could be an example for invasive cancer-like motility

Filopodial migration appears to be a non-conventional mode of motility. A large body of evidence supports the notion that migration modes strongly depend on the underlying substrate^{357,367,214}. Hence, versatile cells facing different substrates can dynamically switch between means of locomotion. It was shown for ovarian cancer cells that they deploy filopodial migration when in contact with peritoneal cells to enable trans-migration⁵⁷². Testis myotube migration occurs always in the same environment that seemingly calls for filopodial locomotion. Accordingly, it is crucial to examine the exact nature of the migration substrates faced during this process. Previous work suggested that pigment cells enclose myotubes, migrating in the opposite direction²⁵⁷. This was demonstrated by marking nuclei. It cannot be excluded that only the elevated part of pigment cells, containing the nucleus, breaches the myotube layer. Using differential interference contrast microscopy, it is very difficult to visualize the very flat cortical regions of pigment cells. The question arises whether these also cover myotubes. To address this, a difference in the expression pattern of Lifeact-EGFP and Lifeact-RFP was utilized. When driven with *htl*-Gal4, Lifeact-EGFP is visible in both pigment cells and myotubes (fig. S7 a'). In contrast, Lifeact-RFP only accumulates in areas with much F-actin and therefore prominently marks cortical F-actin in pigment cells, revealing that these build a continuous layer (fig. S7 a, p = pigment cells). In an overlay (EGFP: green, RFP: magenta), only pigment cells appear white, whereas myotubes appear green. In an orthogonal section, it becomes visible that the cortical regions of pigment cells lay above the myotube layer. (fig. S7 a''-a''', yellow asterisks, cf. to yellow section-line in a). In accordance with the results from Kozopas *et al.*, (1998), it can be concluded that pigment cells build a continuous layer, completely encasing myotubes during migration (fig. S7 b)²⁵⁷. Using anti-beta3 tubulin antibody to stain pigment cells, Detlev Buttgerit came to the same conclusion (unpublished, personal information). Therefore, interesting questions concerning physical interactions due to sheer forces between the pigment sheet and the myotube sheet arise that can be addressed in the future. During RNAi screens for migration defects, some candidates only yielded muscle-coverage defects when driven with *htl*-Gal4 which induces expression in pigment cells and myotubes. When exclusively driven in mesoderm via *mef*-Gal4 no phenotypes arose. This occurred when targeting the RNA of the microtubule plus end-tracker *chromosome bows* (*chb*), the formin *dia*, the GEF *rhogef64c* and *wasp*. Using the pigment-cell specific driver *kr*-Gal4²⁵⁷, defects can be phenocopied but only in rear cases. It could be shown that *kr*-Gal4 is only expressed in single pigment cells in a mosaic-fashion (data not shown). Judging by these non-cell-autonomous muscle defects, it can be assumed that pigment cell dynamics somehow affect myotube behaviour. A possible explanation might be cell-cell adhesions acting as means for force generation, analogous to cell-matrix adhesions. Processes like this are already known from wound closure, where a retrograde flow of adherens junctions was observed to exert force on neighbouring cells, in addition to conventional matrix-adhesion generated force³⁷². In border cells, adjacent cells are the only substrate to migrate on. Therefore, only E-Cadherin-mediated adherens junctions can be used as a substitute for integrin-mediated adhesions to transmit treadmilling-generated force^{353,67}. To test for

such dynamics between pigment cells and myotubes, potential cell-cell adhesion proteins have to be found. Additionally, a complete loss of pigment cells, using better-suited driver lines, could clarify the myotubes dependence on this potential cellular substrate.

As it was shown that myotube migration depends on the β -Integrin subunit *mysospheroid* (*mys*, pub. 2), it could be assumed that migration requires cell-matrix interaction. Therefore, the spatial structure of ECM should be elucidated. To accomplish this, the Collagen IV-marker Viking-EGFP (Vkg-EGFP, protein trap insertion) was analyzed. Basement membrane-like Collagen IV sheets could be visualized. In areas where pigment cells can be detected in orthogonal sections, the seemingly singular sheet is revealed to consist of two layers with pigment cells positioned between (fig. S7 c-c''', asterisks in c'/c'''). In areas with myotubes and pigment cells both ECM-layers enwrap the two cellular sheets. No GFP-marked ECM is detectable between myotubes and pigment cells (fig. S7 c-c''', marked with "myo" in c'/c'''). It can be concluded that myotubes seem only to contact the lower ECM-layer (fig. S7 d). The upper ECM-layer can be detected to ruffle and to partially detach when analysed in top view (fig. S7 c, arrows). This "shedding" process appears to progress throughout myotube migration as in later stages no more upper basement membrane-like ECM can be detected (fig. S7 e-f). However, this process should not affect myotube migration as there seems to be no direct contact. Future experiments must elucidate which tissues secrete the ECM-components. Interestingly, migration does not simply occur on a 2D-interface, despite the flatness of the sheet. The cell has physical contact with a rigid substrate in all spatial dimensions. In conclusion, it migrates *through* and not *on* its environment. This unconventional "2.5D" configuration possibly represents a requirement for the filopodial migration mode. RNAi-based reduction of the matrix metalloprotease *Mmp2* causes strong motility defects in the sheet. MMPs are zinc-dependent peptidases, that enable proteolysis of components of the ECM. They are involved in development, inflammatory processes and cancer invasion ^{reviewed in 240}. Upon *Mmp2* reduction, myotubes are still able to migrate, but the further proximal they are localized in the sheet, the stronger stuck in the substratum they appear. It seems as flexible cells at the front can cope by finding a non-linear way through the meshwork. Cells more rearwards, which are enclosed by neighbours, appear not to be able to do so and are therefore trapped (fig. S8 a-a''', c-c'''). Adult testes display atypical coverage defects, as the tip is dilated but covered in muscles, mimicking adhesion defects (fig. S8 b,d). MMP2 was shown to have a membrane-bound and a released form²⁷⁰. The main difference to the only other *Drosophila* matrix metalloprotease, MMP1, seems to be its substrate specificity, including Collagen IV²⁷⁰. As a working hypothesis, it can be assumed that MMP2 has to be secreted or accumulated in protrusion sites to degrade Collagen-based ECM and thereby allow myotubes to cohesively migrate through the substrate. MMP2 possibly supports controlled delamination of pigment cells from the lower ECM-layer (fig. S8 e). These mechanics closely resemble cancer cell invasive migration ^{61, reviewed in 566}. So far, border cells take the role of a standard-model for invasive motility in *Drosophila*. In terms of motility and trans-migration through tightly adhered tissues, it bears many similarities to cancer cell dynamics and therefore earns this role ^{reviewed in 482}. One behaviour that cannot be investigated in border

cell migration is matrix adhesion-mediated invasion^{353,67} which is a hallmark of cancer cell motility³⁷¹. For this reason, myotube migration in *Drosophila* testis could merit further investigation as a model system for cancer-like collective invasive migration.

Cells not only react to spatial confinement by proteolytic ECM degradation but also through deformation and adaption to the substrate⁵⁵⁵. This could explain why front-cells are still able to migrate so well upon *Mmp2* reduction. In most systems the limiting factor of migration seems to be the nucleus which is much more rigid than the cell body²⁷⁶. Due to the apicobasal narrowness ensured by pigment cells and the cysts, myotubes must cope with confinement even under normal circumstances. Therefore, using the testis migration system as a model for confinement adaptations in the future seems plausible. Especially when it is considered that myotubes even have to carry usually 2–4 nuclei²⁶⁰. Future experiments will have to shed light on how perturbation of nuclear rigidity, *e.g.* by perturbing LaminA, affects migratory behaviour as seen in numerous migration model-systems^{281,106,533,278,238,194,282,280,442,277,492}.

4.9 Conclusion

The described dynamics of testis nascent myotube migration resembles the phenomenon of contact stimulation of migration⁵¹² and gives first insights on how such a cell-behaviour can be regulated mechanically. Myotube migration combines traits from contact inhibition of locomotion typical for mesenchymal cells, and wound closure typical for epithelia. In conclusion, these data confirm the notion that “epithelial” and “mesenchymal” constitute extreme examples on a gradient. Therefore, this simplified classification must be rethought to truly understand the basic mechanisms of collective motility. The newly established testis myotube migration model merits further research as it combines traits from a multitude of other systems. It allows for high resolution live-cell imaging and combines many advantages of an organ culture system with a genetic tractable *in vivo* model system. Nevertheless, further genetical approaches must be established in the future. Currently, all research relies on the conditional expression of RNAi-constructs as it is inherent to multinuclear cells that mitotic recombination-based methods do not work. Presumably, there is a great potential in UAS/Gal4-induced somatic CRISPR-Cas9-based complete deletion of genes³²⁷. Establishing such methods in the future may be worth the effort. A system comparable with established models as *Drosophila* border cell migration or lateral line development in *Danio*, would allow the identification of novel regulators of collective motility.

The establishment of the basic live-cell imaging methods in this work may pave the way for future research on invasion and adaptations to confinement. The substrate adhesive dynamics described, being responsible for “contact stimulation of migration”, might only be possible due to filopodial motility. A similar mechanism was just recently shown to enable cancer-cell trans-migration⁵⁷². In the future, it has to be elucidated which exact conditions cause cells to choose filopodial migration over lamellipodial motility. There might be common rules that apply to cells in development and cancer cells alike. Research in multiple model-systems might allow uncovering such basic axioms. As has been stated previously by others⁴⁸², understanding motility of cancer might be a basic requirement for finding therapeutics that stop the spreading of malign cells.

5. Summary

Cell migration drives most developmental processes, wound closure, as well as immune response. It constitutes a hallmark of cancer. Especially in tumour metastasis and development, cells rely on collective cell migration. Much knowledge about the exact mechanics of collective motility was gathered from a few model systems in which migration processes can be precisely analysed and genetically, mechanically, and pharmacologically influenced. This work aims to extend the existing range of such models by establishing a new *ex vivo* system for collective cell migration.

The testis of *Drosophila* is surrounded by a layer of smooth-like muscles. The precursors of these cells, multinucleated myotubes, have to get to the testis and to migrate toward its distal end during pupal development. Organ-culture conditions were determined, allowing to recapitulate the process *ex vivo*. Thereby, the mechanical rules by which myotubes migrate could be assessed. Testis myotubes seem to use a lamellipodium-independent migration mode that is based entirely on the dynamics of filopodia-like protrusions. In previous studies, a chemoattractive effect mediated by the fibroblast growth factor receptor (FGFR) Heartless (Htl) was discussed, besides its likely role in regulating the number of myoblasts on the genital disc and its possible role in connecting testis and seminal vesicles. The results obtained in this work oppose a chemoattractive function but rather suggest a general role of Htl in the initiation of cell migration. Mathematical and statistical analysis of migration trajectories in the background of genetic, mechanical, and pharmacological perturbation suggest a self-regulating process. The observed dynamics reveal similarities to contact inhibition of locomotion (CIL) since cell-cell contacts provide crucial information for individual cells to enable directionality. Cells seem to inhibit substrate adhesion in filopodia in a contact-dependent manner. This process appears to be controlled by the Rho-GTPases Rac2 and Cdc42. As a result of the contact-dependent loss of adhesion, there is a net-movement into the cell-free space. At the same time, N-Cadherin seems to ensure that cells maintain adhesion to one another. Therefore, there is no repulsive migration as in CIL. Finally, supracellular RhoA/Rock-dependent actomyosin cables appear to support cohesion by closing gaps in the cell cluster at concavely curved edges. These mechanisms presumably result in a process in which all available space is evenly covered by myotubes. Myotube motility appears to be dependent on proteolytic degradation of the matrix. For this reason, in the future, the newly established *ex vivo* system could allow studying the collective dynamics of invasive migration in detail.

5.1 Zusammenfassung

Zellmigration treibt zahlreiche entwicklungsbiologische Prozesse, sowie Wundheilung und Immunreaktionen an und ist ein Merkmal vieler Krebszellen. Besonders in metastasierenden Tumoren, aber auch in der Entwicklung spielt die kollektive Zellmigration eine grundlegende Rolle. Viel Wissen über die exakte Mechanik kollektiver Motilität stammt von wenigen Modellsystemen in denen Migrationsprozesse analysiert und genetisch, mechanisch sowie pharmakologisch beeinflusst werden können. In der vorliegenden Arbeit soll ein neues *ex vivo* System zu Erforschung kollektiver Migration etabliert werden.

Der Testis von *Drosophila* ist von einer Muskelschicht umgeben, die Ähnlichkeit mit glatten Muskeln aufweist. Die Vorläufer dieser Zellen, mehrkernige Myotuben, müssen während der puppalen Entwicklung auf den Testis gelangen und zu seinem distalen Ende migrieren. Es wurden Kulturbedingungen ermittelt, in denen dieser Prozess *ex vivo* rekapituliert werden kann. Dabei konnten die mechanischen Grundlagen der Myotuben-Migration ergründet werden. Testis Myotuben scheinen einen Lamellipodium-unabhängigen Migrationsmodus zu nutzen, der gänzlich auf der Dynamik von Filopodien-artigen Zellfortsätzen beruht. In vorherigen Arbeiten wurde eine chemoattraktive Wirkung, vermittelt über den fibroblast growth factor receptor (FGFR) Heartless (Htl), neben einer wahrscheinlichen Rolle in der Regulation der Myoblasten-Anzahl auf der Genitalscheibe und einer möglichen Rolle bei der Testis-Genitalscheiben-Verbindung, diskutiert. Die Ergebnisse der vorliegenden Arbeit sprechen gegen eine chemoattraktive Funktion, aber für eine generelle Rolle von Htl bei der Initiation der Zellmigration. Mathematische und statistische Analysen der Migrationsbewegungen bei genetischen, mechanischen sowie pharmakologischen Störungen und Beeinflussungen, sprechen für einen selbst-regulierenden Prozess. Dieser hat Ähnlichkeiten zu *contact inhibition of locomotion* (CIL), da Zell-Zell-Kontakte die entscheidenden Informationen zur Richtungsfindung einzelner Zellen geben. Zellen scheinen kontaktabhängig die Matrix-Adhäsion von Filopodien herunterzeregeln. Dieser Prozess scheint von den Rho-GTPase Rac2 und Cdc42 gesteuert zu sein. Als Folge des kontaktabhängigen Adhäsionsverlusts folgt eine Netto-Bewegung in den zellfreien Raum. Gleichzeitig scheint N-Cadherin dafür zu sorgen, dass Zellen ihre Zell-Zelladhäsion zueinander aufrechterhalten, sich also nicht wie bei CIL abstoßen. Schließlich scheinen suprazelluläre RhoA sowie Rock abhängige Actomyosin-Kabel die Kohäsion der Zellcluster zu unterstützen, indem sie Lücken zwischen den Zellen mit konkav gekrümmter Kante schließen. Diese Mechanismen resultieren allem Anschein nach in einem Prozess, indem sämtlicher zur Verfügung stehender Raum gleichmäßig von Myotuben bedeckt wird. Myotuben-Motilität erscheint dabei abhängig von proteolytischer Degradation der Matrix zu sein. Aus diesem Grund könnte das neu etablierte *ex vivo* System es in Zukunft ermöglichen, kollektive Dynamiken invasiver Migration zu erforschen.

6. References

1. Abercrombie, M. & Heaysman, J. E. M. Observations on the social behaviour of cells in tissue culture. I. Speed of movement of chick heart fibroblasts in relation to their mutual contacts. *Exp. Cell Res.* **5**, 111–131 (1953).
2. Abercrombie, M., Heaysman, J. E. M. & Pegrum, S. M. The locomotion of fibroblasts in culture. *Exp. Cell Res.* **62**, 389–398 (1970).
3. Abercrombie, M., Heaysman, J. E. M. & Pegrum, S. M. The locomotion of fibroblasts in culture. IV. Electron microscopy of the leading lamella. *Exp. Cell Res.* **67**, 359–367 (1971).
4. Abercrombie, M., Heaysman, J. E. M. & Pegrum, S. M. The locomotion of fibroblasts in culture. III. Movements of particles on the dorsal surface of the leading lamella. *Exp. Cell Res.* **62**, 389–398 (1970).
5. Abercrombie, M., Joan, E., Heaysman, M. & Pegrum, S. M. The locomotion of fibroblasts in culture. II. ‘Ruffling’. *Exp. Cell Res.* **60**, 437–444 (1970).
6. Abercrombie, M. Contact inhibition in tissue culture. *In Vitro* **6**, 128–142 (1970).
7. Abercrombie, M. & Ambrose, E. J. The surface properties of cancer cells: a review. *Cancer Res.* **22**, 525–548 (1962).
8. Abercrombie, M., Heaysman, J. E. & Pegrum, S. M. Locomotion of fibroblasts in culture. V. Surface marking with concanavalin A. *Exp. Cell Res.* **73**, 536–539 (1972).
9. Abraham, S. *et al.* VE-Cadherin-mediated cell-cell interaction suppresses sprouting via signaling to MLC2 phosphorylation. *Curr. Biol.* **19**, 668–674 (2009).
10. Adams, A. E., Johnson, D. I., Longnecker, R. M., Sloat, B. F. & Pringle, J. R. CDC42 and CDC43, two additional genes involved in budding and the establishment of cell polarity in the yeast *Saccharomyces cerevisiae*. *J. Cell Biol.* **111**, 131–142 (1990).
11. Afewerki, T. L., Ahmed, S. & Warren, D. Emerging regulators of vascular smooth muscle cell migration. *J. Muscle Res. Cell Motil.* **40**, 185–196 (2019).
12. Ahmad, S. M. & Baker, B. S. Sex-Specific Deployment of FGF Signaling in *Drosophila* Recruits Mesodermal Cells into the Male Genital Imaginal Disc. *Cell* **109**, 651–661 (2002).
13. Alexander, S., Koehl, G. E., Hirschberg, M., Geissler, E. K. & Friedl, P. Dynamic imaging of cancer growth and invasion: a modified skin-fold chamber model. *Histochem. Cell Biol.* **130**, 1147–1154 (2008).
14. Alexandrova, A. Y. *et al.* Comparative dynamics of retrograde actin flow and focal adhesions: formation of nascent adhesions triggers transition from fast to slow flow. *PLoS One* **3**, e3234 (2008).
15. Allen, R. D. & Allen, N. S. Cytoplasmic streaming in amoeboid movement. *Annu. Rev. Biophys. Bioeng.* **7**, 469–495 (1978).

16. Allen, R. D. & Taylor, D. L. The molecular basis of amoeboid movement. *Soc. Gen. Physiol. Ser.* **30**, 239–258 (1975).
17. Allen, W. E., Zicha, D., Ridley, A. J. & Jones, G. E. A role for Cdc42 in macrophage chemotaxis. *J. Cell Biol.* **141**, 1147–1157 (1998).
18. Amann, K. J. & Pollard, T. D. The Arp2/3 complex nucleates actin filament branches from the sides of pre-existing filaments. *Nat. Cell Biol.* **3**, 306–310 (2001).
19. Aranjuez, G., Burtscher, A., Sawant, K., Majumder, P. & McDonald, J. A. Dynamic myosin activation promotes collective morphology and migration by locally balancing oppositional forces from surrounding tissue. *Mol. Biol. Cell* **27**, 1898–1910 (2016).
20. Arjonen, A. *et al.* Mutant p53-associated myosin-X upregulation promotes breast cancer invasion and metastasis. *J. Clin. Invest.* **124**, 1069–1082 (2014).
21. Ashburner, M. *Drosophila. A laboratory handbook. Drosophila. A laboratory handbook.* (Cold Spring Harbor Laboratory Press, 1989).
22. Aspenström, P., Lindberg, U. & Hall, A. Two GTPases, Cdc42 and Rac, bind directly to a protein implicated in the immunodeficiency disorder Wiskott-Aldrich syndrome. *Current Biology* vol. 6 70–75 (1996).
23. Astin, J. W. *et al.* Competition amongst Eph receptors regulates contact inhibition of locomotion and invasiveness in prostate cancer cells. *Nat. Cell Biol.* **12**, 1194–1204 (2010).
24. Attieh, Y. *et al.* Cancer-associated fibroblasts lead tumor invasion through integrin- β 3-dependent fibronectin assembly. *J. Cell Biol.* **216**, 3509–3520 (2017).
25. Azoury, J. *et al.* Spindle positioning in mouse oocytes relies on a dynamic meshwork of actin filaments. *Curr. Biol.* **18**, 1514–1519 (2008).
26. Bae, Y. K., Trisnadi, N., Kadam, S. & Stathopoulos, A. The role of FGF signaling in guiding coordinate movement of cell groups guidance cue and cell adhesion regulator? *Cell Adhes. Migr.* **6**, 397–403 (2012).
27. Bailly, M. *et al.* Relationship between Arp2/3 Complex and the Barbed Ends of Actin Filaments at the Leading Edge of Carcinoma Cells after Epidermal Growth Factor Stimulation . *J. Cell Biol.* **145**, 331–345 (1999).
28. Balaban, N. Q. *et al.* Force and focal adhesion assembly: a close relationship studied using elastic micropatterned substrates. *Nat. Cell Biol.* **3**, 466–472 (2001).
29. Balasubramanian, R. & Zhang, X. Mechanisms of FGF gradient formation during embryogenesis. *Semin. Cell Dev. Biol.* **53**, 94–100 (2016).
30. Ballestrem, C., Hinz, B., Imhof, B. A. & Wehrle-Haller, B. Marching at the front and dragging behind: differential α V β 3-integrin turnover regulates focal adhesion behavior. *J. Cell Biol.* **155**, 1319–1332 (2001).
31. Bamburg, J. R. & Bernstein, B. W. Roles of ADF/cofilin in actin polymerization and beyond. *F1000 Biol. Rep.* **2**, 1–7 (2010).
32. Di Bari, M. G. *et al.* Msx2 induces epithelial-mesenchymal transition in mouse mammary epithelial cells through upregulation of Cripto-1. *J. Cell. Physiol.* **219**, 659–666 (2009).

33. Barlan, K. & Gelfand, V. I. Microtubule-based transport and the distribution, tethering, and organization of organelles. *Cold Spring Harb. Perspect. Biol.* **9**, a025817 (2017).
34. Barriga, E. H., Franze, K., Charras, G. & Mayor, R. Tissue stiffening coordinates morphogenesis by triggering collective cell migration in vivo. *Nature* **554**, 523–527 (2018).
35. Bateman, J. R., Lee, A. M. & Wu, C. Site-specific transformation of *Drosophila* via phiC31 integrase-mediated cassette exchange. *Genetics* **173**, 769–777 (2006).
36. Batson, J., Maccarthy-Morrogh, L., Archer, A., Tanton, H. & Nobes, C. D. EphA receptors regulate prostate cancer cell dissemination through Vav2–RhoA mediated cell–cell repulsion. *Biol. Open* **3**, 453–462 (2014).
37. Bear, J. E. & Gertler, F. B. Ena/VASP: Towards resolving a pointed controversy at the barbed end. *J. Cell Sci.* **122**, 1947–1953 (2009).
38. Bear, J. E., Rawls, J. F. & Saxe, C. L. SCAR, a WASP-related protein, isolated as a suppressor of receptor defects in late *Dictyostelium* development. *J. Cell Biol.* **142**, 1325–1335 (1998).
39. Beccari, S., Teixeira, L. & Rørth, P. The JAK/STAT pathway is required for border cell migration during *Drosophila* oogenesis. *Mech. Dev.* **111**, 115–123 (2002).
40. Beningo, K. A., Dembo, M., Kaverina, I., Small, J. V. & Wang, Y. Nascent focal adhesions are responsible for the generation of strong propulsive forces in migrating fibroblasts. *J. Cell Biol.* **153**, 881–888 (2001).
41. Bergert, M., Chandradoss, S. D., Desai, R. A. & Paluch, E. Cell mechanics control rapid transitions between blebs and lamellipodia during migration. *Proc. Natl. Acad. Sci.* **109**, 14434–14439 (2012).
42. Bertani, G. Studies on lysogenesis I.: the mode of phage liberation by lysogenic *Escherichia coli*1. *J. Bacteriol.* **62**, 293 (1951).
43. Bianco, A. *et al.* Two distinct modes of guidance signalling during collective migration of border cells. *Nature* **448**, 362–365 (2007).
44. Bischof, J., Maeda, R. K., Hediger, M., Karch, F. & Basler, K. An optimized transgenesis system for *Drosophila* using germ-line-specific phiC31 integrases. *Proc. Natl. Acad. Sci. U. S. A.* **104**, 3312–3317 (2007).
45. Blanchoin, L., Pollard, T. D. & Hitchcock-DeGregori, S. E. Inhibition of the Arp2/3 complex-nucleated actin polymerization and branch formation by tropomyosin. *Curr. Biol.* **11**, 1300–1304 (2001).
46. Blanchoin, L. *et al.* Direct observation of dendritic actin filament networks nucleated by Arp2/3 complex and WASP/Scar proteins. *Nature* **404**, 1007–1011 (2000).
47. Blanchoin, L. & Pollard, T. D. Hydrolysis of ATP by polymerized actin depends on the bound divalent cation but not profilin. *Biochemistry* **41**, 597–602 (2002).
48. Block, E. R., Matela, A. R., SundarRaj, N., Iszkula, E. R. & Klarlund, J. K. Wounding Induces Motility in Sheets of Corneal Epithelial Cells through Loss of Spatial Constraints. *J. Biol. Chem.* **279**, 24307–24312 (2004).

49. Block, J. *et al.* Filopodia formation induced by active mDia2/Drf3. *J. Microsc.* **231**, 506–517 (2008).
50. Block, J. *et al.* FMNL2 drives actin-based protrusion and migration downstream of Cdc42. *Curr. Biol.* **22**, 1005–1012 (2012).
51. De Bock, K. *et al.* Role of PFKFB3-driven glycolysis in vessel sprouting. *Cell* **154**, 651–663 (2013).
52. Bogdan, S., Schultz, J. & Grosshans, J. Formin' cellular structures. *Commun. Integr. Biol.* **6**, e27634 (2013).
53. Bombardier, J. P. *et al.* Single-molecule visualization of a formin-capping protein 'decision complex' at the actin filament barbed end. *Nat. Commun.* **6**, 1–9 (2015).
54. Borghese, L. *et al.* Systematic analysis of the transcriptional switch inducing migration of border cells. *Dev. Cell* **10**, 497–508 (2006).
55. Borghi, N., Lowndes, M., Maruthamuthu, V., Gardel, M. L. & Nelson, W. J. Regulation of cell motile behavior by crosstalk between cadherin- and integrin-mediated adhesions. *Proc. Natl. Acad. Sci. U. S. A.* **107**, 13324–13329 (2010).
56. Bornschlöggl, T. How filopodia pull: What we know about the mechanics and dynamics of filopodia. *Cytoskeleton* **70**, 590–603 (2013).
57. Brand, A. H. & Perrimon, N. Targeted gene expression as a means of altering cell fates and generating dominant phenotypes. *Development* **118**, 401 LP – 415 (1993).
58. Breitsprecher, D. & Goode, B. L. Formins at a glance. *J. Cell Sci.* **126**, 1–7 (2013).
59. Brenner, S. L. & Korn, E. D. Substoichiometric concentrations of cytochalasin D inhibit actin polymerization. Additional evidence for an F-actin treadmill. *J. Biol. Chem.* **254**, 9982–9985 (1979).
60. Brinkmann, K. *et al.* WHAMY is a novel actin polymerase promoting myoblast fusion, macrophage cell motility and sensory organ development in *Drosophila*. *J. Cell Sci.* **129**, 604–620 (2016).
61. Buccione, R., Caldieri, G. & Ayala, I. Invadopodia: Specialized tumor cell structures for the focal degradation of the extracellular matrix. *Cancer Metastasis Rev.* **28**, 137–149 (2009).
62. Bugyi, B. & Carlier, M.-F. Control of Actin Filament Treadmilling in Cell Motility. *Annu. Rev. Biophys.* **39**, 449–470 (2010).
63. Burbelo, P. D., Drechsel, D. & Hall, A. A Conserved Binding Motif Defines Numerous Candidate Target Proteins for Both Cdc42 and Rac GTPases. *J. Biol. Chem.* **270**, 29071–29074 (1995).
64. Burridge, K. & Mangeat, P. An interaction between vinculin and talin. *Nature* **308**, 744–746 (1984).
65. Burute, M. & Thery, M. Spatial segregation between cell-cell and cell-matrix adhesions. *Curr. Opin. Cell Biol.* **24**, 628–636 (2012).
66. Butler, M. J. *et al.* Discovery of genes with highly restricted expression patterns in the *Drosophila* wing disc using DNA oligonucleotide microarrays. *Development* **130**, 659–670 (2003).

67. Cai, D. *et al.* Mechanical feedback through E-cadherin promotes direction sensing during collective cell migration. *Cell* **157**, 1146–1159 (2014).
68. Cai, D. & Montell, D. J. Diverse and dynamic sources and sinks in gradient formation and directed migration. *Curr. Opin. Cell Biol.* **30**, 91–98 (2014).
69. Calalb, M. B., Polte, T. R. & Hanks, S. K. Tyrosine phosphorylation of focal adhesion kinase at sites in the catalytic domain regulates kinase activity: a role for Src family kinases. *Mol. Cell. Biol.* **15**, 954–963 (1995).
70. Calderwood, D. A., Campbell, I. D. & Critchley, D. R. Talins and kindlins: partners in integrin-mediated adhesion. *Nat. Rev. Mol. cell Biol.* **14**, 503–517 (2013).
71. De Calisto, J., Araya, C., Marchant, L., Riaz, C. F. & Mayor, R. Essential role of non-canonical Wnt signalling in neural crest migration. *Development* **132**, 2587–2597 (2005).
72. Camand, E., Peglion, F., Osmani, N., Sanson, M. & Etienne-Manneville, S. N-cadherin expression level modulates integrin-mediated polarity and strongly impacts on the speed and directionality of glial cell migration. *J. Cell Sci.* **125**, 844–857 (2012).
73. Camand, E., Peglion, F., Sanson, M. & Etienne-manneville, S. N-cadherin expression level modulates integrin-mediated polarity and strongly impacts on the speed and directionality of glial cell migration. 844–857 (2009) doi:10.1242/jcs.087668.
74. Camley, B. A. *et al.* Polarity mechanisms such as contact inhibition of locomotion regulate persistent rotational motion of mammalian cells on micropatterns. *Proc. Natl. Acad. Sci.* **111**, 14770–14775 (2014).
75. Campellone, K. G. & Welch, M. D. A nucleator arms race: cellular control of actin assembly. *Nat. Rev. Microbiol.* **11**, 237–251 (2010).
76. Canel, M. *et al.* Quantitative in vivo imaging of the effects of inhibiting integrin signaling via Src and FAK on cancer cell movement: effects on E-cadherin dynamics. *Cancer Res.* **70**, 9413–9422 (2010).
77. Cao, R. *et al.* Elevated expression of myosin X in tumours contributes to breast cancer aggressiveness and metastasis. *Br. J. Cancer* **111**, 539–550 (2014).
78. Carmona-Fontaine, C. *et al.* Contact inhibition of locomotion in vivo controls neural crest directional migration. *Nature* **456**, 957–961 (2008).
79. Carmona-Fontaine, C. *et al.* Complement fragment C3a controls mutual cell attraction during collective cell migration. *Dev. Cell* **21**, 1026–1037 (2011).
80. Castelli-Gair, J., Greig, S., Micklem, G. & Akam, M. Dissecting the temporal requirements for homeotic gene function. *Development* **120**, 1983 LP – 1995 (1994).
81. Castrillon, D. H. & Wasserman, S. A. diaphanous is required for cytokinesis in *Drosophila* and shares domains of similarity with the products of the limb deformity gene. *Development* **120**, 3367–3377 (1994).
82. Caussinus, E., Colombelli, J. & Affolter, M. Tip-cell migration controls stalk-cell intercalation during *Drosophila* tracheal tube elongation. *Curr. Biol.* **18**, 1727–1734 (2008).

83. Chan, A. Y., Bailly, M., Zebda, N., Segall, J. E. & Condeelis, J. S. Role of Cofilin in Epidermal Growth Factor–Stimulated Actin Polymerization and Lamellipod Protrusion. *J. Cell Biol.* **148**, 531–542 (2000).
84. Chan, C. E. & Odde, D. J. Traction dynamics of filopodia on compliant substrates. *Science* **322**, 1687–1691 (2008).
85. Chang, F., Drubin, D. & Nurse, P. *cdc12p*, a protein required for cytokinesis in fission yeast, is a component of the cell division ring and interacts with profilin. *J. Cell Biol.* **137**, 169–182 (1997).
86. Charras, G. T., Hu, C.-K., Coughlin, M. & Mitchison, T. J. Reassembly of contractile actin cortex in cell blebs. *J. Cell Biol.* **175**, 477–490 (2006).
87. Chen, B. *et al.* Rac1 GTPase activates the WAVE regulatory complex through two distinct binding sites. *Elife* **6**, e29795 (2017).
88. Chen, E. H., Christiansen, A. E. & Baker, B. S. Allocation and specification of the genital disc precursor cells in *Drosophila*. *Dev. Biol.* **281**, 270–285 (2005).
89. Chen, Y. *et al.* Protein phosphatase 1 activity controls a balance between collective and single cell modes of migration. *Elife* **9**, 1–37 (2020).
90. Chen, Z. *et al.* Structure and control of the actin regulatory WAVE complex. *Nature* **468**, 533–538 (2010).
91. Chesarone, M. A., DuPage, A. G. & Goode, B. L. Unleashing formins to remodel the actin and microtubule cytoskeletons. *Nat. Rev. Mol. cell Biol.* **11**, 62–74 (2010).
92. Chhabra, E. S. & Higgs, H. N. INF2 Is a WASP homology 2 motif-containing formin that severs actin filaments and accelerates both polymerization and depolymerization. *J. Biol. Chem.* **281**, 26754–26767 (2006).
93. Choi, C. K. *et al.* Actin and α -actinin orchestrate the assembly and maturation of nascent adhesions in a myosin II motor-independent manner. *Nat. Cell Biol.* **10**, 1039–1050 (2008).
94. Christiansen, A. E., Keisman, E. L., Ahmad, S. M. & Baker, B. S. Sex comes in from the cold: the integration of sex and pattern. *Trends Genet.* **18**, 510–516 (2002).
95. Christiansen, J. J. & Rajasekaran, A. K. Reassessing epithelial to mesenchymal transition as a prerequisite for carcinoma invasion and metastasis. *Cancer Res.* **66**, 8319–8326 (2006).
96. Christopher, L. J., Fletcher, L. D. & Dykstra, C. C. Cloning and Identification of Arp1, an Actin-Related Protein from *Pneumocystis carinii*. *J. Eukaryot. Microbiol.* **42**, 142–149 (1995).
97. Chrzanowska-Wodnicka, M. & Burridge, K. Rho-stimulated contractility drives the formation of stress fibers and focal adhesions. *J. Cell Biol.* **133**, 1403–1415 (1996).
98. Clark, S. W. & Meyer, D. I. ACT3: a putative centractin homologue in *S. cerevisiae* is required for proper orientation of the mitotic spindle. *J. Cell Biol.* **127**, 129–138 (1994).
99. Clark, S. W. *et al.* Beta-centractin: characterization and distribution of a new member of the centractin family of actin-related proteins. *Mol. Biol. Cell* **5**, 1301–1310 (1994).
100. Clark, S. W. & Meyer, D. I. Centractin is an actin homologue associated with the centrosome. *Nature* **359**, 246–250 (1992).

101. Cooper, J. A., Buhle, E. L., Walker, S. B., Tsong, T. Y. & Pollard, T. D. Kinetic evidence for a monomer activation step in actin polymerization. *Biochemistry* **22**, 2193–2202 (1983).
102. Cory, G. O. C., Garg, R., Cramer, R. & Ridley, A. J. Phosphorylation of tyrosine 291 enhances the ability of WASp to stimulate actin polymerization and filopodium formation. Wiskott-Aldrich Syndrome protein. *J. Biol. Chem.* **277**, 45115–45121 (2002).
103. Coyer, S. R. *et al.* Nanopatterning reveals an ECM area threshold for focal adhesion assembly and force transmission that is regulated by integrin activation and cytoskeleton tension. *J. Cell Sci.* **125**, 5110–5123 (2012).
104. Czuchra, A. *et al.* Cdc42 Is Not Essential for Filopodium Formation, Directed Migration, Cell Polarization, and Mitosis in Fibroblastoid Cells. *Mol. Biol. Cell* **16**, 4473–4484 (2005).
105. Dailey, L., Ambrosetti, D., Mansukhani, A. & Basilico, C. Mechanisms underlying differential responses to FGF signaling. *Cytokine Growth Factor Rev.* **16**, 233–247 (2005).
106. Davidson, P. M., Denais, C., Bakshi, M. C. & Lammerding, J. Nuclear deformability constitutes a rate-limiting step during cell migration in 3-D environments. *Cell. Mol. Bioeng.* **7**, 293–306 (2014).
107. DeMali, K. A., Barlow, C. A. & Burridge, K. Recruitment of the Arp2/3 complex to vinculin: coupling membrane protrusion to matrix adhesion. *J. Cell Biol.* **159**, 881–891 (2002).
108. Deng, S., Bothe, I. & Baylies, M. K. The Formin Diaphanous Regulates Myoblast Fusion through Actin Polymerization and Arp2/3 Regulation. *PLOS Genet.* **11**, e1005381 (2015).
109. Derivery, E. & Gautreau, A. Generation of branched actin networks: Assembly and regulation of the N-WASP and WAVE molecular machines. *BioEssays* **32**, 119–131 (2010).
110. Derivery, E., Lombard, B., Loew, D. & Gautreau, A. The wave complex is intrinsically inactive. *Cell Motil. Cytoskeleton* **66**, 777–790 (2009).
111. Derry, J. M. *et al.* WASP gene mutations in Wiskott-Aldrich syndrome and X-linked thrombocytopenia. *Hum. Mol. Genet.* **4**, 1127–1135 (1995).
112. Derry, J. M. J. *et al.* The Mouse Homolog of the Wiskott–Aldrich Syndrome Protein (WASP) Gene Is Highly Conserved and Maps near the Scurfy (sf) Mutation on the X Chromosome. *Genomics* **29**, 471–477 (1995).
113. Derry, J. M. J., Ochs, H. D. & Francke, U. Isolation of a novel gene mutated in Wiskott-Aldrich syndrome. *Cell* **78**, 635–644 (1994).
114. Desai, R. A., Gopal, S. B., Chen, S. & Chen, C. S. Contact inhibition of locomotion probabilities drive solitary versus collective cell migration. *J. R. Soc. Interface* **10**, 20130717 (2013).
115. Deutsch, A., Theraulaz, G. & Vicsek, T. Collective motion in biological systems. *Interface Focus* **2**, 689–692 (2012).
116. Dhanyasi, N. *et al.* Surface apposition and multiple cell contacts promote myoblast fusion in *Drosophila* flight muscles. *J. Cell Biol.* **211**, 191–203 (2015).
117. Didsbury, J., Weber, R. F., Bokoch, G. M., Evans, T. & Snyderman, R. Rac, a novel ras-related family of proteins that are botulinum toxin substrates. *J. Biol. Chem.* **264**, 16378–16382 (1989).

118. Disanza, A. *et al.* CDC42 switches IRSp53 from inhibition of actin growth to elongation by clustering of VASP. *EMBO J.* **32**, 2735–2750 (2013).
119. Diz-Muñoz, A. *et al.* Control of directed cell migration in vivo by membrane-to-cortex attachment. *PLoS Biol.* **8**, (2010).
120. Dominguez, R. & Holmes, K. C. Actin structure and function. *Annu. Rev. Biophys.* **40**, 169–186 (2011).
121. Donà, E. *et al.* Directional tissue migration through a self-generated chemokine gradient. *Nature* **503**, 285–289 (2013).
122. Drenckhahn, D. & Pollard, T. D. Elongation of actin filaments is a diffusion-limited reaction at the barbed end and is accelerated by inert macromolecules. *J. Biol. Chem.* **261**, 12754–12758 (1986).
123. Duchek, P. & Rørth, P. Guidance of cell migration by EGF receptor signaling during *Drosophila* oogenesis. *Science* **291**, 131–133 (2001).
124. Duchek, P., Somogyi, K., Jékely, G., Beccari, S. & Rørth, P. Guidance of Cell Migration by the *Drosophila* PDGF/VEGF Receptor. *Cell* **107**, 17–26 (2001).
125. Dumortier, J. G., Martin, S., Meyer, D., Rosa, F. M. & David, N. B. Collective mesendoderm migration relies on an intrinsic directionality signal transmitted through cell contacts. *Proc. Natl. Acad. Sci.* **109**, 16945–16950 (2012).
126. Dupin, I., Camand, E. & Etienne-Manneville, S. Classical cadherins control nucleus and centrosome position and cell polarity. *J. Cell Biol.* **185**, 779–786 (2009).
127. Edwards, M. *et al.* Capping protein regulators fine-tune actin assembly dynamics. *Nat. Rev. Mol. Cell Biol.* **15**, 677–689 (2014).
128. Egile, C. *et al.* Mechanism of Filament Nucleation and Branch Stability Revealed by the Structure of the Arp2/3 Complex at Actin Branch Junctions. *PLOS Biol.* **3**, e383 (2005).
129. Eickholt, B. J., Mackenzie, S. L., Graham, A., Walsh, F. S. & Doherty, P. Evidence for collapsin-1 functioning in the control of neural crest migration in both trunk and hindbrain regions. *Development* **126**, 2181–2189 (1999).
130. Estrada, B., Casares, F. & Sánchez-Herrero, E. Development of the genitalia in *Drosophila melanogaster*. *Differentiation* **71**, 299–310 (2003).
131. Evangelista, M. *et al.* Bni1p, a yeast formin linking Cdc42p and the actin cytoskeleton during polarized morphogenesis. *Science* **276**, 118–122 (1997).
132. Evangelista, M., Pruyne, D., Amberg, D. C., Boone, C. & Bretscher, A. Formins direct Arp2/3-independent actin filament assembly to polarize cell growth in yeast. *Nat. Cell Biol.* **4**, 260–269 (2002).
133. Faix, J., Breitsprecher, D., Stradal, T. E. B. & Rottner, K. Filopodia: Complex models for simple rods. *Int. J. Biochem. Cell Biol.* **41**, 1656–1664 (2009).
134. Faix, J. & Rottner, K. The making of filopodia. *Curr. Opin. Cell Biol.* **18**, 18–25 (2006).
135. Farooqui, R. & Fenteany, G. Multiple rows of cells behind an epithelial wound edge extend cryptic lamellipodia to collectively drive cell-sheet movement. *J. Cell Sci.* **118**, 51–63 (2005).

136. Fender, S. Charakterisierung von Wnt, MAPK und FGF Signalwegen während der Migration naszierender Myotuben auf die Testes von *Drosophila*. (Philipps-Universität Marburg, 2016).
137. Fenteany, G., Janmey, P. A. & Stossel, T. P. Signaling pathways and cell mechanics involved in wound closure by epithelial cell sheets. *Curr. Biol.* **10**, 831–838 (2000).
138. Fernandes, J., Bate, M. & Vijayraghavan, K. Development of the indirect flight muscles of *Drosophila*. *Development* **113**, 67–77 (1991).
139. Fernandes, J. & VijayRaghavan, K. The development of indirect flight muscle innervation in *Drosophila melanogaster*. *Development* **118**, 215–227 (1993).
140. Fernández-Espartero, C. H. *et al.* GTP exchange factor Vav regulates guided cell migration by coupling guidance receptor signalling to local Rac activation. *J. Cell Sci.* **126**, 2285–2293 (2013).
141. Fincham, V. J. & Frame, M. C. The catalytic activity of Src is dispensable for translocation to focal adhesions but controls the turnover of these structures during cell motility. *EMBO J.* **17**, 81–92 (1998).
142. Fischer, R. S., Lam, P. Y., Huttenlocher, A. & Waterman, C. M. Filopodia and focal adhesions: An integrated system driving branching morphogenesis in neuronal pathfinding and angiogenesis. *Dev. Biol.* **451**, 86–95 (2019).
143. Frankel, S., Heintzelman, M. B., Artavanis-Tsakonas, S. & Mooseker, M. S. Identification of a divergent actin-related protein in *Drosophila*. *J. Mol. Biol.* **235**, 1351–1356 (1994).
144. Fricke, R. *et al.* *Drosophila* Cip4/Toca-1 Integrates Membrane Trafficking and Actin Dynamics through WASP and SCAR/WAVE. *Curr. Biol.* **19**, 1429–1437 (2009).
145. Frieden, C. Polymerization of actin: mechanism of the Mg²⁺-induced process at pH 8 and 20 degrees C. *Proc. Natl. Acad. Sci. U. S. A.* **80**, 6513–6517 (1983).
146. Friedl, P. *et al.* Migration of coordinated cell clusters in mesenchymal and epithelial cancer explants in vitro. *Cancer Res.* **55**, 4557–4560 (1995).
147. Friedl, P. & Gilmour, D. Collective cell migration in morphogenesis, regeneration and cancer. *Nat. Rev. Mol. Cell Biol.* **10**, 445–457 (2009).
148. Friedl, P., Hegerfeldt, Y. & Tusch, M. Collective cell migration in morphogenesis and cancer. *Int. J. Dev. Biol.* **48**, 441–449 (2004).
149. Friedl, P. & Mayor, R. Tuning Collective Cell Migration by Cell – Cell Junction Regulation. 1–18 (2018).
150. Friedl, P. & Wolf, K. Plasticity of cell migration: A multiscale tuning model. *J. Cell Biol.* **188**, 11–19 (2010).
151. Fritz-Laylin, L. K., Lord, S. J. & Mullins, R. D. WASP and SCAR are evolutionarily conserved in actin-filled pseudopod-based motility. *J. Cell Biol.* **216**, 1673–1688 (2017).
152. Fritzen, K. Die Entwicklung der mehrkernigen, glatten Muskeln von *Drosophila melanogaster* - Die Fusion der Testes-relevanten Myoblasten ist abhängig von Arp2/3-gesteuerter Aktin-Polymerisation. (Philipps-Universität Marburg, 2016).
153. Fujiwara, I., Takahashi, S., Tadakuma, H., Funatsu, T. & Ishiwata, S. Microscopic analysis of polymerization dynamics with individual actin filaments. *Nat. Cell Biol.* **4**, 666–673 (2002).

154. Fujiwara, I., Vavylonis, D. & Pollard, T. D. Polymerization kinetics of ADP- and ADP-Pi-actin determined by fluorescence microscopy. *Proc. Natl. Acad. Sci.* **104**, 8827–8832 (2007).
155. Fyrberg, C., Ryan, L., Kenton, M. & Fyrberg, E. Genes Encoding Actin-related Proteins of *Drosophila melanogaster*. *J. Mol. Biol.* **241**, 498–503 (1994).
156. Gabay, L., Seger, R. & Shilo, B.-Z. MAP kinase in situ activation atlas during *Drosophila* embryogenesis. *Development* **124**, 3535–3541 (1997).
157. Gabriele, S. Spatial Confinement Modulates Cell Velocity in Collective Cell Migration. *Biophys. J.* **118**, 603a (2020).
158. Gaggioli, C. *et al.* Fibroblast-led collective invasion of carcinoma cells with differing roles for RhoGTPases in leading and following cells. *Nat. Cell Biol.* **9**, 1392–1400 (2007).
159. Galbraith, C. G., Yamada, K. M. & Sheetz, M. P. The relationship between force and focal complex development. *J. Cell Biol.* **159**, 695–705 (2002).
160. Gammill, L. S., Gonzalez, C. & Bronner-Fraser, M. Neuropilin 2/semaphorin 3F signaling is essential for cranial neural crest migration and trigeminal ganglion condensation. *Dev. Neurobiol.* **67**, 47–56 (2007).
161. Garcia-Arcos, J. M. *et al.* Reconstitution of cell migration at a glance. *J. Cell Sci.* **132**, 0–2 (2019).
162. Gardel, M. L. *et al.* Traction stress in focal adhesions correlates biphasically with actin retrograde flow speed. *J. Cell Biol.* **183**, 999–1005 (2008).
163. Gardel, M. L., Schneider, I. C., Aratyn-Schaus, Y. & Waterman, C. M. Mechanical integration of actin and adhesion dynamics in cell migration. *Annu. Rev. Cell Dev. Biol.* **26**, 315–333 (2010).
164. Gärthner, S. M. K., Rathke, C., Renkawitz-Pohl, R. & Awe, S. Ex vivo culture of *drosophila* pupal testis and single male germ-line cysts: Dissection, imaging, and pharmacological treatment. *J. Vis. Exp.* (2014) doi:10.3791/51868.
165. Gasteier, J. E. *et al.* Activation of the Rac-binding partner FHOD1 induces actin stress fibers via a ROCK-dependent mechanism. *J. Biol. Chem.* **278**, 38902–38912 (2003).
166. Gautreau, A. *et al.* Purification and architecture of the ubiquitous Wave complex. *Proc. Natl. Acad. Sci. U. S. A.* **101**, 4379–4383 (2004).
167. Geiger, B., Spatz, J. P. & Bershadsky, A. D. Environmental sensing through focal adhesions. *Nat. Rev. Mol. cell Biol.* **10**, 21–33 (2009).
168. Geiger, B., Tokuyasu, K. T., Dutton, A. H. & Singer, S. J. Vinculin, an intracellular protein localized at specialized sites where microfilament bundles terminate at cell membranes. *Proc. Natl. Acad. Sci.* **77**, 4127–4131 (1980).
169. Ghabrial, A. S. & Krasnow, M. A. Social interactions among epithelial cells during tracheal branching morphogenesis. *Nature* **441**, 746–749 (2006).
170. Giannone, G. *et al.* Lamellipodial actin mechanically links myosin activity with adhesion-site formation. *Cell* **128**, 561–575 (2007).

171. Giannone, G., Jiang, G., Sutton, D. H., Critchley, D. R. & Sheetz, M. P. Talin1 is critical for force-dependent reinforcement of initial integrin–cytoskeleton bonds but not tyrosine kinase activation. *J. Cell Biol.* **163**, 409–419 (2003).
172. Gildor, B., Massarwa, R., Shilo, B.-Z. & Schejter, E. D. The SCAR and WASp nucleation-promoting factors act sequentially to mediate *Drosophila* myoblast fusion. *EMBO Rep.* **10**, 1043–1050 (2009).
173. Gildor, B., Schejter, E. D. & Shilo, B.-Z. Bidirectional Notch activation represses fusion competence in swarming adult *Drosophila* myoblasts. *Development* **139**, 4040–4050 (2012).
174. Gilmore, A. P. & Burridge, K. Regulation of vinculin binding to talin and actin by phosphatidylinositol-4-5-bisphosphate. *Nature* **381**, 531–535 (1996).
175. Goetsch, K. P., Myburgh, K. H. & Niesler, C. U. In vitro myoblast motility models: Investigating migration dynamics for the study of skeletal muscle repair. *J. Muscle Res. Cell Motil.* **34**, 333–347 (2013).
176. Goley, E. D. & Welch, M. D. The ARP2/3 complex: An actin nucleator comes of age. *Nat. Rev. Mol. Cell Biol.* **7**, 713–726 (2006).
177. Golji, J., Lam, J. & Mofrad, M. R. K. Vinculin activation is necessary for complete talin binding. *Biophys. J.* **100**, 332–340 (2011).
178. Gould, C. J. *et al.* The formin DAD domain plays dual roles in autoinhibition and actin nucleation. *Curr. Biol.* **21**, 384–390 (2011).
179. Grabbe, C., Zervas, C. G., Hunter, T., Brown, N. H. & Palmer, R. H. Focal adhesion kinase is not required for integrin function or viability in *Drosophila*. *Development* **131**, 5795–5805 (2004).
180. Grashoff, C. *et al.* Measuring mechanical tension across vinculin reveals regulation of focal adhesion dynamics. *Nature* **466**, 263–266 (2010).
181. Groth, A. C., Fish, M., Nusse, R. & Calos, M. P. Construction of transgenic *Drosophila* by using the site-specific integrase from phage phiC31. *Genetics* **166**, 1775–1782 (2004).
182. Gryzik, T. & Müller, H.-A. J. FGF8-like1 and FGF8-like2 encode putative ligands of the FGF receptor Htl and are required for mesoderm migration in the *Drosophila* gastrula. *Curr. Biol.* **14**, 659–667 (2004).
183. Gumbiner, B. M. Regulation of cadherin-mediated adhesion in morphogenesis. *Nat. Rev. Mol. Cell Biol.* **6**, 622–634 (2005).
184. Gunage, R. D., Dhanyasi, N., Reichert, H. & VijayRaghavan, K. *Drosophila* adult muscle development and regeneration. *Semin. Cell Dev. Biol.* **72**, 56–66 (2017).
185. Guo, F., Debidda, M., Yang, L., Williams, D. A. & Zheng, Y. Genetic deletion of Rac1 GTPase reveals its critical role in actin stress fiber formation and focal adhesion complex assembly. *J. Biol. Chem.* **281**, 18652–18659 (2006).
186. Guo, W. & Wang, Y. Retrograde fluxes of focal adhesion proteins in response to cell migration and mechanical signals. *Mol. Biol. Cell* **18**, 4519–4527 (2007).

187. Gupta, G. P. & Massagué, J. Cancer Metastasis: Building a Framework. *Cell* **127**, 679–695 (2006).
188. Gupton, S. L. & Gertler, F. B. Filopodia: the fingers that do the walking. *Sci. STKE* **2007**, 1–9 (2007).
189. Haeger, A., Wolf, K., Zegers, M. M. & Friedl, P. Collective cell migration: guidance principles and hierarchies. *Trends Cell Biol.* **25**, 556–566 (2015).
190. Hakim, V. & Silberzan, P. Collective cell migration : a physics perspective. (2017).
191. Hall, A. Ras-related GTPases and the cytoskeleton. *Mol. Biol. Cell* **3**, 475–479 (1992).
192. Hanahan, D. Studies on transformation of Escherichia coli with plasmids. *J. Mol. Biol.* **166**, 557–580 (1983).
193. Hanks, S. K. & Polte, T. R. Signaling through focal adhesion kinase. *Bioessays* **19**, 137–145 (1997).
194. Harada, T. *et al.* Nuclear lamin stiffness is a barrier to 3D migration, but softness can limit survival. *J. Cell Biol.* **204**, 669–682 (2014).
195. Haralalka, S. & Abmayr, S. M. Myoblast fusion in Drosophila. *Exp. Cell Res.* **316**, 3007–3013 (2010).
196. Harata, M., Karwan, A. & Wintersberger, U. An essential gene of Saccharomyces cerevisiae coding for an actin-related protein. *Proc. Natl. Acad. Sci.* **91**, 8258–8262 (1994).
197. Harris, E. S., Li, F. & Higgs, H. N. The mouse formin, FRL α , slows actin filament barbed end elongation, competes with capping protein, accelerates polymerization from monomers, and severs filaments. *J. Biol. Chem.* **279**, 20076–20087 (2004).
198. Harris, T. J. C. & Tepass, U. Adherens junctions: from molecules to morphogenesis. *Nat. Rev. Mol. cell Biol.* **11**, 502–514 (2010).
199. Hartenstein, V. *Atlas of Drosophila development*. (Cold Spring Harbor Laboratory Press, 1993).
200. Heath, I. B. & Steinberg, G. Mechanisms of Hyphal Tip Growth: Tube Dwelling Amebae Revisited. *Fungal Genet. Biol.* **28**, 79–93 (1999).
201. Hegerfeldt, Y., Tusch, M., Bröcker, E.-B. & Friedl, P. Collective cell movement in primary melanoma explants: plasticity of cell-cell interaction, β 1-integrin function, and migration strategies. *Cancer Res.* **62**, 2125–2130 (2002).
202. Heimsath, E. G. & Higgs, H. N. The C terminus of formin FMNL3 accelerates actin polymerization and contains a WH2 domain-like sequence that binds both monomers and filament barbed ends. *J. Biol. Chem.* **287**, 3087–3098 (2012).
203. Hemmings, L. *et al.* Talin contains three actin-binding sites each of which is adjacent to a vinculin-binding site. *J. Cell Sci.* **109**, 2715–2726 (1996).
204. Hidalgo-Carcedo, C. *et al.* Collective cell migration requires suppression of actomyosin at cell–cell contacts mediated by DDR1 and the cell polarity regulators Par3 and Par6. *Nat. Cell Biol.* **13**, 49–59 (2011).

205. Higgs, H. N. & Pollard, T. D. Regulation of Actin Complex and WASp / Scar Proteins. *J. Biol. Chem.* **274**, 32531–32534 (1999).
206. Higgs, H. N. & Pollard, T. D. Activation by Cdc42 and PIP2 of Wiskott-Aldrich Syndrome protein (WASp) stimulates actin nucleation by Arp2/3 complex. *J. Cell Biol.* **150**, 1311–1320 (2000).
207. Higgs, H. N. Formin proteins: a domain-based approach. *Trends Biochem. Sci.* **30**, 342–353 (2005).
208. Higgs, H. N. & Peterson, K. J. Phylogenetic analysis of the formin homology 2 domain. *Mol. Biol. Cell* **16**, 1–13 (2005).
209. Hildebrand, J. D., Schaller, M. D. & Parsons, J. T. Identification of sequences required for the efficient localization of the focal adhesion kinase, pp125FAK, to cellular focal adhesions. *J. Cell Biol.* **123**, 993–1005 (1993).
210. Hill, T. L. & Kirschner, M. W. Bioenergetics and Kinetics of Microtubule and Actin Filament Assembly–Disassembly. in (eds. Bourne, G. H., Danielli, J. F. & Jeon, K. W. B. T.-I. R. of C.) vol. 78 1–125 (Academic Press, 1982).
211. Hoffman, B. D. The detection and role of molecular tension in focal adhesion dynamics. in *Progress in molecular biology and translational science* vol. 126 3–24 (Elsevier, 2014).
212. Horn, C. & Handler, A. M. Site-specific genomic targeting in Drosophila. *Proc. Natl. Acad. Sci. U. S. A.* **102**, 12483–12488 (2005).
213. Horwitz, A., Duggan, K., Buck, C., Beckerle, M. C. & Burridge, K. Interaction of plasma membrane fibronectin receptor with talin—a transmembrane linkage. *Nature* **320**, 531–533 (1986).
214. Hoshino, D., Branch, K. M. & Weaver, A. M. Signaling inputs to invadopodia and podosomes. *J. Cell Sci.* **126**, 2979–2989 (2013).
215. Hotchin, N. A. & Hall, A. The assembly of integrin adhesion complexes requires both extracellular matrix and intracellular rho/rac GTPases. *J. Cell Biol.* **131**, 1857–1865 (1995).
216. Hotulainen, P. & Lappalainen, P. Stress fibers are generated by two distinct actin assembly mechanisms in motile cells. *J. Cell Biol.* **173**, 383–394 (2006).
217. Humphries, M. J. & Newham, P. The structure of cell-adhesion molecules. *Trends Cell Biol.* **8**, 78–83 (1998).
218. Hutson, M. S. *et al.* Forces for morphogenesis investigated with laser microsurgery and quantitative modeling. *Science* **300**, 145–149 (2003).
219. Huttenlocher, A. & Horwitz, A. R. Integrins in cell migration. *Cold Spring Harb. Perspect. Biol.* **3**, 1–16 (2011).
220. Hynes, R. O. Integrins: versatility, modulation, and signaling in cell adhesion. *Cell* **69**, 11–25 (1992).
221. Imamura, H. *et al.* Bni1p and Bnr1p: downstream targets of the Rho family small G-proteins which interact with profilin and regulate actin cytoskeleton in *Saccharomyces cerevisiae*. *EMBO J.* **16**, 2745–2755 (1997).

222. van Impel, A. *et al.* Regulation of the Rac GTPase pathway by the multifunctional Rho GEF Pebble is essential for mesoderm migration in the *Drosophila* gastrula. *Development* **136**, 813–822 (2009).
223. Inaki, M., Vishnu, S., Cliffe, A. & Rørth, P. Effective guidance of collective migration based on differences in cell states. *Proc. Natl. Acad. Sci.* **109**, 2027–2032 (2012).
224. Innocenti, M. *et al.* Abi1 is essential for the formation and activation of a WAVE2 signalling complex. *Nat. Cell Biol.* **6**, 319–327 (2004).
225. Ishizaki, T. *et al.* Coordination of microtubules and the actin cytoskeleton by the Rho effector mDia1. *Nat. Cell Biol.* **3**, 8–14 (2001).
226. Ismail, A. M., Padrick, S. B., Chen, B., Umetani, J. & Rosen, M. K. The WAVE regulatory complex is inhibited. *Nat. Struct. Mol. Biol.* **16**, 561–563 (2009).
227. Jackson-Grusby, L., Kuo, A. & Leder, P. A variant limb deformity transcript expressed in the embryonic mouse limb defines a novel formin. *Genes Dev.* **6**, 29–37 (1992).
228. Jacquemet, G., Hamidi, H. & Ivaska, J. Filopodia in cell adhesion, 3D migration and cancer cell invasion. *Curr. Opin. Cell Biol.* **36**, 23–31 (2015).
229. Jankovics, F. & Brunner, D. Transiently reorganized microtubules are essential for zippering during dorsal closure in *Drosophila melanogaster*. *Dev. Cell* **11**, 375–385 (2006).
230. Jégou, A. *et al.* Individual actin filaments in a microfluidic flow reveal the mechanism of ATP hydrolysis and give insight into the properties of profilin. *PLoS Biol.* **9**, (2011).
231. Jenett, A. *et al.* A GAL4-Driver Line Resource for *Drosophila* Neurobiology. *Cell Rep.* **2**, 991–1001 (2012).
232. Jiang, G., Huang, A. H., Cai, Y., Tanase, M. & Sheetz, M. P. Rigidity sensing at the leading edge through $\alpha\beta 3$ integrins and RPTP α . *Biophys. J.* **90**, 1804–1809 (2006).
233. Johnson, R. P. & Craig, S. W. F-actin binding site masked by the intramolecular association of vinculin head and tail domains. *Nature* **373**, 261–264 (1995).
234. Jory, A. *et al.* A Survey of 6,300 Genomic Fragments for cis-Regulatory Activity in the Imaginal Discs of *Drosophila melanogaster*. *Cell Rep.* **2**, 1014–1024 (2012).
235. Kabsch, W., Mannherz, H. G., Suck, D., Pai, E. F. & Holmes, K. C. Atomic structure of the actin: DNase I complex. *Nature* **347**, 37–44 (1990).
236. Kage, F. *et al.* FMNL formins boost lamellipodial force generation. *Nat. Commun.* **8**, (2017).
237. Karp, G. C. & Solursh, M. Dynamic activity of the filopodia of sea urchin embryonic cells and their role in directed migration of the primary mesenchyme in vitro. *Dev. Biol.* **112**, 276–283 (1985).
238. Kaufmann, A., Heinemann, F., Radmacher, M. & Stick, R. Amphibian oocyte nuclei expressing lamin A with the progeria mutation E145K exhibit an increased elastic modulus. *Nucleus* **2**, 310–319 (2011).
239. Kelleher, J. F., Atkinson, S. J. & Pollard, T. D. Sequences, structural models, and cellular localization of the actin-related proteins Arp2 and Arp3 from *Acanthamoeba*. *J. Cell Biol.* **131**, 385–397 (1995).

240. Kessenbrock, K., Plaks, V. & Werb, Z. Matrix Metalloproteinases: Regulators of the tumor. *Cell* **141**, 52–67 (2010).
241. Kiehart, D. P., Galbraith, C. G., Edwards, K. A., Rickoll, W. L. & Montague, R. A. Multiple forces contribute to cell sheet morphogenesis for dorsal closure in *Drosophila*. *J. Cell Biol.* **149**, 471–490 (2000).
242. Kim, A. S., Kakalis, L. T., Abdul-Manan, N., Liu, G. A. & Rosen, M. K. Autoinhibition and activation mechanisms of the Wiskott-Aldrich syndrome protein. *Nature* **404**, 151–158 (2000).
243. Kim, Y. *et al.* Phosphorylation of WAVE1 regulates actin polymerization and dendritic spine morphology. *Nature* **442**, 814–817 (2006).
244. Klämbt, C., Glazer, L. & Shilo, B. Z. *breathless*, a *Drosophila* FGF receptor homolog, is essential for migration of tracheal and specific midline glial cells. *Genes Dev.* **6**, 1668–1678 (1992).
245. ten Klooster, J. P., Jaffer, Z. M., Chernoff, J. & Hordijk, P. L. Targeting and activation of Rac1 are mediated by the exchange factor β -Pix. *J. Cell Biol.* **172**, 759–769 (2006).
246. Koestner, U., Shnitsar, I., Linnemannstöns, K., Hufton, A. L. & Borchers, A. Semaphorin and neuropilin expression during early morphogenesis of *Xenopus laevis*. *Dev. Dyn. an Off. Publ. Am. Assoc. Anat.* **237**, 3853–3863 (2008).
247. Kohno, H. *et al.* *Bni1p* implicated in cytoskeletal control is a putative target of Rho1p small GTP binding protein in *Saccharomyces cerevisiae*. *EMBO J.* **15**, 6060–6068 (1996).
248. Kollmar, M., Lbik, D. & Enge, S. Evolution of the eukaryotic ARP2/3 activators of the WASP family: WASP, WAVE, WASH, and WHAMM, and the proposed new family members WAWH and WAML. *BMC Res. Notes* **5**, (2012).
249. Korobova, F. & Svitkina, T. Arp2/3 Complex Is Important for Filopodia Formation, Growth Cone Motility, and Neuritegenesis in Neuronal Cells. *Mol. Biol. Cell* **19**, 1561–1574 (2008).
250. Koronakis, V. *et al.* WAVE regulatory complex activation by cooperating GTPases Arf and Rac1. *Proc. Natl. Acad. Sci.* **108**, 14449–14454 (2011).
251. Kovar, D. R., Harris, E. S., Mahaffy, R., Higgs, H. N. & Pollard, T. D. Control of the assembly of ATP- and ADP-actin by formins and profilin. *Cell* **124**, 423–435 (2006).
252. Kovar, D. R., Kuhn, J. R., Tichy, A. L. & Pollard, T. D. The fission yeast cytokinesis formin Cdc12p is a barbed end actin filament capping protein gated by profilin. *J. Cell Biol.* **161**, 875–887 (2003).
253. Kovar, D. R. & Pollard, T. D. Insertional assembly of actin filament barbed ends in association with formins produces piconewton forces. *Proc. Natl. Acad. Sci. U. S. A.* **101**, 14725 LP – 14730 (2004).
254. Kovar, D. R., Wu, J.-Q. & Pollard, T. D. Profilin-mediated competition between capping protein and formin Cdc12p during cytokinesis in fission yeast. *Mol. Biol. Cell* **16**, 2313–2324 (2005).
255. Kozlov, M. M. & Bershadsky, A. D. Processive capping by formin suggests a force-driven mechanism of actin polymerization. *J. Cell Biol.* **167**, 1011–1017 (2004).

256. Kozma, R., Ahmed, S., Best, A. & Lim, L. The GTPase-activating protein n-chimaerin cooperates with Rac1 and Cdc42Hs to induce the formation of lamellipodia and filopodia. *Mol. Cell. Biol.* **16**, 5069–5080 (1996).
257. Kozopas, K. M., Samos, C. H. & Nusse, R. DWnt-2, a Drosophila Wnt gene required for the development of the male reproductive tract, specifies a sexually dimorphic cell fate. *Genes Dev.* **12**, 1155–1165 (1998).
258. Krause, M. *et al.* Lamellipodin, an Ena/VASP ligand, is implicated in the regulation of lamellipodial Dynamics. *Dev. Cell* **7**, 571–583 (2004).
259. Krause, M. & Gautreau, A. Steering cell migration: Lamellipodium dynamics and the regulation of directional persistence. *Nat. Rev. Mol. Cell Biol.* **15**, 577–590 (2014).
260. Kuckwa, J., Fritzen, K., Buttgereit, D., Rothenbusch-Fender, S. & Renkawitz-Pohl, R. A new level of plasticity: Drosophila smooth-like testes muscles compensate failure of myoblast fusion. *Development* **143**, 329–338 (2016).
261. Kudo, R. R. Protozoology. *Protozoology*. 1,174 pp. (1977).
262. Kulesa, P. M. & Fraser, S. E. Neural crest cell dynamics revealed by time-lapse video microscopy of whole embryo chick explant cultures. *Dev. Biol.* **204**, 327–344 (1998).
263. Kulesa, P. M., Bailey, C. M., Kasemeier-Kulesa, J. C. & McLennan, R. Cranial neural crest migration: new rules for an old road. *Dev. Biol.* **344**, 543–554 (2010).
264. Kulesa, P. M. & Fraser, S. E. In ovo time-lapse analysis of chick hindbrain neural crest cell migration shows cell interactions during migration to the branchial arches. *Development* **127**, 1161–1172 (2000).
265. Kuriyama, S. *et al.* In vivo collective cell migration requires an LPAR2-dependent increase in tissue fluidity. *J. Cell Biol.* **206**, 113–127 (2014).
266. Kwong, L., Wozniak, M. A., Collins, A. S., Wilson, S. D. & Keely, P. J. R-Ras promotes focal adhesion formation through focal adhesion kinase and p130Cas by a novel mechanism that differs from integrins. *Mol. Cell. Biol.* **23**, 933–949 (2003).
267. De La Cruz, E. M. & Pollard, T. D. Nucleotide-Free Actin: Stabilization by Sucrose and Nucleotide Binding Kinetics. *Biochemistry* **34**, 5452–5461 (1995).
268. Labernadie, A. *et al.* A mechanically active heterotypic E-cadherin/N-cadherin adhesion enables fibroblasts to drive cancer cell invasion. *Nat. Cell Biol.* **19**, 224–237 (2017).
269. Ladoux, B. & Mège, R. M. Mechanobiology of collective cell behaviours. *Nat. Rev. Mol. Cell Biol.* **18**, 743–757 (2017).
270. LaFever, K. S., Wang, X., Page-McCaw, P., Bhave, G. & Page-McCaw, A. Both Drosophila matrix metalloproteinases have released and membrane-tethered forms but have different substrates. *Sci. Rep.* **7**, 44560 (2017).
271. Lai, F. P. L. *et al.* Arp2/3 complex interactions and actin network turnover in lamellipodia. *EMBO J.* **27**, 982–992 (2008).
272. Lai, F. P. L. *et al.* Cortactin promotes migration and platelet-derived growth factor-induced actin reorganization by signaling to Rho-GTPases. *Mol. Biol. Cell* **20**, 3209–3223 (2009).

273. Lakowicz, J. R. *Principles of fluorescence spectroscopy*. (Springer science & business media, 2013).
274. Lamb, M. C., Anliker, K. K. & Tootle, T. L. Fascin regulates protrusions and delamination to mediate invasive, collective cell migration in vivo. *Dev. Dyn.* 961–982 (2020) doi:10.1002/dvdy.186.
275. Lammel, U. *et al.* The Drosophila FHOD1-like formin Knittrig acts through Rok to promote stress fiber formation and directed macrophage migration during the cellular immune response. *Development* **141**, 1366–1380 (2014).
276. Lammerding, J. Mechanics of the nucleus. *Compr. Physiol.* **1**, 783–807 (2011).
277. Lammerding, J. *et al.* Lamins A and C but not lamin B1 regulate nuclear mechanics. *J. Biol. Chem.* **281**, 25768–25780 (2006).
278. Lammerding, J. *et al.* Lamin A/C deficiency causes defective nuclear mechanics and mechanotransduction. *J. Clin. Invest.* **113**, 370–378 (2004).
279. Lämmermann, T. & Sixt, M. Mechanical modes of ‘amoeboid’ cell migration. *Curr. Opin. Cell Biol.* **21**, 636–644 (2009).
280. Lange, J. R. *et al.* Unbiased high-precision cell mechanical measurements with microconstrictions. *Biophys. J.* **112**, 1472–1480 (2017).
281. Lange, J. R. *et al.* Microconstriction arrays for high-throughput quantitative measurements of cell mechanical properties. *Biophys. J.* **109**, 26–34 (2015).
282. Lautscham, L. A. *et al.* Migration in confined 3D environments is determined by a combination of adhesiveness, nuclear volume, contractility, and cell stiffness. *Biophys. J.* **109**, 900–913 (2015).
283. Law, A. L. *et al.* Lamellipodin and the Scar/WAVE complex cooperate to promote cell migration in vivo. *J. Cell Biol.* **203**, 673–689 (2013).
284. Lawson, C. *et al.* FAK promotes recruitment of talin to nascent adhesions to control cell motility. *J. Cell Biol.* **196**, 223–232 (2012).
285. Leader, B. *et al.* Formin-2, polyploidy, hypofertility and positioning of the meiotic spindle in mouse oocytes. *Nat. Cell Biol.* **4**, 921–928 (2002).
286. Lebensohn, A. M. & Kirschner, M. W. Activation of the WAVE Complex by Coincident Signals Controls Actin Assembly. *Mol. Cell* **36**, 512–524 (2009).
287. Lebreton, G. & Casanova, J. Specification of leading and trailing cell features during collective migration in the Drosophila trachea. *J. Cell Sci.* **127**, 465–474 (2014).
288. Lee, D., Fong, K. P., King, M. R., Brass, L. F. & Hammer, D. A. Differential dynamics of platelet contact and spreading. *Biophys. J.* **102**, 472–482 (2012).
289. Lees-Miller, J. P., Helfman, D. M. & Schroer, T. A. A vertebrate actin-related protein is a component of a multisubunit complex involved in microtubule-based vesicle motility. *Nature* **359**, 244–246 (1992).

290. Lees-Miller, J. P., Henry, G. & Helfman, D. M. Identification of *act2*, an essential gene in the fission yeast *Schizosaccharomyces pombe* that encodes a protein related to actin. *Proc. Natl. Acad. Sci. U. S. A.* **89**, 80–83 (1992).
291. Lehmann, S. *et al.* Hypoxia induces a HIF-1-dependent transition from collective-to-amoeboid dissemination in epithelial cancer cells. *Curr. Biol.* **27**, 392–400 (2017).
292. Lessey, E. C., Guilluy, C. & Burridge, K. From mechanical force to RhoA activation. *Biochemistry* **51**, 7420–7432 (2012).
293. Li, F. & Higgs, H. N. The mouse Formin mDia1 is a potent actin nucleation factor regulated by autoinhibition. *Curr. Biol.* **13**, 1335–1340 (2003).
294. Li, H., Guo, F., Rubinstein, B. & Li, R. Actin-driven chromosomal motility leads to symmetry breaking in mammalian meiotic oocytes. *Nat. Cell Biol.* **10**, 1301–1308 (2008).
295. Li, J. F. & Lowengrub, J. The effects of cell compressibility, motility and contact inhibition on the growth of tumor cell clusters using the Cellular Potts Model. *J. Theor. Biol.* **343**, 79–91 (2014).
296. Li, L., Okura, M. & Imamoto, A. Focal adhesions require catalytic activity of Src family kinases to mediate integrin-matrix adhesion. *Mol. Cell. Biol.* **22**, 1203–1217 (2002).
297. Li, L. *et al.* E-cadherin plays an essential role in collective directional migration of large epithelial sheets. *Cell. Mol. Life Sci.* **69**, 2779–2789 (2012).
298. Liu, Q. *et al.* Cell adhesion molecule cadherin-6 function in zebrafish cranial and lateral line ganglia development. *Dev. Dyn.* **240**, 1716–1726 (2011).
299. Llense, F. & Martín-Blanco, E. JNK signaling controls border cell cluster integrity and collective cell migration. *Curr. Biol.* **18**, 538–544 (2008).
300. Lo, C. M., Wang, H. B., Dembo, M. & Wang, Y. L. Cell movement is guided by the rigidity of the substrate. *Biophys. J.* **79**, 144–152 (2000).
301. Louis, S. F. & Zahradka, P. Vascular smooth muscle cell motility: From migration to invasion. *Exp. Clin. Cardiol.* **15**, (2010).
302. Lyon, C. A., Koutsouki, E., Aguilera, C. M., Blaschuk, O. W. & George, S. J. Inhibition of N-cadherin retards smooth muscle cell migration and intimal thickening via induction of apoptosis. *J. Vasc. Surg.* **52**, 1301–1309 (2010).
303. Maas, R. L., Zeller, R., Woychik, R. P., Vogt, T. F. & Leder, P. Disruption of formin-encoding transcripts in two mutant limb deformity alleles. *Nature* **346**, 853–855 (1990).
304. Machesky, L. M. *et al.* Mammalian actin-related protein 2/3 complex localizes to regions of lamellipodial protrusion and is composed of evolutionarily conserved proteins. *Biochem. J.* **328**, 105–112 (1997).
305. Machesky, L. M. *et al.* Scar, a WASp-related protein, activates nucleation of actin filaments by the Arp2/3 complex. *Proc. Natl. Acad. Sci. U. S. A.* **96**, 3739–3744 (1999).
306. Machesky, L. M., Atkinson, S. J., Ampe, C., Vandekerckhove, J. & Pollard, T. D. Purification of a cortical complex containing two unconventional actins from *Acanthamoeba* by affinity chromatography on profilin-agarose. *J. Cell Biol.* **127**, 107–115 (1994).

307. Machesky, L. M. & Insall, R. H. Scar1 and the related Wiskott-Aldrich syndrome protein, WASP, regulate the actin cytoskeleton through the Arp2/3 complex. *Curr. Biol.* **8**, 1347–1356 (1998).
308. Majumdar, R., Sixt, M. & Parent, C. A. New paradigms in the establishment and maintenance of gradients during directed cell migration. *Curr. Opin. Cell Biol.* **30**, 33–40 (2014).
309. Malinda, K. M., Fisher, G. W. & Ettensohn, C. A. Four-dimensional microscopic analysis of the filopodial behavior of primary mesenchyme cells during gastrulation in the sea urchin embryo. *Dev. Biol.* **172**, 552–566 (1995).
310. Manabe, R., Kovalenko, M., Webb, D. J. & Horwitz, A. R. GIT1 functions in a motile, multi-molecular signaling complex that regulates protrusive activity and cell migration. *J. Cell Sci.* **115**, 1497–1510 (2002).
311. Mandel, M. & Higa, A. Calcium-dependent bacteriophage DNA infection. *J. Mol. Biol.* **53**, 159–162 (1970).
312. Maniatis, T., Fritsch, E. F., Sambrook, J. & Engel, J. Molecular cloning—A laboratory manual. New York: Cold Spring Harbor Laboratory. 1982, 545 S., 42 \$. *Acta Biotechnol.* **5**, 104 (1985).
313. Markstein, M. *et al.* A regulatory code for neurogenic gene expression in the Drosophila embryo. *Development* **131**, 2387–2394 (2004).
314. Martin, P. & Parkhurst, S. M. Parallels between tissue repair and embryo morphogenesis. *Development* **131**, 3021–3034 (2004).
315. Massoumi, R. *et al.* Down-regulation of CYLD expression by Snail promotes tumor progression in malignant melanoma. *J. Exp. Med.* **206**, 221–232 (2009).
316. Matsubayashi, Y., Ebisuya, M., Honjoh, S. & Nishida, E. ERK activation propagates in epithelial cell sheets and regulates their migration during wound healing. *Curr. Biol.* **14**, 731–735 (2004).
317. Matthews, H. K. *et al.* Directional migration of neural crest cells in vivo is regulated by Syndecan-4/Rac1 and non-canonical Wnt signaling/RhoA. *Development* **135**, 1771–1780 (2008).
318. Matthews, H. K., Broders-Bondon, F., Thiery, J. P. & Mayor, R. Wnt11r is required for cranial neural crest migration. *Dev. Dyn. an Off. Publ. Am. Assoc. Anat.* **237**, 3404–3409 (2008).
319. Mayor, R. Collective Cell Migration: Wisdom of the Crowds Transforms a Negative Cue into a Positive One. *Curr. Biol.* **29**, R205–R207 (2019).
320. Mayor, R. Collective Cell Migration: Wisdom of the Crowds Transforms a Negative Cue into a Positive One. *Curr. Biol.* **29**, R205–R207 (2019).
321. Mayor, R. & Carmona-Fontaine, C. Keeping in touch with contact inhibition of locomotion. *Trends Cell Biol.* **20**, 319–328 (2010).
322. Mayor, R. & Etienne-Manneville, S. The front and rear of collective cell migration. *Nat. Rev. Mol. Cell Biol.* **17**, 97–109 (2016).
323. McClay, D. R. The role of thin filopodia in motility and morphogenesis. *Exp. Cell Res.* **253**, 296–301 (1999).

324. McDonald, J. A., Pinheiro, E. M., Kadlec, L., Schupbach, T. & Montell, D. J. Multiple EGFR ligands participate in guiding migrating border cells. *Dev. Biol.* **296**, 94–103 (2006).
325. McDonald, J. A., Pinheiro, E. M. & Montell, D. J. PVF1, a PDGF/VEGF homolog, is sufficient to guide border cells and interacts genetically with Taiman. *Development* **130**, 3469–3478 (2003).
326. McKinney, M. C., Stark, D. A., Teddy, J. & Kulesa, P. M. Neural crest cell communication involves an exchange of cytoplasmic material through cellular bridges revealed by photoconversion of KikGR. *Dev. Dyn.* **240**, 1391–1401 (2011).
327. Meltzer, H. *et al.* Tissue-specific (ts)CRISPR as an efficient strategy for in vivo screening in *Drosophila*. *Nat. Commun.* **10**, 2113 (2019).
328. Miki, H., Miura, K. & Takenawa, T. N-WASP, a novel actin-depolymerizing protein, regulates the cortical cytoskeletal rearrangement in a PIP2-dependent manner downstream of tyrosine kinases. *EMBO J.* **15**, 5326–5335 (1996).
329. Miki, H., Fukuda, M., Nishida, E. & Takenawa, T. Phosphorylation of WAVE downstream of mitogen-activated protein kinase signaling. *J. Biol. Chem.* **274**, 27605–27609 (1999).
330. Miki, H., Sasaki, T., Takai, Y. & Takenawa, T. Induction of filopodium formation by a WASP-related actin-depolymerizing protein N-WASP. *Nature* **391**, 93–96 (1998).
331. Miki, H., Suetsugu, S. & Takenawa, T. WAVE, a novel WASP-family protein involved in actin reorganization induced by Rac. *EMBO J.* **17**, 6932–6941 (1998).
332. Miki, H. & Takenawa, T. Direct binding of the verprolin-homology domain in N-WASP to actin is essential for cytoskeletal reorganization. *Biochem. Biophys. Res. Commun.* **243**, 73–78 (1998).
333. Mitchison, T. & Kirschner, M. Cytoskeletal dynamics and nerve growth. *Neuron* **1**, 761–772 (1988).
334. Montell, D. J. Border-cell migration: the race is on. *Nat. Rev. Mol. cell Biol.* **4**, 13–24 (2003).
335. Montell, D. J., Rorth, P. & Spradling, A. C. slow border cells, a locus required for a developmentally regulated cell migration during oogenesis, encodes *Drosophila* CEBP. *Cell* **71**, 51–62 (1992).
336. Moore, R. *et al.* Par3 controls neural crest migration by promoting microtubule catastrophe during contact inhibition of locomotion. *Development* **140**, 4763–4775 (2013).
337. Morin, X., Daneman, R., Zavortink, M. & Chia, W. A protein trap strategy to detect GFP-tagged proteins expressed from their endogenous loci in *Drosophila*. *Proc. Natl. Acad. Sci.* **98**, 15050 LP – 15055 (2001).
338. Morrell, J. L., Morphew, M. & Gould, K. L. A mutant of Arp2p causes partial disassembly of the Arp2/3 complex and loss of cortical actin function in fission yeast. *Mol. Biol. Cell* **10**, 4201–4215 (1999).
339. Moseley, J. B. *et al.* A conserved mechanism for Bni1- and mDia1-induced actin assembly and dual regulation of Bni1 by Bud6 and profilin. *Mol. Biol. Cell* **15**, 896–907 (2004).
340. Muha, V. & Müller, H.-A. Functions and Mechanisms of Fibroblast Growth Factor (FGF) Signalling in *Drosophila melanogaster*. *Int. J. Mol. Sci.* **14**, 5920–5937 (2013).

341. Muhua, L., Karpova, T. S. & Cooper, J. A. A yeast actin-related protein homologous to that in vertebrate dynactin complex is important for spindle orientation and nuclear migration. *Cell* **78**, 669–679 (1994).
342. Müller, P. M. *et al.* Systems analysis of RhoGEF and RhoGAP regulatory proteins reveals spatially organized RAC1 signalling from integrin adhesions. *Nat. Cell Biol.* **22**, 498–511 (2020).
343. Mullins, R. D., Heuser, J. A. & Pollard, T. D. The interaction of Arp2/3 complex with actin: Nucleation, high affinity pointed end capping, and formation of branching networks of filaments. *Proc. Natl. Acad. Sci. U. S. A.* **95**, 6181–6186 (1998).
344. Mullins, R. D., Stafford, W. F. & Pollard, T. D. Structure, subunit topology, and actin-binding activity of the Arp2/3 complex from *Acanthamoeba*. *J. Cell Biol.* **136**, 331–343 (1997).
345. Mullis, K. B. & Faloona, F. A. B. T.-M. in E. [21] Specific synthesis of DNA in vitro via a polymerase-catalyzed chain reaction. in *Recombinant DNA Part F* vol. 155 335–350 (Academic Press, 1987).
346. Munjal, A., Philippe, J.-M., Munro, E. & Lecuit, T. A self-organized biomechanical network drives shape changes during tissue morphogenesis. *Nature* **524**, 351–355 (2015).
347. Murphy, A. M. & Montell, D. J. Cell type-specific roles for Cdc42, Rac, and RhoL in *Drosophila* oogenesis. *J. Cell Biol.* **133**, 617–630 (1996).
348. Nabeshima, K. *et al.* Front-cell-specific expression of membrane-type 1 matrix metalloproteinase and gelatinase A during cohort migration of colon carcinoma cells induced by hepatocyte growth factor/scatter factor. *Cancer Res.* **60**, 3364–3369 (2000).
349. Nabeshima, K., Inoue, T., Shimao, Y., Kataoka, H. & Koono, M. Cohort migration of carcinoma cells: differentiated colorectal carcinoma cells move as coherent cell clusters or sheets. *Histol. Histopathol.* **14**, 1183–1187 (1999).
350. Nagel, B. M., Bechtold, M., Rodriguez, L. G. & Bogdan, S. *Drosophila* WASH is required for integrin-mediated cell adhesion, cell motility and lysosomal neutralization. *J. Cell Sci.* **130**, 344–359 (2017).
351. Nanda, S. *et al.* Sox100B, a *Drosophila* Group E Sox-domain Gene, Is Required for Somatic Testis Differentiation. *Sex. Dev.* **3**, 26–37 (2009).
352. Nguyen, B. P., Ryan, M. C., Gil, S. G. & Carter, W. G. Deposition of laminin 5 in epidermal wounds regulates integrin signaling and adhesion. *Curr. Opin. Cell Biol.* **12**, 554–562 (2000).
353. Niewiadomska, P., Godt, D. & Tepass, U. D E-Cadherin is required for intercellular motility during *Drosophila* oogenesis. *J. Cell Biol.* **144**, 533–547 (1999).
354. Nikolic, D. L., Boettiger, A. N., Bar-Sagi, D., Carbeck, J. D. & Shvartsman, S. Y. Role of boundary conditions in an experimental model of epithelial wound healing. *Am. J. Physiol. Physiol.* **291**, C68–C75 (2006).
355. Nishita, M. *et al.* Filopodia formation mediated by receptor tyrosine kinase Ror2 is required for Wnt5a-induced cell migration. *J. Cell Biol.* **175**, 555–562 (2006).
356. Nobes, C. D. & Hall, A. Rho, Rac, and Cdc42 GTPases regulate the assembly of multimolecular focal complexes associated with actin stress fibers, lamellipodia, and filopodia. *Cell* **81**, 53–62 (1995).

357. Nürnberg, A., Kitzing, T. & Grosse, R. Nucleating actin for invasion. *Nat. Rev. Cancer* **11**, 117–187 (2011).
358. Oberstein, A., Pare, A., Kaplan, L. & Small, S. Site-specific transgenesis by Cre-mediated recombination in *Drosophila*. *Nat. Methods* **2**, 583–585 (2005).
359. Ochs, H. D. *et al.* The Wiskott-Aldrich syndrome: studies of lymphocytes, granulocytes, and platelets. *Blood* **55**, 243–252 (1980).
360. Oikawa, T. *et al.* PtdIns (3, 4, 5) P 3 binding is necessary for WAVE2-induced formation of lamellipodia. *Nat. Cell Biol.* **6**, 420–426 (2004).
361. Oma, Y. & Harata, M. Actin-related proteins localized in the nucleus. *Nucleus* **2**, 38–46 (2011).
362. Omelchenko, T., Vasiliev, J. M., Gelfand, I. M., Feder, H. H. & Bonder, E. M. Rho-dependent formation of epithelial “leader” cells during wound healing. *Proc. Natl. Acad. Sci.* **100**, 10788–10793 (2003).
363. Oosawa, F. & Asakura, S. *Thermodynamics of the Polymerization of Protein*. (Academic Press, 1975).
364. Otey, C. A., Pavalko, F. M. & Burridge, K. An interaction between alpha-actinin and the beta 1 integrin subunit in vitro. *J. Cell Biol.* **111**, 721–729 (1990).
365. Otomo, T. *et al.* Structural basis of actin filament nucleation and processive capping by a formin homology 2 domain. *Nature* **433**, 488–494 (2005).
366. Ozawa, M., Baribault, H. & Kemler, R. The cytoplasmic domain of the cell adhesion molecule uvomorulin associates with three independent proteins structurally related in different species. *EMBO J.* **8**, 1711–1717 (1989).
367. Paluch, E. K. & Raz, E. The role and regulation of blebs in cell migration. *Curr. Opin. Cell Biol.* **25**, 582–590 (2013).
368. Paul, A. & Pollard, T. The role of the FH1 domain and profilin in formin-mediated actin-filament elongation and nucleation. *Curr. Biol.* **18**, 9–19 (2008).
369. Paul, A. S. & Pollard, T. D. Review of the mechanism of processive actin filament elongation by formins. *Cell Motil. Cytoskeleton* **66**, 606–617 (2009).
370. Paul, A. S. & Pollard, T. D. Energetic requirements for processive elongation of actin filaments by FH1FH2-formins. *J. Biol. Chem.* **284**, 12533–12540 (2009).
371. Paul, C. D., Mistriotis, P. & Konstantopoulos, K. Cancer cell motility: Lessons from migration in confined spaces. *Nat. Rev. Cancer* **17**, 131–140 (2017).
372. Peglion, F., Llense, F. & Etienne-Manneville, S. Adherens junction treadmilling during collective migration. *Nat. Cell Biol.* **16**, 639–651 (2014).
373. Pellegrin, S. & Mellor, H. The Rho Family GTPase Rif Induces Filopodia through mDia2. *Curr. Biol.* **15**, 129–133 (2005).
374. Peng, J., Wallar, B. J., Flanders, A., Swiatek, P. J. & Alberts, A. S. Disruption of the Diaphanous-related formin Drf1 gene encoding mDia1 reveals a role for Drf3 as an effector for Cdc42. *Curr. Biol.* **13**, 534–545 (2003).

375. Perryn, E. D., Czirik, A. & Little, C. D. Vascular sprout formation entails tissue deformations and VE-cadherin-dependent cell-autonomous motility. *Dev. Biol.* **313**, 545–555 (2008).
376. Petrie, R. J. & Yamada, K. M. At the leading edge of three-dimensional cell migration. *J. Cell Sci.* **125**, 5917–5926 (2012).
377. Pfeiffer, B. D. *et al.* Tools for neuroanatomy and neurogenetics in Drosophila. *Proc. Natl. Acad. Sci. U. S. A.* **105**, 9715–9720 (2008).
378. Pfender, S., Kuznetsov, V., Pleiser, S., Kerkhoff, E. & Schuh, M. Spire-type actin nucleators cooperate with Formin-2 to drive asymmetric oocyte division. *Curr. Biol.* **21**, 955–960 (2011).
379. Phng, L. K., Stanchi, F. & Gerhardt, H. Filopodia are dispensable for endothelial tip cell guidance. *Dev.* **140**, 4031–4040 (2013).
380. Pinheiro, E. M. & Montell, D. J. Requirement for Par-6 and Bazooka in Drosophila border cell migration. *Development* **131**, 5243–5251 (2004).
381. Pinto-Costa, R. & Sousa, M. M. Profilin as a dual regulator of actin and microtubule dynamics. *Cytoskeleton* **77**, 76–83 (2020).
382. Plamann, M., Minke, P. F., Tinsley, J. H. & Bruno, K. S. Cytoplasmic dynein and actin-related protein Arp1 are required for normal nuclear distribution in filamentous fungi. *J. Cell Biol.* **127**, 139–149 (1994).
383. Pollard, T. D. Rate constants for the reactions of ATP- and ADP-actin with the ends of actin filaments. *J. Cell Biol.* **103**, 2747–2754 (1986).
384. Pollard, T. D. & Mooseker, M. S. Direct measurement of actin polymerization rate constants by electron microscopy of actin filaments nucleated by isolated microvillus cores. *J. Cell Biol.* **88**, 654–659 (1981).
385. Pollard, T. D. Regulation of actin filament assembly by Arp2/3 complex and formins. *Annu. Rev. Biophys. Biomol. Struct.* **36**, 451–477 (2007).
386. Pollard, T. D., Blanchoin, L. & Mullins, R. D. Molecular Mechanisms Controlling Actin Filament Dynamics in Nonmuscle Cells. *Annu. Rev. Biophys. Biomol. Struct.* **29**, 545–576 (2000).
387. Pollard, T. D. & Borisy, G. G. Cellular Motility Driven by Assembly and Disassembly of Actin Filaments. *Cell* **112**, 453–465 (2003).
388. Ponti, A., Machacek, M., Gupton, S. L., Waterman-Storer, C. M. & Danuser, G. Two distinct actin networks drive the protrusion of migrating cells. *Science* **305**, 1782–1786 (2004).
389. Popp, D., Kabsch, W., Holmes, K. C. & Gebhard, W. Atomic model of the actin filament. *Nature* **347**, 44–49 (1990).
390. Poujade, M. *et al.* Collective migration of an epithelial monolayer in response to a model wound. *Proc. Natl. Acad. Sci.* **104**, 15988–15993 (2007).
391. Prasad, M. & Montell, D. J. Cellular and molecular mechanisms of border cell migration analyzed using time-lapse live-cell imaging. *Dev. Cell* **12**, 997–1005 (2007).
392. Prehoda, K. E., Scott, J. A., Mullins, R. D. & Lim, W. A. Integration of multiple signals through cooperative regulation of the N-WASP-Arp2/3 complex. *Science* **290**, 801–806 (2000).

393. Preibisch, S., Saalfeld, S. & Tomancak, P. Globally optimal stitching of tiled 3D microscopic image acquisitions. *Bioinformatics* **25**, 1463–1465 (2009).
394. Pruyne, D. *et al.* Role of formins in actin assembly: Nucleation and barbed-end association. *Science* **297**, 612–615 (2002).
395. Pruyne, D. Revisiting the phylogeny of the animal formins: two new subtypes, relationships with multiple wing hairs proteins, and a lost human formin. *PLoS One* **11**, e0164067 (2016).
396. Radice, G. L. *et al.* Developmental defects in mouse embryos lacking N-cadherin. *Dev. Biol.* **181**, 64–78 (1997).
397. Ramel, D., Wang, X., Laflamme, C., Montell, D. J. & Emery, G. Rab11 regulates cell–cell communication during collective cell movements. *Nat. Cell Biol.* **15**, 317–324 (2013).
398. Ravasio, A. *et al.* Gap geometry dictates epithelial closure efficiency. *Nat. Commun.* **6**, 1–13 (2015).
399. Reffay, M. *et al.* Interplay of RhoA and mechanical forces in collective cell migration driven by leader cells. *Nat. Cell Biol.* **16**, 217–223 (2014).
400. Ren, X. *et al.* Focal adhesion kinase suppresses Rho activity to promote focal adhesion turnover. *J. Cell Sci.* **113**, 3673–3678 (2000).
401. Renault, L., Bugyi, B. & Carlier, M. F. Spire and Cordon-bleu: multifunctional regulators of actin dynamics. *Trends Cell Biol.* **18**, 494–504 (2008).
402. Rice, A. J. *et al.* Matrix stiffness induces epithelial–mesenchymal transition and promotes chemoresistance in pancreatic cancer cells. *Oncogenesis* **6**, e352–e352 (2017).
403. Ridley, A. J. Life at the leading edge. *Cell* **145**, 1012–1022 (2011).
404. Ridley, A. J., Paterson, H. F., Johnston, C. L., Diekmann, D. & Hall, A. The small GTP-binding protein rac regulates growth factor-induced membrane ruffling. *Cell* **70**, 401–410 (1992).
405. Ridley, A. J. Cell Migration: Integrating Signals from Front to Back. *Science* **302**, 1704–1709 (2003).
406. Ridley, A. J. & Hall, A. The small GTP-binding protein rho regulates the assembly of focal adhesions and actin stress fibers in response to growth factors. *Cell* **70**, 389–399 (1992).
407. Rikitake, Y. & Takai, Y. Directional cell migration regulation by small G proteins, nectin-like molecule-5, and afadin. *Int. Rev. Cell Mol. Biol.* **287**, 97–143 (2011).
408. Ringer, P. *et al.* Multiplexing molecular tension sensors reveals piconewton force gradient across talin-1. *Nat. Methods* **14**, 1090 (2017).
409. Rivelino, D. *et al.* Focal Contacts as Mechanosensors Externally Applied Local Mechanical Force Induces Growth of Focal Contacts by an RhoA-Dependent and Rock-Independent Mechanism. *J. Cell Biol.* **153**, 1175–1186 (2001).
410. Robinson, R. C. Crystal Structure of Arp2/3 Complex. *Science* **294**, 1679–1684 (2001).
411. Robinson, V., Smith, A., Flenniken, A. M. & Wilkinson, D. G. Roles of Eph receptors and ephrins in neural crest pathfinding. *Cell Tissue Res.* **290**, 265–274 (1997).

412. Rodriguez, M. A., LeClaire, L. L. & Roberts, T. M. Preparing to move: Assembly of the MSP amoeboid motility apparatus during spermiogenesis in *Ascaris*. *Cell Motil. Cytoskeleton* **60**, 191–199 (2005).
413. Rohatgi R. *et al.* N-WASP activates the Arp2/3 complex and links Cdc42 and phosphoinositide signals to actin assembly. *Mol. Biol. Cell* **10**, 122A (1999).
414. Rohatgi, R., Ho, H. Y. H. & Kirschner, M. W. Mechanism of N-WASP activation by CDC42 and phosphatidylinositol 4,5-bisphosphate. *J. Cell Biol.* **150**, 1299–1309 (2000).
415. Romero, S. *et al.* Filopodium retraction is controlled by adhesion to its tip. *J. Cell Sci.* **125**, 4999–5004 (2012).
416. Romero, S. *et al.* Formin is a processive motor that requires profilin to accelerate actin assembly and associated ATP hydrolysis. *Cell* **119**, 419–429 (2004).
417. Rørth, P. Collective Cell Migration. *Annu. Rev. Cell Dev. Biol.* **25**, 407–429 (2009).
418. Rørth, P. Initiating and guiding migration: lessons from border cells. *Trends Cell Biol.* **12**, 325–331 (2002).
419. Rothenbusch-Fender, S. *et al.* Myotube migration to cover and shape the testis of *Drosophila* depends on Heartless, Cadherin/Catenin, and myosin II. *Biol. Open* **6**, 1876–1888 (2017).
420. Rottner, K., Behrendt, B., Small, J. V. & Wehland, J. VASP dynamics during lamellipodia protrusion. *Nat. Cell Biol.* **1**, 321–322 (1999).
421. Rottner, K., Hänisch, J. & Campellone, K. G. WASH, WHAMM and JMY: Regulation of Arp2/3 complex and beyond. *Trends Cell Biol.* **20**, 650–661 (2010).
422. Du Roure, O. *et al.* Force mapping in epithelial cell migration. *Proc. Natl. Acad. Sci.* **102**, 2390–2395 (2005).
423. Rudolf, A. *et al.* Distinct genetic programs guide *Drosophila* circular and longitudinal visceral myoblast fusion. *BMC Cell Biol.* **15**, 27 (2014).
424. Ruiz-Gómez, M., Coutts, N., Price, A., Taylor, M. V & Bate, M. *Drosophila* dumbfounded: a myoblast attractant essential for fusion. *Cell* **102**, 189–198 (2000).
425. Sabatini, P. J. B., Zhang, M., Silverman-Gavrila, R., Bendeck, M. P. & Langille, B. L. Homotypic and endothelial cell adhesions via N-cadherin determine polarity and regulate migration of vascular smooth muscle cells. *Circ. Res.* **103**, 405–412 (2008).
426. Sagot, I., Klee, S. K. & Pellman, D. Yeast formins regulate cell polarity by controlling the assembly of actin cables. *Nat. Cell Biol.* **4**, 42–50 (2002).
427. Sagot, I., Rodal, A. A., Moseley, J., Goode, B. L. & Pellman, D. An actin nucleation mechanism mediated by Bni1 and profilin. *Nat. Cell Biol.* **4**, 626–631 (2002).
428. Sahai, E. Mechanisms of cancer cell invasion. *Curr. Opin. Genet. Dev.* **15**, 87–96 (2005).
429. Saiki, R. K. *et al.* Enzymatic amplification of beta-globin genomic sequences and restriction site analysis for diagnosis of sickle cell anemia. *Science* **230**, 1350 LP – 1354 (1985).
430. Santos, A. C. & Lehmann, R. Germ cell specification and migration in *Drosophila* and beyond. *Curr. Biol.* **14**, R578–R589 (2004).

431. Sarmiento, C. *et al.* WASP family members and formin proteins coordinate regulation of cell protrusions in carcinoma cells. *J. Cell Biol.* **180**, 1245–1260 (2008).
432. Sasahara, Y. *et al.* Mechanism of recruitment of WASP to the immunological synapse and of its activation following TCR ligation. *Mol. Cell* **10**, 1269–1281 (2002).
433. Sato, A. *et al.* Profilin is an effector for Daam1 in non-canonical Wnt signaling and is required for vertebrate gastrulation. *Development* **133**, 4219–4231 (2006).
434. Satoh, S. & Tominaga, T. mDia-interacting protein acts downstream of Rho-mDia and modifies Src activation and stress fiber formation. *J. Biol. Chem.* **276**, 39290–39294 (2001).
435. Scarpa, E. *et al.* Cadherin switch during EMT in neural crest cells leads to contact inhibition of locomotion via repolarization of forces. *Dev. Cell* **34**, 421–434 (2015).
436. Scarpa, E. & Mayor, R. Collective cell migration in development. *J. Cell Biol.* **212**, 143–155 (2016).
437. Schäfer, C. *et al.* One step ahead: role of filopodia in adhesion formation during cell migration of keratinocytes. *Exp. Cell Res.* **315**, 1212–1224 (2009).
438. Schafer, D. A. *et al.* Visualization and Molecular Analysis of Actin Assembly in Living Cells. *J. Cell Biol.* **143**, 1919–1930 (1998).
439. Schaks, M. *et al.* Distinct Interaction Sites of Rac GTPase with WAVE Regulatory Complex Have Non-redundant Functions in Vivo. *Curr. Biol.* **28**, 3674–3684.e6 (2018).
440. Schaller, M. D. *et al.* pp125FAK a structurally distinctive protein-tyrosine kinase associated with focal adhesions. *Proc. Natl. Acad. Sci. U. S. A.* **89**, 5192–5196 (1992).
441. Schaller, M. D. *et al.* Autophosphorylation of the focal adhesion kinase, pp125FAK, directs SH2-dependent binding of pp60src. *Mol. Cell. Biol.* **14**, 1680–1688 (1994).
442. Schäpe, J., Prauße, S., Radmacher, M. & Stick, R. Influence of lamin A on the mechanical properties of amphibian oocyte nuclei measured by atomic force microscopy. *Biophys. J.* **96**, 4319–4325 (2009).
443. Schneeberger, D. & Raabe, T. Mbt, a *Drosophila* PAK protein, combines with Cdc42 to regulate photoreceptor cell morphogenesis. *Development* **130**, 427 LP – 437 (2003).
444. Schneider, I. Cell lines derived from late embryonic stages of *Drosophila melanogaster*. *J. Embryol. Exp. Morphol.* **27**, 353–365 (1972).
445. Schnorrer, F. & Dickson, B. J. Muscle building mechanisms of myotube guidance and attachment site selection. *Dev. Cell* **7**, 9–20 (2004).
446. Schnorrer, F., Kalchauer, I. & Dickson, B. J. The transmembrane protein Kon-tiki couples to Dgrip to mediate myotube targeting in *Drosophila*. *Dev. Cell* **12**, 751–766 (2007).
447. Schönichen, A. *et al.* FHOD1 is a combined actin filament capping and bundling factor that selectively associates with actin arcs and stress fibers. *J. Cell Sci.* **126**, 1891–1901 (2013).
448. Schroer, T. A. *et al.* Actin-related protein nomenclature and classification. *J. Cell Biol.* **127**, 1777–1778 (1994).

449. Schuh, M. An actin-dependent mechanism for long-range vesicle transport. *Nat. Cell Biol.* **13**, 1431–1436 (2011).
450. Schulze, N. *et al.* FHOD1 regulates stress fiber organization by controlling the dynamics of transverse arcs and dorsal fibers. *J. Cell Sci.* **127**, 1379–1393 (2014).
451. Schutt, C. E., Myslik, J. C., Rozycki, M. D., Goonesekere, N. C. W. & Lindberg, U. The structure of crystalline profilin- β -actin. *Nature* **365**, 810–816 (1993).
452. Schwob, E. & Martin, R. P. New yeast actin-like gene required late in the cell cycle. *Nature* **355**, 179–182 (1992).
453. Segal, D., Dhanyasi, N., Schejter, E. D. & Shilo, B.-Z. Adhesion and fusion of muscle cells are promoted by filopodia. *Dev. Cell* **38**, 291–304 (2016).
454. Sept, D. & McCammon, J. A. Thermodynamics and kinetics of actin filament nucleation. *Biophys. J.* **81**, 667–674 (2001).
455. Serrels, B. *et al.* Focal adhesion kinase controls actin assembly via a FERM-mediated interaction with the Arp2/3 complex. *Nat. Cell Biol.* **9**, 1046–1056 (2007).
456. Shapiro, L. & Weis, W. I. Structure and biochemistry of cadherins and catenins. *Cold Spring Harb. Perspect. Biol.* **1**, 1–22 (2009).
457. Sharon, E., Rajat, R., Alexandre, V. P., Matthias, M. & Marc, W. K. Mechanism of regulation of WAVE1-induced actin nucleation by Rac1 and Nck. *Nature* **418**, 790–793 (2002).
458. Shaw, T. J. & Martin, P. Wound repair at a glance. *J. Cell Sci.* **122**, 3209 LP – 3213 (2009).
459. Shekhar, S. *et al.* Formin and capping protein together embrace the actin filament in a ménage à trois. *Nat. Commun.* **6**, 1–12 (2015).
460. Shellard, A. & Mayor, R. Supracellular migration—beyond collective cell migration. *J. Cell Sci.* **132**, (2019).
461. Shellard, A., Szabó, A., Trepát, X. & Mayor, R. Supracellular contraction at the rear of neural crest cell groups drives collective chemotaxis. *Science* **362**, 339–343 (2018).
462. Shibue, T., Brooks, M. W. & Weinberg, R. A. An integrin-linked machinery of cytoskeletal regulation that enables experimental tumor initiation and metastatic colonization. *Cancer Cell* **24**, 481–498 (2013).
463. Shimada, A. *et al.* The core FH2 domain of diaphanous-related formins is an elongated actin binding protein that inhibits polymerization. *Mol. Cell* **13**, 511–522 (2004).
464. Silver, D. L. & Montell, D. J. Paracrine signaling through the JAK/STAT pathway activates invasive behavior of ovarian epithelial cells in *Drosophila*. *Cell* **107**, 831–841 (2001).
465. Sixt, M. Cell migration: Fibroblasts find a new way to get ahead. *J. Cell Biol.* **197**, 347–349 (2012).
466. Small, J. V, Isenberg, G. & Celis, J. E. Polarity of actin at the leading edge of cultured cells. *Nature* **272**, 638–639 (1978).

467. Smith, A., Robinson, V., Patel, K. & Wilkinson, D. G. The EphA4 and EphB1 receptor tyrosine kinases and ephrin-B2 ligand regulate targeted migration of branchial neural crest cells. *Curr. Biol.* **7**, 561–570 (1997).
468. Soulie, P. *et al.* Membrane-type-1 matrix metalloproteinase confers tumorigenicity on nonmalignant epithelial cells. *Oncogene* **24**, 1689–1697 (2005).
469. Spillane, M. *et al.* The actin nucleating Arp2/3 complex contributes to the formation of axonal filopodia and branches through the regulation of actin patch precursors to filopodia. *Dev. Neurobiol.* **71**, 747–758 (2011).
470. Squarr, A. J. *et al.* Fat2 acts through the WAVE regulatory complex to drive collective cell migration during tissue rotation. *J. Cell Biol.* **212**, 591–603 (2016).
471. Sroka, J., Von Gunten, M., Dunn, G. A. & Keller, H. U. Phenotype modulation in non-adherent and adherent sublines of Walker carcinosarcoma cells: the role of cell-substratum contacts and microtubules in controlling cell shape, locomotion and cytoskeletal structure. *Int. J. Biochem. Cell Biol.* **34**, 882–899 (2002).
472. Stathopoulos, A., Van Drenth, M., Erives, A., Markstein, M. & Levine, M. Whole-genome analysis of dorsal-ventral patterning in the *Drosophila* embryo. *Cell* **111**, 687–701 (2002).
473. Stedden, C. G. *et al.* Planar-Polarized Semaphorin-5c and Plexin A Promote the Collective Migration of Epithelial Cells in *Drosophila*. *Curr. Biol.* **29**, 908-920.e6 (2019).
474. Steffen, A. *et al.* Rac function is crucial for cell migration but is not required for spreading and focal adhesion formation. *J. Cell Sci.* **126**, 4572 LP – 4588 (2013).
475. Stephenson, R. E. & Miller, A. L. Tools for live imaging of active Rho GTPases in *Xenopus*. *genesis* **55**, e22998 (2017).
476. Stern, C. The growth of testes in *Drosophila*. I. The relation between vas deferens and testis within various species. *J. Exp. Zool.* **87**, 113–158 (1941).
477. Stern, C. The growth of testes in *Drosophila*. II. The nature of interspecific differences. *J. Exp. Zool.* **87**, 159–180 (1941).
478. Stramer, B. *et al.* Clasp-mediated microtubule bundling regulates persistent motility and contact repulsion in *Drosophila* macrophages in vivo. *J. Cell Biol.* **189**, 681–689 (2010).
479. Stramer, B. & Mayor, R. Mechanisms and in vivo functions of contact inhibition of locomotion. *Nat. Rev. Mol. cell Biol.* **18**, 43–55 (2017).
480. Straub, F. B. & Feuer, G. Adenosinetriphosphate the functional group of actin. *Biochim. Biophys. Acta* **4**, 455–470 (1950).
481. Streichan, S. J., Valentin, G., Gilmour, D. & Hufnagel, L. Collective cell migration guided by dynamically maintained gradients. *Phys. Biol.* **8**, 45004 (2011).
482. Stuelten, C. H., Parent, C. A. & Montell, D. J. Cell motility in cancer invasion and metastasis: Insights from simple model organisms. *Nat. Rev. Cancer* **18**, 296–312 (2018).
483. Sturner, T. *et al.* Transient localization of the arp2/3 complex initiates neuronal dendrite branching in vivo. *Dev.* **146**, (2019).

484. Suetsugu, S. *et al.* Sustained activation of N-WASP through phosphorylation is essential for neurite extension. *Dev. Cell* **3**, 645–658 (2002).
485. Sun, J. & Stathopoulos, A. FGF controls epithelial-mesenchymal transitions during gastrulation by regulating cell division and apicobasal polarity. *Development* **145**, (2018).
486. Sun, Z., Guo, S. S. & Fässler, R. Integrin-mediated mechanotransduction. *J. Cell Biol.* **215**, 445–456 (2016).
487. Suraneni, P. *et al.* The Arp2/3 complex is required for lamellipodia extension and directional fibroblast cell migration. *J. Cell Biol.* **197**, 239–251 (2012).
488. Susic-Jung, L. *et al.* Multinucleated smooth muscles and mononucleated as well as multinucleated striated muscles develop during establishment of the male reproductive organs of *Drosophila melanogaster*. *Dev. Biol.* **370**, 86–97 (2012).
489. Sutherland, D., Samakovlis, C. & Krasnow, M. A. branchless encodes a *Drosophila* FGF homolog that controls tracheal cell migration and the pattern of branching. *Cell* **87**, 1091–1101 (1996).
490. Svitkina, T. M. & Borisy, G. G. Arp2/3 complex and actin depolymerizing factor/cofilin in dendritic organization and treadmilling of actin filament array in lamellipodia. *J. Cell Biol.* **145**, 1009–1026 (1999).
491. Svitkina, T. M., Verkhovsky, A. B., McQuade, K. M. & Borisy, G. G. Analysis of the actin–myosin II system in fish epidermal keratocytes: mechanism of cell body translocation. *J. Cell Biol.* **139**, 397–415 (1997).
492. Swift, J. *et al.* Nuclear lamin-A scales with tissue stiffness and enhances matrix-directed differentiation. *Science* **341**, (2013).
493. Symons, M. H. & Mitchison, T. J. Control of actin polymerization in live and permeabilized fibroblasts. *J. Cell Biol.* **114**, 503–513 (1991).
494. Symons, M. *et al.* Wiskott-Aldrich syndrome protein, a novel effector for the GTPase CDC42Hs, is implicated in actin polymerization. *Cell* **84**, 723–734 (1996).
495. Szabo, B. *et al.* Phase transition in the collective migration of tissue cells: experiment and model. *Phys. Rev. E* **74**, 61908 (2006).
496. Takeichi, M. Morphogenetic roles of classic cadherins. *Curr. Opin. Cell Biol.* **7**, 619–627 (1995).
497. Takeichi, M. Cadherins: a molecular family important in selective cell-cell adhesion. *Annu. Rev. Biochem.* **59**, 237–252 (1990).
498. Takeichi, M. The cadherins: cell-cell adhesion molecules controlling animal morphogenesis. *Development* **102**, 639–655 (1988).
499. Takeichi, M., Hatta, K., Nose, A. & Nagafuchi, A. Identification of a gene family of cadherin cell adhesion molecules. *Cell Differ. Dev.* **25**, 91–94 (1988).
500. Takenawa, T. & Miki, H. WASP and WAVE family proteins: Key molecules for rapid rearrangement of cortical actin filaments and cell movement. *J. Cell Sci.* **114**, 1801–1809 (2001).

501. Takeya, R., Taniguchi, K., Narumiya, S. & Sumimoto, H. The mammalian formin FHOD1 is activated through phosphorylation by ROCK and mediates thrombin-induced stress fibre formation in endothelial cells. *EMBO J.* **27**, 618–628 (2008).
502. Tambe, D. T. *et al.* Collective cell guidance by cooperative intercellular forces. *Nat. Mater.* **10**, 469–475 (2011).
503. Teddy, J. M. & Kulesa, P. M. In vivo evidence for short-and long-range cell communication in cranial neural crest cells. *Development* **131**, 6141–6151 (2004).
504. Tepass, U. Genetic analysis of cadherin function in animal morphogenesis. *Curr. Opin. Cell Biol.* **11**, 540–548 (1999).
505. Theriot, J. A. & Mitchison, T. J. Actin microfilament dynamics in locomoting cells. *Nature* **352**, 126–131 (1991).
506. Theveneau, E. *et al.* Collective chemotaxis requires contact-dependent cell polarity. *Dev. Cell* **19**, 39–53 (2010).
507. Theveneau, E. *et al.* Chase-and-run between adjacent cell populations promotes directional collective migration. *Nat. Cell Biol.* **15**, 763–772 (2013).
508. Theveneau, E. & Linker, C. Leaders in collective migration : are front cells really endowed with a particular set of skills ? [version 1 ; referees : 2 approved] Referee Status : **6**, 1–11 (2017).
509. Theveneau, E. & Mayor, R. Can mesenchymal cells undergo collective cell migration ? The case of the neural crest. **5**, 490–498 (2011).
510. Theveneau, E. & Mayor, R. Collective cell migration of epithelial and mesenchymal cells. 3481–3492 (2013) doi:10.1007/s00018-012-1251-7.
511. Thiam, H. R. *et al.* Perinuclear Arp2/3-driven actin polymerization enables nuclear deformation to facilitate cell migration through complex environments. *Nat. Commun.* **7**, (2016).
512. Thomas, L. A. & Yamada, K. M. Contact stimulation of cell migration. *J. Cell Sci.* **103**, 1211–1214 (1992).
513. Thorpe, H. M., Wilson, S. E. & Smith, M. C. Control of directionality in the site-specific recombination system of the *Streptomyces* phage phiC31. *Mol. Microbiol.* **38**, 232–241 (2000).
514. Tinevez, J. Y. *et al.* Role of cortical tension in bleb growth. *Proc. Natl. Acad. Sci. U. S. A.* **106**, 18581–18586 (2009).
515. Titus, M. A. & Goodson, H. V. An evolutionary perspective on cell migration: Digging for the roots of amoeboid motility. *J. Cell Biol.* **216**, 1509–1511 (2017).
516. Torres, E. & Rosen, M. K. Contingent phosphorylation/dephosphorylation provides a mechanism of molecular memory in WASP. *Mol. Cell* **11**, 1215–1227 (2003).
517. Totsukawa, G. *et al.* Distinct roles of MLCK and ROCK in the regulation of membrane protrusions and focal adhesion dynamics during cell migration of fibroblasts. *J. Cell Biol.* **164**, 427–439 (2004).
518. Trappmann, B. *et al.* Matrix degradability controls multicellularity of 3D cell migration. *Nat. Commun.* **8**, 1–8 (2017).

519. Trepap, X. & Fredberg, J. J. Plithotaxis and emergent dynamics in collective cellular migration. *Trends Cell Biol.* **21**, 638–646 (2011).
520. Turner, C. E. & Miller, J. T. Primary sequence of paxillin contains putative SH2 and SH3 domain binding motifs and multiple LIM domains: identification of a vinculin and pp125Fak-binding region. *J. Cell Sci.* **107**, 1583–1591 (1994).
521. Vacquier, V. D. The connection of blastomeres of sea urchin embryos by filopodia. *Exp. Cell Res.* **52**, 571–581 (1968).
522. Vallés, A. M., Beuvin, M. & Boyer, B. Activation of Rac1 by paxillin-Crk-DOCK180 signaling complex is antagonized by Rap1 in migrating NBT-II cells. *J. Biol. Chem.* **279**, 44490–44496 (2004).
523. Vavylonis, D., Kovar, D. R., O’Shaughnessy, B. & Pollard, T. D. Model of formin-associated actin filament elongation. *Mol. Cell* **21**, 455–466 (2006).
524. Veltman, D. M. & Insall, R. H. WASP family proteins: their evolution and its physiological implications. *Mol. Biol. Cell* **21**, 2880–2893 (2010).
525. Venken, K. J. T., He, Y., Hoskins, R. A. & Bellen, H. J. P[acman]: a BAC transgenic platform for targeted insertion of large DNA fragments in *D. melanogaster*. *Science* **314**, 1747–1751 (2006).
526. Vicente-Manzanares, M., Choi, C. K. & Horwitz, A. R. Erratum: Integrins in cell migration - The actin connection (Journal of Cell Science vol. 122 (199-206)). *J. Cell Sci.* **122**, 1473 (2009).
527. Vicente-Manzanares, M., Ma, X., Adelstein, R. S. & Horwitz, A. R. Non-muscle myosin II takes centre stage in cell adhesion and migration. *Nat. Rev. Mol. Cell Biol.* **10**, 778–790 (2009).
528. Vicsek, T., Czirók, A., Ben-Jacob, E., Cohen, I. & Shochet, O. Novel type of phase transition in a system of self-driven particles. *Phys. Rev. Lett.* **75**, 1226 (1995).
529. Villar-Cerviño, V. *et al.* Contact repulsion controls the dispersion and final distribution of Cajal-Retzius cells. *Neuron* **77**, 457–471 (2013).
530. Vishwakarma, M. *et al.* Mechanical interactions among followers determine the emergence of leaders in migrating epithelial cell collectives. *Nat. Commun.* **9**, 1–12 (2018).
531. Vitorino, P. & Meyer, T. Modular control of endothelial sheet migration. *Genes Dev.* **22**, 3268–3281 (2008).
532. Vizcarra, C. L., Bor, B. & Quinlan, M. E. The role of formin tails in actin nucleation, processive elongation, and filament bundling. *J. Biol. Chem.* **289**, 30602–30613 (2014).
533. Vortmeyer-Krause, M. *et al.* Lamin B2 follows lamin A/C-mediated nuclear mechanics and cancer cell invasion efficacy. *bioRxiv* (2020).
534. Wakayama, Y., Fukuhara, S., Ando, K., Matsuda, M. & Mochizuki, N. Cdc42 mediates Bmp-induced sprouting angiogenesis through Fmn13-driven assembly of endothelial filopodia in zebrafish. *Dev. Cell* **32**, 109–122 (2015).
535. Wang, X., He, L., Wu, Y. I., Hahn, K. M. & Montell, D. J. Light-mediated activation reveals a key role for Rac in collective guidance of cell movement in vivo. *Nat. Cell Biol.* **12**, 591–597 (2010).

536. Wang, X. & Ha, T. Defining single molecular forces required to activate integrin and notch signaling. *Science* **340**, 991–994 (2013).
537. Wang, X. *et al.* Analysis of Cell Migration Using Whole-Genome Expression Profiling of Migratory Cells in the Drosophila Ovary. *Dev. Cell* **10**, 483–495 (2006).
538. Watanabe, N. & Mitchison, T. J. Single-molecule speckle analysis of actin filament turnover in lamellipodia. *Science* **295**, 1083–1086 (2002).
539. Webb, D. J. *et al.* FAK–Src signalling through paxillin, ERK and MLCK regulates adhesion disassembly. *Nat. Cell Biol.* **6**, 154–161 (2004).
540. Weber, G. F., Bjerke, M. A. & DeSimone, D. W. A mechanoresponsive cadherin-keratin complex directs polarized protrusive behavior and collective cell migration. *Dev. Cell* **22**, 104–115 (2012).
541. Wegner, A. Head to tail polymerization of actin. *J. Mol. Biol.* **108**, 139–150 (1976).
542. Wegner, A. & Isenberg, G. 12-fold difference between the critical monomer concentrations of the two ends of actin filaments in physiological salt conditions. *Proc. Natl. Acad. Sci. U. S. A.* **80**, 4922–4925 (1983).
543. Wei, S. C. *et al.* Matrix stiffness drives epithelial–mesenchymal transition and tumour metastasis through a TWIST1–G3BP2 mechanotransduction pathway. *Nat. Cell Biol.* **17**, 678–688 (2015).
544. Weijer, C. J. Collective cell migration in development. *J. Cell Sci.* **122**, 3215–3223 (2009).
545. Weiser, D. C., Row, R. H. & Kimelman, D. Rho-regulated myosin phosphatase establishes the level of protrusive activity required for cell movements during zebrafish gastrulation. *Development* **136**, 2375–2384 (2009).
546. Weiss, E. E., Kroemker, M., Rüdiger, A. H., Jockusch, B. M. & Rüdiger, M. Vinculin is part of the cadherin-catenin junctional complex: complex formation between alpha-catenin and vinculin. *J. Cell Biol.* **141**, 755–764 (1998).
547. Welch, M. D., DePace, A. H., Verma, S., Iwamatsu, A. & Mitchison, T. J. The human Arp2/3 complex is composed of evolutionarily conserved subunits and is localized to cellular regions of dynamic actin filament assembly. *J. Cell Biol.* **138**, 375–384 (1997).
548. Wheelock, M. J., Shintani, Y., Maeda, M., Fukumoto, Y. & Johnson, K. R. Cadherin switching. *J. Cell Sci.* **121**, 727–735 (2008).
549. Williams, M. J., Ando, I. & Hultmark, D. Drosophila melanogaster Rac2 is necessary for a proper cellular immune response. *Genes to Cells* **10**, 813–823 (2005).
550. Wilson, A. L. *et al.* Cadherin-4 plays a role in the development of zebrafish cranial ganglia and lateral line system. *Dev. Dyn. an Off. Publ. Am. Assoc. Anat.* **236**, 893–902 (2007).
551. Winter, D., Podtelejnikov, A. V, Mann, M. & Li, R. The complex containing actin-related proteins Arp2 and Arp3 is required for the motility and integrity of yeast actin patches. *Curr. Biol.* **7**, 519–529 (1997).
552. Winter, D., Lechler, T. & Li, R. Activation of the yeast Arp2/3 complex by Bee1p, a WASP-family protein. *Curr. Biol.* **9**, 501–505 (1999).

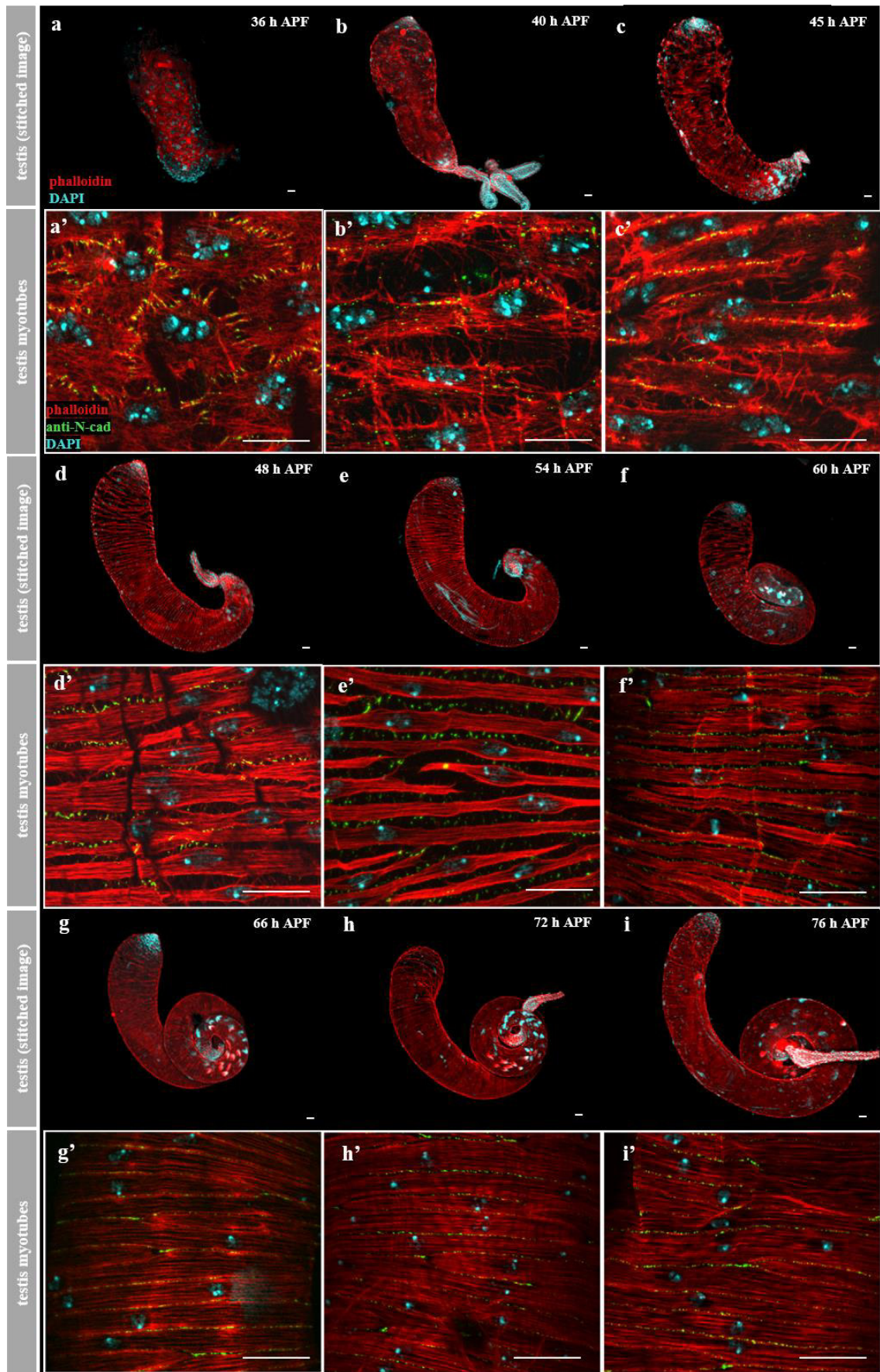
553. Wirtz, D., Konstantopoulos, K. & Searson, P. C. The physics of cancer: The role of physical interactions and mechanical forces in metastasis. *Nat. Rev. Cancer* **11**, 512–522 (2011).
554. Wolf, K. *et al.* Multi-step pericellular proteolysis controls the transition from individual to collective cancer cell invasion. *Nat. Cell Biol.* **9**, 893–904 (2007).
555. Wolf, K. *et al.* Compensation mechanism in tumor cell migration: mesenchymal–amoeboid transition after blocking of pericellular proteolysis. *J. Cell Biol.* **160**, 267–277 (2003).
556. Wong, S., Guo, W.-H. & Wang, Y.-L. Fibroblasts probe substrate rigidity with filopodia extensions before occupying an area. *Proc. Natl. Acad. Sci.* **111**, 17176–17181 (2014).
557. Woodham, E. F. *et al.* Coordination by Cdc42 of Actin, Contractility, and Adhesion for Melanoblast Movement in Mouse Skin. *Curr. Biol.* **27**, 624–637 (2017).
558. Woods, M. L. *et al.* Directional collective cell migration emerges as a property of cell interactions. *PLoS One* **9**, e104969 (2014).
559. Worthylake, R. A., Lemoine, S., Watson, J. M. & Burridge, K. RhoA is required for monocyte tail retraction during transendothelial migration. *J. Cell Biol.* **154**, 147–160 (2001).
560. Woychik, R. P., Stewart, T. A., Davis, L. G., D'Eustachio, P. & Leder, P. An inherited limb deformity created by insertional mutagenesis in a transgenic mouse. *Nature* **318**, 36–40 (1985).
561. Woychik, R. P., Maas, R. L., Zeller, R., Vogt, T. F. & Leder, P. 'Formins': proteins deduced from the alternative transcripts of the limb deformity gene. *Nature* **346**, 850–853 (1990).
562. Wozniak, M. A., Modzelewska, K., Kwong, L. & Keely, P. J. Focal adhesion regulation of cell behavior. *Biochim. Biophys. Acta - Mol. Cell Res.* **1692**, 103–119 (2004).
563. Wu, C. *et al.* Arp2/3 is critical for lamellipodia and response to extracellular matrix cues but is dispensable for chemotaxis. *Cell* **148**, 973–987 (2012).
564. Xia, F. *et al.* Raf activation is regulated by tyrosine 510 phosphorylation in *Drosophila*. *PLoS Biol* **6**, e128 (2008).
565. Xu, Y. *et al.* Crystal structures of a Formin Homology-2 domain reveal a tethered dimer architecture. *Cell* **116**, 711–723 (2004).
566. Yamada, K. M. & Sixt, M. Mechanisms of 3D cell migration. *Nat. Rev. Mol. Cell Biol.* **20**, 738–752 (2019).
567. Yang, C. *et al.* Novel roles of formin mDia2 in lamellipodia and filopodia formation in motile cells. *PLoS Biol.* **5**, 2624–2645 (2007).
568. Yang, S. *et al.* FGF signaling directs myotube guidance by regulating Rac activity. *Dev.* **147**, (2020).
569. Yokoyama, K. *et al.* BANK regulates BCR-induced calcium mobilization by promoting tyrosine phosphorylation of IP3 receptor. *EMBO J.* **21**, 83–92 (2002).
570. Yolland, L. *et al.* Persistent and polarized global actin flow is essential for directionality during cell migration. *Nat. Cell Biol.* **21**, 1370–1381 (2019).
571. Yonemura, S. Cadherin-actin interactions at adherens junctions. *Curr. Opin. Cell Biol.* **23**, 515–522 (2011).

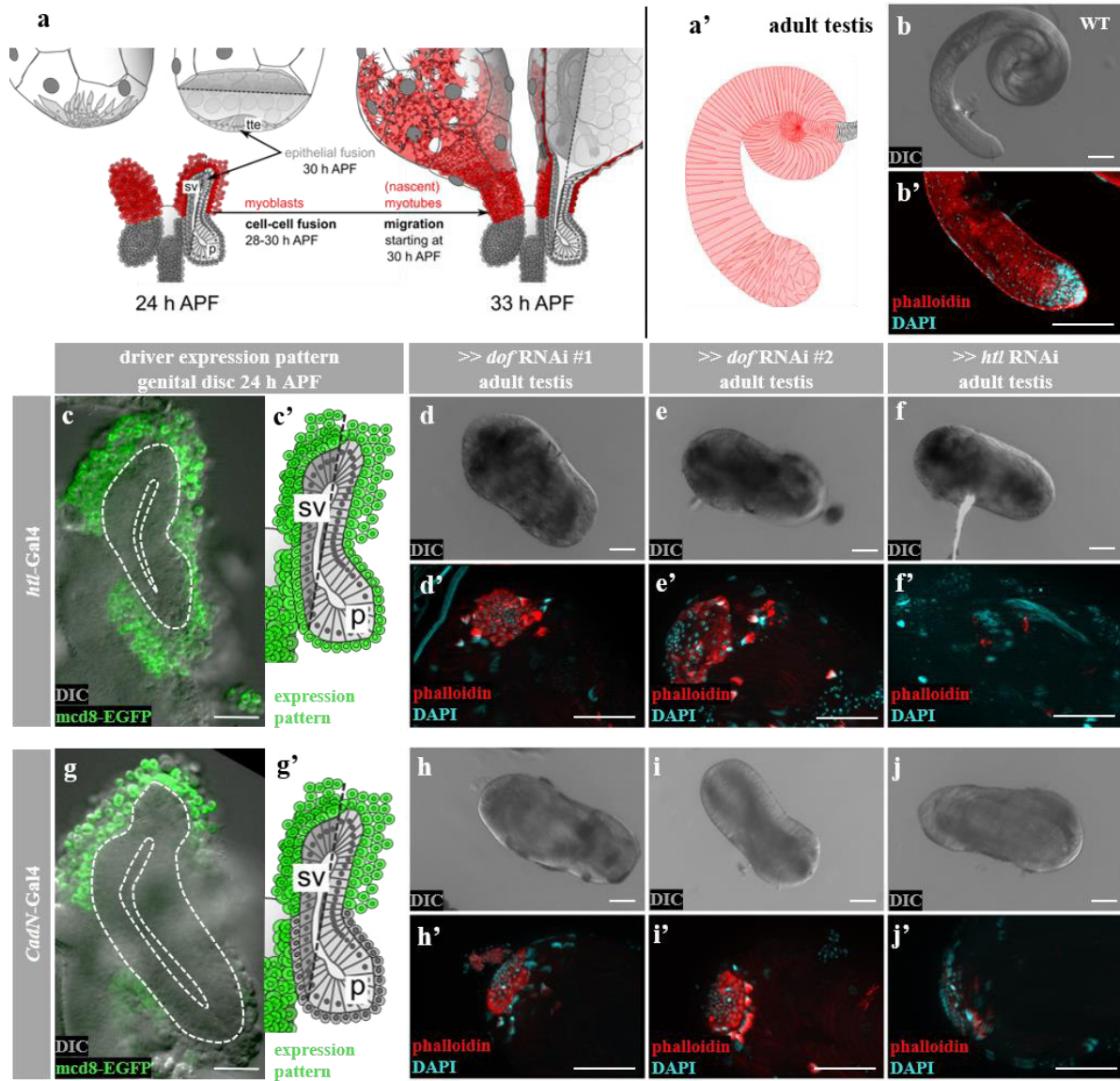
572. Yoshihara, M. *et al.* Filopodia play an important role in the trans-mesothelial migration of ovarian cancer cells. *Exp. Cell Res.* **392**, 112011 (2020).
573. Young, P. E., Richman, A. M., Ketchum, A. S. & Kiehart, D. P. Morphogenesis in *Drosophila* requires nonmuscle myosin heavy chain function. *Genes Dev.* **7**, 29–41 (1993).
574. Yu, H.-H. & Moens, C. B. Semaphorin signaling guides cranial neural crest cell migration in zebrafish. *Dev. Biol.* **280**, 373–385 (2005).
575. Zaidel-Bar, R., Ballestrem, C., Kam, Z. & Geiger, B. Early molecular events in the assembly of matrix adhesions at the leading edge of migrating cells. *J. Cell Sci.* **116**, 4605–4613 (2003).
576. Zaidel-Bar, R., Itzkovitz, S., Ma'ayan, A., Iyengar, R. & Geiger, B. Functional atlas of the integrin adhesome. *Nat. Cell Biol.* **9**, 858–867 (2007).
577. Zeller, R., Jackson-Grusby, L. & Leder, P. The limb deformity gene is required for apical ectodermal ridge differentiation and anteroposterior limb pattern formation. *Genes Dev.* **3**, 1481–1492 (1989).
578. Zhai, J. *et al.* Direct interaction of focal adhesion kinase with p190RhoGEF. *J. Biol. Chem.* **278**, 24865–24873 (2003).
579. Zhang, X. *et al.* Talin depletion reveals independence of initial cell spreading from integrin activation and traction. *Nat. Cell Biol.* **10**, 1062–1068 (2008).
580. Zhao, J., Manuchehrfar, F. & Liang, J. Cell–substrate mechanics guide collective cell migration through intercellular adhesion: a dynamic finite element cellular model. *Biomech. Model. Mechanobiol.* (2020) doi:10.1007/s10237-020-01308-5.
581. Zigmond, S. H. How WASP regulates actin polymerization. *J. Cell Biol.* **150**, 117–119 (2000).
582. Zigmond, S. H. Formin-induced nucleation of actin filaments. *Curr. Opin. Cell Biol.* **16**, 99–105 (2004).
583. Zigmond, S. H. *et al.* Formin leaky cap allows elongation in the presence of tight capping proteins. *Curr. Biol.* **13**, 1820–1823 (2003).

7. Appendix

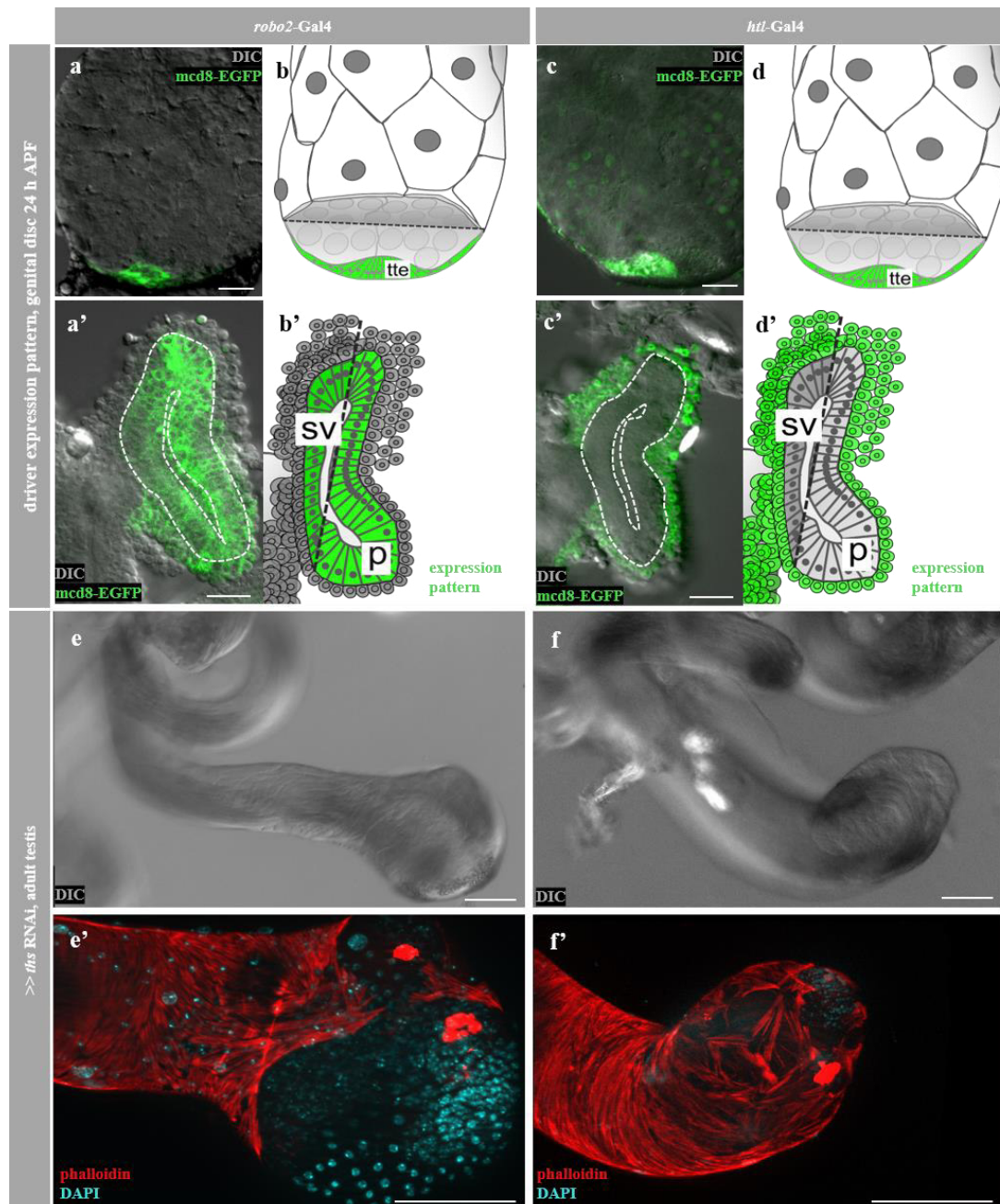
7.1 Supplementary figures

Supplementary figure S1. The development of the *Drosophila* testis myotube layer (following page). Apotome fluorescence micrographs of developing testes stained with phalloidin for F-actin and DAPI for nuclei. The overview images (a–i) are stitched pictures from 40x micrographs taken in culture dishes to sustain natural shape. Detail images (a'–i') are taken using a 40x objective of samples stained with an antibody against N-Cadherin and mounted on object slides. Testis myotubes undergo migration until 40 h APF (a–b'), elongation/condensing from 40–54 h APF (b–e'), and subsequently converge from 54–60 h APF (e–g'). From 66 h APF on, the myotube layer undergoes no more structural changes (g–i'). During all phases, cells are interconnected via N-Cadherin containing filopodia-like protrusion of varying length (a'–i'). Scale bars: 20 μ m

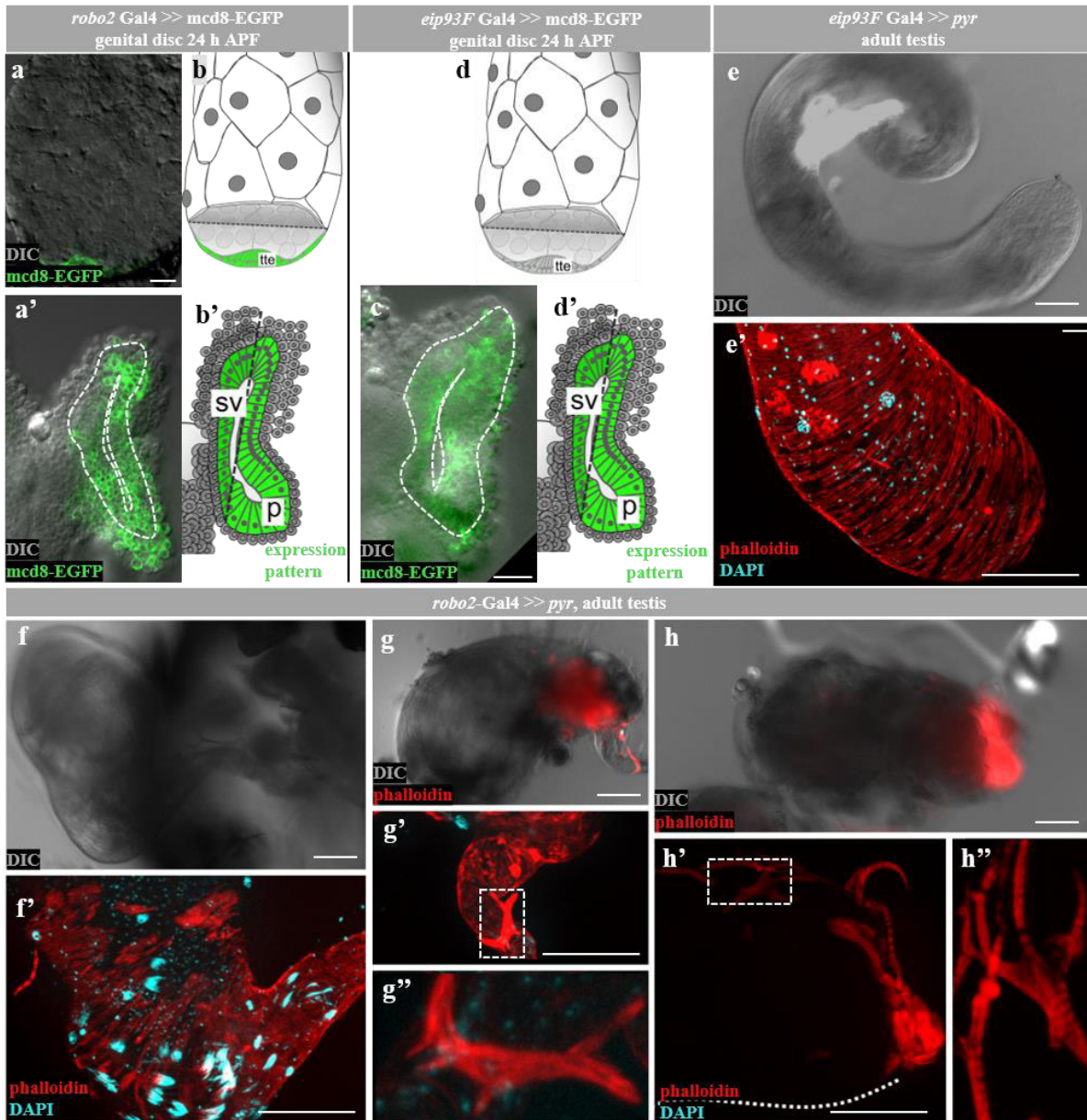




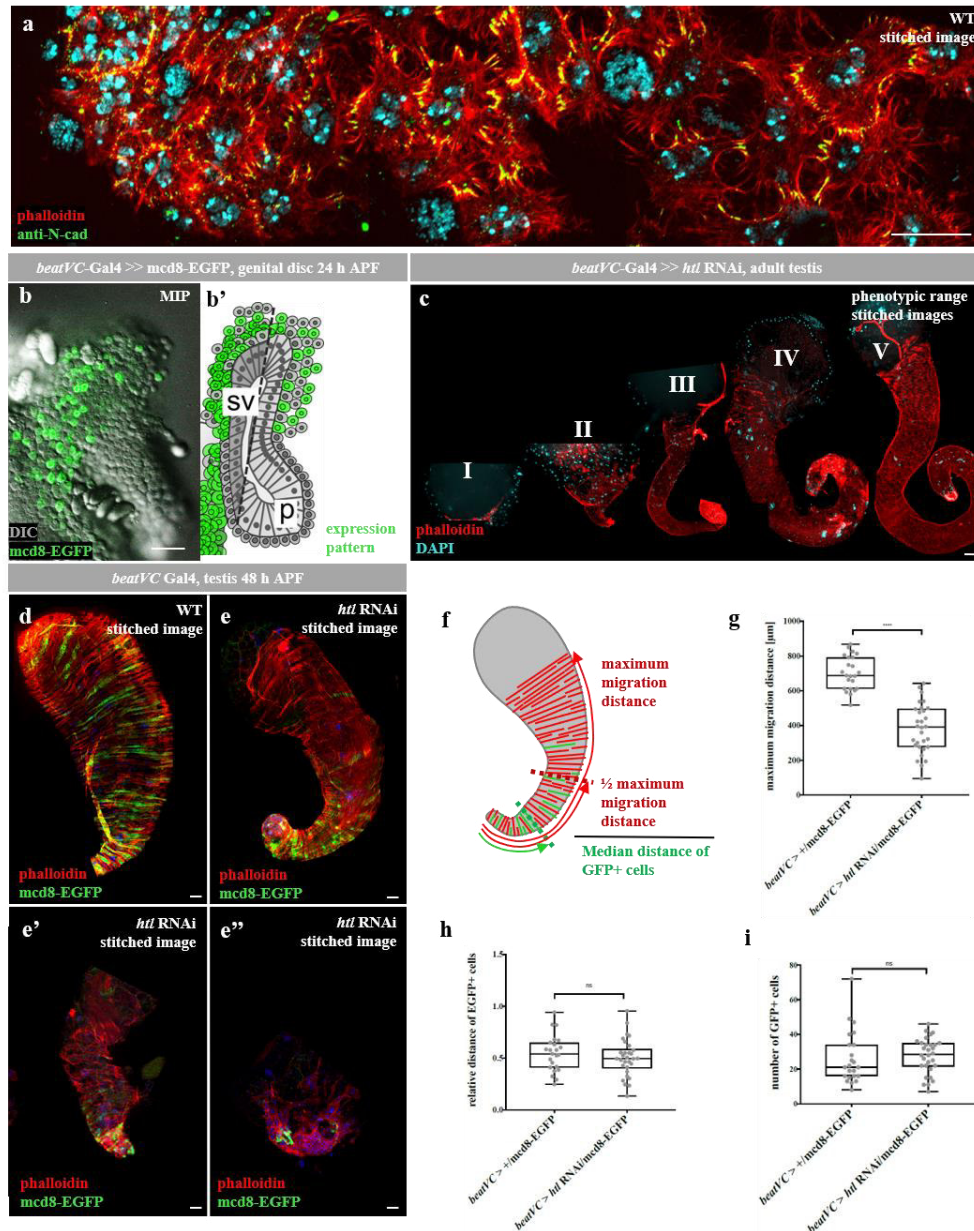
Supplementary figure S2. Reduction of *htl/dof* causes severe muscle coverage defects when using specific myoblast driver lines. Differential interference contrast micrographs (DIC, overview, b, d–f, h–j) and apotome fluorescence micrographs (details, b', d'–f', h'–j') of phalloidin/DAPI stained adult testis in different genetical backgrounds. Combinations of DIC and fluorescence in micrographs of 24 h APF genital discs (c, g). In normal development, genital disc–testis coalescence allows myotubes to migrate on the testis (scheme in a). In the adults stage, the testis is curled in a distinctive 2,5x coiled shape and evenly covered in elongated smooth-like muscles (scheme in a, micrograph in b, b'). UAS-mCD8-EGFP expression shows that *htl*-Gal4 promotes expression in myoblasts of the entire genital disc and *CadN*-Gal4 causes expression in presumptive testis myoblasts (c, g, schemes in c', g', cf. with a). Both driver lines cause near-complete coverage defects using two *dof*-RNAi lines (d, d', e, e'/h, h', i, i') with few non-elongated muscles at the testis base. *htl*-RNAi leads in both cases to a complete loss of muscle coverage (f, f'/j, j'). sv = (prospective) seminal vesicle, p = (prospective) paragonia, tte = testis terminal epithelium. Scale bars: 20 μ m (c, g), 100 μ m (b, b', d–f', h–j').



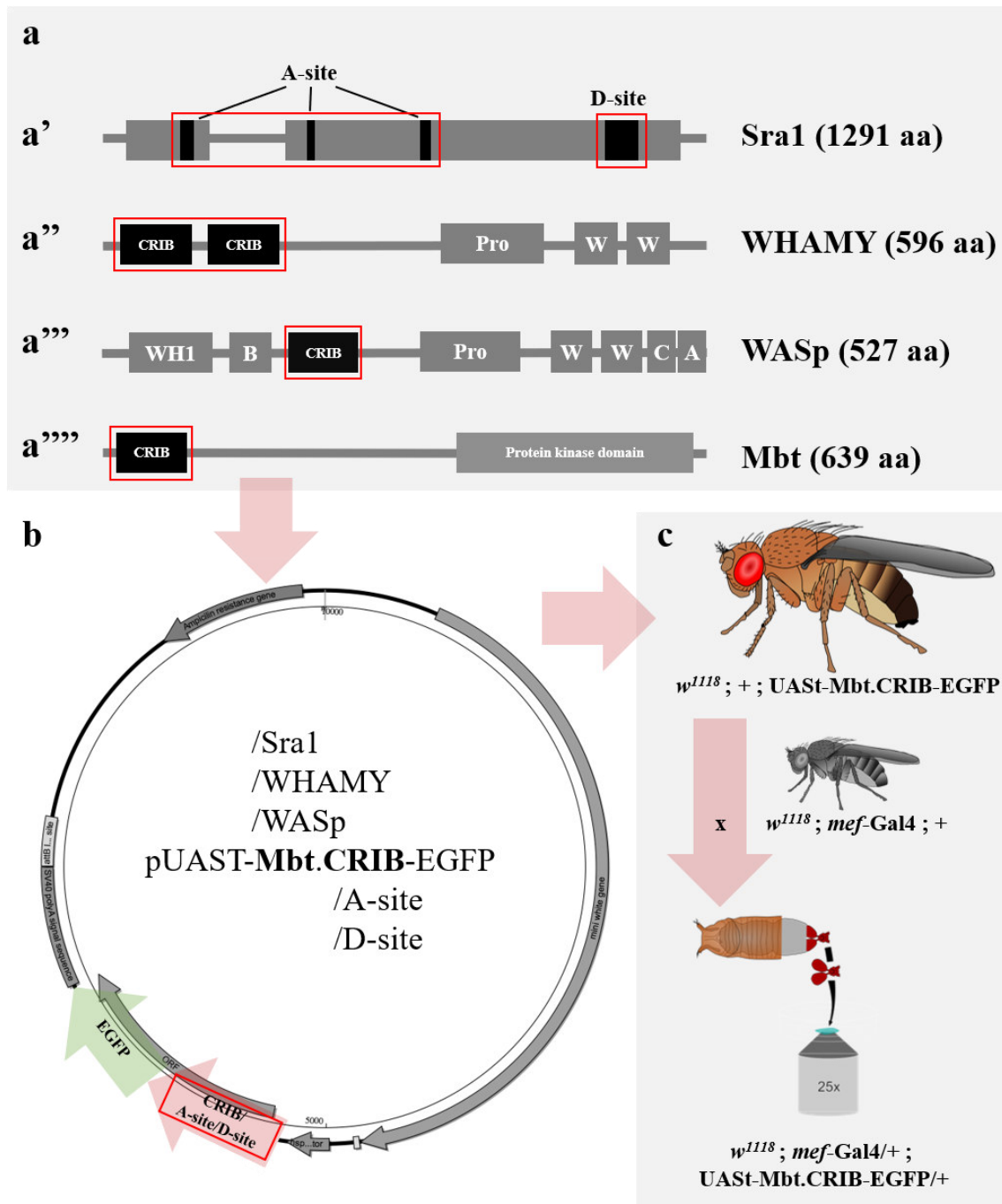
Supplementary figure S3. Reduction of *ths* in the testis terminal epithelium and the seminal vesicle epithelium causes testis muscle coverage defects. Differential interference contrast micrographs (DIC, overview, e, f) and apotome fluorescence micrographs (details, e', f') of phalloidin/DAPI stained adult testis in different genetical backgrounds. Combinations of DIC and fluorescence in micrographs of 24 h APF genital discs and testes (a, a', c, c'). UAS-mCD8-EGFP expression shows that *robo2*-Gal4 promotes expression in testis seminal vesicle epithelium (sv)/terminal epithelium (tte) and *htl*-Gal4 causes expression in myoblasts/tte (a, a', c, c', schemes in b, b', d, d'). Expression of *ths*-RNAi using *robo2*-Gal4 leads to medium muscle coverage defects with a prominently dilated tip. The same RNAi-line when driven with *htl*-Gal4 causes weak coverage defects. p = (prospective) paragonia. Scale bars: 20 μ m (a, a', c, c'), 100 μ m (e–f').



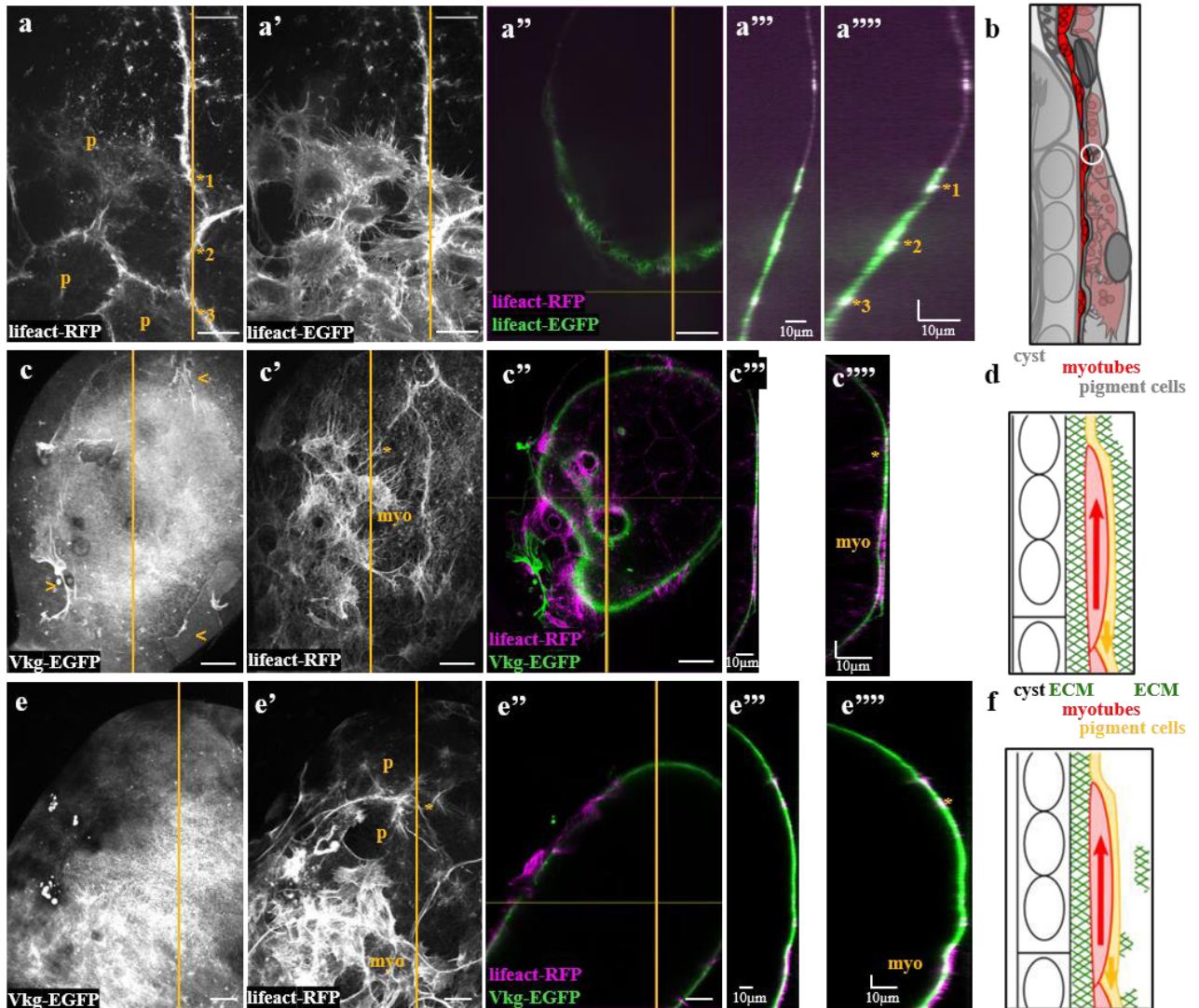
Supplementary figure S4. Ectopic expression of *pyr* in the testis terminal epithelium and the seminal vesicle epithelium causes testis muscle coverage defects. Differential interference contrast micrographs (DIC, overview, e–h) and apotome fluorescence micrographs (details, e’–h’’) of phalloidin/DAPI stained adult testis in different genetical backgrounds. Combinations of DIC and fluorescence in micrographs of 24 h APF genital discs and testes (a, a’, c). UAS-mCD8-EGFP expression shows that *robo2*-Gal4 promotes expression in testis seminal vesicle epithelium(sv)/terminal epithelium (tte) and *eip93F*-Gal4 causes expression in sv but not tte (a, a’, c, schemes in b, b’, d, d’). Ectopic expression of *pyr* with the latter causes weak coverage defects with loosely packed muscles at the dilated testis tip (e, e’). Expression of *pyr* with *robo2*-Gal4 causes strong coverage defects (f, f’). On some testes, ectopic muscles are present on the seminal vesicle (g, g’, dashed box from g’ magnified in g’’) or cover thickly the terminal testis epithelium, interrupting testis-genital disc connection (h, h’, dashed box from h’ magnified in h’’). p = (prospective) paragonia. Scale bars: 20 μ m (a, a’, c), 100 μ m (e–h’’).



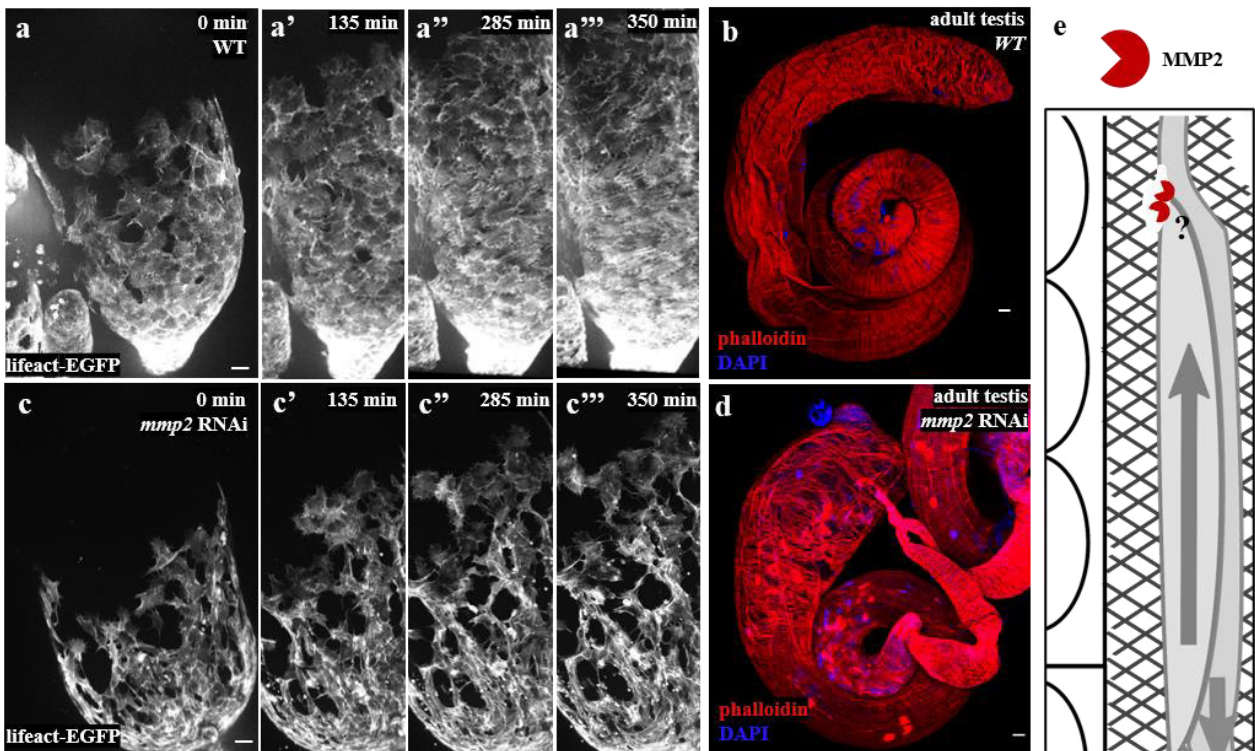
Supplementary figure S5. Mosaic-like expression of *htl*-RNAi suggests plithotactic direction of immobilized cells. Apotome fluorescence stitched micrographs of phalloidin/DAPI stained 36 h APF (a), 48 h APF (d–e’), and adult testis (c) in different genetical backgrounds. Combinations of DIC and fluorescence in micrographs of 24 h APF genital discs (b). Immunofluorescent staining of N-Cadherin in wild type shows that all myotubes are interconnected during migration (a). UAS-mCD8-EGFP expression shows that *beatVC*-Gal4 promotes expression in a mosaic pattern in myoblasts (b, scheme in b’). Expression of *htl* RNAi causes a broad range of coverage phenotypes (c). Shortly after migration in wild type, *beatVC*>>*mCD8*-GFP marked cells distribute along the testis axis (d). The same is true if single cells get immobilized via *beatVC*>>*mCD8*-GFP/*htl*-RNAi e-e’’. Quantification (summarized in f) reveals, that the maximum migration distance of unaffected cells is strongly disturbed (g). Relative distance and cell number of GFP positive affected cells remain unaffected. sv = (prospective) seminal vesicle, p = (prospective) paragonia, tte = testis terminal epithelium. Scale bars: 20 µm.



Supplementary figure S6. Cdc42 and Rac activity sensors are derived from GTPase binding domains of different targets. Sra1, WHAMY, WASp and Mbt contain sites with high affinity for activated Rac (Sra1, WHAMY, a', a'') and Cdc42 (WASp, Mbt, a''', a'''). These were inserted in pUASTattb-rfa-GFP and thereby fused with EGFP under the control of a UAS-promoter (b). Subsequently, transgenic fly stocks were created, using PhiC31 Integrase-mediated transgenesis. Transgenic UAS-GTPase-sensor animals must be crossed with Gal4 driver-line expressing flies, to generate offspring that can be analysed for sensor expression (c). Domain structures obtained from ^{60,87}, Pfam version 33.1.



Supplementary figure S7. Collagen localization studies suggests two basement membrane-like ECM-layers covering myotube/pigment cell layer from both sides. Confocal images of testes 33 h APF (a–a''''', c–c''''') and 36 h APF (e–e'''''). Therein, maximum intensity projections of stacks (a, a', c, c', e, e'), single slides (a'', c'', e''), orthogonal sections (a''', c''', e''', position: yellow line in pictures on the left), and orthogonal sections with a twofold stretched z-axis (a''''', c''''', e'''''). Expression of lifact-RFP causes a strong signal in cortical actin of pigment cells (p) using *htl*-Gal4 as driver (a). lifact-EGFP is evenly distributed in myotubes and pigment cells (a'). Cortical actin in the orthogonal sections in traversed three times (a, *1–*3) and lies on top of the myotube layer (a'''–a''''', scheme in b). Vkg-EGFP marks ECM (c). Lifact-RFP stainings allows to discriminate between pigment-cell covered area and myotube/pigment cell covered area (c'). An orthogonal section traverses myotube/pigment cell area (c', myo), and area uncovered by myotubes (c', asterisk) and reveals two thin basement membrane-like ECM layers (c''–c'''''). One layer lies under both cell-sheets, the other covers both cell sheets (c''''', white circle in scheme in d). During migration the upper layer starts to ruffle (c, arrowheads). Simmilar stainings in later stages revealed the absence of an upper ECM-layer (e–e''''', scheme in f). Scale bars: 20 μm if not stated otherwise.

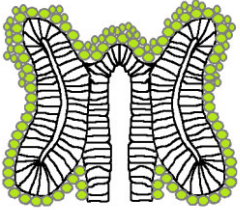
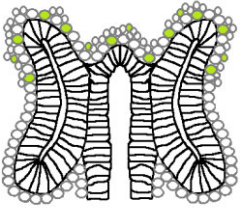
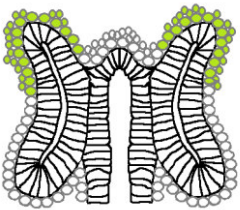
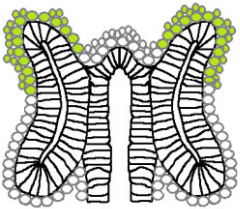
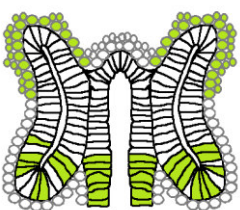
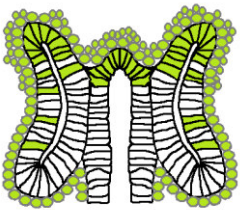


Supplementary figure S8. Pan-mesodermal reduction of *Mmp2* causes migration defects. Spinning disc fluorescence micrographs of 7 h-long *ex vivo* cultured testes expressing UAS-lifeact-EGFP under the control of *mef-Gal4* (a–a''', c–c'''). Confocal fluorescence micrographs of adult testes stained with phalloidin for F-actin and DAPI for nuclei (b,d). Live-cell imaging revealed that *Mmp2* RNAi still allows front cells to migrate non-directional but disrupts cells the stronger, the further they are in the rear of the sheet (c, *cf.* with wild type in a). This causes adult testis coverage defects in which the tip is dilated due to large gaps between muscles (d, *cf.* with wild type in b). This suggests a role of MMP2 in proteolytic ECM degradation by the collective that allows more confined myotubes in the rear to freely migrate through the substrate (scheme in e). Scale bars: 20 μm .

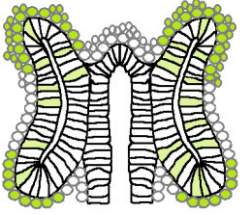
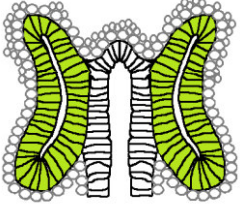
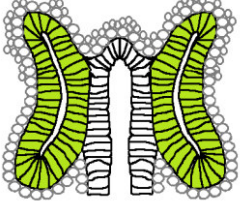
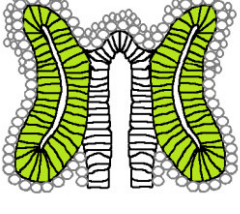
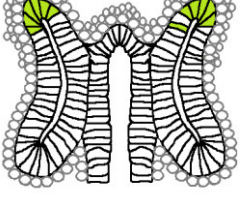
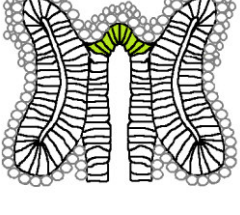
7.2 Vector Maps

Vector maps and gene cards can be found on the enclosed compact disc.

7.3 Gal4 driver lines screened for genital disc/testis nascent myoblast expression

driver	fly line ID	expression pattern	schematic (genital disc 24 h APF)
<i>hhl</i> Gal4	BL-40669	At 24 h APF in all genital disc myoblasts, pigment cells, and the terminal testis epithelium. At 33 h APF in testis nascent myotubes and pigment cells.	
<i>beatVC</i> Gal4	BL-40654	At 24 h APF scattered in some testis myoblasts in a mosaic fashion. At 33 h APF scattered in some testis nascent myotubes in a mosaic fashion.	
<i>lbe</i> Gal4	BL-47974	At 24 h APF in prospective testis myoblasts (weak). At 33 h APF in testis nascent myotubes (weak). (characterized by D. Buttgerit, unpublished)	
<i>CadN</i> Gal4	BL-45206	At 24 h APF in prospective testis myoblasts.	
<i>CadN</i> Gal4	BL-45579	At 24 h APF in prospective testis myoblasts and some epithelial cells of the prospective paragonia and ductus ejaculates.	
<i>eip93F</i> Gal4	BL-40475	At 24 h APF in all genital disc myoblasts, some epithelial cells of the prospective seminal vesicle and the terminal epithelium.	

Appendix

<i>pnt</i> Gal4	BL-46271	At 24 h APF in genital disc myoblasts at the poles of the prospective seminal vesicle and prospective paragonia, some epithelial cells of the prospective seminal vesicle and prospective paragonia.	
<i>eip93F</i> Gal4	BL-40473	At 24 h APF in all epithelial cells of the prospective seminal vesicle and prospective paragonia.	
<i>robo2</i> Gal4	BL-48074	At 24 h APF in all epithelial cells of the prospective seminal vesicle, the prospective paragonia, and the testis terminal epithelium.	
<i>doc1</i> Gal4	BL-50193	At 24 h APF in all epithelial cells of the prospective seminal vesicle and prospective paragonia.	
<i>dWnt2</i> Gal4	BL-45974	At 24 h APF in some epithelial cells of the prospective seminal vesicle at the tip. (characterized by D. Buttgerit, unpublished)	
<i>gt</i> Gal4	BL-47597	At 24 h APF in some epithelial cells of the prospective ductus ejaculatus at the tip.	
<i>kr</i> Gal4	80	At 33 h APF in a few pigment cells in a mosaic fashion ³⁵¹ .	

7.4 UAS effector screen for adult testis shaping defect

effector (A-Z)	fly line ID	construct ID	driver	phenotypic strength
<i>abi</i> RNAi	v36142	GD14302	<i>mef</i> Gal4	no phenotype
<i>abi</i> RNAi	v100714	KK108071	<i>mef</i> Gal4	no phenotype
<i>abi</i> RNAi	BL-36707	TRiP.HMS01597	<i>mef</i> Gal4	no phenotype
<i>abi</i> RNAi	NIG 9749R-2	-	<i>mef</i> Gal4	no phenotype
<i>α-Cat</i> RNAi	v40882	GD8808	<i>mef</i> Gal4	weak adhesion/migration defects
<i>α-Cat</i> RNAi	v20123	GD8808	<i>mef</i> Gal4	no phenotype
<i>α-Cat</i> RNAi	v19182	GD8808	<i>mef</i> Gal4	no phenotype
<i>α-Catr</i> RNAi	v7182	GD1632	<i>mef</i> Gal4	no phenotype
<i>α-Catr</i> RNAi	v104566	KK107455	<i>mef</i> Gal4	no phenotype
<i>actn</i> RNAi	v7762	GD1354	<i>htl</i> Gal4	weak migration defects
<i>actn</i> RNAi	v106162	KK103517	<i>htl</i> Gal4	no phenotype
<i>actn</i> RNAi	v7761	GD1354	<i>htl</i> Gal4	no phenotype
<i>actn</i> RNAi	v15171	GD4964	<i>htl</i> Gal4	no phenotype
<i>arm</i> RNAi	BL-35004	TRiP.HMS01414	<i>mef</i> Gal4	no phenotype
<i>arp3</i> RNAi	v108951	KK102278	<i>htl</i> Gal4	medium migration defects
<i>arp3</i> RNAi	v108951	KK102278	<i>mef</i> Gal4	medium migration defects
<i>arp3</i> RNAi	v35258	GD12273	<i>htl</i> Gal4	medium migration defects
<i>arp3</i> RNAi	v35258	GD12273	<i>mef</i> Gal4	medium migration defects
<i>arp3</i> RNAi	BL-32921	TRiP.HMS00711	<i>htl</i> Gal4	no phenotype
<i>arp3</i> RNAi	v35260	GD12273	<i>htl</i> Gal4	no phenotype
<i>arp2</i> RNAi	v29943	GD14716	<i>mef</i> Gal4	medium migration defects
<i>bicC</i> RNAi	BL-34997	TRiP.HMS01407	<i>htl</i> Gal4	no phenotype
<i>bicC</i> RNAi	BL- 35631	TRiP.GL00478	<i>htl</i> Gal4	no phenotype
<i>bru1</i> RNAi	BL-38983	TRiP.HMS01899	<i>htl</i> Gal4	no phenotype
<i>cad99C</i> RNAi	v3733	GD151	<i>htl</i> Gal4	no phenotype
<i>capu</i> RNAi	v34278	GD34278	<i>htl</i> Gal4	no phenotype
<i>chb</i> RNAi	BL-34669	TRiP.HMS01146	<i>htl</i> Gal4	strong migration defects
<i>chb</i> RNAi	BL-34669	TRiP.HMS01146	<i>kr</i> Gal4	occasional medium migration defects
<i>chb</i> RNAi	BL-34669	TRiP.HMS01146	<i>mef</i> Gal4	no phenotype
<i>chb</i> RNAi	BL-35442	TRiP.GL00367	<i>htl</i> Gal4	no phenotype
<i>cip4</i> ^{ΔSH3} #1	144		<i>mef</i> Gal4	no phenotype
<i>cip4</i> ^{ΔSH3} #2	144		<i>mef</i> Gal4	no phenotype
<i>cip4</i> ^{ΔSH3} #10	144		<i>mef</i> Gal4	no phenotype
<i>cip4</i> ^{ΔSH3} #10.3	144		<i>mef</i> Gal4	no phenotype
<i>cip4</i> RNAi	NIG 15015R-3	-	<i>mef</i> Gal4	club-like testis, complete muscle coverage
<i>cip4</i> RNAi	v18492		<i>mef</i> Gal4	club-like testis, complete muscle coverage

<i>Cdc42.F89</i>	BL-6286	-	<i>htl</i> Gal4	no phenotype
<i>Cdc42.L89</i>	BL-6389	-	<i>htl</i> Gal4	no phenotype
<i>Cdc42.N17</i>	BL-6288	-	<i>htl</i> Gal4	weak migration defects
<i>Cdc42.V12</i>	B-4854	-	<i>htl</i> Gal4	no phenotype
<i>cdc42 RNAi</i>	BL-28021	TRiP.JF02855	<i>htl</i> Gal4	strong-medium migration defects
<i>cdc42 RNAi</i>	BL-28021	TRiP.JF02855	<i>mef</i> Gal4	strong-medium migration defects
<i>cdc42 RNAi</i>	v100794	KK100794	<i>mef</i> Gal4	medium migration defects
<i>cortactin RNAi</i>	v105289	KK108594	<i>htl</i> Gal4	no phenotype
<i>cortactin RNAi</i>	NIG 3637R-3	-	<i>htl</i> Gal4	no phenotype
<i>cortactin RNAi</i>	BL-32871	TRiP.HMS00658	<i>htl</i> Gal4	no phenotype
<i>cyri RNAi</i>	v107318	KK108589	<i>mef</i> Gal4	no phenotype
<i>cyri RNAi</i>	v107318	KK108589	<i>lbe</i> Gal4	no phenotype
<i>cyri RNAi</i>	v44825	GD8705	<i>mef</i> Gal4	no phenotype
<i>daam RNAi</i>	BL-39058	TRiP.HMS01978	<i>htl</i> Gal4	no phenotype
<i>daam RNAi</i>	v24885	GD8382	<i>htl</i> Gal4	no phenotype
<i>Dia.CA</i>	BL-27616	-	<i>htl</i> Gal4	lethal
<i>Dia.CA</i>	BL-27616	-	<i>mef</i> Gal4	lethal
<i>Dia.CA</i>	BL-27616	-	<i>lbe</i> Gal4	no phenotype
<i>Dia.NC</i>	Gift from J. Großhans		<i>mef</i> Gal4	no phenotype
<i>dia RNAi</i>	v20518	GD9442	<i>htl</i> Gal4	strong migration defects
<i>dia RNAi</i>	v20518	GD9442	<i>kr</i> Gal4	occasional medium-strong migration defects
<i>dia RNAi</i>	v20518	GD9442	<i>mef</i> Gal4	no phenotype
<i>dock RNAi</i>	BL-43176	TRiP.GL01519	<i>htl</i> Gal4	no phenotype
<i>dock RNAi</i>	BL-27728	TRiP.JF02810	<i>htl</i> Gal4	no phenotype
<i>dof RNAi</i>	v105603	KK100350	<i>htl</i> Gal4	strong migration defects
<i>dof RNAi</i>	v105603	KK100350	<i>lbe</i> Gal4	no phenotype
<i>dof RNAi</i>	v105603	KK100350	<i>Ncad</i> Gal4	strong migration defects
<i>dof RNAi</i>	v21317	GD10225	<i>htl</i> Gal4	strong migration defects
<i>dof RNAi</i>	v21317	GD10225	<i>lbe</i> Gal4	medium migration defects
<i>dof RNAi</i>	v21317	GD10225	<i>Ncad</i> Gal4	strong migration defects
<i>drl RNAi</i>	BL-29602	TRiP.JF03281	<i>htl</i> Gal4	no phenotype
<i>dscam1 RNAi</i>	BL-29628	TRiP.JF03307	<i>htl</i> Gal4	no phenotype
<i>dscam1 RNAi</i>	BL-38945	TRiP.HMS01859	<i>htl</i> Gal4	no phenotype
<i>dscam2 RNAi</i>	BL-51839	TRiP.HMC03411	<i>htl</i> Gal4	no phenotype
<i>dWnt2.k</i>	BL-6961	-	<i>eip 93F</i> Gal4	no phenotype
<i>dWnt2.k</i>	BL-6961	-	<i>robo2</i> Gal4	no phenotype
<i>dome RNAi</i>	BL-53890	TRiP.HMJ21208	<i>htl</i> Gal4	no phenotype
<i>egfr RNAi</i>	BL-36770	TRiP.JF02283	<i>htl</i> Gal4	no phenotype

Appendix

<i>egfr</i> RNAi	BL-25781	TRiP.JF01368	<i>htl</i> Gal4	no phenotype
<i>ena</i> RNAi	v43056	GD8910	<i>htl</i> Gal4	no phenotype
<i>ena</i> RNAi	v106484	KK107752	<i>htl</i> Gal4	no phenotype
<i>FAK56-eGFP</i>	¹⁷⁹		<i>mef</i> Gal4	lethal
<i>fak56</i> RNAi	v17957	GD6840	<i>mef</i> Gal4	no phenotype
<i>fhos</i> RNAi	v45837	GD2374	<i>htl</i> Gal4	no phenotype
<i>fhos</i> RNAi	v45837	GD2374	<i>htl</i> Gal4	no phenotype
<i>fhos</i> RNAi	v34034	GD10435	<i>htl</i> Gal4	no phenotype
<i>fhos</i> RNAi	v34035	GD10435	<i>htl</i> Gal4	no phenotype
<i>fhos</i> RNAi	v108347	KK108388	<i>htl</i> Gal4	no phenotype
<i>fhos</i> RNAi	BL-51391	TRiP.HMJ21037	<i>htl</i> Gal4	no phenotype
<i>fhos</i> RNAi	BL-31400	TRiP.JF01606	<i>htl</i> Gal4	no phenotype
<i>f</i> RNAi	v24630	GD7893	<i>htl</i> Gal4	no phenotype
<i>f</i> RNAi	v103813	KK102771	<i>htl</i> Gal4	no phenotype
<i>form3</i> RNAi	v107473	KK110697	<i>htl</i> Gal4	no phenotype
<i>form3</i> RNAi	v45594	GD12856	<i>htl</i> Gal4	no phenotype
<i>form3</i> RNAi	v42302	GD14823	<i>htl</i> Gal4	no phenotype
<i>fra</i> RNAi	BL-31664	TRiP.JF01457	<i>htl</i> Gal4	no phenotype
<i>frl</i> RNAi	v34412	GD10799	<i>htl</i> Gal4	no phenotype
<i>frl</i> RNAi	v34413	GD10799	<i>htl</i> Gal4	no phenotype
<i>frl</i> RNAi	BL-32447	TRiP.HMS00445	<i>htl</i> Gal4	no phenotype
<i>gef64c</i> RNAi	v47121	GD16275	<i>htl</i> Gal4	strong-medium migration defects
<i>gef64c</i> RNAi	v47121	GD16275	<i>kr</i> Gal4	occasional medium migration defects
<i>gef64c</i> RNAi	v47121	GD16275	<i>mef</i> Gal4	no phenotype
<i>gef64c</i> RNAi	v105252	KK103071	<i>htl</i> Gal4	no phenotype
<i>gef64c</i> RNAi	v34470	GD10829	<i>htl</i> Gal4	no phenotype
<i>Htl.λ</i>	BL-5367	-	<i>lbe</i> Gal4	no phenotype
<i>Htl.λ</i>	BL-5367	-	<i>htl</i> Gal4	thicker testis with ectopic striated muscles
<i>Htl.λ</i>	BL-5367	-	<i>tgx</i> Gal4	no phenotype
<i>htl</i> RNAi	v6692	GD84	<i>htl</i> Gal4	missing testis-genital disc connection
<i>htl</i> RNAi	v6692	GD84	<i>lbe</i> Gal4	weak-medium migration defects
<i>htl</i> RNAi	v6692	GD84	<i>Ncad</i> Gal4	missing testis-genital disc connection
<i>htl</i> RNAi	v6692	GD84	<i>beatVC Gal4</i>	strong-weak migration defects
<i>htl</i> RNAi	BL-35024	TRiP.HMS01437	<i>htl</i> Gal4	medium migration defects
<i>htl</i> RNAi	BL-35024	TRiP.HMS01437	<i>lbe</i> Gal4	no phenotype
<i>htl</i> RNAi	BL-35024	TRiP.HMS01437	<i>Ncad</i> Gal4	medium migration defects
<i>if</i> RNAi	BL-27544	TRiP.JF02695	<i>htl</i> Gal4	lethal
<i>itgaPS4</i> RNAi	BL-44534	TRiP.HMC02928	<i>htl</i> Gal4	no phenotype
<i>itgbn</i> RNAi	BL-28601	TRiP.HM05089	<i>htl</i> Gal4	no phenotype

Appendix

<i>mbc</i> RNAi	v16044	GD6965	<i>htl</i> Gal4	no phenotype
<i>mew</i> RNAi	BL-44553	TRiP.HMS02849	<i>htl</i> Gal4	no phenotype
<i>mew</i> RNAi	BL-27543	TRiP.JF02694	<i>htl</i> Gal4	no phenotype
<i>mmp1</i> RNAi	BL-31489	TRiP.JF01336	<i>htl</i> Gal4	no phenotype
<i>mmp2</i> RNAi	BL-61309	TRiP.HMJ23143	<i>htl</i> Gal4	club-like testis, complete muscle coverage (low density at the tip)
<i>mmp2</i> RNAi	BL-61309	TRiP.HMJ23143	<i>mef</i> Gal4	club-like testis, complete muscle coverage (low density at the tip)
<i>msn</i> RNAi	BL-28791	TRiP.JF03219	<i>htl</i> Gal4	no phenotype
<i>msn</i> RNAi	v101517	KK 108948	<i>htl</i> Gal4	strong migration defects
<i>mtl</i> RNAi	v108427	KK110274	<i>mef</i> Gal4	no phenotype
<i>myo10a</i> RNAi	v101729	KK108171	<i>mef</i> Gal4	no phenotype
<i>myo10a</i> RNAi	v33486	GD9734	<i>mef</i> Gal4	no phenotype
<i>mys</i> RNAi	v103704	KK100518	<i>htl</i> Gal4	lethal
<i>mys</i> RNAi	v103704	KK100518	<i>mef</i> Gal4	lethal
<i>mys</i> RNAi	v103704	KK100518	<i>lbe</i> Gal4	medium-no migration defects
<i>mys</i> RNAi	v103704	KK100518	<i>Ncad</i> Gal4	missing testis-genital disc connection
<i>mys</i> RNAi	BL-33642	TRiP.HMS00043	<i>htl</i> Gal4	lethal
<i>mys</i> RNAi	BL-27735	TRiP.JF02819	<i>htl</i> Gal4	no phenotype
<i>Ncad.fl</i>	Gift from S. Önel		<i>mef</i> Gal4	lethal
<i>Ncad-GFP</i>	Gift from C.-H. Lee		<i>mef</i> Gal4	lethal
<i>Ncad-GFP</i>	Gift from C.-H. Lee		<i>lbe</i> Gal4	missing testis-genital disc connection
<i>Ncad-GFP</i>	Gift from C.-H. Lee		<i>Ncad</i> Gal4	medium migration defects
<i>Ncad</i> RNAi	v101642	KK105304	<i>mef</i> Gal4	defective adhesion
<i>Ncad2</i> RNAi	v101659	KK105358	<i>mef</i> Gal4	no phenotype
<i>Ncad2</i> RNAi	v36166	GD14316	<i>mef</i> Gal4	no phenotype
<i>p120ctn</i> RNAi	v103063	KK113572	<i>mef</i> Gal4	no phenotype
<i>pak1</i> RNAi	v12553	GD4035	<i>htl</i> Gal4	no phenotype
<i>pak3</i> RNAi	NIC 14895R-1	-	<i>htl</i> Gal4	strong-medium migration defects
<i>pak3</i> RNAi	NIC 14895R-1	-	<i>kr</i> Gal4	occasional medium migration defects
<i>pak3</i> RNAi	NIC 14895R-1	-	<i>mef</i> Gal4	no phenotype
<i>pak3</i> RNAi	NIC 14895R-2	-	<i>htl</i> Gal4	no phenotype
<i>pak3</i> RNAi	v39844	GD8481	<i>htl</i> Gal4	no phenotype
<i>pak3</i> RNAi	v39843	GD8481	<i>htl</i> Gal4	no phenotype
<i>Pyr.DN</i>	BL-58430	-	<i>htl</i> Gal4	no phenotype
<i>Pyr-HA</i>	Gift from A. Müller		<i>eip 93F</i> Gal4	Adhesion defects at the testis tip
<i>Pyr-HA</i>	Gift from A. Müller		<i>robo2</i> Gal4	strong migration defects, ectopic striated muscle cells at the seminal vesicles/terminal testis epithelium
<i>Pyr-HA</i>	Gift from A. Müller		<i>htl</i> Gal4	lethal

<i>Pyr-HA</i>	Gift from A. Müller		<i>gt</i> Gal4	no phenotype
<i>pyr</i> RNAi	BL-37520	TRiP.HMS01662	<i>htl</i> Gal4	no phenotype
<i>pyr</i> RNAi	v36523	GD14793	<i>eip 93F</i> Gal4	no phenotype
<i>pyr</i> RNAi	v36523	GD14793	<i>robo2</i> Gal4	no testis defects, strong leg phenotypes
<i>pyr</i> RNAi	v36523	GD14793	<i>doc1</i> Gal4	no phenotype
<i>pyr</i> RNAi	v36523	GD14793	<i>gt</i> Gal4	no phenotype
<i>pyr</i> RNAi	v36523	GD14793	<i>dWnt2</i> Gal4	no phenotype
<i>pyr</i> RNAi	v36523	GD14793	<i>lsp</i> Gal4	no phenotype
<i>pyr</i> RNAi	v36523	GD14793	<i>htl</i> Gal4	no phenotype
<i>Rac1.N17</i>	BL-6292	-	<i>mef</i> Gal4	lethal
<i>Rac1.N17</i>	BL-6292	-	<i>lbe</i> Gal4	no phenotype
<i>Rac1</i> RNAi	BL-28985	TRiP.JF02813	<i>mef</i> Gal4	no phenotype
<i>Rac1</i> RNAi	NIG-2248R-1	-	<i>mef</i> Gal4	no phenotype
<i>Rac1</i> RNAi	NIG-2248R-2	-	<i>mef</i> Gal4	no phenotype
<i>Rac1</i> RNAi	BL-34910	TriP.HMS01258	<i>mef</i> Gal4	no phenotype
<i>Rac1</i> RNAi	v49246	GD17411	<i>mef</i> Gal4	no phenotype
<i>Rac2</i> RNAi	NIG-8356R-3	-	<i>mef</i> Gal4	strong migration defects
<i>Rac2</i> RNAi	NIG-8356R-1	-	<i>mef</i> Gal4	strong migration defects
<i>Rac2</i> RNAi	v28926	GD13964	<i>mef</i> Gal4	no phenotype
<i>Rac2</i> RNAi	v50349	GD17536	<i>mef</i> Gal4	no phenotype
<i>Rac2</i> RNAi	v50350	GD17536	<i>mef</i> Gal4	no phenotype
<i>rassf8</i> RNAi	v105823	KK100500	<i>mef</i> Gal4	no phenotype
<i>rho1</i> RNAi	BL-27727	TriP.JF02809	<i>mef</i> Gal4	lethal
<i>rho1</i> RNAi	BL-27727	TriP.JF02809	<i>lbe</i> Gal4	lethal
<i>rho1</i> RNAi	BL-32383	TriP.HMS00375	<i>mef</i> Gal4	lethal
<i>rho1</i> RNAi	BL-32383	TriP.HMS00375	<i>lbe</i> Gal4	medium migration defects
<i>rho1</i> RNAi	BL-32383	TriP.HMS00375	<i>Ncad</i> Gal4	strong migration defects
<i>rho1</i> RNAi	v12734	GD4726	<i>mef</i> Gal4	lethal
<i>rho1</i> RNAi	v109420	KK108182	<i>mef</i> Gal4	no phenotype
<i>rhoL</i> RNAi	v102461	KK111715	<i>mef</i> Gal4	no phenotype
<i>rib</i> RNAi	BL-50682	TriP.HMC03083	<i>htl</i> Gal4	no phenotype
<i>robo1</i> RNAi	BL- 9285	-	<i>htl</i> Gal4	no phenotype
<i>robo2</i> RNAi	BL-34589	TriP.HMS01063	<i>htl</i> Gal4	no phenotype
<i>robo2</i> RNAi	BL-27317	TriP.JF02626	<i>htl</i> Gal4	no phenotype
<i>robo3</i> RNAi	BL-44539	TriP.HMC02934	<i>htl</i> Gal4	missing testis-genital disc connection
<i>robo3</i> RNAi	BL-44539	TriP.HMC02934	<i>mef</i> Gal4	no phenotype
<i>robo3</i> RNAi	BL-44539	TriP.HMC02934	<i>kr</i> Gal4	no phenotype
<i>robo3</i> RNAi	BL-29398	TriP.JF03331	<i>htl</i> Gal4	no phenotype
<i>rtGef</i> RNAi	v100583	KK108300	<i>mef</i> Gal4	no phenotype
<i>rtGef</i> RNAi	v17966	GD6845	<i>mef</i> Gal4	no phenotype

<i>scab</i> RNAi	BL-27545	TriP.JF02696	<i>htl</i> Gal4	no phenotype
<i>scab</i> RNAi	BL-38959	TriP.HMS01873	<i>htl</i> Gal4	no phenotype
<i>scar</i> RNAi	NIG 4636R-1	-	<i>htl</i> Gal4	medium migration defects
<i>scar</i> RNAi	NIG 4636R-1	-	<i>mef</i> Gal4	medium migration defects
<i>scar</i> RNAi	BL-51803	TriP.HMC03361	<i>mef</i> Gal4	medium migration defects
<i>scar</i> RNAi	BL-36121	TriP.HMS01536	<i>mef</i> Gal4	no phenotype
<i>scar</i> RNAi	BL-31126	TriP.JF01599	<i>mef</i> Gal4	no phenotype
<i>shg</i> RNAi	v8024	GD2659	<i>htl</i> Gal4	no phenotype
<i>shg</i> RNAi	v27082	GD14421	<i>htl</i> Gal4	no phenotype
<i>Shi.K44</i> (DN)	BL-5811	-	<i>mef</i> Gal4	lethal
<i>Shi.K44</i> (DN)	BL-5811	-	<i>lbe</i> Gal4	lethal
<i>shi</i> RNAi	v3799	GD1529	<i>mef</i> Gal4	weak migration defects
<i>sos</i> RNAi	v42848	GD1539	<i>htl</i> Gal4	no phenotype
<i>sqh</i> RNAi	v109493	KK107557	<i>mef</i> Gal4	medium migration defects
<i>sqh</i> RNAi	v7916	GD1695	<i>mef</i> Gal4	strong migration defects
<i>sqh</i> RNAi	v7917	GD1695	<i>mef</i> Gal4	medium migration defects
<i>Src42A</i> .DN	Gift from S. Luschnig		<i>mef</i> Gal4	club-like testis, complete muscle coverage
<i>Src42A</i> .DN	Gift from S. Luschnig		<i>htl</i> Gal4	club-like testis, complete muscle coverage
	-			
<i>src42A</i> RNAi	v17644	GD8338	<i>htl</i> Gal4	no phenotype
<i>src42A</i> RNAi	v17643	GD8338	<i>htl</i> Gal4	no phenotype
<i>src42A</i> RNAi	BI-44039	TriP.HMS02755	<i>htl</i> Gal4	no phenotype
<i>swip</i> RNAi	v31308	GD7047	<i>mef</i> Gal4	medium migration defects
<i>swip</i> RNAi	v107033	KK102466	<i>mef</i> Gal4	no phenotype
<i>swip</i> RNAi	v31307	GD7047	<i>mef</i> Gal4	no phenotype
<i>swip</i> RNAi	v31307	GD7047	<i>htl</i> Gal4	no phenotype
<i>swip</i> RNAi	v31308	GD7047	<i>htl</i> Gal4	no phenotype
<i>swip</i> RNAi	v107033	KK102466	<i>htl</i> Gal4	no phenotype
<i>eGFP-Ths-Cherry</i>	Gift from A. Müller		<i>eip 93F</i> Gal4	no phenotype
<i>eGFP-Ths-Cherry</i>	Gift from A. Müller		<i>robo2</i> Gal4	no phenotype
<i>eGFP-Ths-Cherry</i>	Gift from A. Müller		<i>gt</i> Gal4	no phenotype
<i>Ths</i>	BL-28106	-	<i>eip 93F</i> Gal4	no phenotype
<i>Ths</i>	BL-28106	-	<i>robo2</i> Gal4	no phenotype
<i>Ths</i>	BL-28106	-	<i>gt</i> Gal4	no phenotype
<i>ths</i> RNAi	v102441	KK111662	<i>eip 93F</i> Gal4	no phenotype
<i>ths</i> RNAi	v102441	KK111662	<i>robo2</i> Gal4	no phenotype
<i>ths</i> RNAi	v102441	KK111662	<i>doc1</i> Gal4	no phenotype

Appendix

<i>ths</i> RNAi	v102441	KK111662	<i>gt</i> Gal4	no phenotype
<i>ths</i> RNAi	v102441	KK111662	<i>dWnt2</i> Gal4	no phenotype
<i>ths</i> RNAi	v24536	GD7730	<i>eip 93F</i> Gal4	no phenotype
<i>ths</i> RNAi	v24536	GD7730	<i>robo2</i> Gal4	medium migration defects
<i>ths</i> RNAi	v24536	GD7730	<i>htl</i> Gal4	weak-medium migration defects
<i>ths</i> RNAi	v24536	GD7730	<i>doc1</i> Gal4	no phenotype
<i>ths</i> RNAi	v24536	GD7730	<i>gt</i> Gal4	no phenotype
<i>ths</i> RNAi	v24536	GD7730	<i>dWnt2</i> Gal4	no phenotype
<i>ths</i> RNAi	v24536	GD7730	<i>lsp</i> Gal4	no phenotype
<i>trio</i> RNAi	v40138	GD9531	<i>htl</i> Gal4	no phenotype
<i>tsr.S3A</i>	BL-9236	-	<i>htl</i> Gal4	no phenotype
<i>tsr</i> RNAi	v110599	KK108706	<i>lbe</i> -Gal4	medium migration defects
<i>tsr</i> RNAi	v110599	KK108706	<i>htl</i> Gal4	lethal
<i>tsr</i> RNAi	v110599	KK108706	<i>mef</i> Gal4	lethal
<i>unc-5</i> RNAi	BL-33756	TriP.HMS01099	<i>htl</i> Gal4	no phenotype
<i>velo</i> RNAi	BL-32389	TriP.HMS00383	<i>htl</i> Gal4	no phenotype
<i>vinc</i> RNAi	v105956	KK100863	<i>mef</i> Gal4	no phenotype
<i>wasp</i> RNAi	BL-36119	TriP.HMS01534	<i>mef</i> Gal4	no phenotype
<i>wasp</i> RNAi	BL-36119	TriP.HMS01534	<i>htl</i> Gal4	medium migration defects
<i>wasp</i> RNAi	BL-36119	TriP.HMS01534	<i>kr</i> Gal4	occasional medium migration defects
<i>wasp</i> RNAi	v13759	GD1559	<i>htl</i> Gal4	medium migration defects
<i>wasp</i> RNAi	v13759	GD1559	<i>kr</i> Gal4	occasional strong-medium migration defects
<i>wasp</i> RNAi	v13759	GD1559	<i>mef</i> Gal4	no phenotype
<i>wasp</i> RNAi	BL-25955	TriP.JF01975	<i>mef</i> Gal4	no phenotype
<i>wasp</i> RNAi	BL-25955	TriP.JF01975	<i>htl</i> Gal4	medium migration defects
<i>wasp</i> RNAi	BL-25955	TriP.JF01975	<i>kr</i> Gal4	occasional medium migration defects
<i>zip</i> RNAi	v7819	GD1566	<i>mef</i> Gal4	strong migration defects

7.5 List of mutant fly lines analysed for adult testis shaping defects

mutant	fly line ID/source	phenotypic strength
<i>f¹</i>	BL- 36	no phenotype
<i>sn³</i>	BL- 113	no phenotype
<i>swip^{Δ1}</i>	Franziska Lehne (unpublished)	no phenotype
<i>wasp³</i>	BL- 39725	strong shaping defects. Myoblasts in phalloidin staining not visible, due to strong F-actin signal in pigment cells.

7.6 Author Contributions

7.6.1 Publication 1

Rothenbusch-Fender, S., K. Fritzen, **M. C. Bischoff**, D. Buttgereit, S. F. Önel, & R. Renkawitz-Pohl (2017): Myotube migration to cover and shape the testis of *Drosophila* depends on Heartless, Cadherin/Catenin, and myosin II.

Biology Open 6 (12), 1876–1888.

- Critical reading of the manuscript and planning/execution of the experiments as explained in the following.

Fig. 5 D: Characterization of *htl*-Gal4 expression pattern in genital disc myoblasts to deduce *htl* expression.

Fig. 6 D: Characterisation and documentation of *ths^{e02026}/Df(2R)ths238* (hypomorphic allele/deficiency)-induced coverage defects in adult testis. These results indicate a function of Ths and constitute the only RNAi-independent muscle coverage defects.

Fig. 7: N-cadherin/phospho-Myosin II light chain antibody staining on wild type, *mef*-Gal4>>*dof* RNAi, and *mef*-Gal4>>*htl* RNAi. The results indicated that Myosin II light chain phosphorylation is reduced downstream of FGF-signalling. Conversely, N-Cadherin seems unaffected.

Fig. 8 B: Conceptualization and drawing of a preliminary version of the scheme that was adapted using photoshop by Susanne F. Önel.

7.6.2 Publication 2

Bischoff, M.C., S. Lieb, R. Renkawitz-Pohl, & S. Bogdan (2020):

Filopodia-based contact stimulated collective migration drives tissue morphogenesis.

Prof. Dr. Renate Renkawitz-Pohl initiated the original project. Prof. Dr. Sven Bogdan and Maik Bischoff designed the project, made the figures, the movies and wrote the manuscript. Maik Bischoff performed all experiments and statistics. Sebastian Lieb programmed the computer simulation and worked with Maik Bischoff on the planning and implementation. All authors commented on the manuscript.

7.7 Verzeichnis der akademischen Lehrer/-innen

Meine akademischen Lehrenden waren in Gießen:

Dr. C. Albrecht

Dr. M. Althaus

Prof. Dr. A. Becker

Prof. Dr. W. Clauß

Prof. Dr. R. Dammann

Prof. Dr. A. Dorresteyn

Dr. A. Holz

Prof. Dr. M. Düren

Dr. K. Ehlers

Dr. K. Ekschmitt

Junior-Prof. Dr. J. Encarnação

Prof. Dr. R. Göttlich

Prof. Dr. J. Hafke

Prof. Dr. J. Hughes

Prof. Dr. G. Klug

Prof. Dr. R. Lakes-Harlan

Prof. Dr. M. U. Martin

Prof. C. Müller PhD

Prof. Dr. A. Pingoud

Prof. Dr. R. Renkawitz

Prof. Dr. S. Schindler

Prof. Dr. R. Schmidt

Dr. P. Schubert

Prof. Dr. B. Spengler

Prof. Dr. T. Trenczek

Apl-Prof. Dr. B. Werding

PD Dr. B. Westermann

Prof. Dr. T. Wilke

Prof. Dr. V. Wolters

7.8 Danksagung

Ich möchte mich bei meinen Freunden und meiner Familie bedanken, die immer Verständnis hatten, wenn ich mal nicht so viel Zeit hatte und mich an allen Enden unterstützt haben. Besonders möchte ich mich bei meiner Freundin bedanken, die immer für mich da war, als es am härtesten war. Das Kapitel „Doktor“ neigt sich jetzt dem Ende, nur damit sich ein noch spannenderes anschließen kann.

Für das kritische Lesen und korrigieren der vorliegenden Arbeit möchte ich mich bei Vignesh Viswanathan bedanken. *आपकी मदद के लिए बहुत बहुत शुक्रिया। मुझे आशा है कि Google अनुवादक काम करता है!* Außerdem möchte ich mich bei Alexander Hirschhäuser bedanken, der viele gute Vorschläge hatte, die ich gerne umgesetzt habe. Ich möchte mich ganz besonders bei Dr. Uwe Töpfer bedanken, der trotz seiner Arbeit und seiner jungen Familie, die Zeit fand meine Arbeit auf „Herz und Nieren“ zu prüfen, und noch so einiges fand, dass mir durch die Lappen ging. *Danke Uwe, ohne Dich sähe diese Arbeit ganz anders aus.* Ich möchte mich bei Napasorn „Mo“ Suwanwela für die sprachliche Überarbeitung der Arbeit bedanken.

ขอบคุณไม่ถ้าไม่มีคุณวิทยานิพนธ์นี้จะมีเครื่องหมายจุลภาคมากกว่านี้และมีความหมายน้อยกว่านี้มากฉันหวังว่า Google Translate จะทำได้! Dafür, dass sie mir die Fliegen-genetik und das wissenschaftliche Arbeiten beigebracht hat, möchte ich mich bei Dr. Anne Holz bedanken.

Allen Mitarbeitern und Studenten der Abteilung Molekulare Zellphysiologie, die ich nicht erwähnt habe, möchte ich danken, da es ohne ein so gutes Team im Rücken, nicht möglich wäre so etwas wie diese Arbeit zu stemmen.

Zu guter Letzt möchte ich mich ganz besonders gleichermaßen bei Prof Dr. Renate Renkawitz-Pohl und bei Prof. Dr. Sven Bogdan bedanken. Bei beiden zusammen möchte ich mich für das Thema, bedanken. Bei Frau Prof Renkawitz dafür, dass sie es sich initial ausgedacht hat und bei Herrn Prof. Bogdan dafür, dass es sich durch ihn sich zu dem weiterentwickelt hat, was die vorliegende Arbeit abbildet. Ich nutzte im Laufe meines Promotionszeit Labore und Ausstattung von Frau Prof. Renkawitz und von Herrn Prof. Bogdan und muss mich auch hierfür bei beiden bedanken. Schließlich möchte ich mich dafür bedanken, dass ich auf sämtliche Unterstützung bauen konnte, die man sich vorstellen kann.

7.9 Ehrenwörtliche Erklärung

„Ich erkläre ehrenwörtlich, dass ich die dem Fachbereich Medizin Marburg zur Promotionsprüfung eingereichte Arbeit mit dem Titel: **New principles in collective cell migration during *Drosophila* organ development** im Institut für Physiologie und Pathophysiologie unter Leitung von Prof. Dr. S. Bogdan mit Unterstützung durch Prof. Dr. R. Renkawitz-Pohl ohne sonstige Hilfe selbst durchgeführt und bei der Abfassung der Arbeit keine anderen als die in der Dissertation aufgeführten Hilfsmittel benutzt habe. Ich habe bisher an keinem in- oder ausländischen Medizinischen Fachbereich ein Gesuch um Zulassung zur Promotion eingereicht, noch die vorliegende oder eine andere Arbeit als Dissertation vorgelegt.

Ich versichere, dass ich sämtliche wörtlichen oder sinngemäßen Übernahmen und Zitate kenntlich gemacht habe.

Mit dem Einsatz von Software zur Erkennung von Plagiaten bin ich einverstanden.

Vorliegende Arbeit wurde in folgenden Publikationsorganen veröffentlicht:

Rothenbusch-Fender, S., Fritzen, K., Bischoff, M. C., Buttgereit, D., Oenel, S. F., & Renkawitz-Pohl, R. (2017). Myotube migration to cover and shape the testis of *Drosophila* depends on Heartless, Cadherin/Catenin, and myosin II. *Biology open* 6 (12), 1876-1888.

Ort, Datum, Unterschrift Doktorandin/Doktorand

„Die Hinweise zur Erkennung von Plagiaten habe ich zur Kenntnis genommen.“

Ort, Datum, Unterschrift Referentin/Referent